INTEGRATING EXPERIMENTAL AND PHYSIOLOGICALLY BASED PHARMACOKINETIC MODELING APPROACHES TO EVALUATE NEUROTOXICITY OF THE HERBICIDE ATRAZINE ACROSS THE LIFESPAN

by

ZHOUMENG LIN

(Under the Direction of Nikolay M. Filipov)

ABSTRACT

Atrazine (ATR) is a widely used chlorotriazine herbicide. Available experimental evidence and computational tools are insufficient for proper assessment of ATR's risk to human health. This dissertation project aimed to determine neurotoxicity of ATR overexposure during adulthood, development, or in vitro, and to create physiologically based pharmacokinetic (PBPK) models for ATR across the lifespan in rodents.

In adult male C57BL/6 mice, short-term oral ATR exposure (5-250 mg/kg) caused dose-dependent reduced performance in a novel object recognition test (NOR), open field hypoactivity and increased swimming time in a forced swim test at higher doses; the latter effects were accompanied with altered dopamine and serotonin homeostasis in the striatum and prefrontal cortex. Low-level drinking water (DW) ATR exposure (3 mg/L) during gestation and lactation resulted in hyperactivity and decreased NOR performance in mouse dams, hyperactivity in male and female juvenile offspring, decreased swimming time in male juveniles, increased marble burying in female juveniles, and decreased NOR performance in female adults. Neurochemically, DW ATR exposure increased striatal dopamine in dams and juvenile

offspring. In vitro exposure (24-48 h; 12-300 μM) to ATR or its main metabolite didealkylatrazine (DACT) affected morphological differentiation of N27 dopaminergic cells with ATR mainly targeting soma enlargement (dose-dependent effect) and DACT decreasing neurite outgrowth (high-dose effect).

A PBPK model for ATR and its metabolites desethylatrazine, desisopropylatrazine and DACT was developed in adult male mice and then extrapolated to rats. This adult rodent model and recent experimental data were the foundation for a subsequent developmental PBPK model that accurately described ATR's kinetic behavior during fetal, neonatal, pregnant and lactating stages in rats. Model simulations aligned well with experimental data, including with a new pharmacokinetic study conducted with pregnant mice orally exposed to ATR, validating the cross-species extrapolation of the gestational model.

In conclusion, ATR overexposure affects multiple behavioral domains and perturbs brain dopamine and serotonin homeostasis, with some effects on the offspring being sex-specific. ATR- and/or DACT-induced neuronal differentiation disruption may contribute to the observed developmental neurotoxicity. The newly developed PBPK models can be used in brain dosimetry predictions and, together with the experimental data, may improve ATR's risk assessment.

INDEX WORDS: Atrazine, Pesticides, Toxicity, Brain, Behavior, Dopamine, Serotonin, PBPK modeling, Developmental exposure, Neuronal differentiation

INTEGRATING EXPERIMENTAL AND PHYSIOLOGICALLY BASED PHARMACOKINETIC MODELING APPROACHES TO EVALUATE NEUROTOXICITY OF THE HERBICIDE ATRAZINE ACROSS THE LIFESPAN

by

ZHOUMENG LIN

B.Med., Southern Medical University, China, 2009

A Dissertation Submitted to the Graduate Faculty of The University of Georgia in Partial Fulfillment of the Requirements for the Degree

DOCTOR OF PHILOSOPHY

ATHENS, GEORGIA

2013

INTEGRATING EXPERIMENTAL AND PHYSIOLOGICALLY BASED PHARMACOKINETIC MODELING APPROACHES TO EVALUATE NEUROTOXICITY OF THE HERBICIDE ATRAZINE ACROSS THE LIFESPAN

by

ZHOUMENG LIN

Major Professor:	Nikolay M. Filipov
Committee:	Jia-Sheng Wang
	Mary Alice Smith
	Julie A. Coffield
	Xiaoqin Ye

Electronic Version Approved:

Maureen Grasso
Dean of the Graduate School
The University of Georgia
December 2013

ACKNOWLEDGEMENTS

Firstly, I would like to thank my advisor Dr. Nikolay M. Filipov for proper guidance, continuous support and readily-available help throughout my PhD training. I really appreciate him and will always remember what he has taught or given me, such as (1) a variety of techniques and knowledge, (2) the opportunities to receive comprehensive training in the field of toxicology by learning in vitro, in vivo, and computational techniques, (3) the ways of experimental design, scientific thinking and effective writing, (4) the opportunities to receive professional training (e.g., grant writing, public presentation, and leadership), (5) the suggestions on my career development, and (6) many others. I am also grateful for his confidence in my ability to become a successful toxicologist in the future. I enjoy the time working with him, especially during the most impressive weekly mentor meetings. To me, he is not only an excellent advisor, but also a great friend.

Secondly, I would like to express my sincere gratitude to Dr. Jeffrey W. Fisher. I was fortunate to take the last course of PBPK modeling offered by Dr. Fisher before he moved to FDA. Even though he works far away from Athens and is not in my Advisory Committee, he is so nice that he keeps mentoring me various computational modeling techniques throughout my graduate study and providing me with excellent professional suggestions to help me find a job.

To my respected Advisory Committee members, Dr. Jia-Sheng Wang, Dr. Mary Alice Smith, Dr. Xiaoqin Ye and Dr. Julie A. Coffield, I would like to say Thank You so much for helping me review my research proposal and dissertation, attend annual Committee Meetings, provide a number of constructive suggestions and write multiple reference letters. Special thanks

are also given to my Society of Toxicology Mentor Match Program mentor, Dr. Joshua A. Harrill, for excellent professional advice and helping me revise my CV and Cover Letter. Additionally, I would like to give my warm appreciation to my undergraduate advisor and friend, Dr. Lang Yao in the Department of Toxicology at the Southern Medical University in Guangzhou, China, who brought me into this exciting field of Toxicology and keeps encouraging me to pursue my dream.

Many thanks are given to my lab members, Dr. Celia A. Dodd, Irina I. Georgieva, and Saritha Krishna. Celia and Irina showed me many techniques and Saritha taught me a lot of oral presentation skills. I really enjoyed the time working with them. Additionally, to my good friends, Dr. Sheppard A. Martin, Dr. Shuang Li, Dr. Shuo Xiao, Fei Zhao, Rong Li, and Xia Guo, thank you for helping me a lot in my dissertation research.

I sincerely appreciate the Interdisciplinary Toxicology Program, Graduate School, and Department of Physiology and Pharmacology for offering me research assistantships. My home department, the Department of Physiology and Pharmacology is really an excellent environment that allows me to focus on research. Dr. Gaylen L. Edwards, Kali King and Misty Patterson in my home department, and Dr. Brain S. Cummings, Dr. Mary Alice Smith, and Joanne Mauro in the Interdisciplinary Toxicology Program always provide me with a variety of timely assistance. Thanks are given to them.

Last but not least, I would like to thank my family. My parents have been doing their best to raise, educate, support and encourage me. While I was not able to be with them most of the time during the last four years, they had never complained. Instead, they always understand, support, and encourage me. I am in particularly indebted to my wife Chunla He, who is also a PhD student at the University of Georgia. We have been studying together for nine years. She

has been constantly supporting and helping me in my research and in my life without any complaints, regardless of success or failure. Even endless thanks cannot express my gratitude.

For those many other friends at the University of Georgia, thank you for helping me in my daily life.

Once again, I would like sincerely thank my advisor, committee members, mentors, friends, and my family. Without your support and help, I would not have completed this dissertation project.

TABLE OF CONTENTS

LIST OF TABLES

Page

LIST OF FIGURES

Page

ABBREVIATIONS

ABC: ATP-binding cassette

AChE: acetylcholine esterase

ANOVA: analysis of variance

ATR: atrazine, 2-chloro-4-(ethylamino)-6-(isopropylamino)-s-triazine

AUC: area under the curve

BW: body weight

^{14}C-ATR: ^{14}C-atrazine

Cl-TRIs: chlorinated metabolites of ATR, including DE, DIP, and DACT

DA: dopamine

DACT: didealkylatrazine, didealkyl atrazine, diaminochlorotriazine, 2-chloro-4,6-diamino-1,3,5-triazine

DAT: dopamine transporter

DE: desethylatrazine, desethyl atrazine, 2-chloro-4-amino-6-(isopropylamino)-s-triazine

DIP: desisopropylatrazine, desisopropyl atrazine, 2-amino-4-chloro-6-(ethylamino)-s-triazine

DOPAC: 3,4-dihydroxyphenylacetic acid

Drd1: dopamine receptor D1

Drd2: dopamine receptor D2

Drd4: dopamine receptor D4

EPA: Environmental Protection Agency

FST: forced swim test

GD: gestational day

GI tract: gastrointestinal tract

GnRH: gonadotropin-releasing hormone

5-HIAA: 5-hydroxyindoleacetic acid

HRP: horseradish peroxidase

5-HT: serotonin

HVA: homovanillic acid

ip: intraperitoneal

LOAEL: lowest observed adverse effect level

MCL: maximum contaminant level

MHPG: 3-methoxy-4-hydroxyphenylglycol

3-MT: 3-methoxytyramine

N: Newton

NE: norepinephrine

NOAEL: no observed adverse effect level

NOR: novel object recognition test

NSC: normalized sensitivity coefficient

Nurr1: nuclear receptor related 1

PAD: population adjusted dose

PBPK: physiologically based pharmacokinetic

PC: tissue:blood partition/distribution coefficient

PD: Parkinson's disease

PND: postnatal day

po: by oral gavage

RBC: red blood cell

RfD: reference dose

SRM: selected reaction monitoring

TH: tyrosine hydroxylase

VMAT-2: vesicular monoamine transporter 2

VTA: ventral tegmental area

CHAPTER 1

INTRODUCTION

Problem statement

Pesticides are substances or mixture of substances intended for preventing, destroying, or mitigating any pest. Over the last several decades, the global use of pesticides has increased steadily, which has substantially improved crop yields (LeBaron et al., 2008). In order to meet the need for increased crop yields to feed a growing world population, it is predicted that pesticides' global use will continue to increase. However, the expanded use of pesticides has resulted in ubiquitous residues in air, water and food, which has led to widespread concern about their potential adverse effects on human health (Tadeo, 2008). In particular, emerging evidence suggests that pesticide exposure is a risk factor of Parkinson's disease (PD; Brown et al., 2006; Tanner et al., 2011). PD is the second most common neurodegenerative disease that affects approximately 4 million people worldwide (de Lau and Breteler, 2006). It is characterized pathologically by a progressive loss of dopamine (DA) neurons in the substantial nigra and a severe reduction of striatal DA. While the etiology of PD has yet to be established, recent studies suggest over 90% of PD is likely related to environmental causes, pesticide exposure in particular (Tanner et al., 1999; Hatcher et al., 2008). Therefore, it has become a critical research problem to identify specific pesticides as causative factors to PD.

Atrazine (ATR) is a chlorotriazine herbicide that is widely used in most countries, such as the US (EPA, 2003). Because it is relatively persistent in the water, it has become a ubiquitous water contaminant (Battaglin et al., 2009). Humans can be exposed to ATR via consuming ATR-

contaminated drinking water and food (Mosquin et al., 2012); while occupational population can be exposed to much higher amounts of ATR via inhalation and dermal routes (Catenacci et al., 1993). ATR and its metabolites are commonly detected in human biological samples, including urine samples from ATR applicators, their families, and the general populations, as well as from umbilical plasma samples and breast milk samples (Balduini et al., 2003; Whyatt et al., 2003; Curwin et al., 2007; Chevrier et al., 2011). As a result, there is a great concern about the potential toxic effects of ATR to humans, which is also an important research problem.

Animal studies suggest that ATR overexposure causes PD-like dopaminergic toxicities (Coban and Filipov, 2007; Bardullas et al., 2011) and a recent epidemiology study has associated higher concentrations of ATR in ground water with increased incidence of PD (Shaw, 2011). Therefore, ATR overexposure might be a risk factor of PD. Due to ATR's potential toxicity to humans, it has been banned in Europe since 2003 (Sass and Colangelo, 2006). Different decisions on the use of ATR among countries are mainly due to insufficient scientific evidence about its potential toxicity, mode of action, and assessing tools for proper risk assessment. For example, while some evidence suggests that ATR targets the DA pathway and causes DA-related motor dysfunction, there is much unknown about ATR's effects on other neural pathways, other behaviors, and the underlying mechanism(s). The dose-dependency of ATR's effects and its most sensitive neural target are also largely unknown, which are key components in the risk assessment process. In addition, while it is known that developing nervous system is much more sensitive to ATR than adult nervous system (Giusi et al., 2006; Belloni et al., 2011), it is unknown whether ATR exposure disrupts any of the nervous system developmental events, such as differentiation. Moreover, little is known about the neurobehavioral and neurochemical effects of human-relevant (i.e., drinking water, low doses) ATR exposure during vulnerable gestational

and lactational periods on the dams and offspring. These questions are crucial in assessing the risk of ATR in sensitive subpopulations, including the fetus, neonate, and pregnant women.

From the perspective of risk assessment, while experimental evidence is vital, quantitative assessing tools, such as physiologically based pharmacokinetic (PBPK) models, also play an important role. PBPK models are mathematical descriptions of chemical disposition in the body. They play an increasingly important role in the risk assessment of chemicals because they can be used to predict target organ dosimetry and conduct species extrapolation. In the case of ATR, PBPK models are available in adult rats (Timchalk et al., 1990; McMullin et al., 2003; McMullin et al., 2007b), and these models have properly simulated the kinetic behavior of ATR and its metabolites in the plasma. However, none of these existing adult rat models has been successfully extrapolated to other species, such as mice, which is important in the future extrapolation to humans. Also, there are no PBPK models for ATR in other age stages (e.g. fetal, neonatal, pregnant, or lactating periods) in any animal species. Additionally, the available models can only be used to predict the plasma dosimetry of ATR and its metabolites. Thus, they cannot be used to predict target organ (i.e, the brain) dosimetry, which is essential in establishment of target organ dose-response relationship.

Objectives, hypotheses, and specific aims

Considering the data gaps related to ATR's neurotoxicity and the modeling of its kinetic behavior, in order to provide experimental evidence and computational tools to help assess the risk of ATR neurotoxicity, the overall objectives of this dissertation were to (1) determine the neurochemical and neurobehavioral effects of ATR exposure during adulthood or development and (2) develop rodent PBPK models for ATR across the lifespan. To meet these objectives, the following hypotheses were developed: (1) overexposure to ATR will cause adverse effects on

regional brain monoamine homeostasis, which will result in subsequent behavioral abnormalities; ATR's adverse effects will be more prominent when exposure is during the period of nervous system development; (2) new PBPK models for ATR in rodents across the lifespan will be successfully developed and these models will be able to predict accurately the measured concentrations of ATR and its metabolites from available pharmacokinetic studies as well as from a newly-conducted study as part of this dissertation project in multiple tissues, including the brain. These hypotheses were addressed in the following Specific Aims:

Specific Aim 1: To determine the effects of short-term exposure to a wide dose range of ATR (5-250 mg/kg) on the behavioral, neurochemical and molecular endpoints associated with DA and other monoamine systems in adult male mice. The dose-dependency of each index and the differential sensitivity among different endpoints were evaluated in this Aim.

Specific Aim 2: To develop a PBPK model for ATR and its metabolites DE, DIP, and DACT in adult male mice. This model described the dosimetry of ATR and its metabolites in the mouse brain, other organs, plasma, and urine and it was extrapolated to rats.

Specific Aim 3: To develop PBPK models for ATR and its metabolites DE, DIP, and DACT in rat fetuses, neonates, and dams. The development of these models was based on the adult model of Specific Aim 2 and on recently published experimental rat data (Fraites et al., 2011). A pharmacokinetic study of ATR in pregnant mice was also performed and data were used to extrapolate the gestational model from rats to mice in order to test the model's cross-species extrapolation ability.

Specific Aim 4: Determine the effects of ATR and its major metabolite DACT on the morphological differentiation of dopaminergic neurons in vitro. N27 cell line (Prasad et al., 1994), an immortalized TH-positive neuronal cell line derived from rat mesencephalic tissue at

the peak of DA neuron generation (E12), was used in this Aim. N27 cells were exposed to a concentration-range (12-300 μM) of ATR or DACT during different states of differentiation.

Specific Aim 5: Determine the effects of exposure to a low drinking water concentration of ATR (3 mg/L) during gestation and lactation on regional monoamine neurochemistry and associated behaviors in the mouse dam, juvenile and adult offspring. Selected brain regions included prefrontal cortex, nucleus accumbens, striatum, perirhinal cortex, and/or hippocampus. Behavioral tests comprised open field, pole, grip strength, marble burying, novel object recognition, and/or forced swim tests.

The results (presented later) from these studies greatly advance our understanding about the effects of ATR on the nervous system, especially on the sensitive developing nervous system. Specifically, data from Aim 1 suggest that ATR exposure not only affects the nigrostriatal DA pathway and motor function, but also disrupts other monoamine systems (serotonin and norepinephrine) and changes other behavioral domains (emotion and cognition). Aim 5 provides evidence that maternal low-dose ATR exposure disrupts nervous system development, resulting in delayed or long-term behavioral and neurochemical changes in the offspring. Aim 4 identified potential mechanisms of developmental neurotoxicity of ATR. The PBPK models from Aim 2 and Aim 3 substantially increase our understanding about ATR's kinetic behavior in the body across the lifespan. Overall, these studies suggest that ATR exposure affects multiple behavioral domains and perturbs brain monoamine homeostasis, with some effects on the offspring being delayed or persistent. ATR- and/or DACT-induced neuronal differentiation disruption may contribute to the observed developmental neurotoxicity. The PBPK models and the experiment data together can be used to establish dose-response relationship of ATR's neurotoxicity, thereby contributing to the risk assessment of this widely used herbicide.

CHAPTER 2

LITERATURE REVIEW

Pesticides

Overview

Pesticides are defined as any substance or mixture of substances intended for preventing, destroying, repelling, or mitigating pests (Echobicon, 2001). They can be classified on the basis of their chemical structures (e.g., organochlorine, organophosphate, pyrethroid, or triazine) or the organisms designed to control (e.g., herbicides, insecticides, fungicides, rodenticides, or pediculicides). Over the last century, the worldwide pesticide use has increased steadily (Kiely et al., 2004; Grube et al., 2011). Concurrently, the agricultural yields have improved, with estimated yield improvements for major crops, such as corn, cotton, sorghum, soybean, and wheat in the US ranging from 238% to 811% (LeBaron et al., 2008). Currently, herbicides constitute around 40% of the total pesticide use in both the world (e.g., 5.2 billion pounds [2.4 billion kg] in 2007) and the US (e.g., 1.1 billion pounds [0.5 billion kg] in 2007; Grube et al., 2011). In the US, pesticides are used on more than 90% of the cultivated area, representing 87 million ha of cropland (Gianessi and Reigner, 2007). Due to the need for continued increases in crop yields not only to feed a growing world population, but also for greater biofuel market demand (OECD-FAO, 2007), it is anticipated that the worldwide use of pesticides will continue to increase in the foreseeable future.

The widespread use of pesticides expectedly results in environmental residues found in the air, soil, water, and food. The general population can be chronically exposed to low levels of

pesticides and/or their environmental metabolites through drinking water, food, air, and dust. For example, according to the National Water-Quality Assessment Program, around 50% of the US domestic water supply sites were contaminated with at least one pesticide (Kolpin et al., 1998; Squillace et al., 2002; Gilliom, 2007). The occupational pesticide exposures, on the other hand, are typically much higher and occur primarily via inhalation and dermal routes (Konradsen, 2007). In occupational settings, acute pesticide poisoning has become a global public health problem, with an estimated worldwide occurrence of 3 million severe cases and a minimum of 0.3 million death each year (Jeyaratnam, 1990; Konradsen, 2007).

Excessive exposure to pesticides has been associated with adverse health outcomes involving alterations of various organ systems, including the reproductive, immune, endocrine, or nervous system (Bretveld et al., 2006; Tanner et al., 2011; Corsini et al., 2013). The negative consequences of pesticide overexposure on the nervous system are of utmost concern due to the nervous system's heightened sensitivity to toxic insults (Costa et al., 2008). In this regard, the association between pesticide exposure and neurodegenerative diseases, such as Parkinson's disease (PD) and Alzheimer's disease, is particularly strong (Baldi et al., 2003; Parron et al., 2011; Tanner et al., 2011).

Pesticides and neurotoxicity

A number of pesticides are specifically designed or have been demonstrated to be neurotoxicants (Echobicon, 2001). Insecticides (e.g., organophosphates, carbamates, pyrethroids, and organochlorines), are specifically designed to kill insects by targeting insect's nervous system. However, they are also neurotoxic to non-target mammalians, including humans. For example, organophosphate and carbamate insecticides can disrupt acetylcholine neurotransmission in laboratory animals and humans by inhibiting mammalian brain

acetylcholine esterase activity, resulting in accumulation of acetylcholine at cholinergic synapses in the nervous system and a range of behavioral abnormalities (Costa, 2006; Costa et al., 2008). Similarly, excessive exposure of non-target species to pyrethroid insecticides can prolong opening of sodium channels, leading to a stable hyperexcitable state (Costa et al., 2008).

Herbicides are designed to kill or severely injure plants generally via biochemical pathways that are unique to plants. However, certain herbicides can be highly toxic to non-target mammalian species, including to humans. For example, the herbicide paraquat is classified as a highly toxic pesticide, with an oral LD_{50} of 100 mg/kg in rats (Costa et al., 2008). Short-term exposure to non-lethal doses of paraquat results in decreased striatal dopamine (DA) levels and reduced number of DA neurons in the substantia nigra, leading to PD-like symptoms, such as motor dysfunction (Cannon et al., 2009; Litteljohn et al., 2009). Fungicides are mainly used to protect crops from fungi and molds. However, certain fungicides can also cause mammalian neurotoxicity in mammals. For example, the dithiocarbamate fungicide maneb has been shown to produce nigrostriatal DA degeneration when given in combination with paraquat, and to directly affect DA neurons by inhibiting mitochondrial function (Thiruchelvam et al., 2000; Zhang et al., 2003). In the context of pesticide neurotoxicity, whether exposure to certain pesticides may contribute to the etiology of some neurodegenerative diseases (most notably PD) and/or to other less defined behavioral alterations has become a topic of public concern, and more research is needed in this field (Costa et al., 2008; Kamel, 2013).

Pesticides and Parkinson's disease (PD)

PD is the second most common neurodegenerative disorder that is typified pathologically by a progressive depletion of dopaminergic neurons in the substantia nigra and a severe reduction of striatal DA content (de Lau and Breteler, 2006). The prevalence of PD increases

with age and in industrialized countries it is estimated at about 1-2% of people over 60 years old and at 3-5% in people above 85 years of age (de Lau and Breteler, 2006). While the etiology of PD has yet to be established, recent epidemiological studies suggest only a small fraction of PD is attributable to genetic factors and over 90% of PD is likely related to environmental causes, pesticide exposure in particular (Tanner et al., 1999; Hatcher et al., 2008). For example, exposure to pesticides as a group (Brown et al., 2006; Parron et al., 2011), to paraquat (Tanner et al., 2011), to rotenone (Tanner et al., 2011), or to the combination of paraquat and maneb (Costello et al., 2009) has been associated with increased incidence of PD. In addition, elevated levels of pesticides (e.g., organochlorines) have been found in brains of PD cases compared to controls (Fleming et al., 1994; Corrigan et al., 2000). While pesticide exposure and PD have been associated in multiple epidemiological studies, lack of association between pesticide exposure and PD has also been reported (Brown et al., 2006; Berry et al., 2010). The variation in the associations among studies may be due to the differences in duration and frequency of exposure, types of pesticides, and inter-subject variation (Allen et al., 2013). In particular, age-related differences in the nervous system and pharmacokinetics may play an important role in the differential sensitivity to pesticide neurotoxicity (Ginsberg et al., 2005; Timchalk et al., 2006).

Pesticide neurotoxicity and age – windows of vulnerability

Adverse effects of pesticide overexposure on the nervous system in most cases are age-dependent with the young (Zheng et al., 2000; Vidair, 2004) and the elderly (Weiss, 2000b; Ginsberg et al., 2005) typically affected the most. While in some cases (Hiller-Sturmhöfel and Swartzwelder, 2005) adult brains may be more sensitive than immature ones, the differential nervous system sensitivity to pesticides across the lifespan is frequently manifested with greater sensitivity of the developing nervous system (Weiss, 2000a; Winneke, 2011). This

greater sensitivity is attributed mainly to increased vulnerability of the developing brain due to the complex emergence of various neurodevelopmental events and the lack of a mature blood-brain barrier (Rice and Barone, 2000). Nervous system development extends from the embryonic period through adolescence, and encompasses the temporal and regional emergence of following processes: proliferation, migration, differentiation, synaptogenesis, myelination, and apoptosis (Rice and Barone, 2000). Developing brain's vulnerability is a function of exposure timing and exposure level. Exposure timing is critical for developmental neurotoxicity; when exposure to pesticides is coincident with the ontogeny of developmental processes and it interferes with the cascade of these developmental events, it is more likely to cause neurotoxicity (Rice and Barone, 2000). Exposure level relates to the amounts of pesticides and/or their active metabolites that reach the developing brain. For example, due to the higher permeability of the immature blood-brain barrier (BBB) of embryos, fetuses, and infants (Kearns et al., 2003), pesticides/metabolites are expected to pass through BBB more readily. Therefore, in order to fully reveal the impact of a specific pesticide on the mammalian nervous system, it is important to consider age-related physiological and pharmacokinetic differences.

Pesticide neurotoxicity, metabolism, and pharmacokinetics

Besides having an immature and rapidly developing brain, fetuses and neonates can have greater sensitivity to pesticides than adults due to pharmacokinetic factors, including absorption, distribution, metabolism, and elimination. For example, fetuses can be directly exposed to pesticides because many pesticides are lipophilic and can pass the blood-placenta barrier efficiently (Salama et al., 1993; Abdel-Rahman et al., 2002). In neonates, absorption of chemicals is slower than in adults, mainly because of lower gastric emptying and intestinal motility and decreased activity of intestinal drug-metabolizing enzymes (Kearns et al., 2003).

However, despite slower absorption, neonates frequently have higher bioavailability because of lower total plasma protein levels (including albumin), resulting in increased free chemical fraction (Kearns et al., 2003). The age-dependent increase in the overall expression and activity of phase I and phase II metabolizing enzymes results in lower adult levels of parent compounds compared to their levels in the fetus, neonate and the young infant (Hines and McCarver, 2002; McCarver and Hines, 2002). In addition, developmental changes in renal function can dramatically alter the plasma clearance of chemicals with extensive renal elimination (Chen et al., 2006). Therefore, it is critical to reveal the physiological stage- and age-related differences in pesticide pharmacokinetics for proper and full evaluation of the human health risks associated with their use.

Pesticide neurotoxicity and physiologically based pharmacokinetic (PBPK) modeling

The evaluation of the risks of pesticide exposure to human health, including to the nervous system, usually starts with the establishment of dose-response relationships based on toxicological and pharmacokinetic studies in laboratory animals. While toxicological studies are helpful for identifying the critical points of departure, i.e., LOAEL (lowest observed adverse effect level) and NOAEL (no observed adverse effect level), the associated target organ pesticide/metabolite dosimetry is usually unknown due to lack of dose-relevant pharmacokinetic studies. In this regard, physiologically based pharmacokinetic (PBPK) modeling is helpful and can be used for target organ dosimetry prediction associated with LOAEL, NOAEL and actual exposure levels; these in turn can be used to derive human equivalent doses, a key step in the pesticide risk assessment process (Crowell et al., 2011). Therefore, in order to help improve the neurotoxicity risk assessment of a specific pesticide, it is vital to conduct both experimental and PBPK modeling studies.

Atrazine

Overview

Atrazine [ATR; 2-chloro-4-(ethylamino)-6-(isopropylamino)-s-triazine, CAS# 1912-24-9; Fig. 2.1] is a broad-spectrum chlorotriazine herbicide that was first registered in 1958 by JR Geigy SA (currently known as Syngenta). For more than half a century, it has been extensively used to control broadleaf weeds; at present ATR is one of the two most widely used pesticides in the US (EPA, 2003). The US Environmental Protection Agency (EPA) estimates that ATR's annual use, which is applied on crops such as corn, sugarcane, sorghum, and pineapples (>98% of total use in the US), is approximately 76.5 million pounds (34.7 million kg) of active ingredient (EPA, 2003). Besides crop use, ATR is also used in forestry (such as Christmas tree farms and on sod farms), golf courses, and residential lawns (for a combined <2% of total use; EPA, 2003).

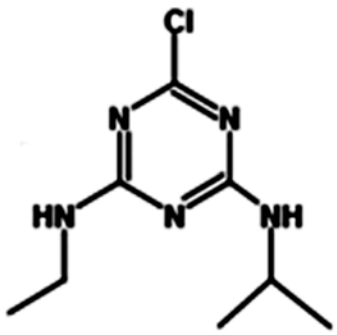

Figure 2.1. Chemical structure of atrazine. Adapted from ATSDR (2003).

Due to its widespread use, relative persistence in the water (half-life >6 months), and extreme persistence in the soil (detectable 22 years after application), ATR has become a ubiquitous environmental contaminant (ATSDR, 2003; Jablonowski et al., 2009). In places with

heavy ATR use, such as the Midwestern US, surface and drinking water ATR concentrations (up to 224 and 34 μg/L, respectively) substantially exceed the current maximum contaminant levels (MCL) for both the US and Europe, which are 3 and 0.1 μg/L, respectively (ATSDR, 2003; Mosquin et al., 2012).

Human exposures to ATR and its metabolites occur mostly through oral ingestion of ATR-contaminated drinking water or food products for the general population, as well as via inhalation and dermal absorption for occupational and residential applicators (Catenacci et al., 1993; ATSDR, 2003; Mosquin et al., 2012). For the general population, the estimated acute and chronic dietary exposures to ATR are 0.234-0.857 and 0.046-0.286 μg/kg/day, respectively (Gammon et al., 2005), which are relatively low compared to the human reference dose (100 μg/kg/day) and the population adjusted dose (10 μg/kg/day). On the other hand, the exposure levels could reach up to 151000 μg per work shift or >2 mg/kg/day (assuming a standard 70 kg body weight) for ATR manufacturing workers, suggesting a much higher occupational risk for overexposure (Catenacci et al., 1993).

ATR and its metabolites are commonly detected in urine samples from farmers, their families, and the general population, including pregnant women and young children (Barr et al., 2007; Curwin et al., 2007; Chevrier et al., 2011). They are also detected in umbilical cord plasma and in breast milk samples (Balduini et al., 2003; Whyatt et al., 2003). These findings have raised the public concern about the potential health impacts of ATR exposure to sensitive human subpopulations, such as the fetus and neonate. As a result, ATR has been banned in Europe since 2003 (Sass and Colangelo, 2006). However, ATR is still used extensively in the US and many other countries, such as China, Brazil, Argentina, and Mexico (Sass and Colangelo, 2006). In

these countries of heavy ATR use, there is a huge controversy as to whether or not ATR should be banned due to the increasing evidence about ATR toxicity (Sass and Colangelo, 2006).

Atrazine toxicity: adults

Effects on the endocrine, reproductive, and immune systems

In laboratory animals, excessive exposure to ATR causes various adverse effects on multiple organ systems, including endocrine, reproductive, immune, and nervous systems (Cooper et al., 2000; Pruett et al., 2003; Cooper et al., 2007; Bardullas et al., 2011). Observed endocrine effects include perturbations of the hypothalamic-pituitary-gonadal (HPG) and hypothalamic-pituitary-adrenal (HPA) axis functions. Specifically, ATR (75-300 mg/kg) exposure decreases luteinizing hormone (LH) surge in ovariectomized estrogen- (Cooper et al., 2000) or estrogen plus progesterone-primed (McMullin et al., 2004; Foradori et al., 2009a), as well as in intact female rats (Cooper et al., 2007). Prolactin levels and follicle-stimulating hormone (FSH) surge are also attenuated by ATR in ovariectomized, estrogen-primed (Cooper et al., 2000) and estrogen plus progesterone-primed (Foradori et al., 2009a) female rats, respectively. In the case of HPA axis, ATR (5-300 mg/kg) exposure increases plasma concentrations of adrenocorticotropic hormone, corticosterone, and adrenal progesterone in rodents (Pruett et al., 2003; Laws et al., 2009; Pruett et al., 2009; Foradori et al., 2011; Hotchkiss et al., 2012).

The altered endocrine homeostasis caused by ATR (50-300 mg/kg) exposure also contributes to a range of reproductive abnormalities, including disrupted estrous cyclicity (Cooper et al., 1996; Shibayama et al., 2009), increased pre- and post-implantation loss (Cummings et al., 2000), and full-litter resorption (Narotsky et al., 2001) in females. In males, ATR (50-300 mg/kg) exposure decreases testosterone levels and alters testicular and epididymal

sperm numbers, motility, viability, morphology, and daily sperm production (Kniewald et al., 2000; Stoker et al., 2000; Trentacoste et al., 2001; Abarikwu et al., 2010; Victor-Costa et al., 2010). In line with these rodent studies, epidemiological studies suggest that environmental ATR exposure is associated with menstrual cycle length irregularity (Cragin et al., 2011) and poor semen quality (Swan et al., 2003; Swan, 2006).

In terms of immune toxicity, repeated (14 days) ATR (250-500 mg/kg) oral exposure reduces host resistance to B16F10 melanoma and alters cell-mediated immune function in female mice (Karrow et al., 2005). Acute ATR (100-300 mg/kg) intraperitoneal injection disrupts cell-mediated and humoral immune functions by decreasing the percentage of $CD4^{+}CD8^{+}$ cells in the thymus, the number of nucleated cells in the spleen, the expression of MHC class II molecules on splenocytes, splenic natural killer cell activity, and the lgG1 and lgG2a responses to keyhole limpet hemocyanin (Pruett et al., 2003).

Effects on the nervous system

In the nervous system, ATR disrupts hypothalamic control of HPG axis by inhibiting pulsatile gonadotropin-releasing hormone (GnRH) release without altering GnRH RNA or protein levels, or pituitary sensitivity to a GnRH receptor agonist in rats (Foradori et al., 2009b; Foradori et al., 2013). ATR also targets DA circuitries, especially the nigrostriatal system. For example, ATR alters DA homeostasis in catecholaminergic PC12 cells (Das et al., 2000), rat striatal slices (Filipov et al., 2007) and striatal synaptic vesicles (Hossain and Filipov, 2008). In vivo, short-term ATR (125-250 mg/kg) exposure decreases striatal DA concentration and reduces substantia nigra and ventral tegmental area (VTA) DA (tyrosine hydroxylase [TH] positive) neurons in juvenile male mice (Coban and Filipov, 2007). Behavioral analysis of ATR-treated (10 mg/kg, 1 year) rats reveals altered locomotor activity, motor coordination, and spatial

memory that are accompanied by decreased striatal DA content (Bardullas et al., 2011). Recent studies, associating pesticide-contaminated well water consumption (Gatto et al., 2009) and higher concentrations of ATR in groundwater (Shaw, 2011) with increased incidence of PD, provide a potential epidemiological correlate for the experimental data reviewed above and suggest that ATR overexposure could potentially be a risk factor or a risk modifier for PD.

While available evidence suggests that altered nigrostriatal DA function underlies ATR-induced behavioral abnormalities, little is known about ATR's effects on other neurotransmitter systems, such as serotonin (5-HT), or on other brain structures, such as prefrontal cortex and hippocampus, which receive dopaminergic projections from the VTA (Alcaro et al., 2007), a target region of ATR (Coban and Filipov, 2007). The molecular targets of ATR within the dopaminergic circuitries are also largely unknown. Moreover, the dose-dependency of ATR's effects on multiple behaviors, especially in adult mice, has not been investigated.

Atrazine toxicity: developmental effects

Non-nervous system effects

Laboratory studies suggest that developmental exposure to ATR affects birth outcomes and the development of multiple organ systems, including reproductive, immune, and nervous systems. Regarding birth outcomes, Cummings et al. (2000) found that ATR (≥50 mg/kg) exposure during early pregnancy (gestational day [GD] 1-8) increases the percent of both preimplantation loss and postimplantation loss in rats in a strain-dependent manner, with F344 and Holtzman rats being most susceptible to preimplantation and postimplantation effects, respectively. Likewise, Narotsky et al. (2001) reported that exposure to ATR (≥50 mg/kg) during early pregnancy (GD6-10) causes prenatal loss, full-litter resorption, and delayed parturition, with F344 rats being more sensitive than Sprague-Dawley and Long Evans rats. In addition, in

rats, ATR exposure (100 mg/kg) during late pregnancy (GD14-21) results in decreased birth weight and increased postnatal mortality (Davis et al., 2011; Fraites et al., 2011).

In agreement with these laboratory studies, several epidemiological studies have reported that ATR exposure during pregnancy is associated with various adverse birth outcomes, such as fetal growth restriction, small-for-gestational-age, preterm birth, and birth defects (Munger et al., 1997; Villanueva et al., 2005; Ochoa-Acuña et al., 2009; Chevrier et al., 2011; Rinsky et al., 2012). For instance, Villanueva et al. (2005) found that the risk of small-for-gestational-age is increased with the number of months of the third trimester of pregnancy occurring from May to September, months with the highest ATR levels in drinking water based on data from 1990 to 1998 in a general population cohort from northwest France. In the state of Indiana (US), ATR in the drinking water (>0.1 μg/L) during the third trimester or during the entire pregnancy is associated with a significant increase in the prevalence of small-for-gestational-age from 1993 to 2007 (Ochoa-Acuña et al., 2009). In addition, quantifiable levels of ATR (≥0.05 μg/L) or a specific ATR metabolite (e.g., atrazine mercapturate: ≥0.02 μg/L) in the first-morning-void urine samples collected during early pregnancy (4-19 weeks) are associated with increased incidence of fetal growth restriction and small head circumference for sex and gestational age (Chevrier et al., 2011).

In the reproductive system, developmental exposure (gestational, lactational, or combined) to ATR (100 mg/kg) delays vaginal opening, increases vaginal opening body weight (lactational and combined groups), and delays mammary gland development (all groups) in female Long-Evans rats (Rayner et al., 2004). In male rats, peripubertal ATR exposure (100-200 mg/kg; PND22-47) affects reproductive tract development, as evidenced by decreased seminal vesicle and ventral prostate weights, as well as reduced serum and intratesticular testosterone

concentrations (Trentacoste et al., 2001). Developmental ATR exposure in zebrafish (0.3-30 μg/L; from 1 to 72 h post fertilization) also results in altered expression of multiple genes involving neuroendocrine and reproductive system development and function, such as *CYP17A1*, a gene with important role in the steroid hormone biosynthesis (Weber et al., 2013).

In the immune system, ATR (35 mg/kg) exposure during gestation and lactation (GD10–PND23) decreases primary antibody and delayed-type hypersensitivity responses in male offspring, but not in female rat offspring (Rooney et al., 2003). Perinatal ATR exposure via a subcutaneously implanted time-release pellet (approximately 0.7 mg/kg) from GD11 to PND11±1 results in a significant immunopotentiation at 3 months that is not apparent at 6 months in male offspring, as well as a significant depression of the immune function at 6 months, but not at 3 months, in female offspring (Rowe et al., 2006; Rowe et al., 2008). These results suggest that the effects of ATR on the immune system development are sex-specific, dose- and time-dependent (Rooney et al., 2003; Rowe et al., 2006; Rowe et al., 2008). Besides in utero and lactational periods, the period from PND30 to sexual maturity has also been shown as a window of vulnerability to ATR for the developing immune system (Filipov et al., 2005). Specifically, 14-day exposure of one-month-old male C57BL/6 mice to ATR (5-250 mg/kg) decreases immune organ cellularity, weights, and lymphocyte distribution of spleen and thymus, with certain effects persisting long (i.e., 7 weeks) after exposure has been terminated (Filipov et al., 2005).

Developmental neurotoxicity of atrazine: in vivo

ATR has been suggested as a potential developmental neurotoxicant based on two reports. In the first study (Giusi et al., 2006), ATR exposure caused extensive neurodegenerative alterations in cortical, striatal, hippocampal and hypothalamic areas of adult offspring delivered

from mouse dams exposed (oral gavage) to environmentally relevant low dose (0.1 mg/kg/day) of ATR from GD14 to PND21. In the other study, same exposure paradigm was used and ATR's effects on offspring's behavior were evaluated (Belloni et al., 2011). This study found that ATR exposure results in changes in exploratory profile (i.e., hyperactivity; 0.001 or 0.1 mg/kg/day) and in affiliative/investigative behavior (0.001 or 0.1 mg/kg/day) in juvenile offspring, as well as altered learning performance (i.e., delayed step-through response in the passive avoidance test; 0.1 mg/kg/day) in adult offspring. Of note, the LOAEL of ATR (0.001 mg/kg) associated with developmental neurotoxicity is much lower than the effective doses that cause developmental toxicity on other organ systems (i.e., reproductive or immune organs, typically ≥0.7 mg/kg; Rowe et al., 2006) or neurotoxicity in adult animals (≥10 mg/kg; Coban and Filipov, 2007; Bardullas et al., 2011), indicating that developing nervous system is particularly sensitive to ATR. However, the behavioral effects of developmental ATR exposure via drinking water, the most common route of human exposure to ATR (ATSDR, 2003; Mosquin et al., 2012), have not been examined. The neurochemical substrates associated with the behavioral effects of developmental ATR exposure have also not been investigated. In particular, while early pregnancy (e.g., GD6-13 in mice), when dopaminergic neurons are still undifferentiated/proliferating (e.g., GD6-10.5 in mice) or at the beginning of differentiation (e.g., GD10.5-13), is a known vulnerable period of the brain development to toxic insults (Rice and Barone, 2000; Prakash and Wurst, 2006), developmental neurotoxicity studies for ATR that include exposure during this period have not been reported, which is a critical data gap.

Developmental toxicity and neurotoxicity of atrazine: in vitro

Effects of in vitro exposure to ATR on the differentiation and maturation of several cell types have been examined, including blood, immune and neuronal cells. Magnelli et al. (1989)

investigated the effects of ATR (15 μg/ml; 70 μM) on erythroid differentiation and found that ATR inhibits hexamethylene-bis-acetamide-induced differentiation of undifferentiated mouse erythroleukaemic cells by around 10%. Pinchuk et al. (2007) demonstrated that ATR exposure disrupts the phenotypic and functional maturation of JAWSII mouse bone marrow-derived dendritic cells at non-cytotoxic concentrations (1 μM; cytotoxicity was observed at ≥200 μM ATR). With respect to neuronal differentiation, Solari et al. (2010) reported that ATR at relatively lower concentrations (≤9.3 μM) does not alter the expression of retinoic acid-induced differentiation markers (stage-specific embryonic antigen-1 [embryonic marker] and βIII-tubulin [neuronal marker]) in mouse P19 embryonic stem cells. The effects of in vitro exposure to ATR or its metabolites on the differentiation of dopaminergic neurons have not been investigated.

Pharmacokinetics of atrazine

Absorption

Human exposure to ATR is primarily via oral, dermal, and inhalation routes. Upon oral exposure, ATR is rapidly and extensively absorbed through gastrointestinal (GI) tract, with an absorption half-life of 2.6 h in rats exposed to a single dose of 30 mg/kg ^{14}C-atrazine (^{14}C-ATR; Timchalk et al., 1990). In rats, approximately 80-82% of the given dose is absorbed within 72 h after a single dose of ^{14}C-ATR (1.5 or 30 mg/kg; Bakke et al., 1972; Timchalk et al., 1990). Similarly, in monkeys, 65-79% of radioactivity is absorbed within 7 days after a single oral dose of ^{14}C-ATR (1, 10, and 100 mg/monkey; Hui et al., 2011). The average oral bioavailability in monkeys is 62-73% (Hui et al., 2011).

In studies where the actual ATR and its metabolites were measured, additional important kinetic data were obtained. For example, in rats, plasma ATR concentrations peak quickly (i.e., within 0.5 h) and then fall; a second minor peak occurs at 2 h, followed by a rapid decline and

subsequent plateau up to 48 h following single oral gavage (100 or 150 mg/kg; Brzezicki et al., 2003; McMullin et al., 2007b). In mice, similar biphasic plasma concentration curve was observed, with the first and second peaks detected at 1 and 12 h after dosing, respectively (Ross and Filipov, 2006; Ross et al., 2009). These data indicates that uptake of ATR in mice and rats is similar.

The absorption efficiency of ATR following dermal exposure is far less efficient than its oral absorption. For example, the fractional skin (mid-dorsal skin) penetration of ^{14}C-ATR (53.9-577.9 μg/cm^2) is 3.2-9.6% and 2.8-7.7% in young and adult rats, respectively, and the absorption percentage decreases with increasing ^{14}C-ATR dose (Hall et al., 1988). Likewise, in humans exposed to ^{14}C-ATR via forearm dermal patches for 24 h, only 0.3-5.1% of the applied dose was absorbed over a 7-day monitoring period (Buchholz et al., 1999). These results are consistent with an in vitro study using human skin samples exposed to ^{14}C-ATR, which found that: (1) approximately 16.4% of applied ^{14}C-ATR was absorbed in a 24-h period, (2) most of the absorbed radioactivity (15% of the applied dose) remained in the skin, and (3) less than 5% penetrated through the skin and reached the receptor fluid (Ademola et al., 1993). While dermal absorption of ATR in humans is not as substantial as oral, significant amounts of ATR and its metabolites have been detected in the urine of workers exposed to ATR primarily via dermal contact (Catenacci et al., 1993). Hence, dermal occupational exposure to ATR should not be de-emphasized.

Published data regarding absorption of ATR in humans or laboratory rodents exposed to ATR via inhalation are not available.

Distribution

Upon exposure, ATR and its metabolites are well distributed throughout the body. Earlier studies showed that ^{14}C-ATR was detected in the plasma, liver, brain, heart, lung, kidney, digestive tract, omental fat, leg muscle, and whole skin of rats exposed to 1.5 or 30 mg/kg ^{14}C-ATR (Bakke et al., 1972; Timchalk et al., 1990). Using modern analytical technologies, both ATR and its individual metabolites are detected in multiple organs. In mice exposed to ATR (5, 25, 125 or 250 mg/kg) via a single oral gavage, ATR and its metabolites desethylatrazine (DE), desisopropylatrazine (DIP), and didealkylatrazine (DACT) were all detected in the liver (Ross et al., 2009), with DACT being the most predominant metabolite. In the kidney, brain, spleen and thymus, the levels of ATR and DACT were generally lower than those in liver, and the levels of DE and DIP were exceedingly low (close to limits of quantification; Ross et al., 2009).

Similar to adult rodents, in rat dams orally exposed to ATR (5 or 25 mg/kg) during gestation (GD18–20 or GD14–20), DACT was the predominant metabolite, accounting for ~86% and 55-92% of total chlorotriazines in the maternal plasma and tissues, respectively (Fraites et al., 2011). ATR was detectable in both plasma and tissues, but its levels were substantially lower than DE, DIP, or DACT. Interestingly, higher levels of ATR were detected in the adrenal and mammary tissues (5- to 12-fold of plasma ATR levels), indicating a potential of ATR accumulation in these two tissues during late gestation (Fraites et al., 2011). In the fetus, DACT was also the main metabolite, accounting for 60-90% of the total chlorotriazines (Fraites et al., 2011). Overall, the levels of ATR, DE, DIP and DACT in the fetus were similar to those in the maternal plasma, indicating that all of them can cross the blood-placenta barrier efficiently. However, the concentrations of ATR and its metabolites in individual fetal tissues or in the placenta have not been reported.

Upon perinatal exposure (GD14–PND10), the concentrations and distribution of ATR and its metabolites in the maternal plasma and tissues were similar to those observed in the dams exposed to ATR during gestation (Fraites et al., 2011). In the milk obtained from neonatal stomach (Fraites et al., 2011), the levels of ATR, DE, DIP, and DACT were approximately 0.5-fold of their respective levels in maternal plasma. In the milk, neonatal plasma and brain, DACT accounted for 91-93%, 99% and 92-96% of total chlorotriazines, respectively (Fraites et al., 2011). ATR was found at relatively higher concentrations in the neonatal brain (2-5% of total chlorotriazines) compared to other neonatal tissues or fluids. Only DACT was detected in the neonatal gonads (ovary or testes). However, the concentrations of ATR and its metabolites in maternal/neonatal plasma/tissues and fetuses are available only at a single time point, i.e., 2 h after the lasting dosing in Fraites et al. (2011), thus, their time-course kinetic behaviors during pregnancy and lactation have not been reported. In addition, while ATR pharmacokinetic data are available in the pregnant and lactating rat (Fraites et al., 2011), there are no such data in the mouse, which are important for species comparison and extrapolation.

Consistent with the findings in animal studies (Fraites et al., 2011), ATR was detected in human umbilical cord plasma samples (1-12 pg/g; 20% positive of 211 samples) from residentially exposed, low risk urban population in New York (Whyatt et al., 2003), and in breast milk samples (0.3-1.3 μg/L; 30% positive of 10 samples) from a general population cohort in eastern France (Balduini et al., 2003). These results indicate that in utero and lactational exposures may be important routes for ATR and its metabolites to reach the developing fetus and the neonate, respectively. Because developing organisms, especially the developing nervous system, are vulnerable to ATR (Giusi et al., 2006; Belloni et al., 2011), ATR exposure during pregnancy and lactation may be of particular concern.

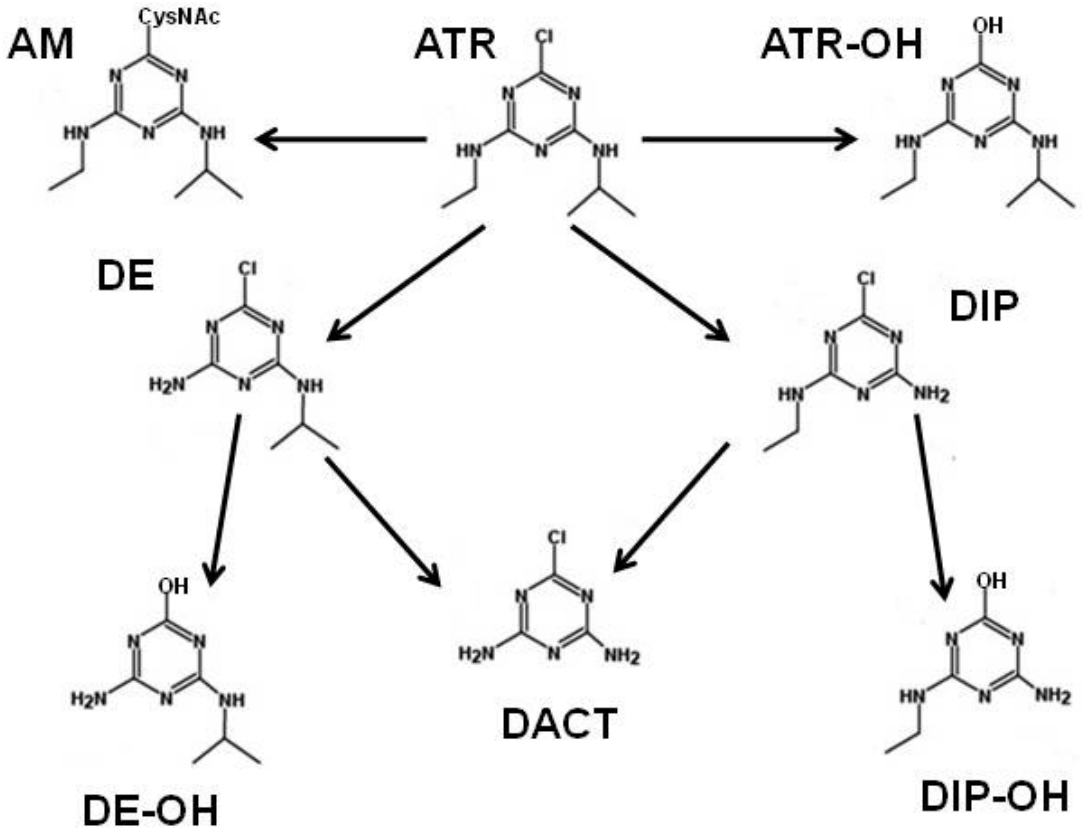

Figure 2.2. Metabolism of ATR in mammals. Abbreviations: ATR, atrazine; ATR-OH, hydroxyatrazine; AM, atrazine mercapturate; DACT, diaminochlorotriazine; DE, desethylatrazine; DE-OH, hydroxydesethylatrazine; DIP, desisopropylatrazine; DIP-OH, hydroxydesisopropylatrazine. DE, DIP, and DACT are ATR's major metabolites, accounting for more than 90% of total ATR-related metabolites in rodents and humans. AM and ATR-OH are detected at low levels in ATR-treated rodents. AM, ATR-OH, DE-OH and DIP-OH are detected in ATR-exposed humans. Adapted and modified from Barr et al. (2007), Ross et al. (2009) and Fraites et al. (2011).

Metabolism

In the body, ATR is rapidly and extensively metabolized primarily by hepatic cytochrome P450 enzymes (e.g., CYP1A1/2, CYP2B1/2, CYP2D1, and CYP2E1; Hanioka et al., 1998a; Hanioka et al., 1999a) to yield chlorinated mono-dealkylated metabolites, DE and DIP (Fig. 2.2). Subsequent metabolism of DE and DIP by P450s produces DACT, which is the major in vivo ATR metabolite in rats (Brzezicki et al., 2003; McMullin et al., 2007b; Fraites et al., 2009; Fraites et al., 2011), mice (Ross and Filipov, 2006; Ross et al., 2009), and, apparently, humans (Catenacci et al., 2002; Barr et al., 2007). In mammals, P450s can be found in virtually all organs, but mainly in the liver (300 pmol of total P450s/mg microsomal protein; Martignoni et al., 2006). Among the major ATR-metabolizing P450 isoforms, CYP1A1, CYP1A2, and CYP2E1 show strong conservation among species, with an identity to human 80% for rats and mice, and 95% for monkeys (Martignoni et al., 2006). CYP2B is detected in the liver of all species, highly expressed in the intestine of rat and mouse, but undetectable in the human intestine. CYP2D has been identified in the liver of humans and other mammalian species. However, CYP2D family shows genetic polymorphism resulting in intraspecies and interspecies variation in terms of catalytic activity (Martignoni et al., 2006). CYP1A1, CYP1A2, CYP2B, and CYP2E1 are all inducible in humans, rats, and mice, but induction of CYP2D has not been reported as of yet.

In line with the greater similarities and lesser differences in terms of the expression and activity of main ATR-metabolizing P450s, the overall pathways for metabolism of ATR are consistent qualitatively across mammalian species, but quantitative differences (mainly the amounts of the intermediate metabolites: DE and DIP) exist due to variations between species in the kinetics of individual steps. For example, in ATR-exposed rats, plasma levels of DIP are

generally 3- to 9-fold higher than DE (McMullin et al., 2007b; Fraites et al., 2009; Fraites et al., 2011), whereas in ATR-treated mice, plasma DIP levels are only 1.2- to 1.5-fold larger than DE (Ross et al., 2009). This is not unexpected as the maximum in vitro metabolic rate of ATR to DIP is approximately 11- and 3-fold higher than that of ATR to DE in rats and mice, respectively (Hanioka et al., 1999b).

To a much lesser extent, ATR also undergoes phase II metabolism by glutathione transferases to generate atrazine mercapturate (AM; Fig. 2.2). For example, AM was also found in the plasma and urine of ATR-exposed mice, but its levels were far lower than other metabolites, e.g. 1000-fold less than DACT (Ross et al., 2009). Hydroxylation of ATR and its chlorinated metabolites (DE and DIP) is another minor pathway of ATR metabolism in mammals (Fig. 2.2). For instance, ATR-OH was detected, at much lower levels compared with other metabolites, in maternal plasma and tissues, fetuses, milk, and neonatal tissues following repeated daily exposure to rat dams (Fraites et al., 2011). In occupational population, ATR-OH, DE-OH, and DIP-OH (abbreviations defined in Fig. 2.2) were also detected in the urine as minor metabolites (Barr et al., 2007).

Available in vitro and in vivo evidence suggests that the metabolism of ATR is auto-inducing. For example, short-term ATR exposure induces the expression and activity of total P450s in zebrafish (Dong et al., 2009). In mammals, specific major ATR-metabolizing P450 isoforms such as rat CYP1A1, CYP1A2, CYP2B, and CYP2B1 (Hanioka et al., 1998b; Islam et al., 2002; Pogrmic-Majkic et al., 2012), and human CYP1A2, CYP2A6, CYP2B6, and CYP3A4 (Abass et al., 2012), are all induced by ATR exposure. Increased expressions of these enzymes (e.g., CYP1A1/2 and CYP2B1/2), in turn, increase the metabolism of ATR to DE and DIP in rats (Hanioka et al., 1999a). Due to ATR's autoinduction metabolism, in rats, relatively longer

exposures (7-day: GD14-20; or 19-day: GD14-PND10) to ATR (25 mg/kg) produce lower concentrations of ATR, DE, and DIP in maternal/neonatal plasma/tissues and/or fetuses compared to shorter exposure (3-day: GD18-20; Fraites et al., 2011).

Elimination

Urine is the primary elimination route for ATR regardless of exposure routes (Timchalk et al., 1990; Catenacci et al., 1993; Buchholz et al., 1999; Barr et al., 2007; Ross et al., 2009). For example, earlier studies using ^{14}C-ATR (1.5 or 30 mg/kg) showed that 65.5-67% and 18-20% of radioactivity was recovered in the urine and feces, respectively, in rats 72 h after dosing, with 85-95% of that excreted in the urine appearing during the first 24 h after dosing (Bakke et al., 1972; Timchalk et al., 1990). The elimination half-life of total radioactivity was calculated as 10.8-11.2 h using one-compartment pharmacokinetic model (Timchalk et al., 1990). Similarly, in humans, 50% of the ATR-related compounds were excreted via the urine in the first 8 h following an 8-h occupational exposure in an ATR production plant (Catenacci et al., 1993). These data indicate that the elimination of ATR and its metabolites is rapid and primarily urinary. A recent study showed that, although ATR was detected in fecal extracts, none of the metabolites was detected at significant amounts in limited analysis of fecal extracts from ATR-exposed mice (Ross et al., 2009). These data indicate that measured fecal radioactivity in earlier studies (Bakke et al., 1972; Timchalk et al., 1990) might be a result of unabsorbed ATR that had traversed the GI tract.

Milk secretion is another important elimination route for ATR and its metabolites. Following a single oral gavage to the lactating dam (2 or 4 mg ^{14}C-ATR/rat dam) on PND3, approximately 0.007% of radioactivity was distributed to the neonatal stomach contents (surrogate for milk) after a 30-min nursing period (2.5-3 h after dosing; Stoker and Cooper,

2007). Following gestational and lactational exposure (GD14–PND10) to the dam (5 or 25 mg/kg), significant concentrations of ATR, DE, DIP, and DACT were detected in the milk; their levels were generally half of ATR/metabolites respective maternal plasma levels (Fraites et al., 2011).

Salivary excretion is another elimination route for ATR, but it is a minor one. For example, Lu et al. (1997) found that there was a high correlation between saliva and plasma ATR concentrations in rats after a single oral dosing (105 mg/kg), which was independent of variations in salivary flow rates. Although of limited importance for ATR's kinetic behavior, this elimination pathway is important for exposure assessment as salivary ATR levels might be used for biomonitoring (Denovan et al., 2000; Hines et al., 2006).

Physiologically based pharmacokinetic models of atrazine

Physiologically based pharmacokinetic (PBPK) modeling is a process that uses mathematical equations and computer programming to describe the absorption, distribution, metabolism, and elimination of chemicals in an organism. PBPK models play an important role in the risk assessment processes (WHO, 2010). By incorporating mode of action evidence of chemicals' toxicity and relevant in vitro and in vivo experimental data, the major advantage of PBPK models' use is to conduct valuable extrapolations across species, routes and doses. Increasing number of PBPK models in rodents have been developed for various toxicants, including pesticides (Mirfazaelian et al., 2006; Timchalk et al., 2007; Timchalk and Poet, 2008; Lu et al., 2010; Tornero-Velez et al., 2010; Crowell et al., 2011). Some of these models (Lu et al., 2010; Crowell et al., 2011) have been extrapolated to humans to estimate internal/external exposures and to calculate human equivalent doses based on points of

departures (LOAEL and NOAEL) observed in rodent studies, which is important for improved regulatory decision making process.

At present, there are three PBPK models for ATR in adult rats (Timchalk et al., 1990; McMullin et al., 2003; McMullin et al., 2007b), but none in adult mice or humans. There are also no PBPK models for ATR during the fetal, neonatal, pregnant, or lactating periods in any animal species. The first ATR PBPK model (Timchalk et al., 1990) is a one-compartment model that described the time-course of radioactivity in the plasma of male rats exposed to single dose of ^{14}C-ATR (30 mg/kg). As an initial step, this model provided helpful information, such as absorption and elimination rate constants. Based on this simple model, McMullin et al. (2003) constructed a four-compartment (i.e., blood, liver, brain, and rest of body) PBPK model in male rats exposed to single or multiple doses of ^{14}C-ATR (1-100 mg/kg). This model simulated the time-course of two pools of compounds: (1) ATR and its chlorinated metabolites in the plasma, red blood cells (RBC) and urine; (2) glutathione conjugates (e.g., AM) in the plasma and urine. This second model can be used to predict plasma, RBC, and urine chlorotriazine dosimetry. However, the common drawbacks of these earlier models are: (1) an inability to separate parent compound from individual metabolites, (2) a lack of simulations of target tissue dosimetry, and (3) a deficiency of description of saturable oxidative metabolism of ATR and its metabolites.

To address the shortcomings of earlier models, McMullin et al. (2007b) developed a set of PBPK models that described the plasma time-course of ATR and its individual metabolites in female rat orally exposed to single dose of ATR or each metabolite at one molar equivalent dose (i.e., 150 mg/kg ATR). Each model consisted of blood, liver, and lumped body compartments. Each individual model was linked together into a final composite model to describe the time-courses of ATR and its major metabolites. Major advances of this model include (1)

mathematical description of ATR metabolic pathways using Michaelis-Menten equations and (2) simulations of plasma time-courses of ATR and its individual metabolites. However, in part due to the lack of experimental data, this model did not include the target organ-brain compartment; neither did it consider dose-dependency. Thus, more comprehensive PBPK models for ATR in adult rodents are needed. Moreover, to help improve ATR's risk assessment in the vulnerable subpopulations (fetuses and neonates; Giusi et al., 2006; Belloni et al., 2011), it is urgently needed to develop ATR PBPK models during fetal, neonatal, gestational, and lactation stages.

CHAPTER 3

SHORT-TERM ATRAZINE EXPOSURE CAUSES BEHAVIORAL DEFICITS AND DISRUPTS MONOAMINERGIC SYSTEMS IN MALE C57BL/6 MICE[1]

[1] Lin, Z., Dodd, C.A., Filipov, N.M. 2013. Neurotoxicology and Teratology. 39C:26-35.

Reprinted here with permission of the publisher.

Abstract

Excessive exposure to the widely used herbicide atrazine (ATR) affects several organ systems, including the brain, where neurochemical alterations reflective of dopamine (DA) circuitry perturbation have been reported. The present study aimed to investigate effects of short-term oral exposure to a dose-range (0, 5, 25, 125, or 250 mg/kg) of ATR on behavioral, neurochemical, and molecular indices of toxicity in adult male C57BL/6 mice. The experimental paradigm included open field, pole and grip tests (day 4), novel object recognition (NOR) and forced swim tests (FST; day 9), followed by tissue collection 4 h post dosing on day 10. After 4 days of exposure, ATR decreased locomotor activity (≥125 mg/kg). On day 9, ATR-exposed mice exhibited dose-dependent decreased performance in the NOR test (≥25 mg/kg) and spent more time swimming and less time immobile during the FST (≥125 mg/kg). Neurochemically, short-term ATR exposure increased striatal DA and DA turnover (its metabolite homovanillic acid [HVA] and the HVA/DA ratio; ≥125 mg/kg). In addition, ATR exposure increased the levels of the serotonin metabolite 5-hydroxyindoleacetic acid (5-HIAA) in the striatum (≥125 mg/kg) and it also increased DA turnover (≥125 mg/kg), 5-HIAA (125 mg/kg), and norepinephrine (≥125 mg/kg) levels in the prefrontal cortex. In the hippocampus, the only effect of ATR was to increase the norepinephrine metabolite 3-methoxy-4-hydroxyphenylglycol (MHPG; 250 mg/kg). At the molecular level, the expression of key striatal (protein) or nigral (mRNA) markers associated with nigrostriatal DA function, such as tyrosine hydroxylase, DA transporter, vesicular monoamine transporter 2, and DA receptors, was not affected by ATR. These results indicate that short-term ATR exposure targets multiple monoamine pathways at the neurochemical level, including in the striatum, and induces behavioral abnormalities suggestive of impaired motor and cognitive functions and increased anxiety. Impaired performance in the

NOR behavioral test, seen in the absence of neurochemical alterations, was the most sensitive endpoint affected by ATR; this should be taken into consideration for future low-dose ATR studies and for the assessment of risk associated with overexposure to this herbicide.

Keywords: Atrazine, Pesticides, Novel object recognition test, Forced swim test, Dopamine

Introduction

Atrazine [ATR; 2-chloro-4-(ethylamino)-6-(isopropylamino)-s-triazine, CAS# 1912-24-9] is a widely used chlorotriazine herbicide (LeBaron et al., 2008). ATR and/or its metabolites are frequently detected in the soil, ground, surface, and drinking water (Battaglin et al., 2009; Krutz et al., 2010; Mosquin et al., 2012), in farm households (Lozier et al., 2012), and in urine samples from pesticide applicators and the general population (Curwin et al., 2007). ATR's wide use and frequent detection raise concerns about potential adverse health effects due to overexposure.

In laboratory studies, excessive exposure to ATR is detrimental to several organ systems, including the immune (Filipov et al., 2005), reproductive (Cooper et al., 2007), and nervous systems. In the brain, ATR disrupts hypothalamic control of the hypothalamic–pituitary–gonadal axis by affecting luteinizing hormone release characteristics (Foradori et al., 2009a), apparently, indirectly (Cooper et al., 2007; Foradori et al., 2013). ATR also targets dopamine (DA) circuitries, including the nigrostriatal system. For example, ATR disrupts DA homeostasis in catecholaminergic PC12 cells (Das et al., 2000), rat striatal slices (Filipov et al., 2007) and striatal synaptic vesicles (Hossain and Filipov, 2008). ATR also disrupts the morphological differentiation of N27 dopaminergic cells (Lin et al., 2013a). In vivo, short-term ATR exposure decreases striatal DA concentration and reduces nigral and ventral tegmental area (VTA) DA [tyrosine hydroxylase (TH) positive] neurons in juvenile male mice (Coban and Filipov, 2007).

In orally exposed mice (5-250 mg/kg; Ross et al., 2009) or rats (5-25 mg/kg; Fraites et al., 2011), both ATR and its main metabolite didealkylatrazine (DACT) enter the brain readily where they are detected at levels similar to their plasma levels. Hence, the fact that ATR affects the brain, including the nigrostriatal system, is not surprising. Recent reports associating pesticide-contaminated well water consumption (Gatto et al., 2009) and higher concentration of ATR in groundwater (Shaw, 2011) with increased incidence of Parkinson's disease (PD) provide a potential epidemiological correlate for the experimental data reviewed above and suggest that ATR overexposure could potentially be a risk factor or a risk modifier for PD.

While effects of ATR on DA in the striatum (striatal tissues) and catecholamine-producing cells are reported in several studies (Das et al., 2000; Filipov et al., 2007), little is known about its effects on other monoamines, such as serotonin (5-HT). It is also unknown whether ATR affects other brain structures, such as prefrontal cortex and hippocampus, which receive dopaminergic projections from the VTA (Alcaro et al., 2007). In addition, little is known about the molecular targets of ATR within the dopaminergic circuitries. For example, ATR disrupts DA homeostasis in the striatum and in PC12 cells neurochemically, but it does not affect the protein expression of TH, the rate-limiting enzyme in the synthesis of DA (Das et al., 2003; Coban and Filipov, 2007). Moreover, effects of ATR in an oral exposure paradigm on the protein and/or mRNA levels of other important dopaminergic markers, such as dopamine receptors D1 (Drd1), D2 (Drd2), and D4 (Drd4), dopamine transporter (DAT), vesicular monoamine transporter 2 (VMAT-2), α-synuclein, or nuclear receptor related 1 (Nurr1; Lotharius and Brundin, 2002; Smidt et al., 2003), are largely unknown. Behaviorally, chronic dietary exposure of rats to ATR impairs motor coordination, disrupts spontaneous

locomotor activity, and alters spatial memory (Bardullas et al., 2011). However, the dose-dependency of ATR's effects on different behaviors in adult rodents has not been investigated.

Compared to long-term studies, short-term studies cost less, take less time, and have been a widely used approach to explore toxic potentials, early effects, and mechanism(s) of action of toxicants (Middlemore-Risher et al., 2010; Speed et al., 2012). In the case of ATR, short-term ($\leq$ 21 days) ATR exposure (ranging from 5 to 500 mg/kg) impairs reproductive (Cooper et al., 1996; Cooper et al., 2000; Foradori et al., 2009a; Foradori et al., 2009b; Fraites et al., 2009) and immune functions (Filipov et al., 2005; Karrow et al., 2005). In line with these short-term studies and taking into account the absence of behavioral or neurochemical data associated with short-term ATR exposure in adult mice, the specific objectives of the present study were: (1) to evaluate the behavioral and neurochemical effects of short-term oral exposure to a dose range (5–250 mg/kg) of ATR in mice and (2) to investigate potential molecular mechanism(s) involved in the effects of ATR on the brain nigrostriatal system. For behavioral analyses, we used the following tests: open field, pole test, grip strength, novel object recognition (NOR), and forced swim tests (FST). These tests are commonly used to evaluate motor, object recognition memory and depressive-like behaviors that are dependent, at least in part, on the normal function of brain regions receiving rich monoaminergic innervation, including the striatum, prefrontal cortex, and hippocampus (Petit-Demouliere et al., 2005; Alcaro et al., 2007; Taylor et al., 2010; Antunes and Biala, 2012). These regions and another potential target region, the hypothalamus (Cooper et al., 2007), were selected for the analysis of monoamine levels. To identify potential molecular mechanism(s) involved in ATR's effects on the nigrostriatal pathway, we determined the expression levels of several key protein (striatum) and/or mRNA (substantia nigra) dopaminergic markers including TH, DAT, VMAT-2, Drd1, Drd2, Drd4, and Nurr1.

Materials and methods

Animals and chemicals

Adult male C57BL/6 mice (2–3 months old, 22.4 ± 0.22 g, Taconic, Hudson, NY) were housed (5 mice/cage) with water and food available ad libitum under constant temperature (22 °C) on a 12-h light/dark cycle in an AAALAC accredited facility throughout the study. Animals were allowed to acclimate at least one week before experimentation. All animal procedures were in accord with the Animal Welfare Act and the Guide for the Care and Use of Laboratory Animals (NIH, 2011) and were approved in advance by the Institutional Animal Care and Use Committee (IACUC) of the University of Georgia.

Atrazine (Lot #: 421-55A, 98.9% purity) was purchased from Chem Service (West Chester, PA) and was dissolved in corn oil (Sigma; St. Louis, MO). Monoamine HPLC standards for DA, 3,4-dihydroxyphenylacetic acid (DOPAC), homovanillic acid (HVA), 3-methoxytyramine (3-MT), 5-HT, 5-hydroxyindoleacetic acid (5-HIAA), norepinephrine (NE), and 3-methoxy-4-hydroxyphenylglycol (MHPG) were obtained from Sigma. All chemicals (i.e., $NaH_2PO_4H_2O$, octyl sodium sulfate, EDTA disodium salt, triethylamine, and methanol) for the mobile phase used for HPLC analysis (described below) were purchased from Thermo Fisher (Fair Lawn, NJ). Rabbit anti-TH antibody was from Millipore (Billerica, MA). Rabbit anti-DAT, anti-VMAT-2, anti-Drd2, anti-α-synuclein, and anti-β-actin antibodies were from Santa Cruz Biotechnology Inc. (Santa Cruz, CA). Goat anti-rabbit secondary antibody coupled to horseradish peroxidase (HRP) and Bradford reagent for total protein determination were purchased from Bio-Rad (Hercules, CA). Super Signal West Pico Chemiluminescent substrate and Gentle ReView™ buffer were from Pierce (Rockford, IL) and Amresco (Solon, OH), respectively. qScript cDNA SuperMix kit was from Quanta Biosciences (Gaithersburg, MD).

RT^2 Real-Time™ SYBR Green/Rox PCR master mix and certified mouse-specific PCR primers for dopamine receptor D1a (Drd1a), dopamine receptor D2 (Drd2), dopamine receptor D4 (Drd4), tyrosine hydroxylase (TH), vesicular monoamine transporter 2 (VMAT-2), dopamine transporter (DAT), α-synuclein, nuclear receptor related 1 (Nurr1), and GAPDH were from Qiagen (Valencia, CA). All other chemicals, unless specified, were obtained from Sigma.

Treatment and tissue collection

The experimental design and the timeline for the present study are depicted in Fig. 3.1. In brief, animals were assigned randomly into 5 treatment groups (n = 5/group) and treated daily with corn oil vehicle or a dose range of ATR (5, 25, 125, or 250 mg/kg) by oral gavage for 10 days at a volume of 5 mL/kg. These doses were selected based on previous short-term ATR exposure studies focusing on its effects on the reproductive, endocrine, immune, or brain functions; the rationale for this dose regimen selection is described in detail in these studies (Cooper et al., 1996; Cooper et al., 2000; Filipov et al., 2005; Karrow et al., 2005; Coban and Filipov, 2007; Foradori et al., 2009a; Foradori et al., 2009b; Fraites et al., 2009). All dosing was performed mid-morning and animals were weighted daily prior to treatment. On behavioral test day (days 4 and 9) and sacrifice day (day 10), the dosing was staggered (with treatment randomized in a counter-balanced design) such that behavioral tests or tissue collection were conducted 4 h after dosing. This time point was selected based on our earlier pharmacokinetic studies (Ross and Filipov, 2006; Ross et al., 2009) to allow plasma and tissue, i.e., brain, levels of ATR and its main metabolite DACT to reach maximal concentrations.

Four hours after the last dosing on day 10, animals were euthanized (CO_2; followed by decapitation) and the brain tissues were collected and processed similar to Coban and Filipov (2007). Briefly, the whole brain was immediately extracted, washed in ice-cold HEPES-buffered

Hank's saline solution (pH 7.4) and split sagittally into two hemispheres; one-half of the brain was frozen on dry ice and stored at − 80 °C, while the other half was fixed in 4% paraformaldehyde. In addition, spleens, livers and thymuses were collected and weighted.

Behavioral analysis

Behavioral tests were performed on days 4 and 9, 4 h after dosing. Specifically, on day 4, mice were subjected sequentially to open field, pole, and grip strength tests (~10 min between tests). On day 9, novel object recognition (NOR) and forced swim tests (FST) were performed. For the NOR, mice were habituated to the open field arena for 30 min on day 8 and the test was conducted beginning 4 h after dosing on day 9. The FST was conducted 1.5 h after completion of the NOR. All five treatment groups underwent behavioral testing on day 4; only control, 25, 125, and 250 mg/kg groups were subjected to the NOR and FST behavioral tests on day 9 in order to complete these tests within the allotted testing window. Animals were naïve to the testing ambience prior to testing initiation and all tests were performed in a specially equipped behavioral testing room separate from the one where the mice were housed.

Open field

Each mouse was individually monitored in an open field arena (l × w × h: 25 × 25 × 40 cm, divided into 16 square grids; Coulbourn Instruments, Whitehall, PA) with Limelight video tracking software (Actimetrics, Wilmette, IL) for 30 min. Parameters evaluated included: (1) total distance traveled (cm) and number of crossings, analyzed per 5 min interval (horizontal activity); (2) number of rearings during the first 5 min, counted using the Limelight software by an experimenter blinded to the treatment (vertical activity); and (3) time spent in the periphery or in the center, analyzed per 5 min interval (location parameters).

Pole test

The pole test was performed as previously described (Matsuura et al., 1997; Royl et al., 2009) with minor modifications. Briefly, mice were placed gently head-up facing the top of a vertical metal pole with a gauze-wrapped rough surface (d × h; 1 × 55 cm). Turning criterion was a full body turn with the head facing down the pole. The maximum time allowed for turning was 60 s and the maximum total time (for a complete turn plus descent) per trial was 120 s. A total of 4 trials were conducted for each mouse with a 4–5 min resting period between each trial. The average time to turn, time to descend, and total time spent on the pole from all 4 trials were used for statistical analysis (Royl et al., 2009).

Grip strength

A strength gauge (Bioseb, France) with attached mouse-specific square wire grid (6 × 6 cm) was used to measure forelimb grip strength, similar to Miller et al. (2010). Briefly, mice were carefully placed in front of the wire grid and allowed to grab hold with both fore paws. Once grip was established, the maximum grip strength was recorded (in Newtons [N]). For each animal, 4 measurements (1 min apart) were taken to obtain an average value for the maximum grip strength; this value was used for statistical analysis (Miller et al., 2010).

Novel object recognition (NOR)

The NOR was carried out according to Sik et al. (2003) and Stranahan et al. (2008) with minor modifications. On day 8, mice were habituated to the open field arenas for 30 min; 24 h later, they were placed in the arenas with two plastic cube objects, identical in size (36 cm^3), shape and color, and allowed to explore for 5 min. After a 1-h rest period in their home cages, mice were placed back into the arena for a 5-min exploration with one familiar object (one of the two identical objects) and one novel object (different shape and color, but similar in size). The

two objects were placed in two adjacent corners about 3 cm away from the wall. The order of objects and object location (novel vs. familiar) used per subject per session was randomized. To prevent the use of odor cues, the objects and the test arenas were cleaned thoroughly between sessions with 0.4% Roccal-D Plus (Pfizer Inc., New York, NY). The number of approaches towards the novel (N_n) vs. the familiar object (N_f) was counted using the Limelight video tracking software. Successful approach was defined as follows: directing the nose towards the object at a distance of no more than 2 cm and/or touching the object with the nose (Sik et al., 2003). Continuous object exploration, without shifting attention to the other object, the wall, or walking away, was counted as a single approach. In addition, the arena was divided into 9 square grids and the time the mice spent in the square with the novel (T_n) vs. the time in the square with the familiar object (T_f) was determined with the Limelight software. Novelty preference index (NPI) was calculated using the following equations: $NPI = (N_n - N_f) / (N_n + N_f)$, or $NPI = (T_n - T_f) / (T_n + T_f)$ (Sik et al., 2003).

Forced swim test (FST)

After completion of NOR, mice were placed in their home cages for a 1.5-h rest. At 6.5 h post dosing (day 9), FST was performed according to the method previously reported (Petit-Demouliere et al., 2005; Perona et al., 2008) with minor modifications. Briefly, mice were placed gently in a large cylindrical container (18 × 25 cm; d × h) filled approximately two-thirds with tap water (3 L, 29 ± 1 °C) for 15 min. Fresh water and clean container were used for every mouse. The total time spent swimming vs. immobile and the number of climbings were scored by an experimenter blinded to treatment groups with the aid of the Limelight video tracking software.

Neurochemistry for monoamines and their metabolites

Brain tissue punching and determination of monoamines and their metabolites were similar as described in our earlier study (Coban and Filipov, 2007). Micropunches from the striatum, prefrontal cortex, hippocampus (all 1.5-mm diameter), and hypothalamus (0.75-mm diameter) were collected from 500-μm thick sections, placed in centrifuge tubes containing 100 μL of 0.2 N perchloric acid, sonicated, and centrifuged (13,200 *g* at 4 °C for 10 min). An aliquot (20 μL) of the supernatant was injected into HPLC with an electrochemical detector (Waters Alliance, Waters Co., Milford, MA) for determination of: (1) DA and its metabolites DOPAC, HVA and 3-MT; (2) 5-HT and its metabolite 5-HIAA; and (3) NE and its metabolite MHPG. The analytes were separated on a C_{18}, 5-μm base-deactivated reverse-phase column (4.6 mm × 25 cm; Supelco, Sigma) using a flow rate of 1 mL/min. The mobile phase was composed of 84 mM $NaH_2PO_4H_2O$, 1.15 mM octyl sodium sulfate, 0.09 mM EDTA disodium salt, 0.25 mM triethylamine, and 17.5% methanol, with final pH of 3.65 (adjusted with 5 M phosphoric acid). The electrochemical detector (Waters 2465) was set at 0.83 V with respect to Ag/AgCI reference electrode. Data were analyzed with a chromatographic software (Empower, Waters Co.) and normalized on a per mg protein basis. Protein pellets were digested with 0.5 M NaOH and tissue protein concentrations were determined by the Bradford method using bovine serum albumin (Gemini Bio-Products, West Sacramento, CA) as a standard.

Western blot for TH, DAT, VMAT-2, Drd2, and α-synuclein

Striatal protein expression of TH, DAT, VMAT-2, Drd2 and α-synuclein was determined by western blots following the procedure we have described in detail in Coban and Filipov (2007). Briefly, 10 μg protein from each sample was loaded and separated on 10% SDS gels. Proteins were transferred onto PVDF membranes for 45 min using semi-dry transfer apparatus

(Bio-Rad). Membranes were blocked for 90 min in blocking buffer (5% milk), followed by overnight incubation at 4 °C with primary antibodies against TH (1:3000), DAT, VMAT-2, Drd2, or α-synuclein (all 1:1000). The next day, membranes were washed (4×) and incubated with a secondary antibody (goat anti-rabbit HRP, 1:10,000 to 1:100,000) for 90 min. Bands of interest were visualized by adding a chemiluminescent substrate. Membranes were then stripped and re-probed for β-actin (1:1000). Proteins of interest were quantified (pixel density) with the Quantity One software (Bio-Rad) and then normalized to β-actin prior to statistical analysis with at least 3 animals per group.

mRNA analysis for Drd1a, Drd2, Drd4, TH, VMAT-2, DAT, α-synuclein, and Nurr1

Substantia nigra punches (0.75-mm diameter) were obtained from 500-μm thick brain sections. Total RNA was extracted using E.Z.N.A. MicroElute total RNA kit (Omega Bio-Tek, Inc., Norcross, GA) according to manufacturer's instructions. In short, the tissue was suspended in TRK lysis buffer supplemented with 1 mM 2-mercaptoethanol (Invitrogen, Grand Island, NY), followed by homogenization using a rotor–stator homogenizer for 15 s. One volume of 70% ethanol was added to promote selective binding of RNA to the membrane of the MicroElute RNA column. Following a series of washes (3×), total RNA was eluted in nuclease free water and quantified on an Epoch microtiter plate reader (BioTek Instruments, Inc., Winooski, VT). Using a Peltier thermal cycler (Bio-Rad; 5 min 25 °C, 30 min 42 °C, and 5 min 85 °C), 75 ng RNA was converted to cDNA with qScript cDNA SuperMix (Quanta Bioscience, Gaithersburg, MD). qPCR was run using RT^2 Real-Time™ SYBR Green/Rox PCR master mix and certified primers for Drd1a, Drd2, Drd4, TH, VMAT-2, DAT, α-synuclein, Nurr1, and GAPDH. cDNA representing 0.5 ng of starting RNA was added to each reaction well and amplifications were performed in a Mx3005P qPCR machine (Stratagene) programmed for an initial warming

(10 min, 95 °C) followed by 45 amplification cycles (15 s, 95 °C; 1 min, 60 °C) with each sample run in triplicate. Treatment differences were calculated as a fold change using the $^{\Delta\Delta}C_T$ method with GAPDH used as a house-keeping gene.

Statistical analysis

All data are presented as means ± SEM and were analyzed using SigmaStat 2.03 (SPSS Inc., Chicago, IL) by one-way analysis of variance (ANOVA), unless specifically mentioned below. The open field test data were analyzed by a two-way ANOVA to determine the effect of an additional factor, interval (5-min time period), on horizontal and location parameters. Student's t-test was used to compare the difference between approaching the familiar vs. the novel object in the NOR within each ATR dose. Striatal DA concentration data were not of equal variance, so Student's t-test was used to compare each treatment group with control. If significance was detected by ANOVA, the Fisher's LSD multiple comparison *post hoc* test was used to evaluate the differences between treatments with a significance level set at $p \leq 0.05$.

Results

Body weight and general appearance

Ten-day ATR exposure did not cause significant decrements in body weight ($p = 0.08$) or alterations in the general appearance of the mice, but there was a numerical trend towards a decrease in body weight at the highest exposure level, i.e., the body weights of the control and 250 mg/kg groups after 10-day ATR exposure were 23.5 ± 0.57 and 22.0 ± 0.48 g, respectively. In addition, weights (g/kg BW) of spleen ($p = 0.57$), thymus ($p = 0.19$) and liver ($p = 0.49$) were not affected by ATR. However, there was a trend ($p = 0.06$) towards an increase in the relative brain weight of the 250 mg/kg ATR group (control vs. 250 mg/kg ATR: 18.3 ± 0.57 vs. 20.2 ± 0.36 g/kg; other data not shown).

Behavioral analysis

Open field

ATR-treated (125 or 250 mg/kg) mice exhibited a significant decrease in the mean distance traveled ($p \leq 0.001$) and the number of crossings ($p \leq 0.01$) per 5 min interval (Fig. 3.2A, B). Similarly, vertical activity (number of rearings), which was evaluated during the first 5 min exploration period, was decreased by ATR exposure (125 or 250 mg/kg; $p \leq 0.001$; Fig. 3.2C). On the other hand, control and ATR-exposed mice spent equal time in the periphery ($p = 0.14$) or the center ($p = 0.15$) of the arenas. For example, the mean time spent in the periphery/center per 5 min interval was $203.1 \pm 11.51/95.2 \pm 11.53$ and $223.1 \pm 11.51/76.4 \pm 11.53$ s in control and 250 mg/kg groups, respectively (other data not shown).

Pole test

No significant effects of ATR on the average time to turn ($p = 0.32$; e.g., control vs. 250 mg/kg group: 7.6 ± 3.68 vs. 4.1 ± 0.88 s), time to descend ($p = 0.22$; e.g., control vs. 250 mg/kg group: 9.6 ± 2.42 vs. 11.7 ± 2.60 s), and total time ($p = 0.12$; e.g., control vs. 250 mg/kg group: 17.2 ± 5.05 vs. 15.8 ± 2.89 s) were found (other data not shown).

Grip strength

There was an apparent trend towards a decrease of the mean grip strength at the 250 mg/kg exposure level (Fig. 3.3), but this decrease was not statistically significant ($p = 0.13$) due, in part, to the somewhat higher variability of the control group.

NOR

As expected, control mice exhibited novel object bias by showing greater than 50% preference for the novel object ($p \leq 0.01$); this bias was not present in the ATR-treated mice

(≥ 25 mg/kg; Fig. 3.4). Specifically, in the 25 mg/kg group, the number of approaches towards the novel vs. the familiar object was not significantly different ($p = 0.24$); at the two higher doses, ATR-exposed mice approached the familiar object more than the novel one (125 mg/kg: $p \leq 0.05$; 250 mg/kg: $p \leq 0.001$). Similarly, ATR-exposed mice spent equal time with the novel vs. the familiar object in the 25 mg/kg group ($p = 0.63$), and more time with the familiar than with the novel object in the 125 or 250 mg/kg groups ($p \leq 0.001$; data not shown). If these data are expressed as NPI, ATR exposure resulted in a dose-dependent decrease of the NPI ($p \leq 0.001$; Fig. 3.4, inset).

FST

During the entire 15-min FST, mice exposed to ATR (125 or 250 mg/kg) spent more time swimming ($p \leq 0.01$) and less time immobile ($p \leq 0.01$) than the control mice, whereas the number of climbings was not significantly different between groups ($p = 0.40$; Fig. 3.5). Effects of ATR (125 or 250 mg/kg) on the times spent swimming or immobile were not restricted to a particular time interval because similar results were observed during the first ($p \leq 0.05$), second ($p \leq 0.01$), and last 5-min ($p \leq 0.01$) intervals (data not shown).

Neurochemistry for monoamines and their metabolites

Striatal DA levels were increased by 7.4% and 12.2% in the 125 ($p \leq 0.05$ vs. control) and 250 ($p \leq 0.01$ vs. control) mg/kg ATR groups, respectively (Fig. 3.6A). ATR (125 or 250 mg/kg) also increased striatal levels of the DA's metabolite HVA ($p \leq 0.001$; Fig. 3.6B), but it did not affect the other two DA metabolites: DOPAC ($p = 0.35$) and 3-MT ($p = 0.41$; Table A1, Appendix A). As a result, striatal HVA/DA ratio was increased ($p \leq 0.001$) by ATR (125 or 250 mg/kg), while the DOPAC/DA ratio was not changed ($p = 0.39$; Table A1, Appendix A). In addition, ATR treatment did not alter striatal 5-HT levels ($p = 0.31$), but it increased 5-HIAA

(125 or 250 mg/kg; $p \leq 0.001$; Fig. 3.6C) and the 5-HIAA/5-HT ratio (125 mg/kg; $p \leq 0.01$; Table A1, Appendix A).

In the prefrontal cortex, the two DA metabolites HVA (125 or 250 mg/kg; $p \leq 0.001$) and DOPAC (125 mg/kg; $p \leq 0.01$), the 5-HT metabolite 5-HIAA (125 mg/kg; $p \leq 0.05$) and NE (125 or 250 mg/kg; $p \leq 0.05$) were all increased by ATR (Table A2, Appendix A). DA was also marginally increased, but only at the lowest dose (5 mg/kg; $p \leq 0.01$ vs. control), with levels returning to control values at 25–250 mg/kg.

The effects of ATR on hippocampal monoamine levels were minimal; the only significant effect that was observed was an increase of MHPG at 250 mg/kg ($p \leq 0.01$; Table A2, Appendix A).

In the hypothalamus, no significant changes of monoamines or their metabolites were found ($p \geq 0.13$; data not shown).

Striatal levels of TH, DAT, VMAT-2, Drd2, and α-synuclein

No significant differences due to ATR exposure were found in the striatal protein expression of TH, DAT, VMAT-2, Drd2, or α-synuclein ($p \geq 0.22$; Fig. 3.7).

Nigral mRNA levels of Drd1a, Drd2, Drd4, TH, VMAT-2, DAT, α-synuclein, and Nurr1

At the mRNA level in the substantia nigra, ATR treatment did not alter the expression of DAT ($p \geq 0.12$), VMAT-2 ($p \geq 0.37$), Drd1a ($p \geq 0.17$), Drd2 ($p \geq 0.39$), Drd4 ($p \geq 0.07$), α-synuclein ($p \geq 0.23$), or Nurr1 ($p \geq 0.17$; Table 3.1). TH mRNA was not affected by ATR treatment as well, but a trend ($p \geq 0.06$) towards a decrease in the 125 and 250 mg/kg groups was observed (Table 3.1).

Discussion

The major findings of this study are: (1) short-term exposure to the herbicide ATR at doses not associated with overt signs of toxicity induces multiple behavioral abnormalities; (2) ATR targets monoamine pathways, mainly nigrostriatal and mesocortical; (3) while the majority of the ATR-induced perturbations were observed at the two highest (125 and 250 mg/kg) doses, performance in the NOR (behavior) was the most sensitive endpoint in our study, i.e., behavioral deficits in this test were seen at doses as low as 25 mg/kg. Within the context of ATR exposure, the NOR and FST findings, as well as ATR's effects on 5-HT homeostasis, are novel.

The NOR is based on the spontaneous tendency of rodents to spend more time exploring a novel object than a familiar one. It measures their novelty preference, which reflects the use of recognition memory (Antunes and Biala, 2012). Our NOR data suggest that short-term ATR exposure affects object recognition memory of mice. In line with our finding, chronic (1 year) dietary exposure to ATR (10 mg/kg) disrupts spatial memory in rats by increasing the number of errors made in a non-delayed random foraging task (Bardullas et al., 2011) and mouse offspring from dams orally exposed to ATR (0.1 mg/kg) beginning day 14 of gestation through weaning exhibit delayed step-through response in a passive avoidance test (Belloni et al., 2011). Thus, in terms of ATR's effects on memory function, our NOR data with short-term oral exposure has good correspondence with other chronic (Bardullas et al., 2011) and developmental oral exposure studies (Belloni et al., 2011). Interestingly, at the two higher doses (125 or 250 mg/kg), due to the dose-dependent decreased novelty preference, ATR-treated mice exhibited higher familiar object preference. It is well known that novel stimuli, such as unfamiliar objects, create conflict in rodents by concurrently evoking both approach and avoidance behaviors (Montgomery, 1955; Hoebel et al., 2008). Hence, the dose-dependent decreased novelty

preference may reflect increased avoidance of the novel object, indicative of increased anxiety (Ramos and Mormede, 1998; Li et al., 2010). Somewhat consistent with this finding, rats exposed to a single dose of ATR (25–200 mg/kg), exhibit taste aversion to sucrose, a substance that is normally preferred by rodents (Hotchkiss et al., 2012). Additionally, exposures to other unrelated and structurally different monoamine modulators, such as the synthetic cannabinoid CP 55,940 (O'Shea et al., 2004) or 3,4-methylenedioxymethamphetamine (Morley et al., 2001), alter performance in NOR and induce anxiety-like behavior in rodents.

Object recognition memory relies on the integrity of the hippocampus and the prefrontal cortex (Wallace et al., 2007; Antunes and Biala, 2012). In part accounting for the observed memory deficits, we found that ATR disrupts the homeostasis of DA, 5-HT and NE in the prefrontal cortex and of NE in the hippocampus, but not at the 25 mg/kg dose that also affects animals' performance in the NOR. These results are consistent with previous reports that lower level exposures to other toxicants, such as arsenic or methylone, alter behavior in the absence of neurochemical (monoamine) changes (Bardullas et al., 2009; den Hollander et al., 2013). One possible explanation for this is that there may be other neurotransmitter systems and/or brain regions not evaluated in our study that are sensitive targets of ATR overexposure. In terms of neurotransmitter systems, acetylcholine is one potential target. For example, ATR decreases the activity and mRNA expression of brain acetylcholine esterase (AChE) in fish (Xing et al., 2010a; Xing et al., 2010b) and decreased brain AChE activity has been associated with object recognition memory impairment in rats exposed to excessive amounts of iron or proline (Perez et al., 2010; Roecker et al., 2012). Regarding other brain regions, the nucleus accumbens (Nelson et al., 2010) also plays a role in object recognition memory, but we did not measure monoamines/metabolites in this brain structure, which is something that needs to be done in

future studies. Alternatively, because neurochemical analyses were done at a single time point (at 4 h after a 10-day exposure) and in whole tissues, it is possible that monoamines were altered at lower levels of exposure in a time-dependent fashion and/or that neurotransmitter release characteristics were altered, which is an effect that cannot be detected by measuring neurotransmitter tissue levels. To determine if this is the case, more sensitive means, such as microdialysis, need to be employed (Nowak et al., 2006).

Possible explanation for the FST results may be that ATR-treated mice are hyperactive after 9 days of exposure. However, open field test data in this study indicate that these mice were hypoactive on day 4 and possible hyperactivity on day 9 would suggest a biphasic response. Such biphasic locomotor activity disruption caused by ATR has been observed in a long-term, chronic exposure paradigm, i.e., ATR (10 mg/kg) decreases and increases locomotor activity after 8 and 12 months of exposure, respectively (Bardullas et al., 2011). As locomotor activity was not measured on day 9 in our study, we cannot discount this possibility, but we consider it remote. The FST results may also suggest that ATR exposure causes antidepressive effects (Petit-Demouliere et al., 2005). Because antidepressants typically enhance monoaminergic neurotransmission by inhibiting neurotransmitter degradation or reuptake (Baudry et al., 2011), the observed increases in DA and NE levels, as well as in DA, NE and 5-HT turnover at 4 h after exposure may indicate that ATR exposure induces a short-term enhancement of monoaminergic neuron activity, leading to perhaps transient antidepressive-like effects. This interpretation is consistent with Page et al. (2003), who report greater increase of extracellular NE by antidepressant treatment, which, ultimately, would lead to increased NE breakdown. In this regard, immobile time during FST has been suggested to reflect learning and memory; FST-related learned helplessness is associated with widespread perturbation of NE homeostasis,

including in the locus coeruleus (Weiss et al., 1981; West, 1990). Thus, the observed short-term increase in prefrontal cortical NE and hippocampal MHPG suggests that the FST results may also be due to inhibition of learning, which is consistent with the NOR results. However, whether these effects last or exist in long-term exposure paradigms remains to be determined.

Another explanation, which is most likely in our view, is that the increased time swimming was due to increased anxiety. In this regard, mice subjected to cold stress also exhibit increased time swimming in FST; this effect was reversed by an anxiolytic treatment (Hata et al., 1995; Hata et al., 1999). The serotonergic system is involved in the regulation of anxiety (Gordon and Hen, 2004). Exposure of non-depressed mice to psoralidin or amitriptyline increases swimming time in the FST in conjunction with altered 5-HT homeostasis (e.g., increased 5-HIAA) in the striatum and prefrontal cortex (Yi et al., 2008). In line with this, our data suggest that ATR-induced increased swimming in the FST is accompanied by altered 5-HT homeostasis in both the striatum and prefrontal cortex. Hence, higher doses of ATR (125 or 250 mg/kg) may induce anxiety-like behavior by disrupting serotonergic pathways. Of note, we found that 125 mg/kg ATR was, for the most part, more potent in causing neurochemical alterations than the 250 mg/kg dose. This is likely due to the dose-dependent autoinduction metabolism of ATR (Hanioka et al., 1998b; Fraites et al., 2011; Pogrmic-Majkic et al., 2012).

Our finding that mice exposed to ATR for 4 days were hypoactive agrees with previous studies by Ugazio et al. (1991) and Rodriguez et al. (2013), who found hypoactivity in the open field test after short-term exposure of rats to ATR orally (1000 mg/kg) or ip (100 mg/kg), suggesting that ATR's effects on motor activity are independent of exposure routes. Multiple studies (Coban and Filipov, 2007; Bardullas et al., 2011; Rodriguez et al., 2013), including the current one, have demonstrated that ATR targets dopaminergic pathways. Dopaminergic systems

are known to participate in motor control (Schultz, 2007). Hence, it is not surprising that ATR exposure induces motor deficits, probably due perturbations of DA circuitries, nigrostriatal pathway in particular. At the neurochemical level, our data suggest that ATR exposure disrupts striatal DA homeostasis at doses that also cause locomotor activity alterations (125 or 250 mg/kg). Altered striatal DA homeostasis was observed in rats exposed to ATR for one-year (10 mg/kg; Bardullas et al., 2011) or in rats (Rodriguez et al., 2013) or juvenile mice exposed to ATR for two weeks (Coban and Filipov, 2007). However, in these studies striatal DA levels were decreased, whereas we found a 7.4–12.2% increase in striatal DA and a 30–100% increase in striatal HVA levels after a 10-day exposure (125 or 250 mg/kg). In agreement with our findings, in a preliminary study, increased striatal levels of DA and its metabolites (DOPAC and HVA) were also observed in rats at 90 min or 4 h after a single ATR (100 mg/kg; ip) injection, with HVA being more prominently affected than DOPAC (Rodriguez et al., 2007b). These data indicate that ATR's effects on striatal DA are time-dependent. This is not unique to ATR, as short-term exposure (1 week) to another DA toxicant, the herbicide paraquat, increases, whereas longer exposure (3 weeks) decreases striatal DA levels (Litteljohn et al., 2009). Such initial increases of DA and its turnover may ultimately contribute to DA neuronal degeneration and/or DA depletion through the generation of free radicals and toxic metabolites (Lotharius and Brundin, 2002), as reported in longer exposure studies (Coban and Filipov, 2007; Bardullas et al., 2009). In this regard, ATR exposure has been shown to induce oxidative stress in multiple organs, including the brain (Singh et al., 2011; Xing et al., 2012).

While increasing evidence documents adverse effects of ATR on DA systems, not much is known about its mechanism of action. The present study shows that the neurochemical and behavioral alterations induced by short-term ATR exposure are not accompanied by significant

alterations in the striatal protein or nigral mRNA levels of selected dopaminergic markers, including TH, VMAT-2, DAT, DA receptors, or α-synuclein. The lack of ATR effect on TH expression in this study is in line with other in vitro (Das et al., 2003), ex vivo (Filipov et al., 2007), or in vivo (Rodriguez et al., 2013) studies, whereas the lack of ATR effect on DA receptors was also reported in a recent rat study (Rodriguez et al., 2013). Thus, at least at earlier stages and/or lower exposures, ATR exerts dopaminergic toxicity through mechanisms independent of the abundance of these selected markers, but it may do so by affecting the function of some of these key molecules. For example, we have found that ATR disrupts VMAT-2-mediated vesicular uptake of DA (Hossain and Filipov, 2008). Others have shown that acute ATR exposure (100 mg/kg, ip) increases the levels of phosphorylated TH (Ser 19 and 40; Rodriguez et al., 2007b), which is consistent with the short-term increase of striatal DA, the trend for a decreased nigral TH mRNA observed in our study, as well as with the acutely increased striatal DA reported by Rodriguez et al. (2007b).

Among existing rodent neurotoxicity studies with ATR, in spite of the differences in exposure duration, doses, and exposure routes and in agreement with our current findings, the most consistent effects are changes in striatal DA homeostasis and locomotor activity (Ugazio et al., 1991; Coban and Filipov, 2007; Rodriguez et al., 2007b; Bardullas et al., 2011; Rodriguez et al., 2013). However, it should be noted that two-week ATR exposure (100 mg/kg, 3 ip injections/week) affected ventral midbrain mRNA levels of TH, DAT, and VMAT-2 (Rodriguez et al., 2013), but by using similar exposure levels (125 or 250 mg/kg) and via oral gavage for 10 days we only observed a trend towards a decrease of nigral TH mRNA level, suggesting that some neural effects of ATR might be impacted by ATR's reported first-pass metabolism (Ross et al., 2009; Rodriguez et al., 2013); this should be considered in comparing study findings and in

designing future studies. Of note, in this study, by using behavioral tasks not used before, we found that short-term ATR exposure alters performance in the NOR at doses (i.e., 25 mg/kg) that do not affect locomotor activity. This indicates that novelty seeking behavior may be more sensitive to ATR than locomotor activity; this novel finding should be taken into consideration.

Conclusions

Our results indicate that short-term exposure to ATR induces multiple behavioral abnormalities involving motor, cognitive and emotional functions and it targets monoamine pathways. The fact that altered performance in the NOR occurs at doses that do not change motor activity and brain monoamines indicates that certain behavioral domains may be particularly sensitive to ATR and highlights the potential for other brain regions, besides the nigrostriatal system, to be targeted by ATR. Our findings also underscore the importance of considering behavioral deficits in assessing the risk of ATR overexposure as the lowest observed adverse effect level (LOAEL) in our study (25 mg/kg) is almost 3-fold lower than the current EPA LOAEL (70 mg/kg), which is based on ATR's adverse effects on the reproductive (endocrine) system (EPA, 2003).

Conflict of interest statement

The authors declare that there are no conflicts of interest.

Table 3.1. mRNA levels[a] in the substantia nigra of mice exposed to ATR (0-250 mg/kg) for 10 days.

Group	TH	DAT	VMAT-2	Drd1a	Drd2	Drd4	α-synuclein	Nurr1
Vehicle	1.00 ± 0.10	1.00 ± 0.21	1.00 ± 0.24	1.00 ± 0.08	1.00 ± 0.14	1.00 ± 0.13	1.00 ± 0.11	1.00 ± 0.13
5 mg/kg	1.20 ± 0.16	1.37 ± 0.08	1.20 ± 0.10	0.98 ± 0.11	1.15 ± 0.11	1.06 ± 0.14	0.89 ± 0.10	1.12 ± 0.10
25 mg/kg	1.21 ± 0.05	1.47 ± 0.09	1.30 ± 0.17	1.06 ± 0.07	1.20 ± 0.06	0.63 ± 0.09	1.05 ± 0.01	1.34 ± 0.08
125 mg/kg	0.62 ± 0.12	1.65 ± 0.36	1.27 ± 0.30	0.85 ± 0.07	0.91 ± 0.08	0.84 ± 0.05	1.07 ± 0.15	1.06 ± 0.15
250 mg/kg	0.80 ± 0.09	1.30 ± 0.24	1.04 ± 0.15	0.95 ± 0.03	1.04 ± 0.14	0.90 ± 0.06	0.78 ± 0.06	1.07 ± 0.12

TH: tyrosine hydroxylase; DAT: dopamine transporter; VMAT-2: vesicular monoamine transporter 2; Drd1a: dopamine receptor D1a; Drd2: dopamine receptor D2; Drd4: dopamine receptor D4; α-synuclein: alpha-synuclein; Nurr1: nuclear receptor related 1.

[a] Data represent means ± SEM of fold differences relative to vehicle control determined by the $^{\Delta\Delta}C_T$ method with GAPDH as a house-keeping gene.

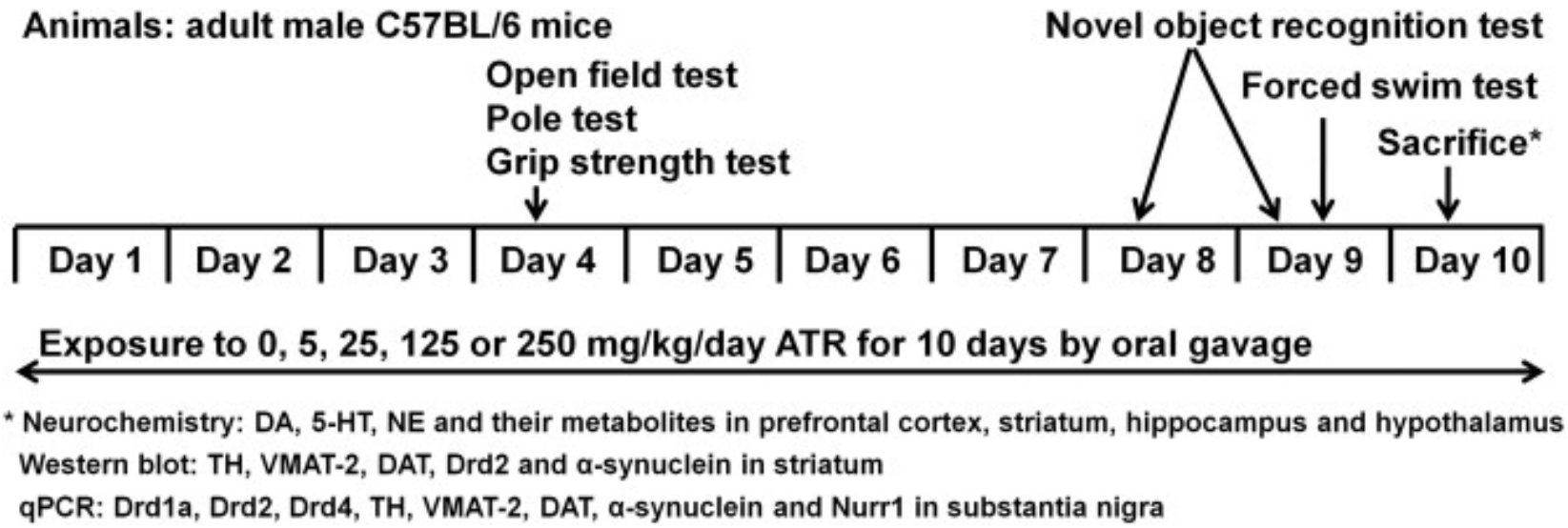

Figure 3.1. Experimental design and a timeline of the 10-day ATR exposure study.

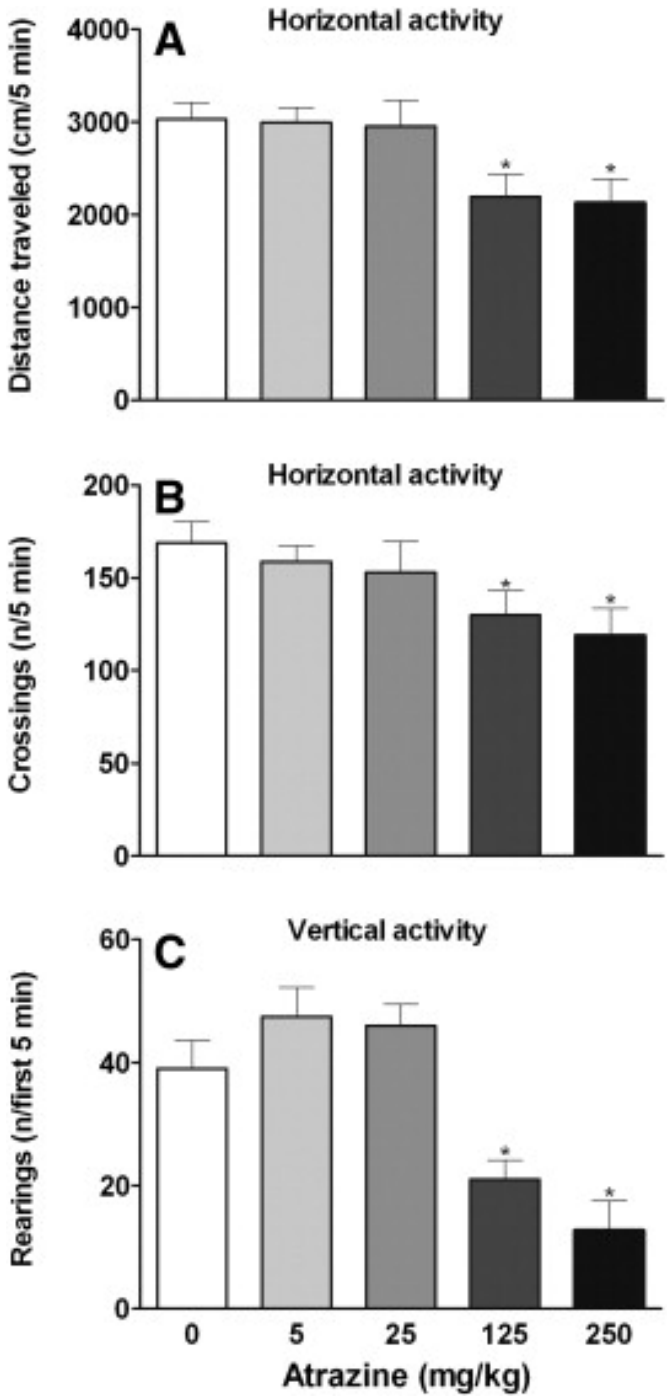

Figure 3.2. Effects of 4-day exposure to ATR (0–250 mg/kg) on spontaneous locomotor activity. Parameters include mean distance traveled per 5 min (A), mean number of crossings per 5 min (B), and the number of rearings during the first 5 min (C). * Indicates significant difference from the control group ($p \leq 0.05$).

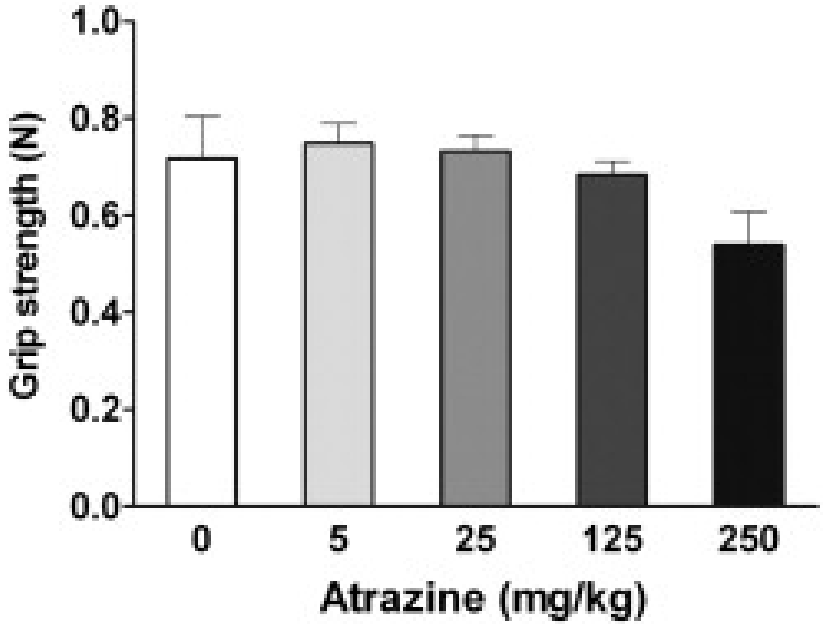

Figure 3.3. Effects of 4-day exposure to ATR (0–250 mg/kg) on mean grip strength.

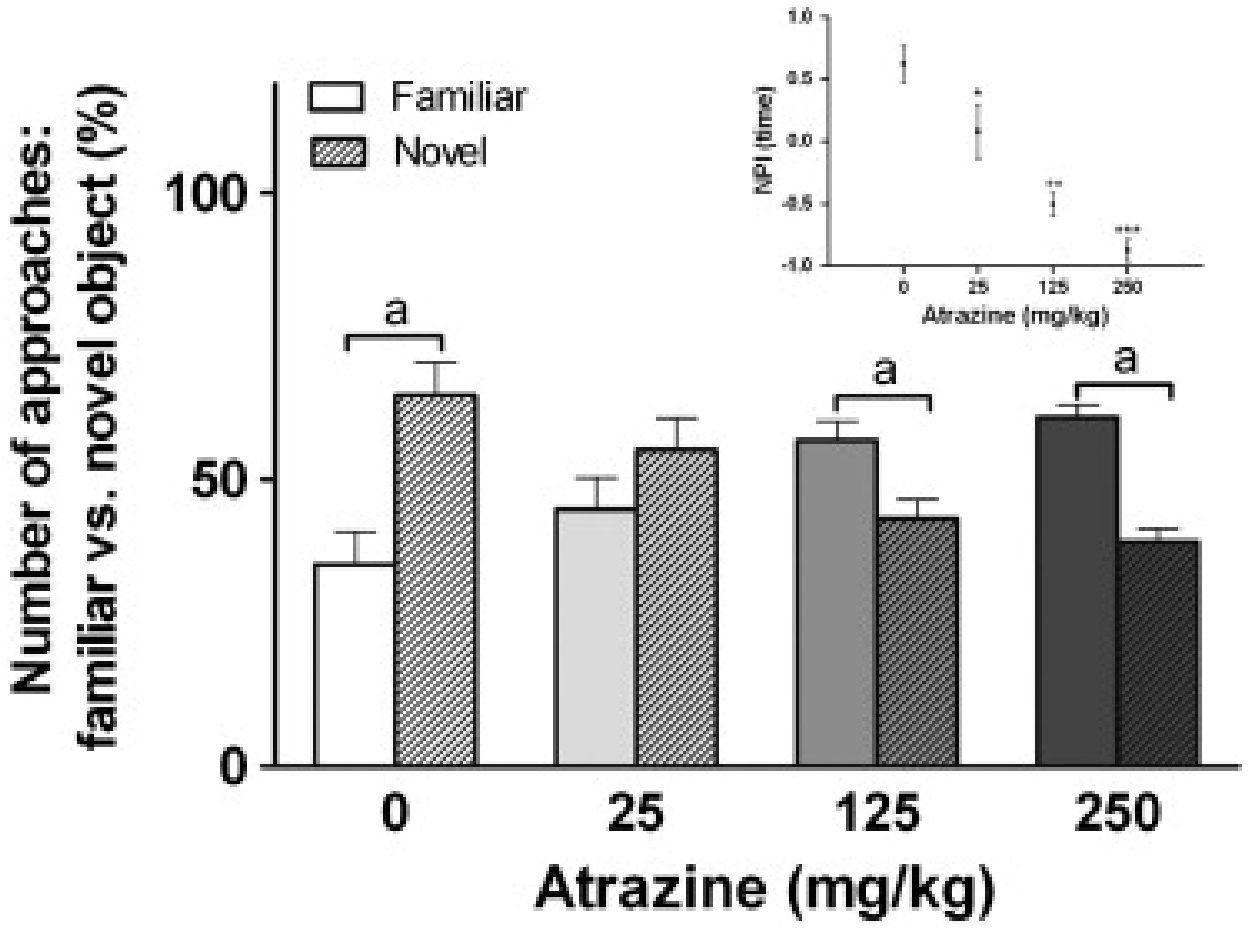

Figure 3.4. Effects of 9-day exposure to ATR (0–250 mg/kg) on the number of approaches towards a familiar vs. a novel object (%) in a novel object recognition test (NOR). The inset represents the novelty preference index (NPI) calculated based on times spent exploring the familiar vs. novel object. [a] Indicates significant difference between novel and familiar within ATR dose ($p \leq 0.05$). *, ** and *** indicate significant difference from the control group ($p \leq 0.05$). Means not sharing the same number of asterisks are significantly different ($p \leq 0.05$).

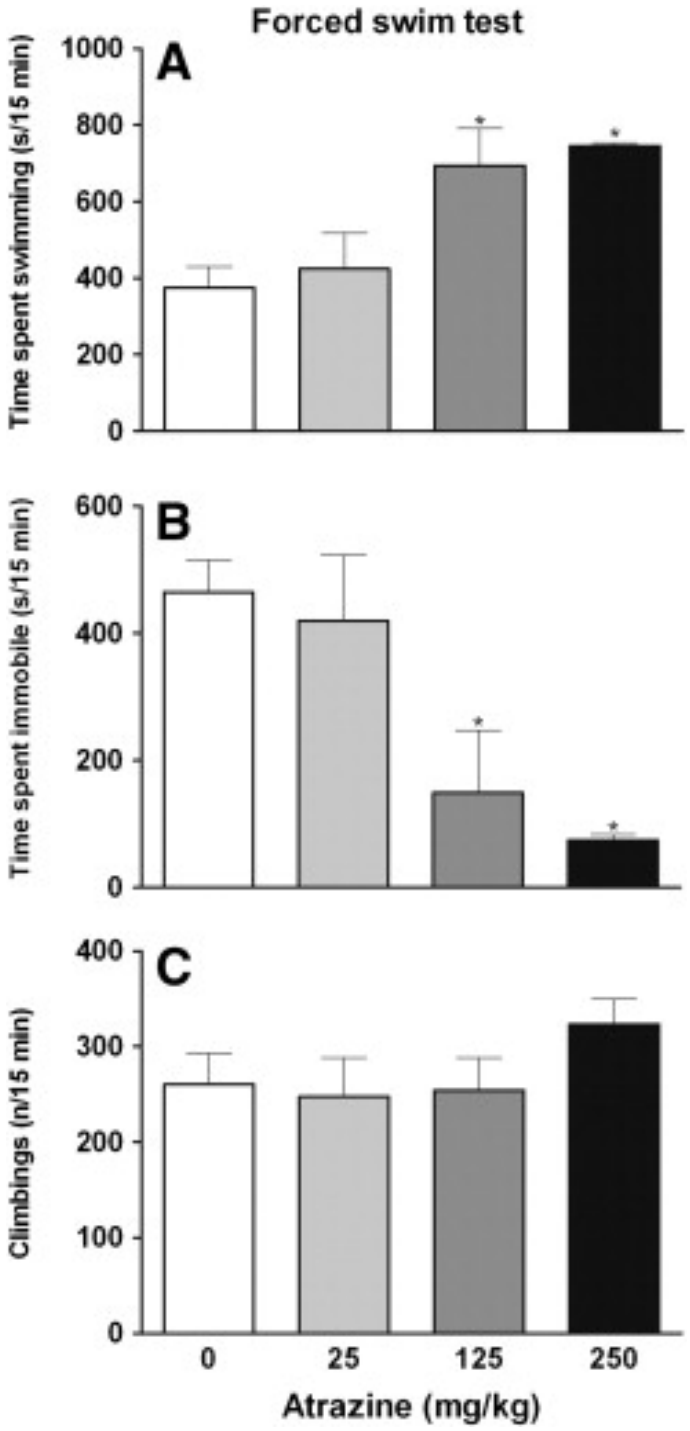

Figure 3.5. Effects of 9-day exposure to ATR (0–250 mg/kg) on the time spent swimming (A), immobile (B), and the number of climbings (C) in a forced swim test (FST). * Indicates significant difference from the control group ($p \leq 0.05$).

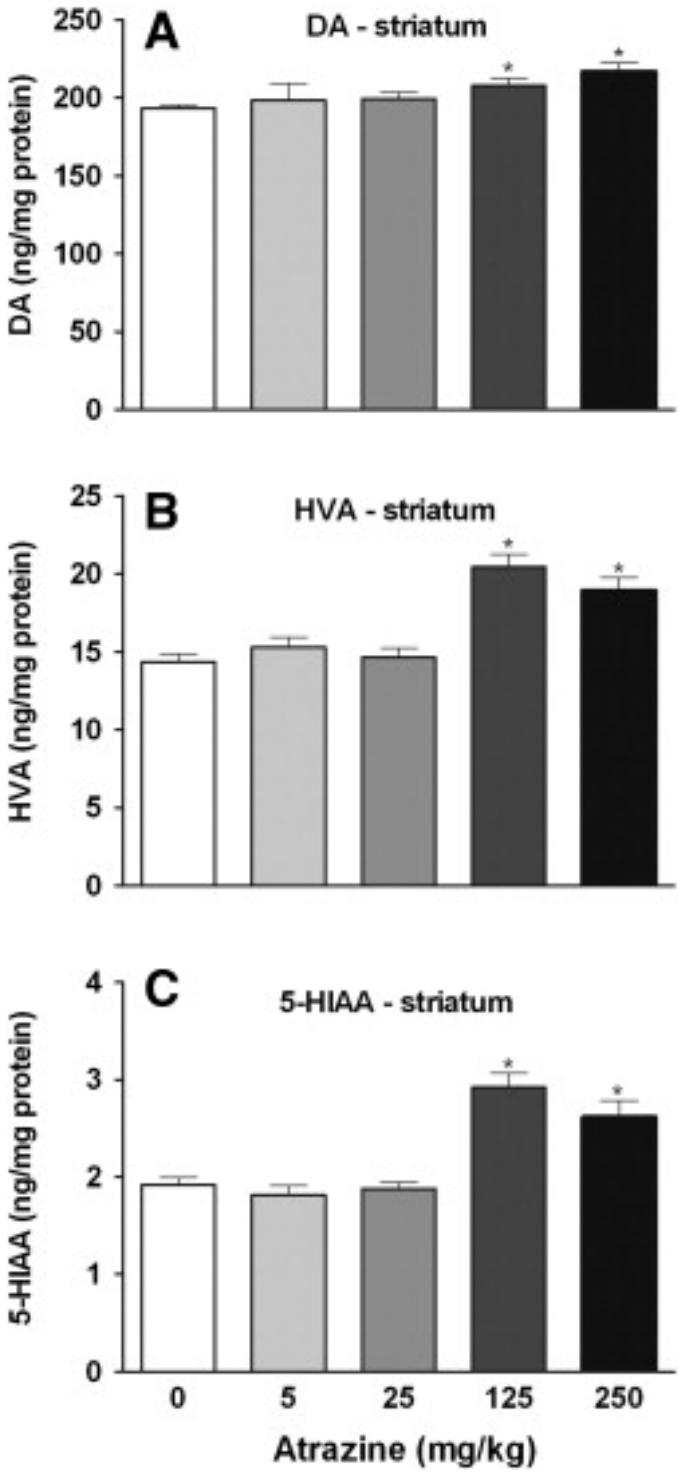

Figure 3.6. Effects of 10-day exposure to ATR (0–250 mg/kg) on striatal levels of DA (A), HVA (B), and 5-HIAA (C). * Indicates significant difference from the control group ($p \leq 0.05$).

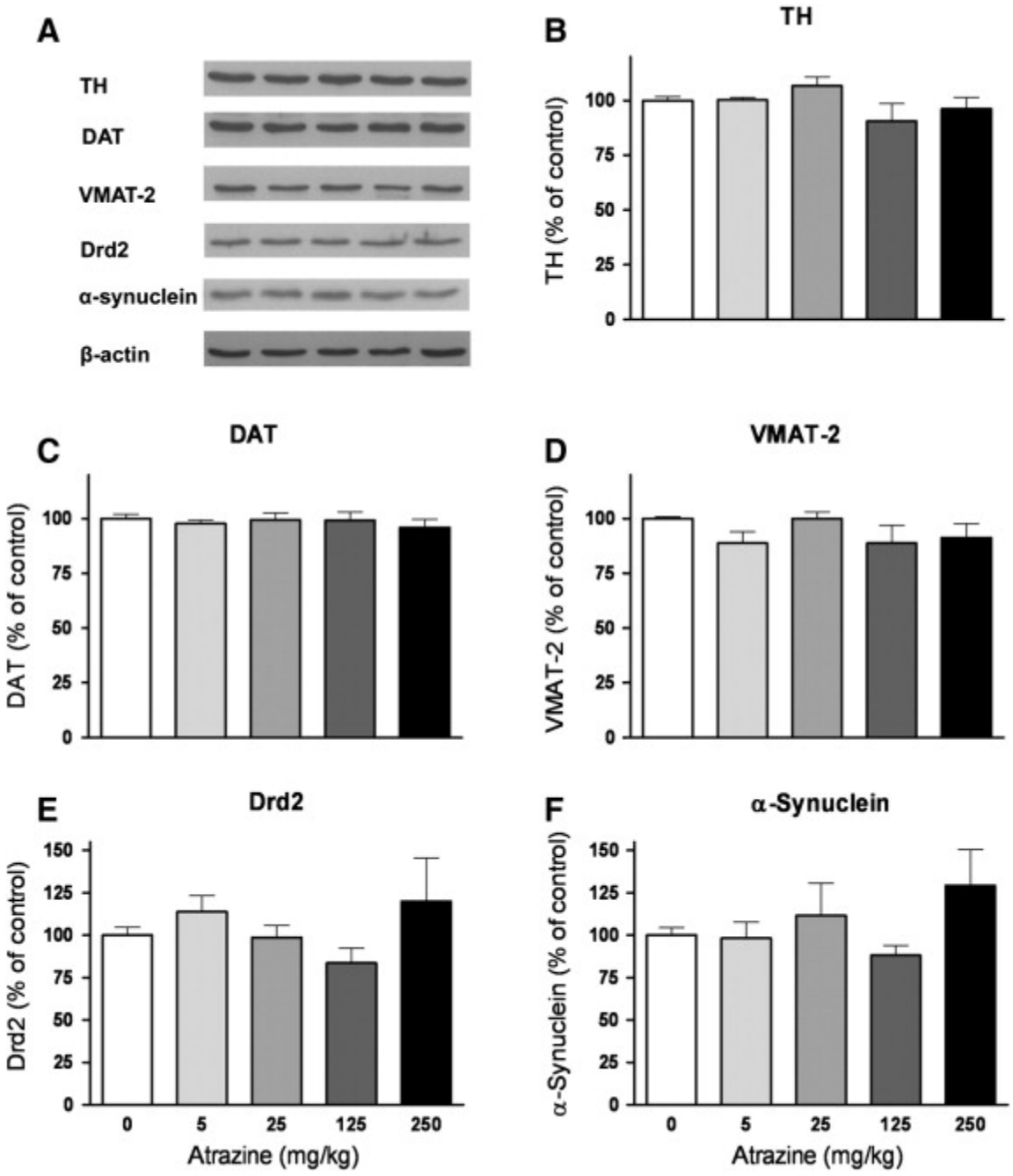

Figure 3.7. Effects of 10-day exposure to ATR (0–250 mg/kg) on striatal TH (B), DAT (C), VMAT-2 (D), Drd2 (E), and α-synuclein (F) protein levels determined by western blot analysis as described in the Materials and methods section. Representative bands (n = 3–4/group) for each protein of interest and the house-keeping protein β-actin are provided in panel A.

CHAPTER 4

A PHYSIOLOGICALLY BASED PHARMACOKINETIC MODEL FOR ATRAZINE AND ITS MAIN METABOLITES IN THE ADULT MALE C57BL/6 MOUSE[1]

[1] Lin, Z., Fisher, J.W., Ross, M.K., Filipov, N.M. 2011. Toxicology and Applied Pharmacology. 251(1):16-31. Reprinted here with permission of the publisher.

Abstract

Atrazine (ATR) is a chlorotriazine herbicide that is widely used and relatively persistent in the environment. In laboratory rodents, excessive exposure to ATR is detrimental to the reproductive, immune, and nervous systems. To better understand the toxicokinetics of ATR and to fill the need for a mouse model, a physiologically based pharmacokinetic (PBPK) model for ATR and its main chlorotriazine metabolites (Cl-TRIs) desethyl atrazine (DE), desisopropyl atrazine (DIP), and didealkyl atrazine (DACT) was developed for the adult male C57BL/6 mouse. Taking advantage of all relevant and recently made available mouse-specific data, a flow-limited PBPK model was constructed. The ATR and DACT sub-models included blood, brain, liver, kidney, richly and slowly perfused tissue compartments, as well as plasma protein binding and red blood cell binding, whereas the DE and DIP sub-models were constructed as simple five-compartment models. The model adequately simulated plasma levels of ATR and Cl-TRIs and urinary dosimetry of Cl-TRIs at four single oral dose levels (250, 125, 25, and 5 mg/kg). Additionally, the model adequately described the dose dependency of brain and liver ATR and DACT concentrations. Cumulative urinary DACT amounts were accurately predicted across a wide dose range, suggesting the model's potential use for extrapolation to human exposures by performing reverse dosimetry. The model was validated using previously reported data for plasma ATR and DACT in mice and rats. Overall, besides being the first mouse PBPK model for ATR and its Cl-TRIs, this model, by analogy, provides insights into tissue dosimetry for rats. The model could be used in tissue dosimetry prediction and as an aid in the exposure assessment to this widely used herbicide.

Keywords: Atrazine, PBPK modeling, DACT, Chlorotriazine herbicides

Introduction

Atrazine (ATR; 2-chloro-4-(ethylamino)-6-(isopropylamino)-*s*-triazine, CAS# 1912-24-9) is a chlorotriazine herbicide that was introduced by JR Geigy SA (subsequently known as Ciba-Geigy, Novartis, and, currently, Syngenta) in the 1950s (Gammon et al., 2005). For more than half-century, ATR has been used worldwide for the control of broadleaf weeds and is applied on crops such as corn, sugarcane, and sorghum (EPA, 2003). In the United States alone, ATR's annual use is approximately 65–80 million pounds/year (Gianessi and Marcelli, 2000; EPA, 2003), with little variation over the past few decades (Kiely et al., 2004).

Due to its widespread use and relative persistence in ground water, excessive human exposure to ATR is a concern, with pesticide applicators, farmers, and their families being at increased risk (Curwin et al., 2007). The primary routes of exposure to ATR in these populations are inhalation, dermal, and oral (Chevreuil et al., 1996; Squillace et al., 2002).

Limited human data (Hoppin et al., 2002; Hessel et al., 2004) and extensive rodent data indicate that exposure to high levels of ATR is detrimental to the reproductive, immune, and nervous systems. For example, oral exposure to ATR disrupts the estrus cycle and alters reproductive hormone balance in rats (Eldridge et al., 1994a; Eldridge et al., 1994b; Simic et al., 1994; Wetzel et al., 1994; Cooper et al., 1996; Cooper et al., 2000). We (Filipov et al., 2005; Pinchuk et al., 2007) and others (Pruett et al., 2003; Karrow et al., 2005; Rowe et al., 2006) have demonstrated that excessive ATR exposure has a negative impact on the immune system. In addition, several studies, including ours, indicate that ATR is detrimental to the brain (Rodriguez et al., 2005; Giusi et al., 2006; Filipov et al., 2007), with the basal ganglia being a target in both rats (Rodriguez et al., 2005) and mice (Filipov et al., 2007). While data pertaining to ATR's toxicity in mammals are increasing, there is still much unknown about its

pharmacokinetic behavior, in vivo metabolism, and tissue dosimetry, which are all critical in establishing dose–response relationships and in identifying potential toxic metabolites.

In vitro, cytochrome P450s metabolize ATR to the mono-dealkylated products desethyl atrazine (DE; 2-chloro-4-amino-6-(isopropylamino)-*s*-triazine) and desisopropyl atrazine (DIP; 2-chloro-4-(ethylamino)-6-amino-*s*-triazine) (Hanioka et al., 1999b, a). Apparently, the mono-dealkylated metabolites DE and DIP are the two major products of in vitro metabolism of ATR by liver microsomes across mammals as reported for mice (Ross and Filipov, 2006), rats, pigs (Lang et al., 1996), and, importantly, humans (Lang et al., 1996; Joo et al., 2010). In vivo, following oral exposure, ATR is absorbed and metabolized rapidly. Following initial generation of DE and DIP, subsequent metabolism of DE and DIP produces didealkyl atrazine (DACT; 2-chloro-4,6-diamino-*s*-triazine), which appears to be the major in vivo ATR metabolite in rats (Brzezicki et al., 2003; McMullin et al., 2003), mice (Ross and Filipov, 2006; Ross et al., 2009), and, apparently, humans (Barr et al., 2007). Importantly, compared to ATR, much higher levels of DACT were detected in target tissues, such as the brain (Ross et al., 2009).

Physiologically based pharmacokinetic (PBPK) models have been useful tools to perform dose–response analysis and risk assessment of toxic chemicals, including pesticides (Mirfazaelian et al., 2006; Timchalk et al., 2007; Timchalk and Poet, 2008; Tornero-Velez et al., 2010). At present, there are three PBPK models for ATR in the rat (Timchalk et al., 1990; McMullin et al., 2003; McMullin et al., 2007b) and none in the mouse. The first PBPK model (Timchalk et al., 1990) describes the time course of radioactivity in the plasma of rats given ^{14}C-ATR orally and was used as a foundation for subsequent models. While an extremely valuable initial step, drawbacks of this initial model were the lack of tissue compartments and the inability to distinguish ATR from its metabolites. McMullin et al. developed the other PBPK

models for ATR in the rat (McMullin et al., 2003; McMullin et al., 2007b), with the latest model successfully describing the time course of ATR and its chlorinated metabolites (Cl-TRIs) in the rat plasma. However, in part due to the lack of experimental data, this model did not include the brain compartment, an important target organ for ATR, nor did it consider dose–response tissue dosimetry data for its development.

To generate dose-dependent tissue dosimetry data for ATR in the mouse, which is a species frequently used in toxicity assessment, including that of ATR (NTP, 1994; Pruett et al., 2003; Filipov et al., 2005; Giusi et al., 2006; Rowe et al., 2006), we conducted a complete disposition study of ATR in adult male C57BL/6 mice (Ross et al., 2009). In this study, time course data on ATR and its Cl-TRIs in plasma, tissues, and urine across four oral doses (250–5 mg/kg) were generated. Taking advantage of these new data, the objective of the present study was to develop a comprehensive PBPK model for ATR and its Cl-TRIs in the mouse.

Methods

Experimental data

In vivo study

The experimental in vivo data used for model development and evaluation have been described in detail elsewhere (Ross et al., 2009). Briefly, ATR, dissolved in corn oil, was administered to adult male C57BL/6 mice (3–4 months old) at single doses of 250, 125, 25, and 5 mg/kg body weight by oral gavage (po). This dose regimen was selected to closely resemble the doses used in the National Toxicology Program mouse study (NTP, 1994). At 0.5, 1, 2, 4, 6, 12, and 24 h after ATR administration, groups of mice were sacrificed. Plasma and tissue samples were harvested and frozen at −80 °C for subsequent analysis. Twenty-four-hour urine samples were collected at 24, 48, and 72 h post treatment, representing urinary excretion that

occurred from 0- to 24-, 25- to 48-, and 49- to 72- h, respectively. After collection, samples were processed for LC/MS analysis for ATR and its Cl-TRIs following procedure described in detail elsewhere (Ross and Filipov, 2006; Ross et al., 2009). The units of relevant data used in the model development are "l" for volume, "μmol" for amount, and "μmol/l (μM)" for concentration in both tissues and plasma. The unit of the dose "mg/kg" was converted to "μmol/kg" by dividing molecular weight of ATR (215.69 g/mol) and then multiplying the unit with a factor of 1000, to accommodate the model output.

In vitro metabolism of ATR by intestinal microsomes

This study was conducted in order to determine whether intestinal metabolism of ATR takes place and needs to be incorporated in the model development. Briefly, pooled human intestinal microsomes (HIM) were purchased from Xenotech (Lenexa, KS). Incubations were performed in a total volume of 250 μl essentially as described previously (Ross and Filipov, 2006). In short, ATR (50 μM final concentration) was pre-incubated for 5 min at 37 °C with HIM (0.5 mg protein/ml) in 40 mM Tris–HCl buffer (pH 7.4) containing 13 mM $MgCl_2$ and 1 mM EDTA. NADPH was added to each reaction mixture at a final concentration of 1 mM to begin the reaction. Control reactions received water instead of NADPH. After 60 min, reactions were quenched with an equal volume of cold acetonitrile containing simazine (internal standard). After centrifuging for 5 min, the supernatants (10 μl aliquot) were analyzed with the LC-MS method reported in Ross and Filipov (2006). These data are presented as Fig. B1 (Appendix B).

PBPK model development

Simulation software

ACSLX simulation software Version 2.5 (Aegis Technologies Group, Inc., Huntsville, AL) was used to develop the PBPK model for ATR and its Cl-TRIs. Key sets of differential

equations used in the final model are provided in the Appendix B. Computer code for the model could be obtained upon request from the corresponding author. The structure of the model is presented in Fig. 4.1 and described in detail below.

Model structure

The most currently published PBPK model for ATR and its Cl-TRIs in the adult rat (McMullin et al., 2007b) was used as a starting point for the present mouse model. As previously described (McMullin et al., 2007b), the present model was constructed based on the following assumptions: saturable metabolism, flow-limited distribution, and first-order urine excretion for Cl-TRIs. The model consisted of four sub-models for ATR, DE, DIP, and DACT. Each sub-model described a separate chemical and was linked together through systemic circulation into an integrated model (Fig. 4.1). The ATR and DACT sub-models contained six compartments: blood, liver (primary site of metabolism), brain (target organ), kidney (primary site of elimination), and lumped tissues (richly and slowly perfused tissues) to account for the remaining volume of distribution. Since data exist indicating that ATR and DACT could bind to plasma protein (primarily albumin) and red blood cells (RBC, primarily hemoglobin; Lu et al., 1998; McMullin et al., 2003; Dooley et al., 2006; Dooley et al., 2007), plasma and RBC in the blood compartment in ATR and DACT sub-models were described as separate compartments in order to evaluate the binding characteristics of ATR and DACT with plasma protein and RBC, respectively. Due to the lack of such evidence for DE and DIP, and the lack of time course data of DE and DIP in the kidney, the DE and DIP sub-models were composed of five compartments: blood, liver, brain, richly and slowly perfused tissues.

The present model described the uptake of ATR using a two-compartment model as described by Staats et al. (1991) and by Abbas and Fisher (1997), who found that the two-

compartment model provided a good description of gastrointestinal (GI) absorption of lipophilic chemicals that exhibited an initial rapid uptake phase, followed by a slow, sustained uptake into systemic circulation (Fig. 4.1). Briefly, the model assumes that following oral administration, ATR is absorbed rapidly from the stomach lumen into the blood supply of the GI tract, with a gastric absorption rate constant K1 (h^{-1}). Simultaneously, ATR is distributed into the intestinal lumen by force of gastric emptying, with a gastric-emptying rate constant K2 (h^{-1}). This is followed by a slower absorption of ATR from the intestinal lumen into the GI tract's blood supply, with an intestinal absorption rate constant K3 (h^{-1}). The three constant values were determined by visually fitting the predicted plasma concentrations of ATR and its Cl-TRIs to actual time course data at a 250 mg/kg dose (Ross et al., 2009).

The rate of change for each chemical in each compartment was described using mass balance differential equations as described in Evans et al. (2008) and Mirfazaelian and Fisher (2007). As in the previous PBPK models for ATR in rats (Timchalk et al., 1990; McMullin et al., 2003; McMullin et al., 2007b), we assumed that all compartments are flow-limited, meaning the compound's distribution was determined mainly through blood flow (Medinsky and Valentine, 2001). As an example, the flow-limited liver compartment differential rate equation for ATR is:

RL = QL*(CA-CVL)+RAO-RATR_DEmet-RATR_DIPmet……...(4.1)

where RL is the rate of distribution of ATR in the liver, μmol/h; QL is the volume of blood flow to the liver per hour, l/h; CA is the arterial blood concentration of ATR, μM; CVL is the liver venous blood concentration of ATR, μM; RAO is the absorption rate of ATR from the GI tract via portal vein, μmol/h; RATR_DEmet and RATR_DIPmet are the oxidative metabolism rates of ATR converting to DE and to DIP in the liver, respectively, μmol/h. Other key differential equations are described in the Appendix B.

The model described oxidative metabolism of ATR to DE, ATR to DIP, DE to DACT, and DIP to DACT in the liver using Michaelis–Menten equations, whereas the brain, kidney, richly and slowly perfused compartments were assumed to be non-metabolizing organs. For instance, the conversion from ATR to DE is described as follows:

RATR_DEmet = VmaxATR_DE*CVL/(KmATR_DE+CVL)……..…(4.2)

where RATR_DEmet is the oxidative metabolism rate from ATR to DE, μmol/h; VmaxATR_DE is the maximal metabolic rate constant from ATR to DE, μmol/h; KmATR_DE is the Michaelis–Menten constant, μM.

Based on the dose and the average mouse body weight (Ross et al., 2009), the amount of ATR that was administrated to each mouse was calculated to be 29.348, 14.674, 2.935, and 0.587 μmol for the 250, 125, 25, and 5 mg/kg doses, respectively. Based on the reported 0- to 24-, 25- to 48-, and 49- to 72-h cumulative urine concentrations of ATR and its Cl-TRIs (Ross et al., 2009), we calculated the 72-h cumulative urine elimination amount of ATR, DE, DIP, and DACT. For ATR, the cumulative elimination amount was 0.02722, 0.0221, 0.00169, and 0.00042 μmol for the 250, 125, 25, and 5 mg/kg doses, respectively. Since the elimination amount of ATR accounted for less than 0.1% of the total administrated amount, urine elimination of non-metabolized ATR was considered negligible and urine elimination equation was not included in the ATR sub-model. The same procedure was used to calculate the percent of the eliminated amount of DE, DIP, and DACT. The majority of the administered ATR dose was excreted in the urine as DACT, with 29.3%, 30.0%, 44.6%, and 49.7% of administered ATR being eliminated as DACT for the 250, 125, 25, and 5 mg/kg doses, respectively. The amount of administered ATR excreted as DE or DIP across all four doses was approximately 0.5% and 0.4%, respectively. Thus, urine elimination equations were incorporated in the sub-models for

each Cl-TRI metabolite. Urine elimination of Cl-TRIs was described as a first-order elimination process. For example, the urine elimination rate equation for DACT is:

Rurine3 = Kurine3*CVK3*VK……..…(4.3)

where Rurine3 is the elimination rate of DACT via the urine, μmol/h; Kurine3 is the urine elimination rate constant for DACT, h^{-1}; CVK3 is the kidney venous blood concentration of DACT, μM; VK is the volume of kidney, l.

Plasma protein and RBC binding

Previous investigations indicated that ATR and/or DACT could bind to plasma protein, primarily albumin (Lu et al., 1998; McMullin et al., 2003; Dooley et al., 2007), and to RBC/hemoglobin (McMullin et al., 2003; Dooley et al., 2006). The binding reaction pathways of ATR and DACT with plasma protein and RBC protein were incorporated into the model via second-order equations (McMullin et al., 2003; Leavens and Borghoff, 2009) as shown below:

RAPlasmaFree = QC*(CV-CPlasmaFree)+RARBCunbind-RARBCbind+RAPlasmaunbind-RAPlasmabind……..…..(4.4)

RAPlasmabind = KaATRPlasma*BMaxPlasmaRemain*APlasmaFree……(4.5)

RAPlasmaunbind = KdATRPlasma*APlasmabound……....(4.6)

RARBCbind = KaATRrbc*BMaxRBCRemain*APlasmaFree…….(4.7)

RARBCunbind = KdATRrbc*ARBCbound……..(4.8)

where RAPlasmaFree is the rate of change of the amount of free ATR in the plasma, μmol/h; CPlasmaFree is the plasma concentration of free ATR, μM; RARBCunbind is the rate of unbinding of RBC-ATR complex, μmol/h; RARBCbind is the rate of binding of ATR with RBC, μmol/h; RAPlasmaunbind is the rate of unbinding of plasma protein–ATR complex, μmol/h; RAPlasmabind is the rate of binding of ATR with plasma protein, μmol/h; KaATRPlasma is the

binding rate constant of ATR with plasma protein, /(h*μmol); KaATRrbc is the binding rate constant of ATR with RBC, /(h*μmol); KdATRPlasma is the unbinding rate constant of plasma protein–ATR complex, h^{-1}; KdATRrbc is the unbinding rate constant of RBC-ATR complex, h^{-1}; BMaxPlasmaRemain is the remaining binding capacity of plasma protein with ATR, μmol; BMaxRBCRemain is the remaining binding capacity of RBC with ATR, μmol; APlasmaFree is the amount of free ATR in the plasma, μmol; APlasmabound is the amount of plasma protein–ATR complex, μmol.

Model parameters

Values for physiological parameters, such as tissue volumes and blood flow, were from literature, i.e., Brown et al. (1997), and the body weight was from Ross et al. (2009). Dose-specific tissue/plasma distribution coefficients (PCs, otherwise known as tissue/plasma partition coefficients) were derived from the published time course data (Ross et al., 2009) and are included in the Appendix B. The PCs for ATR and DACT in liver, brain, and kidney were calculated as the ratio of the AUC of the tissue concentration to the AUC of the plasma concentration (Gentry et al., 2004; Mirfazaelian et al., 2006). AUCs were calculated using the trapezoidal rule (Perrier and Gibaldi, 1982). As a result, four sets of dose-specific PCs for both ATR and DACT in liver, brain, and kidney were obtained. For the model development, PCs based on the highest (250 mg/kg) dose of ATR were used. We chose the PCs from the 250 mg/kg dose to develop the model because the model was built based on the data set at the highest dose and then extrapolated to the lower doses. Due to limited data availability (Ross et al., 2009), the PCs for DE and DIP in the liver were calculated as the ratio of the 4-h time point concentration in the liver to that in the plasma. Due to lack of time course data for DE and DIP in the brain, the brain PCs for DE and DIP were set equal to that of ATR based on structural

similarity. The PCs for richly and slowly perfused tissues for ATR and its metabolites were assumed to be equal to those of liver and brain, respectively.

The elimination rate constants for DE, DIP, and DACT were estimated by visually fitting the simulated cumulative urine elimination amounts of DE, DIP, and DACT to the measured data, respectively.

Approximately 26% (18% to 37%) of plasma ATR is bound to plasma protein in rats at steady-state plasma concentrations of ATR between 0.14 and 1.85 μM (Lu et al., 1998), and approximately 1.5% of the total ATR and its Cl-TRIs are bound to RBC in rats given 30 mg/kg ATR po (Timchalk et al., 1990). Based on these data, in the present model, we assumed that the percent of DACT bound to plasma protein is equal to that of ATR, i.e., 26%. As there is no conclusive evidence that DE and DIP bind to hemoglobin and, compared to DACT, the amount of plasma DE and DIP is much smaller, we assumed that the 1.5% of the total ATR and its Cl-TRIs that bound to RBC was composed of ATR and DACT only. Of the total ATR and DACT bound to RBC, 99.3% was DACT, which was calculated based on the average AUC ratios of plasma DACT concentration to plasma ATR concentration (AUC_{DACT}/AUC_{ATR}). Using published data on the RBC volume for the mouse (Suckow et al., 2001), the concentrations of the RBC-bound ATR and RBC-bound DACT were calculated. Due to the lack of plasma protein and RBC binding relevant constants, we arbitrarily set all dissociation rate constants of plasma protein–ATR complex, plasma protein–DACT complex, RBC–ATR complex, and RBC–DACT complex to be 1. In addition, we assumed that the maximal binding capacities of RBC with ATR or DACT are 10-fold higher than the calculated concentrations of RBC–ATR complex and RBC–DACT complex. The maximal binding capacities of plasma protein with ATR and DACT were set equal to the maximal plasma concentration of ATR and DACT observed at the highest

dose level (250 mg/kg). After fixing the dissociation rate constants and maximal binding capacity constants, the association rate constants were estimated by manually adjusting to meet the criteria that approximately 26% of ATR and DACT in the plasma were bound the plasma protein and the simulated amounts of ATR and DACT that bound to RBC were close to the calculated amounts.

Currently, there are no reported in vivo metabolic rate parameters for ATR and its Cl-TRIs for rodents. A starting point for the estimation of the metabolic rate constants of ATR to DE, and ATR to DIP was an in vitro study with mouse liver microsomes (Hanioka et al., 1999b) as in vitro techniques have been shown to be a valuable a priori parameterization, with in vitro metabolic rates typically being 2- to 3-fold lower than corresponding in vivo values (Kramer et al., 2001). There are no in vitro data on the metabolic rate constants of DE to DACT and DIP to DACT, as, in vitro, the DE/DIP to DACT conversion is minimal across mammals (Lang et al., 1996; McMullin et al., 2003; Joo et al., 2010), including conversion by mouse microsomal preparations (Hanioka et al., 1998a; Hanioka et al., 1999b, a; Ross and Filipov, 2006). In the present mouse model, the in vivo hepatic oxidative metabolic parameters of ATR to DE and ATR to DIP were estimated by manually adjusting based on the corresponding in vitro metabolic rates, and optimal simulations of plasma concentrations for ATR and its Cl-TRIs were obtained when the in vivo metabolic rates were 2-fold higher than the in vitro metabolic rates. As for DE and DIP metabolism to DACT, we estimated the mouse's metabolic parameters based on the rat metabolic rates used in the most current PBPK model for ATR in the rat (McMullin et al., 2007b). Parameter estimations were performed where model outputs were visually fitted to experimental data. The values and units of the physiological parameters and chemical-specific parameters are provided in Tables 4.1-4.3.

Dose extrapolation

After calibration of the model at the 250 mg/kg dose (Fig. 4.2), the model was employed to simulate three additional lower doses (125, 25, and 5 mg/kg). Considering the absorption characteristics of ATR, which suggest that the absorption rate constant of ATR is inversely proportional to ATR dose (McMullin et al., 2003; McMullin et al., 2007b), we also used a higher K1 (0.3 h^{-1}) for the 5 mg/kg dose besides the K1 (0.14 h^{-1}) used for the three other (250, 125, and 25 mg/kg) doses. In addition, the tissue/plasma PCs derived from the time course data at the 5 mg/kg dose (Ross et al., 2009) were also incorporated into the model to simulate the kinetic behavior for the lowest dose (5 mg/kg) of ATR. The lowest (5 mg/kg) dose model simulations that used PCs determined from 250 mg/kg dose data were compared to the model simulations that used PCs derived from 5 mg/kg dose data, as shown on Figs. 4.3-4.6.

Model validation

Model validation was performed by incorporating pharmacokinetic data for mice and rats from previous studies that were not used in the present model development and parameter estimation. The same chemical-specific parameters utilized in the present mouse model as shown in Table 4.2 were employed to model the kinetics of ATR in both male C57BL/6 mice and female Sprague–Dawley rats reported in earlier experimental studies (Brzezicki et al., 2003; Ross and Filipov, 2006). In the rat model, the physiological parameters such as body weight, tissue volume, and blood flow were changed to rat-specific values based on Brown et al. (1997). The metabolic rates of ATR to DE, and ATR to DIP for rats used in the rat model were obtained using the same approach as the mouse model by setting the values of in vivo metabolic rates 2-fold to the corresponding in vitro metabolic rates determined in rat liver microsomes (Hanioka et al., 1999b), whereas the metabolic rates of DE and DIP to DACT were set same as

the rates in the mouse model due to lack of in vitro metabolic rates of DE to DACT and DIP to DACT. The criteria for a validated model suggested by Corley et al. (2005), namely, if the simulations are in reasonable agreement with the external experimental data (generally within a factor of two of the measured values and/or with similar kinetic behavior over the uptake, distribution, and clearance phases), the model is considered "validated", were adopted.

Sensitivity analysis

Sensitivity analysis was performed to identify critical model parameters with major influence on the AUC plasma and brain concentration of ATR and DACT. Each parameter was increased by 10% and the corresponding dose metrics were computed. Normalized Sensitivity Coefficients (NSCs) were calculated using the following equation (Evans and Andersen, 2000; Sweeney et al., 2003; Mirfazaelian et al., 2006):

$$NSC = \Delta r/r * p/\Delta P \quad (4.9)$$

where r is the response variable (e.g., AUC plasma concentration for ATR), Δr is the change of the response variable value, p is the value of the parameter of interest (e.g., PC of brain for ATR), and Δp is the change of the parameter value. Each model parameter was categorized as having low, medium, or high impact on the selected AUC plasma and brain concentration of ATR and DACT based on the following criteria (Yoon et al., 2009a): low: NSC < 0.2; medium: 0.2 ≤ NSC < 0.5; High: 0.5 ≤ NSC.

Results

Model Development

The PBPK model predictions of plasma, liver, and brain dosimetry of ATR and its Cl-TRIs were compared to measured data of mice dosed orally with 250 mg/kg ATR, as shown in Fig. 4.2. Initially, we set all the absorption rate constants (K1, K2, and K3) to be 1 and

incorporated the published in vitro metabolic rate constants of ATR to DE, and ATR to DIP determined using liver microsomes (Hanioka et al., 1999b) into the mouse model. The result was an overestimation of plasma ATR levels and an underestimation of plasma Cl-TRIs levels, which was the same problem that McMullin et al. (2007b) met after incorporation of the in vitro metabolic rate of ATR determined using rat hepatocytes (McMullin et al., 2007a) into the rat model. Next, we increased the in vivo metabolic rates of ATR to DE, and ATR to DIP 2-fold; incorporated the visually estimated metabolic rate constants of DE and DIP to DACT for the mouse; and slightly adjusted the absorption rate constants based on relevant data in the rat model (McMullin et al., 2003). These adjustments resulted in adequate description of plasma levels of ATR and its Cl-TRIs at the 250 mg/kg dose (Fig. 4.2). After model calibration for plasma ATR and its Cl-TRIs, we initially simulated the liver and brain levels of ATR and DACT with all PCs set to be 1, as it was assumed in the rat model published earlier (McMullin et al., 2007b). As a result, the liver level of ATR was greatly underestimated. We then incorporated the PCs calculated using the area method with data from Ross et al. (2009), which resulted in an adequate description of tissue levels of both ATR and DACT (Fig. 4.2). The calculated brain PC for ATR and the PCs for its Cl-TRIs were close to 1 (Table 4.2), therefore in line with the estimated PCs for ATR and its Cl-TRIs used in the rat PBPK model (McMullin et al., 2007b). On the other hand, the calculated liver and kidney PCs (51.81, 14.15 for the 250 mg/kg dose) for ATR are higher than the estimated PCs that were used in the rat PBPK model for ATR (approximately 1; McMullin et al., 2007b). Initial setting of all urine elimination rate constants to 1 resulted in underestimation of the cumulative urine elimination amount of Cl-TRIs. Visually fitting the simulations to actual data (Ross et al., 2009) resulted in adequate prediction when the Kurine values were set at 3, 1.5, and 20 h^{-1} for DE, DIP, and DACT, respectively (Fig. 4.6).

Dose Extrapolation

We built the model based on the time course data at the highest (250 mg/kg) dose and then performed dose extrapolation to the 125, 25, and 5 mg/kg doses. As shown in Fig. 4.2 and Fig. 4.3, the experimental dose–response plasma dosimetry data consistently agree with the 250 mg/kg-based model predicted levels for ATR and its Cl-TRIs across four dose levels. In addition, liver and brain concentrations of both ATR and DACT were well predicted across three doses (250, 125, and 25 mg/kg) but were somewhat underestimated at the lowest dose (5 mg/kg; Figs. 4.3-4.5). Based on earlier model assuming that lower doses of ATR exhibit higher absorption rate constants, i.e., 0.07 h^{-1} at 90 mg/kg vs. 0.2 h^{-1} at 30 mg/kg, in rats (McMullin et al., 2003), we increased the absorption rate constant (0.14 h^{-1} at 250, 125, and 25 mg/kg vs. 0.3 h^{-1} at 5 mg/kg) for the 5 mg/kg dose group. To better simulate the low-dose kinetics for ATR and its Cl-TRIs, we also incorporated the PCs derived from the dataset at the 5 mg/kg dose using the area method. This adjustment markedly improved the simulation of brain and liver DACT concentrations at 5 mg/kg dose, but the ATR liver and brain levels even though improved were still somewhat underestimated (Fig. 4.4 and Fig. 4.5).

Model Evaluation

Generally good agreements were obtained between model predicted and measured plasma concentrations of ATR and its Cl-TRIs during the absorption and distribution phase within 24 h after ATR administration at all four oral doses (Fig. 4.2 and Fig. 4.3). The experimental data showed apparent biphasic concentration curves for plasma ATR, with a first peak at 1 h and a minor second peak at 12 h post dosing at all doses. The present model simulates the first peak accurately, but it slightly underestimates the minor second peak. In addition, it appears that metabolism of ATR to DE and DIP may be not fast enough since the

elimination phase of the ATR curves seem to be flatten out more than the experimental data. Several approaches were undertaken to address this issue. For example, when we increased by 10-fold both the gastric absorption rate constant (K1) and the metabolic rate constants of ATR to DE, and ATR to DIP, rapid elimination of ATR from the plasma was indeed observed. However, tissue ATR, as well as plasma and urine dosimetry of Cl-TRIs, was sacrificed since tissue ATR was not eliminated as fast as plasma ATR, and plasma levels of Cl-TRIs were all substantially overestimated at the early time points (up to 12 h post ATR administration). More importantly, due to the increased K1, the cumulative urine elimination amounts of Cl-TRIs were also greatly overestimated. This is why this approach was abandoned. Overall, even with the underestimation of the second ATR peak observed experimentally, the model provides adequate prediction of plasma ATR across all four dose levels as the experimental and simulated AUCs are similar (Table B2, Appendix B).

As ATR was rapidly cleared from the plasma, the concentrations of DACT concomitantly increased and reached peak concentrations at 2 h post treatment at all dose levels. The model accurately simulated the formation and clearance of DACT across all doses (Fig. 4.2 and Fig. 4.3). The measured plasma DE and DIP levels showed complex concentration curves, with apparent biphasic curves at the three higher dose levels and almost straight line concentration curves at the lowest (5 mg/kg) dose. Regardless of the complex plasma behavior of DE and DIP, the model recapitulated the general distribution behaviors of both DE and DIP across all doses fairly accurately (Fig. 4.2 and Fig. 4.3).

Due to the extensive metabolism, complex pharmacokinetics, and multiple metabolites, predicting tissue dosimetry for ATR is challenging. The present model provided good simulations of liver and brain levels of ATR at the higher dose levels (250, 125 mg/kg) but

somewhat under predicted the tissue levels of ATR at low doses (25, 5 mg/kg) (Fig. 4.2, Fig. 4.4 and Fig. 4.5). On the other hand, the model simulated quite well the formation, distribution, and elimination phases of the most predominant metabolite, DACT, in both liver and brain within 24 h post dosing at all dose levels (Fig. 4.2, Fig. 4.4, and Fig. 4.5). Inclusion of 5 mg/kg-specific PCs in the model markedly improved the simulation of brain and liver ATR and DACT (Fig. 4.4 and Fig. 4.5).

In addition, the simulations of cumulative urinary excretion amounts of DACT, DE, and DIP at four dose levels were plotted and compared to the experimental observations, all of which showed a very good agreement (Fig. 4.6), with the urinary excretion rate constants for DE, DIP, and DACT set at 3, 1.5, and 20 h^{-1}, respectively, whereas the urinary elimination of ATR in the present mouse model, in agreement with the experimental data (Ross et al., 2009), was negligible.

Model Validation

Validation in mice using 3-month-old male C57BL/6 mouse data from (Ross and Filipov, 2006)

In this study, mice were exposed to four oral doses of ATR (250, 125, 25, and 5 mg/kg body weight) via same administration route/vehicle, and, ATR and its Cl-TRIs in the plasma were determined with the same method (LC-MS), short of minor optimizations, used in the study we used for model development (Ross et al., 2009). Model simulations of the plasma concentrations of ATR and DACT were plotted with experimental data and examples for the high (250 mg/kg) and low (5 mg/kg) doses are shown in Fig. 4.7. Plasma ATR levels were adequately simulated, whereas plasma DACT levels were simulated fairly well at the high dose but were somewhat under predicted at the low-dose levels.

Validation in rats using female Sprague Dawley rat data from (Brzezicki et al., 2003)

In this study, rats were given a single dose of 100 mg ATR/kg body weight in a different vehicle (1% methylcellulose). The measured plasma levels of ATR and DACT (by a different method, GS-MS) were compared to model predictions and are shown in Fig. 4.7. The model provided a similar disposition behavior of ATR in the plasma over absorption, distribution, and clearance phases, but the model simulation of plasma ATR was 3-fold higher than the experimental level. This may be due to the different metabolic rates of ATR between mice and rats as demonstrated in vitro (Hanioka et al., 1998a; Hanioka et al., 1999b, a), different analytical methods, sex-dependent differences, or slightly different absorption rates of ATR due to different administration vehicles. On the other hand, the model accurately predicted both the kinetic behavior and plasma level of the predominant metabolite DACT (Fig. 4.7).

Model application

The present model was expanded to simulate cumulative urinary DACT (cumulative for the first 24-h post exposure) amounts across a wide dose range, from 0.01 mg/kg to 1500 mg/kg, representing an environmentally relevant low exposure level (Battaglin et al., 2000) and an exceedingly high exposure level (Pommery et al., 1993), respectively. Since the gastric absorption constant is higher at the low dose ($K1 = 0.3\ h^{-1}$) than at the high dose ($K1 = 0.14\ h^{-1}$), we plotted two simulations with two different linear regression equations. As shown in Fig. 4.8, the model accurately predicted the experimentally determined urinary DACT amounts from 5 mg/kg to 250 mg/kg, with the low- and high-dose regression lines being closely aligned. This suggests a potential use of the model for reverse dosimetry application for an expanded dose range.

Sensitivity Analysis

NSCs were calculated for 53 model parameters for four dose metrics, including AUCs for plasma and brain concentrations of ATR and DACT. Of the 53 model parameters and 4 dose metrics, 212 NSCs were obtained. Of all these NSCs, only parameters with at least one absolute value of NSC more than or equal to 0.2 (Yoon et al., 2009a) were plotted and are presented in Fig. 4.9. All four dose metrics were moderately positively sensitive to the gastric absorption rate constant (K1) and intestinal absorption rate constant (K3) and were moderately negatively sensitive to the GI transfer rate constant (K2). AUCs for brain concentrations of ATR and DACT were highly positively sensitive to the PCs for brain of ATR and DACT (PBR and PBR3), which is biologically plausible (Mirfazaelian et al., 2006). AUCs for plasma concentrations of ATR and DACT were moderately positively sensitive to the maximal binding capacity of ATR and DACT in the plasma (BMaxplasmac and BMaxplasmac3) and the binding rate constants (KaATRplasma and KaDACTplasma) but were moderately negatively sensitive to the dissociation rate constants (KdATRplasma and KdDACTplasma). In addition, the metabolic rate of ATR to DIP (VmaxATR_DIP) was highly negatively sensitive, whereas the Michaelis–Menten constant (KmATR_DIP) was highly positively sensitive to the ATR-related dose metrics, but with little association with DACT-related dose metrics. Urine elimination rate constant (Kurine3) and the kidney volume (VKC) were highly negatively sensitive to the DACT-related dose metrics.

Discussion

Besides being the first mouse model for ATR and its Cl-TRIs, this PBPK model successfully simulates brain dosimetry across a wide dose range (250–5 mg/kg), which is a unique feature and can be used for a target site-specific dose–response considerations and for in

vitro to in vivo data extrapolation. Another major model characteristic is that the model accurately predicts the urinary concentration of each of the Cl-TRIs, including the concentration of the ATR's major metabolite DACT, over a wide dose range, suggesting the potential use of the model in reverse dosimetry analysis. Importantly, this model also incorporates simultaneous dose–response simulations of plasma, tissue, and urine dosimetry for ATR and its Cl-TRIs using linked sub-models via systemic circulation, which, compared to the already existing PBPK models for ATR in the rat (Timchalk et al., 1990; McMullin et al., 2003; McMullin et al., 2007b), is another unique feature.

After calibration using the 250 mg/kg dose group data, dose extrapolation was performed, which showed good simulations of plasma and tissue dosimetry of ATR and its Cl-TRIs at the 125 and 25 mg/kg dose levels, whereas tissue levels of ATR and DACT at the 5 mg/kg dose were somewhat underestimated. Incorporation of low-dose (5 mg/kg-specific) PCs only slightly improved simulations of plasma levels of ATR and its Cl-TRIs, but it did improve substantially liver and brain ATR and, particularly, DACT simulations. These results suggest that if low-dose exposure modeling is the goal, use of low-dose-specific PCs will result in more accurate predictions of actual tissue, including target organ, i.e., brain, dosimetry. The underestimation of the tissue levels of ATR and DACT using 250 mg/kg-specific PCs based PBPK model for the low-dose ATR could mean the binding properties of ATR and DACT with tissue proteins may not be described adequately due to the lack of concrete evidence in mammals that ATR could bind to tissues. Based on our pharmacokinetic data (Ross et al., 2009) and the model simulations, we hypothesize that portions of ATR and DACT in tissues, such as liver and brain, are bound to tissue proteins and not available for systemic circulation, which is apparent particularly at the low dose. In this regard, several pesticides, such as pentachlorophenol, thiocarbamate, and

molinate, have been demonstrated to be able to bind to tissue proteins (Tsai et al., 2003; Zimmerman et al., 2004; Campbell et al., 2008). Importantly, studies with pituitary cells have identified several proteins as targets for covalent modification by DACT (Dooley et al., 2008). In addition, a very recent study has identified stable DACT-protein adducts in the brains of rats orally exposed to ATR (Dooley et al., 2010), thus presenting the distinct possibility that DACT and perhaps ATR bind to proteins in multiple tissues, including the liver and the brain. The underestimation of ATR tissue levels at low doses may also reflect the inadequacy of the detection limits of the analytical methods for measuring low concentrations of ATR and its Cl-TRIs in tissues as we have discussed earlier (Ross and Filipov, 2006; Ross et al., 2009).

An important goal of this model was to lay the foundation for cross-species (rats and, eventually, humans) extrapolation and dosimetry simulations. As a first step, the present model shows successful simulation of plasma DACT in rats receiving 100 mg/kg ATR po by changing the physiological parameters to be rat-specific and using the rat-specific metabolic rates of ATR to DE and to DIP. This indicates that the model can be used for species extrapolation since DACT is the apparent final and predominant ATR metabolite across several mammalian species. In order to extend the model to low-dose ATR exposure for humans, more data such as (1) the binding characteristics of low concentration ATR and DACT with tissue proteins, especially in the liver and brain; (2) pharmacokinetic data of rodents receiving low-dose ATR, less than 5 mg/kg (for analyzing such data, more sensitive analytical methods need to be used/developed); and (3) detailed urinary metabolite profile data from humans with known recent exposure to ATR, are needed.

Due to the relatively high (for a small molecule) molecular weight (more than a 100 Da) of ATR (215.69) and DACT (145.55), we tried to refine the current flow-limited model by using

a modified asymmetric diffusion-limited PBPK model, which incorporated the asymmetric permeability area cross product (PA term) into each compartment for ATR and DACT sub-models. Although the tissue dosimetry simulations of brain and liver for ATR and DACT sub-models were slightly improved across the entire dose range (data not shown), the plasma and urine simulations were almost identical to the simulations achieved with the simpler flow-limited model. Due to the increased variability of the asymmetric diffusion-limited model, which contained 20 more estimated PA terms than the present flow-limited model, and the fact that the overall simulations in the revised model were only slightly improved, we concluded that the simpler flow-limited model is appropriate for ATR and is in line with previous ATR PBPK models for rats (Timchalk et al., 1990; McMullin et al., 2003; McMullin et al., 2007b). Moreover, this simpler flow-limited model assumption has worked well for a variety of chemicals, including drugs (Bjorkman, 2003), solvents (Andersen, 1995), and, importantly, other herbicides (Evans et al., 2008).

At present, there are three ATR PBPK models for the rat and none for the mouse. The available rat models have been very helpful in revealing some of the pharmacokinetic characteristics of ATR in the rat, with the latest model (McMullin et al., 2007b) successfully describing plasma dosimetry of ATR and its Cl-TRIs. However, the existing models have several drawbacks, in part due to lack of experimental data. For example, they do not include target organs, such as the brain, as separate compartments, nor do they consider dose–response relationship in the modeling process. Compared to the rat models, our mouse model describes the pharmacokinetics for ATR in greater detail, especially the absorption characteristics of ATR and the urinary elimination characteristics of its individual metabolites, including its primary metabolite DACT.

Our model suggests that at low doses, dose-dependent parameterization for oral uptake, as shown in Table 4.2, may be necessary. A single gastric absorption rate can be used for doses of 25 mg/kg and higher, but this parameter is best to be increased for simulations of low (5 mg/kg) dose kinetics. Thus, in our model, the gastric absorption rate ($K1 = 0.3\ h^{-1}$) for the 5 mg/kg dose was 2-fold higher than that ($K1 = 0.14\ h^{-1}$) of the higher doses (250, 125, and 25 mg/kg). McMullin et al. (2003) arrived at similar conclusions when constructing their rat PBPK model, i.e., in the rat, the gastric absorption rates were estimated to be $0.07\ h^{-1}$ at 90 mg/kg vs. $0.2\ h^{-1}$ at 30 mg/kg. This dose-dependent absorption property is not unique to ATR, as it has been observed in other chemicals, such as isopropanol (Clewell et al., 2001). The causes of this dose-dependent absorption characteristic of ATR are unknown but may be related to an effect of higher doses of ATR on gastric absorption or gastric emptying. On the other hand, the absorption rate of environmentally relevant doses that are often much lower than 5 mg/kg may be greater than $0.3\ h^{-1}$. Thus, more kinetic data of low-dose ATR exposure in rodents are needed in order to optimize the model for environmentally relevant dose modeling.

In the most recent rat model, the authors incorporated in vitro metabolic rates of ATR to DE and DIP into the model development and assumed that there is approximately 64% of ATR eliminated via intestinal metabolism since incorporation of in vitro kinetic constants alone consistently underestimated the plasma levels of Cl-TRIs while overestimating the plasma level of ATR. However, our study with human intestinal microsomes demonstrates that intestinal metabolism of ATR by enterocytes is not measurable (Fig. B1, Appendix B). Moreover, there is no evidence that ATR can be metabolized to DE, DIP, or DACT by cytochrome P450s present in the normal gut flora. While certain soil and water bacteria degrade ATR quite efficiently by hydrolytic dechlorination and are considered for bioremediation purposes (Rousseaux et al.,

2001; Satsuma, 2009; Govantes et al., 2010), mammalian gut flora bacteria, such as *E. coli*, do not. However, they can be engineered and reprogrammed to do so, which is another strategy for ATR elimination from the environment that may be employed in the future (Sinha et al., 2010). Based on these observations and the fact that ATR is metabolized similarly by rat, mouse, pig, and human liver microsomes, i.e., DE and DIP are the two major in vitro cytochrome P450 metabolites (Lang et al., 1996; Hanioka et al., 1998a; Hanioka et al., 1999b, a; Ross and Filipov, 2006; McMullin et al., 2007a; Joo et al., 2010), we did not include intestinal metabolism in our model. Rather, we incorporated in vivo metabolic rates of ATR that are 2-fold higher than the reported mouse-specific in vitro values. This approach resulted in adequate plasma dosimetry simulation of ATR and, importantly, is in line with a study demonstrating that in vivo metabolic rates can be 2- to 3-fold higher than in vitro values (Kramer et al., 2001). Furthermore, although in vitro techniques could be a valuable a priori parameterization for PBPK modeling (Kramer et al., 2001), differences in binding characteristics, as well as an apparent differential metabolic capacity for ATR, between in vitro and in vivo might be contributing to these different metabolic rates, signifying the need for metabolic rate optimization.

A major unique feature of the present ATR PBPK model is the inclusion of a dose-dependent urinary clearance of individual Cl-TRIs metabolites. Inclusion and successful simulation of urinary clearance of individual metabolites, particularly DACT, are critical because the model could be used to establish urine as an appropriate surrogate matrix for reverse dosimetry analysis of ATR in a dose-dependent manner. DACT has been recommended to be the best candidate metabolite to conduct future biomonitoring studies (Barr et al., 2007; Ross et al., 2009). However, the disadvantage of using DACT as a biomarker is its lack of specificity since DACT is also formed from other structurally related triazine herbicides, such as simazine

(Adams et al., 1990). Therefore, DACT by itself cannot be used to predict type of exposure. Nonetheless, once the exposure type, i.e., ATR, is known, DACT would be very good biomarker for ATR exposure and for estimation of target tissue levels because of its abundance. With the help of the current model, cumulative urine excretion DACT over a defined period of time, i.e., 24 h, can be used to predict ATR exposures over a wide dose range, including doses representative of environmentally relevant, low-level exposures (Battaglin et al., 2000). Compared to plasma, urine samples are relatively easier to collect. Thus, using urinary biomarker of exposure has practical applications in aiding the risk assessment process for ATR.

The model described here also differs from other published models in that it can be used as a quantitative tool to predict internal brain concentrations of ATR and DACT. This will help in assessing the contribution of ATR and DACT to the neurotoxicity of ATR over a wide dose range since the model provides generally good simulations of brain dosimetry of both ATR and DACT. Several studies have demonstrated that ATR exposure is detrimental to nervous system in both the rats (Rodriguez et al., 2005) and mice (Filipov et al., 2007). Although the exact mode of action of ATR in the brain is still unclear, our recent study has demonstrated that ATR is perhaps the primary compound that acutely affects the brain (inhibition of vesicular dopamine uptake) as observed using isolated synaptic vesicles (Hossain and Filipov, 2008). While ATR may be responsible for the acute effects, our current model and the recently published pharmacokinetic study (Ross et al., 2009) indicate that, compared to ATR, much greater amounts of DACT are present in the brain. Thus, the chronic and long-term effects of ATR exposure may be caused by potential protein-damaging properties of DACT since several studies have demonstrated that both ATR and DACT can covalently bind with proteins, such as albumin and hemoglobin, and form stable protein adducts. Importantly, DACT also forms protein adducts

with pituitary and brain proteins that play important homeostatic roles (Lu et al., 1998; Dooley et al., 2006; Dooley et al., 2007; Dooley et al., 2008; Dooley et al., 2010). This mechanism, however, needs further investigation, especially within the brain.

Besides effects on the nervous system, ATR exposure can adversely affect immune organs, such as thymus and spleen (Pruett et al., 2003; Filipov et al., 2005; Karrow et al., 2005; Rowe et al., 2006), as well as reproductive organs, such as testis (Victor-Costa et al., 2010), of laboratory rodents. The physiological parameters of these organs can be easily obtained from the literature, i.e., Brown et al. (1997) and, with some additional organ-specific tissue dosimetry data, our model could be extended to incorporate simulation of tissue dosimetry of ATR and its Cl-TRIs in additional target organs.

In conclusion, we have developed the first mouse PBPK model for ATR and its Cl-TRIs. The mouse model improves existing rat models by incorporating dose–response simulations and by accurately describing liver, brain, and urine levels of ATR and its Cl-TRIs over a broad dose range. This model can be used in internal (target organ) dosimetry prediction and as an aid in the exposure assessment process for different dosage and exposure scenarios to this widely used herbicide. Finally, the model can employ urinary metabolite data as a surrogate matrix for reverse dosimetry analysis.

Conflict of interest statement

The authors declare that there are no conflicts of interest.

Acknowledgements

We thank Dr. Sheppard A. Martin and Dr. Shuang Li from the Department of Environmental Health Science, College of Public Health, University of Georgia, Athens, GA, for modeling assistance.

Table 4.1. Physiological parameters used in the model development.

Parameter	Description	Values chosen	Source
Blood flows			
QCC	Cardiac output (l/h/kg0.75)	16.5	Brown et al. (1997)
QLC	Fraction of blood flow to liver (unitless)	0.161	Brown et al. (1997)
QBRC	Fraction of blood flow to brain (unitless)	0.033	Brown et al. (1997)
QKC	Fraction of blood flow to kidney (unitless)	0.091	Brown et al. (1997)
QR	blood flow to richly perfused tissue		QR = 0.76*QC-QL-QK
QS	blood flow to slowly perfused tissue		QS = 0.24*QC-QBR
QR1	blood flow to richly perfused tissue (specific to DE and DIP sub-models)		QR1 = 0.76*QC-QL
Tissue volumes			
BW	Body weight (kg)	0.0253	Ross et al. (2009)
VLC	Fraction liver tissue (unitless)	0.0549	Brown et al. (1997)
VBRC	Fraction brain tissue (unitless)	0.0165	Brown et al. (1997)
VKC	Fraction kidney tissue (unitless)	0.0167	Brown et al. (1997)
VbloodC	Fraction blood volume (unitless)	0.049	Brown et al. (1997)
VR	Richly perfused tissue volume		VR = 0.09*BW-VL-VK
VS	Slowly perfused tissue volume		VS = 0.82*BW-VBR
VR1	Richly perfused tissue volume(specific to DE and DIP sub-models)		VR1= 0.09*BW-VL

Table 4.2. Chemical-specific parameters used for the developing of PBPK model of ATR in mice.

Parameter		ATR	DE	DIP	DACT
Partition/Distribution coefficients (PCs)[a]					
PL[b]	Liver:blood PC	51.81 (78.09)	1.89 (5)	0.42 (6.4)	0.63 (2.11)
PBR[b]	Brain:blood PC	0.48 (2.08)	0.48 (0.48)	0.48 (0.48)	0.55 (2.08)
PK[b]	Kidney:blood PC	14.15 (125.36)	-	-	0.29 (1.83)
PR[c]	Richly perfused tissue:blood PC	51.81 (78.09)	1.89 (5)	0.42 (6.4)	0.63 (2.11)
PS[d]	Slowly perfused tissue:blood PC	0.48 (2.08)	0.48 (0.48)	0.48 (0.48)	0.55 (2.08)
Absorption constants					
K1[e] (h^{-1})	Gastric absorption rate constant	0.14	-	-	-
K2 (h^{-1})	Gastric-emptying rate constant	1	-	-	-
K3 (h^{-1})	Intestinal absorption rate constant	0.01	-	-	-
Elimination constants					
Kurine (h^{-1})	Urine excretion constant	-	3	3	20
Plasma protein binding					
Bmax[f] (μmol)	Maximal binding capacity	2.79	-	-	109.76
Ka (/(h*μmol))	Association rate constant	180	-	-	5
Kd (h^{-1})	Dissociation rate constant	1	-	-	1
Red blood cell binding					
Bmax[g] (μmol)	Maximal binding capacity	59	-	-	8439
Ka (/(h*μmol))	Association rate constant	720	-	-	5
Kd (h^{-1})	Dissociation rate constant	1	-	-	1

- Indicates parameter not included in the model. [a] PC values in parentheses represent PCs determined from the 5 mg/kg dose group data. [b] Unitless, calculated. [c] Unitless, set equal to liver. [d] Unitless, set equal to brain. [e] K1 = 0.3 h^{-1} at the 5 mg/kg dose group. [f] Set equal to maximal plasma concentrations of ATR and DACT observed at the highest dose level (250 mg/kg). [g] Set to be 10 fold of the calculated concentrations of ATR and DACT bound to RBC.

Table 4.3. Hepatic metabolic parameters of ATR, DE and DIP in mice used in the model and determined in vitro.

	Vmaxc (in vivo)[a]	Vmax (in vivo)[b]	Km (in vitro)[c]	Vmax (in vitro)[d]	Vmax (in vivo)/Vmax (in vitro)
ATR to DE	139.67	8.86	52.5[a]	4.43	2
ATR to DIP	406.07	25.76	29.5[a]	12.88	2
DE to DACT	14	0.89	13[e]	-	-
DIP to DACT	42	2.66	13[e]	-	-

[a] Estimated, scalable by $(BW)^{0.75}$, μmol/h/$kg^{0.75}$. [b] Estimated, for 0.0253 kg mouse, μmol/h. [c] Hanioka et al. (1999b), μM. [d] Hanioka et al. (1999b), μmol/h. Description about the unit conversion from pmol/min/mg protein to μmol/h is shown in Appendix B. [e] McMullin et al. (2007b), μM.

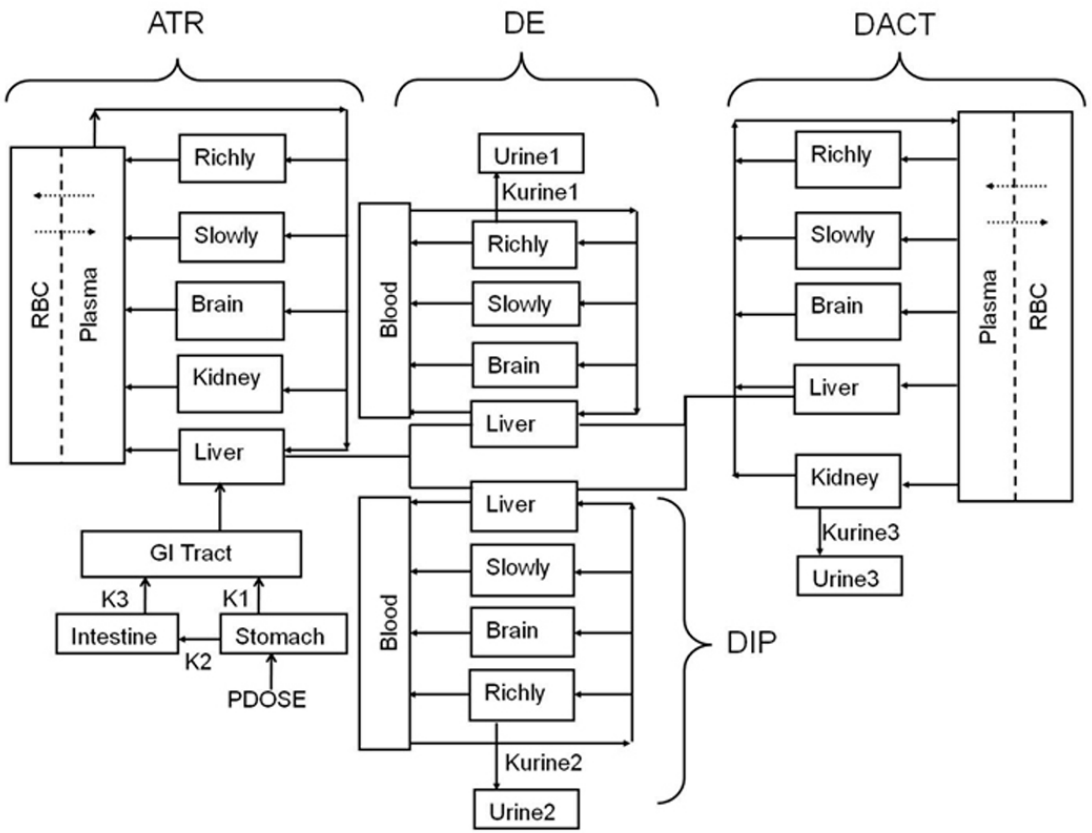

Figure 4.1. Physiologically based pharmacokinetic (PBPK) model structure for ATR (atrazine) and its main chlorotriazine metabolites: DE (desethyl atrazine), DIP (desisopropyl atrazine), and DACT (didealkyl atrazine) in male C57BL/6 mice exposed to ATR orally.

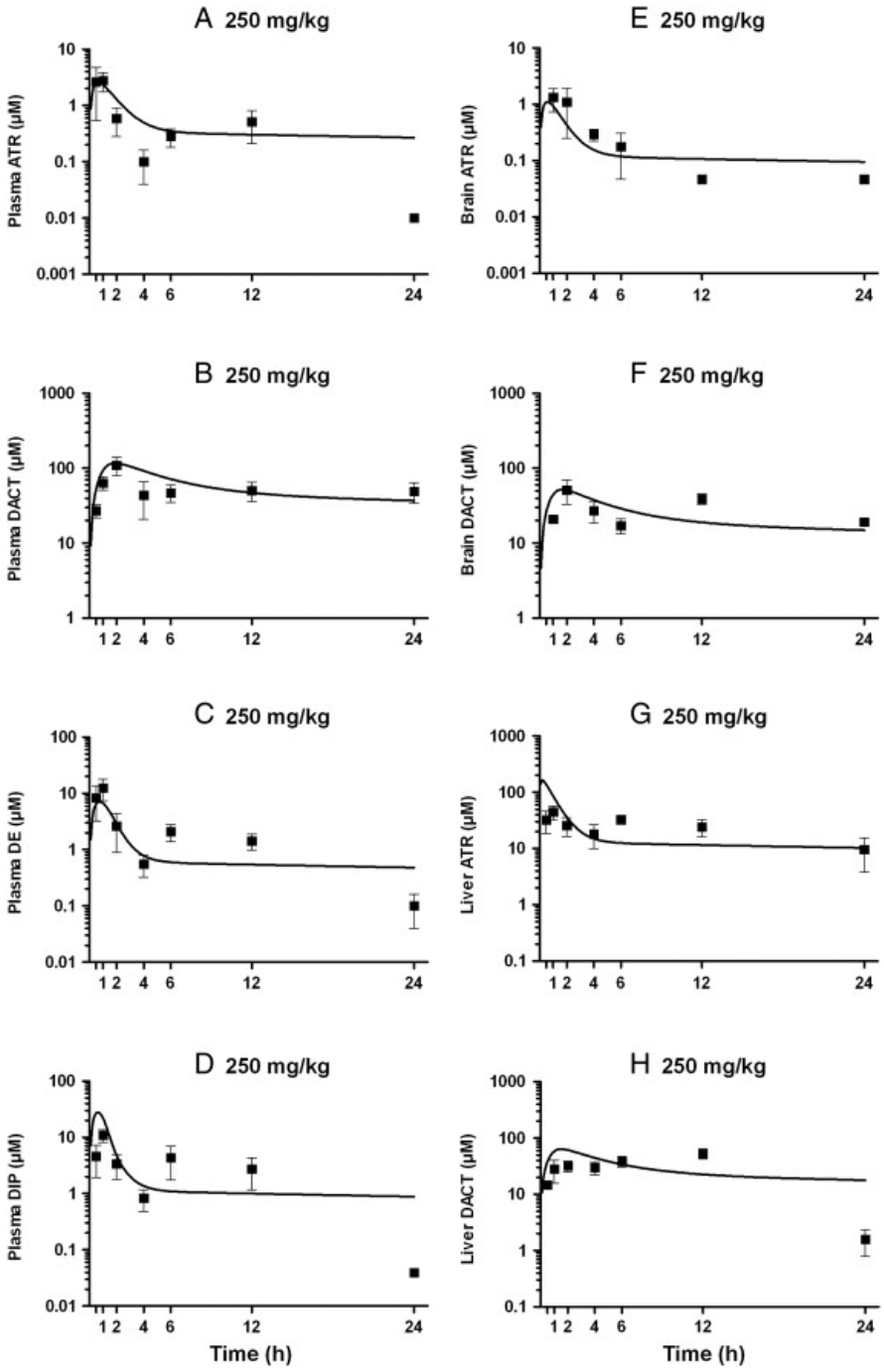

Figure 4.2. Model predictions (solid lines) and measured levels (■) (Ross et al., 2009) of ATR and DACT in the plasma (A-B), brain (E-F) and liver (G-H), and of DE and DIP in the plasma (C-D), of mice dosed po with 250 mg/kg ATR. Solid lines represent model simulations using PC values determined from the 250 mg/kg dose.

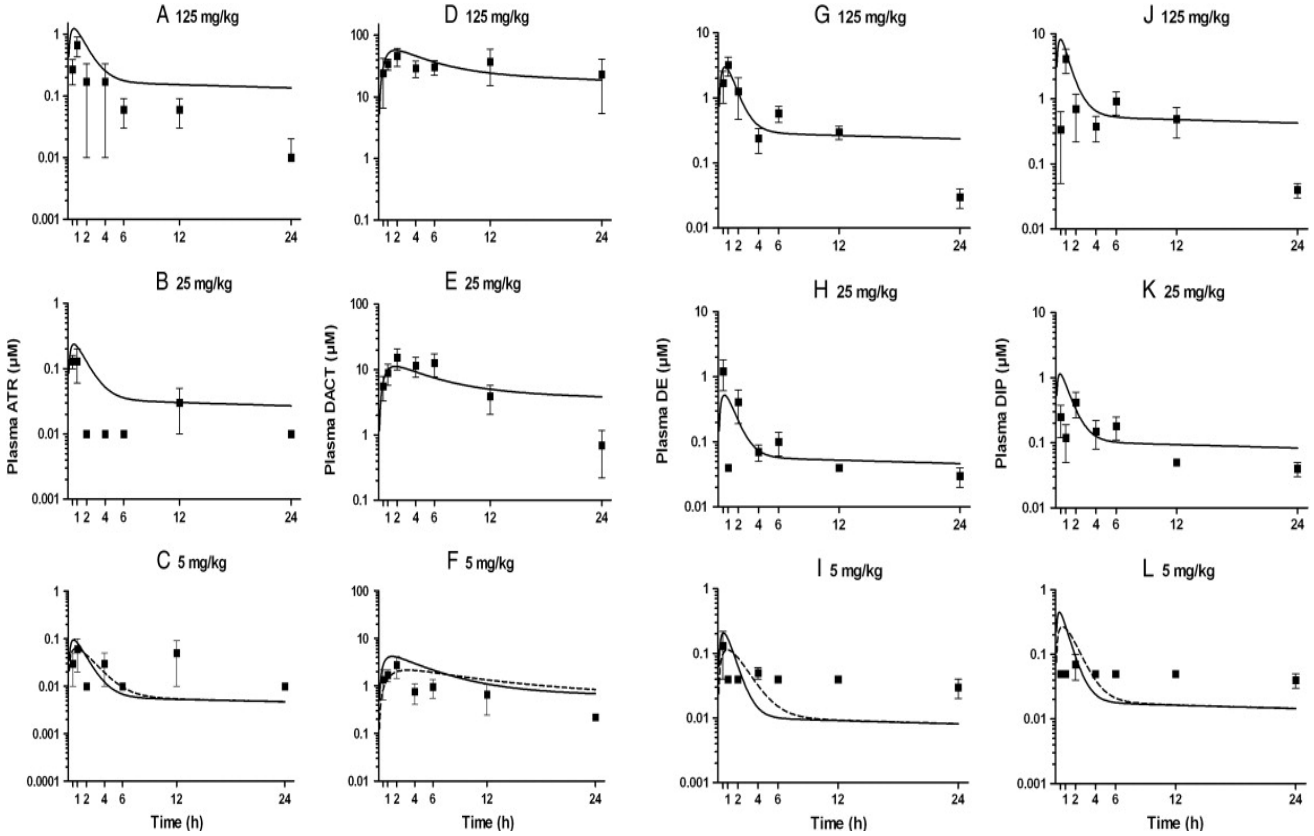

Figure 4.3. Model predictions (solid and dashed lines) and measured levels (■) (Ross et al., 2009) of plasma concentrations of ATR (A-C), DACT (D-F), DE (G-I) and DIP (J-L) in mice dosed po with three single dose levels of 125, 25, and 5 mg/kg ATR, respectively. Solid lines represent model simulations using PC values determined from a 250 mg/kg dose. Dashed lines represent model simulations using PC values determined from a 5 mg/kg dose.

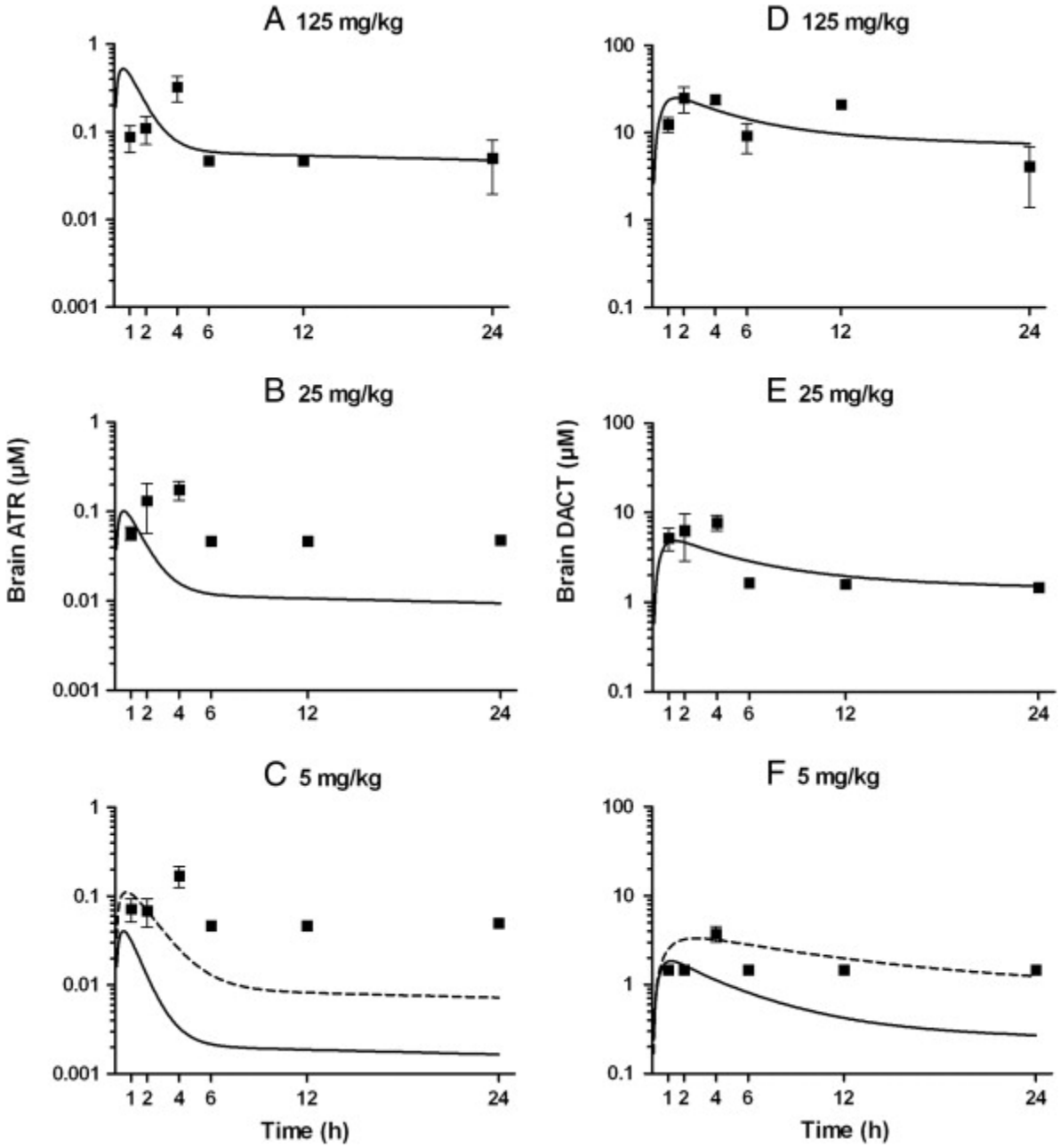

Figure 4.4. Model predictions (solid and dashed lines) and measured levels (■) (Ross et al., 2009) of brain concentrations of ATR (A-C), and DACT (D-F) in mice dosed po with three single dose levels of 125, 25, and 5 mg/kg ATR, respectively. Solid lines represent model simulations using PC values determined from a 250 mg/kg dose. Dashed lines represent model simulations using PC values determined from a 5 mg/kg dose.

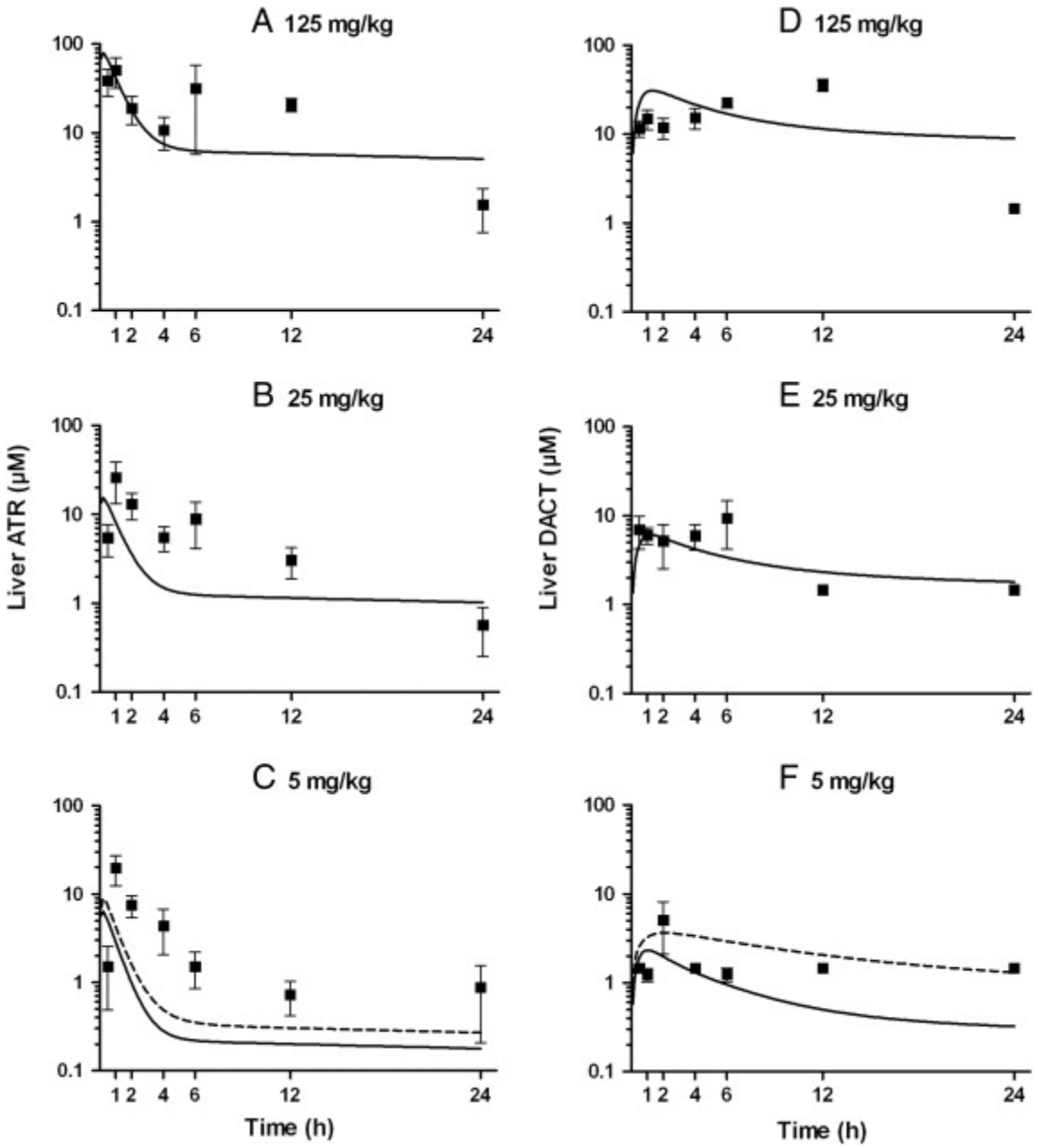

Figure 4.5. Model predictions (solid and dashed lines) and measured levels (■) (Ross et al., 2009) of liver concentrations of ATR (A-C), and DACT (D-F) in mice dosed po with three single dose levels of 125, 25, and 5 mg/kg ATR, respectively. Solid lines represent model simulations using PC values determined from a 250 mg/kg dose. Dashed lines represent model simulations using PC values determined from a 5 mg/kg dose.

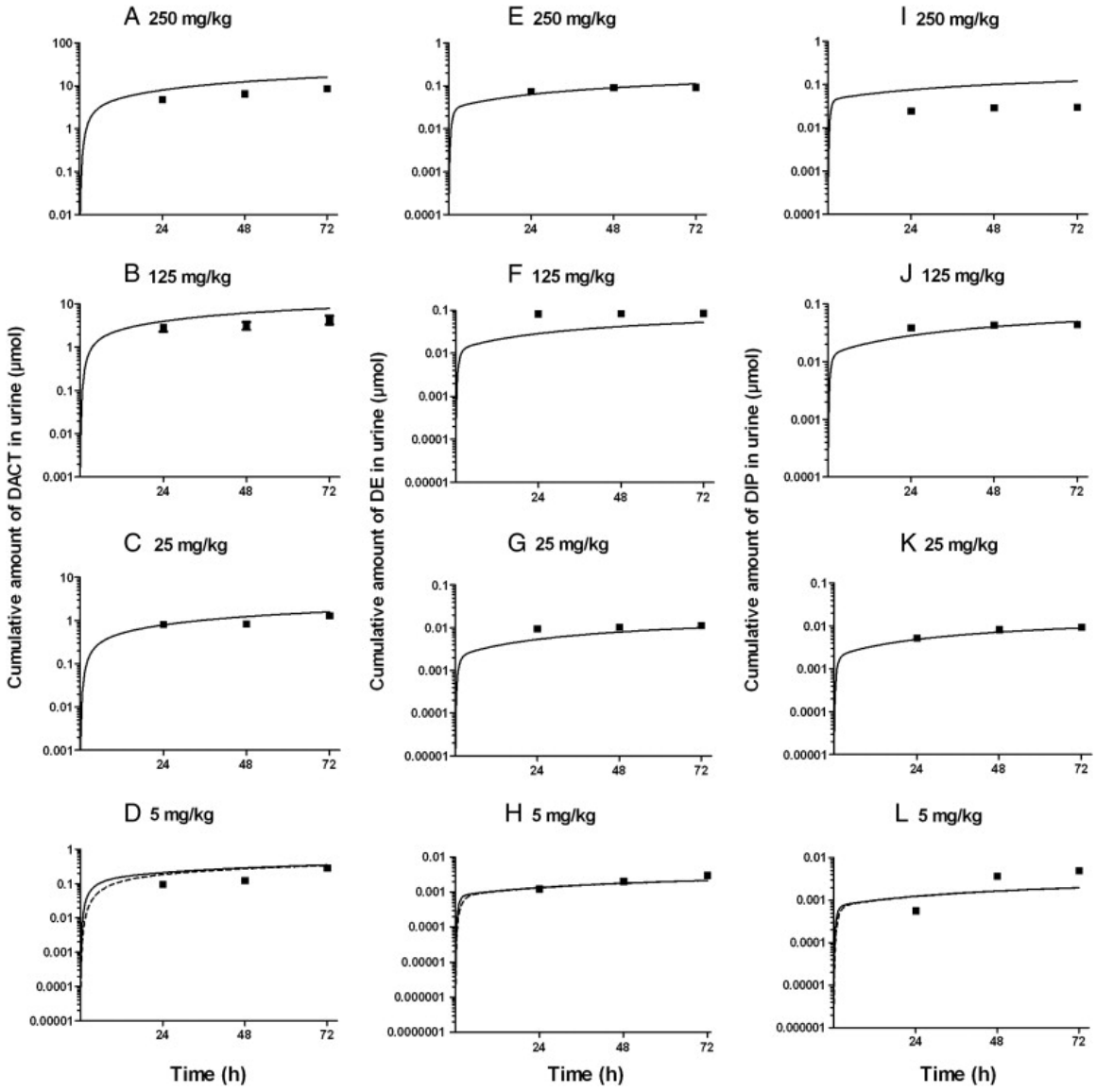

Figure 4.6. Model predictions (solid and dashed lines) and measured levels (■) (Ross et al., 2009) of cumulative urine excretion amount of Cl-TRIs: DACT (A-D), DE (E-H) and DIP (I-L) in mice dosed po with four single dose levels of 250, 125, 25 and 5 mg/kg, respectively. Solid lines represent model simulations using PC values determined from a 250 mg/kg dose. Dashed lines represent model simulations using PC values determined from a 5 mg/kg dose.

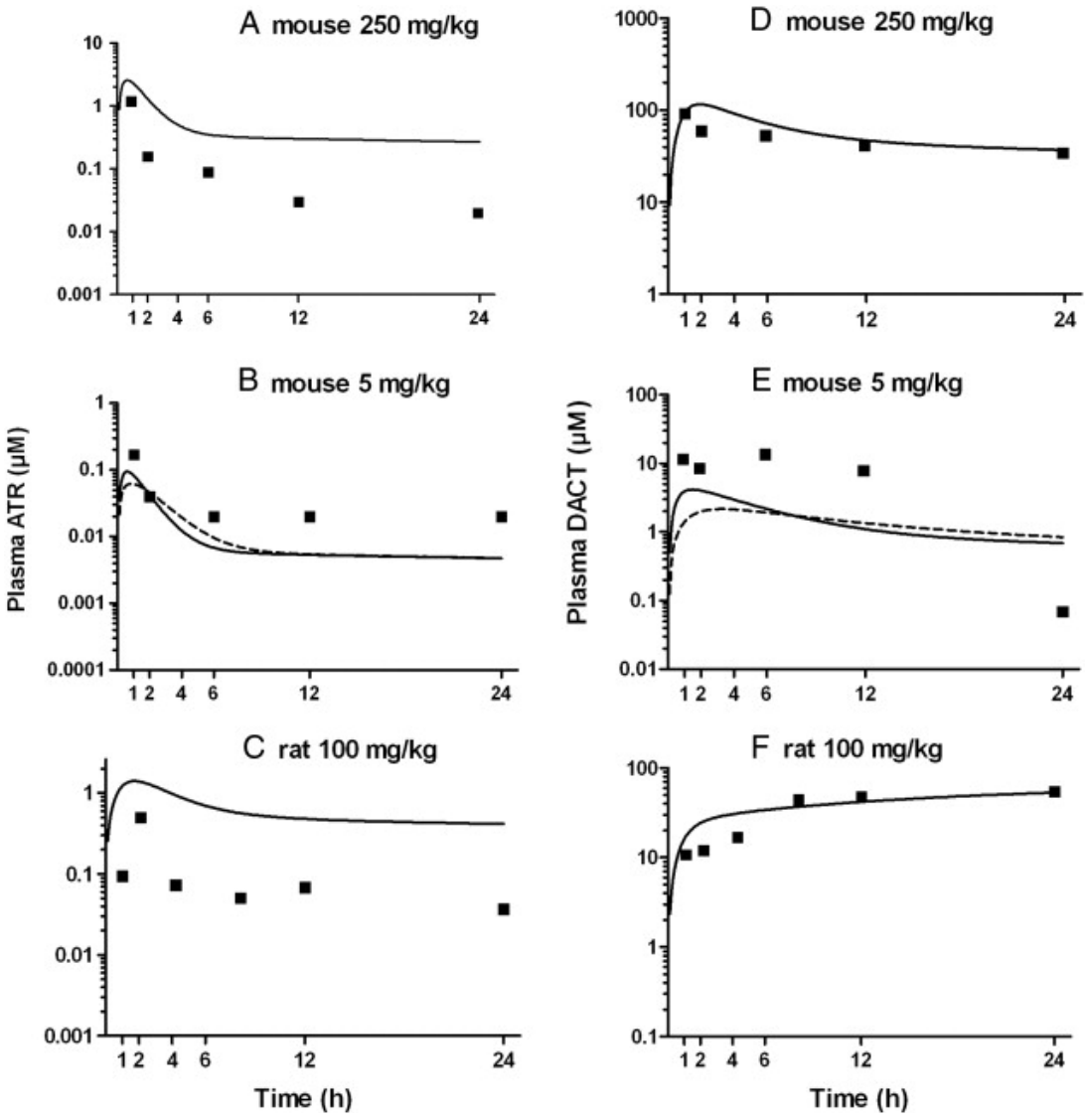

Figure 4.7. Model predictions (solid and dashed lines) and measured levels (■) of plasma concentrations of ATR (A-C), and DACT (D-F) for a male C57BL/6 mouse dosed po with 250 or 5 mg/kg ATR (Ross and Filipov, 2006), and for a female Sprague Dawley rat dosed po with 100 mg/kg ATR (Brzezicki et al., 2003), respectively. These data were used for model validation. Solid lines represent model simulations using PC values determined from a 250 mg/kg dose. Dashed lines represent model simulations using PC values determined from a 5 mg/kg dose.

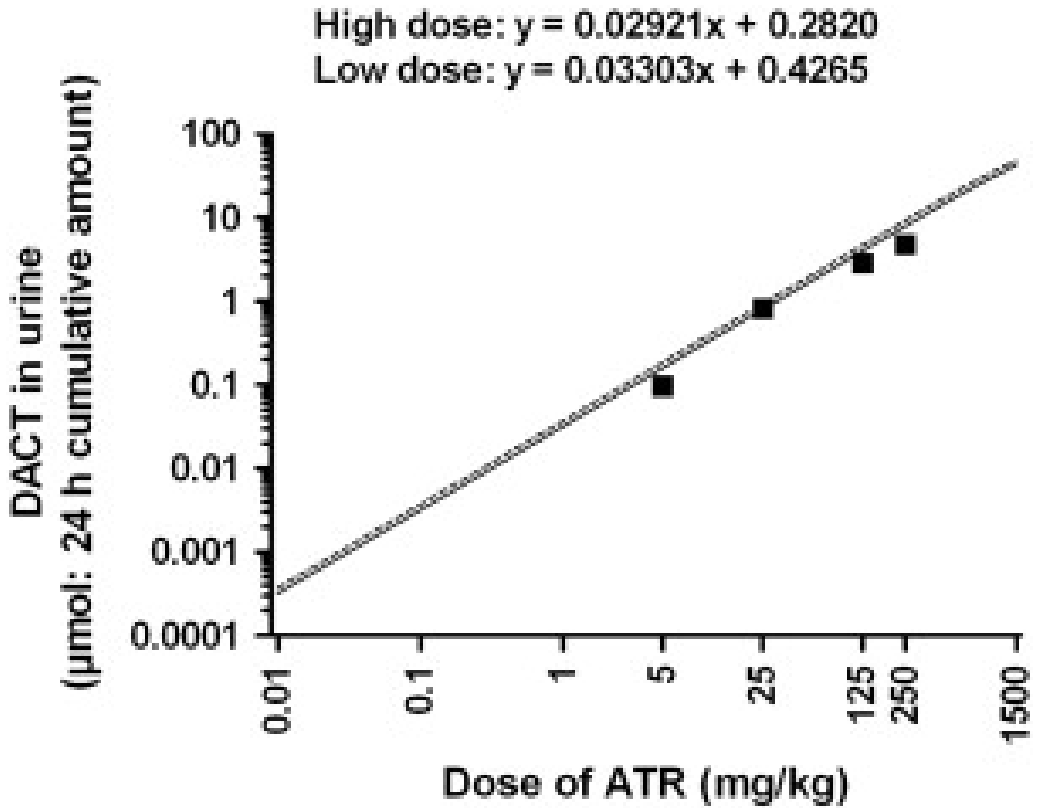

Figure 4.8. Simulations of a dose-dependent 24-h cumulative urine elimination amount of DACT across a wide ATR dose range (0.01 to 1500 mg/kg). Each time point represents the measured cumulative levels (■) of DACT in a 24-h urine sample (Ross et al., 2009). Solid line represent model simulations using PC values determined from a 250 mg/kg dose, with K1 = 0.14. Dashed lines represent model simulations using PC values determined from a 5 mg/kg dose, with K1 = 0.3. Regression equations from the two simulations (high dose and low dose are also included in the figure).

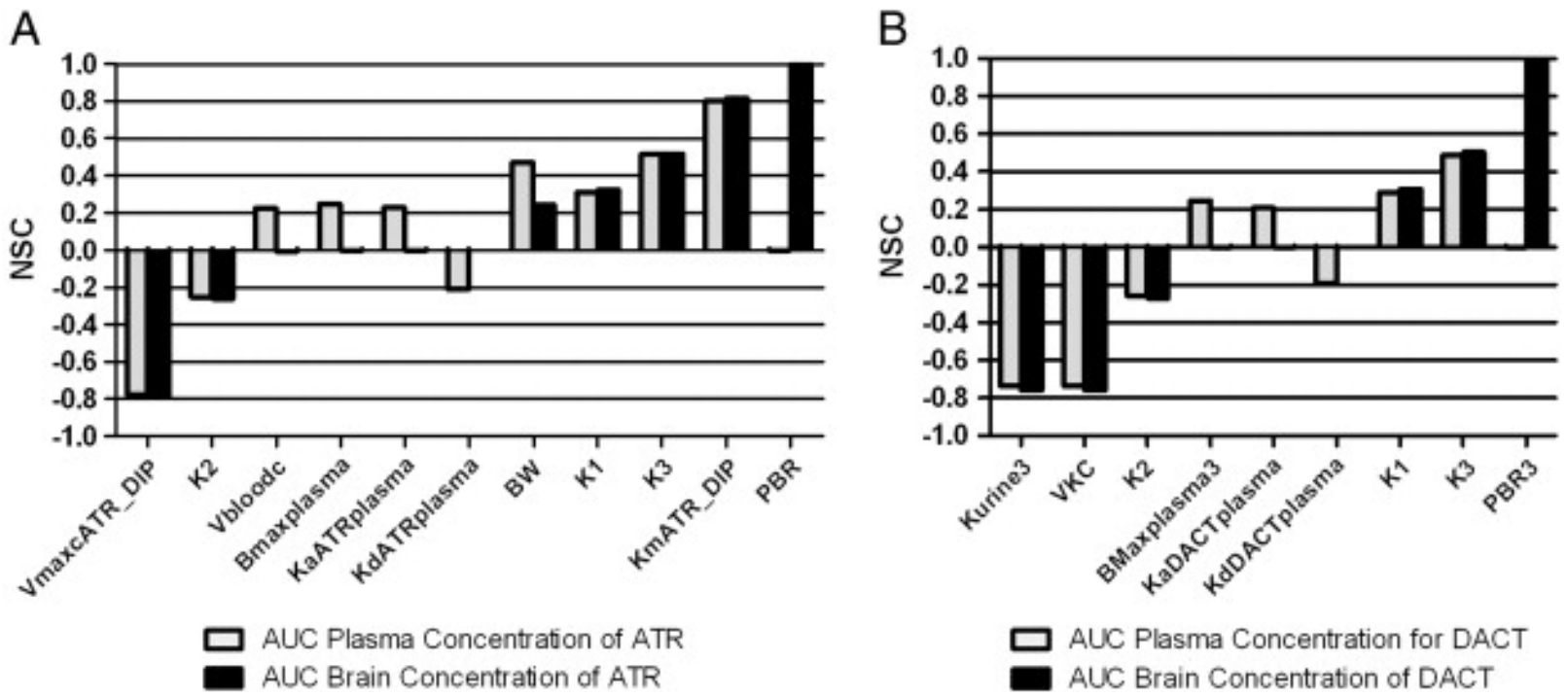

Figure 4.9. Normalized Sensitivity Coefficients (NSCs) for several model parameters using AUCs for plasma and brain ATR (A) and DACT (B) concentrations as the dose metrics. The simulations were based on the 250 mg/kg dose. Only parameters with at least one absolute value of NSC greater than 0.2 are presented.

CHAPTER 5

ESTIMATION OF PLACENTAL AND LACTATIONAL TRANSFER AND TISSUE DISTRIBUTION OF ATRAZINE AND ITS MAIN METABOLITES IN RODENT DAMS, FETUSES, AND NEONATES WITH PHYSIOLOGICALLY BASED PHARMACOKINETIC MODELING[1]

[1] Lin, Z., Fisher, J.W., Wang, R., Ross, M.K., Filipov, N.M. 2013. Toxicology and Applied Pharmacology. 273(1):140-158. Reprinted here with permission of the publisher.

Abstract

Atrazine (ATR) is a widely used chlorotriazine herbicide, a ubiquitous environmental contaminant, and a potential developmental toxicant. To quantitatively evaluate placental/lactational transfer and fetal/neonatal tissue dosimetry of ATR and its major metabolites, physiologically based pharmacokinetic models were developed for rat dams, fetuses and neonates. These models were calibrated using pharmacokinetic data from rat dams repeatedly exposed (oral gavage; 5 mg/kg) to ATR followed by model evaluation against other available rat data. Model simulations corresponded well to the majority of available experimental data and suggest that: (1) the fetus is exposed to both ATR and its major metabolite didealkylatrazine (DACT) at levels similar to maternal plasma levels, (2) the neonate is exposed mostly to DACT at levels two-thirds lower than maternal plasma or fetal levels, while lactational exposure to ATR is minimal, and (3) gestational carryover of DACT greatly affects its neonatal dosimetry up until mid-lactation. To test the model's cross-species extrapolation capability, a pharmacokinetic study was conducted with pregnant C57BL/6 mice exposed (oral gavage; 5 mg/kg) to ATR from gestational day 12 to 18. By using mouse-specific parameters, the model predictions fitted well with the measured data, including placental ATR/DACT levels. However, fetal concentrations of DACT were overestimated by the model (10-fold). This overestimation suggests that only around 10% of the DACT that reaches the fetus is tissue-bound. These rodent models could be used in fetal/neonatal tissue dosimetry predictions to help design/interpret early life toxicity/pharmacokinetic studies with ATR and as a foundation for scaling to humans.

Keywords: Atrazine, PBPK modeling, Pesticides, Developmental toxicity, Pregnancy, Lactation

Introduction

Atrazine [ATR; 2-chloro-4-(ethylamino)-6-(isopropylamino)-s-triazine, CAS# 1912-24-9] is a chlorotriazine herbicide used extensively on crops to control broadleaf weeds (EPA, 2003). Due to its widespread use, relative persistence in water (ATSDR, 2003) and extreme persistence in soil (Jablonowski et al., 2009), ATR is ubiquitous in the environment (Battaglin et al., 2009).

Possible exposure sources for ATR include contaminated air (dust), food, and drinking water (García et al., 2012; Lozier et al., 2012; Mosquin et al., 2012). Surface and drinking water ATR concentrations (up to 224 and 34 μg/L, respectively) in places with heavy ATR use, such as the Midwestern U.S., substantially exceed current maximum contaminant levels (MCL), i.e., 3 and 0.1 μg/L in U.S. and Europe, respectively (ATSDR, 2003; Mosquin et al., 2012). According to the EPA guidelines for acute exposure risk assessment of ATR, the lowest observed adverse effect level (LOAEL), no observed adverse effect level (NOAEL), reference dose (RfD) and population adjusted dose (PAD) are 70,000, 10,000, 100 and 10 μg/kg/day, respectively (EPA, 2003). For the general population in the U.S., the estimated acute and chronic dietary exposures to ATR are 0.234–0.857 and 0.046–0.286 μg/kg/day, respectively, which is relatively low (Gammon et al., 2005). On the other hand, the exposure levels could reach up 151,000 μg per work shift for ATR manufacturing workers, indicating a much higher occupational overexposure risk (Catenacci et al., 1993).

ATR and/or its metabolites have been frequently detected in spot urine samples from pesticide applicators (ATR equivalents [ATR and up to 8 identifiable metabolites, of which DE, DIP and DACT, abbreviations defined below, account for >85%]: 100–510 μg/L; detected in every sample; Barr et al., 2007), their families (ATR mercapturate: 0.024–4.9 μg/L, 27% positive samples) and the general population (ATR mercapturate: ≤3.8 μg/L [creatinine normalized]; 14%

positive samples; Curwin et al., 2007), including pregnant women and young children (Curwin et al., 2007; Chevrier et al., 2011). Quantifiable levels of ATR (>0.05 μg/L) or one of its metabolites (ATR mercapturate: >0.02 μg/L) in pregnant women's first-morning-void urine have been associated with adverse birth outcomes, such as fetal growth restriction (Chevrier et al., 2011).

ATR and its metabolites have also been detected in plasma, urine and multiple tissues (including the brain, liver and kidney) of ATR-treated rodents (Ross et al., 2009; Fraites et al., 2011), in fetuses and in the milk of orally exposed rat dams (Fraites et al., 2011), in human umbilical cord plasma samples from residentially exposed, low risk, urban population (Whyatt et al., 2003), and in breast milk samples collected from a general population in France (Balduini et al., 2003). Thus, in utero and lactational exposures may be important routes for ATR to reach the developing fetus or neonate.

In the body, ATR is metabolized by several hepatic P450s (e.g., CYP2B1, CYP2D1, and CYP2E1; Hanioka et al., 1998a) fairly rapidly to desethylatrazine (DE; 2-chloro-4-amino-6-isopropylamino-s-triazine, CAS# 6190-65-4) and desisopropylatrazine (DIP; 2-amino-4-chloro-6-ethylamino-s-triazine, CAS# 1007-28-9), which, in turn, are metabolized to didealkylatrazine (DACT; 2-chloro-4,6-diamino-1,3,5-triazine, CAS# 3397-62-4), the major in vivo metabolite of ATR in mice (Ross and Filipov, 2006; Ross et al., 2009), rats (Brzezicki et al., 2003), and, apparently, humans (Barr et al., 2007; Fig. 5.1). During gestational and/or lactational stages, ATR is also extensively metabolized following a similar pattern (Fraites et al., 2011). Emerging evidence suggests that the metabolism of ATR is auto-inducing and is physiological stage-independent, i.e., short-term ATR exposure increases its own metabolism and/or the expression of ATR-metabolizing P450 isoforms in peripubertal (Pogrmic-Majkic et al., 2012), adult

(Hanioka et al., 1998b), and pregnant and/or lactating rats (Fraites et al., 2011). However, there is still much unknown about the pharmacokinetic behavior of ATR in dams, fetuses, and neonates. Of note, while some such pharmacokinetic data are available in the rat (Fraites et al., 2011), there is no gestational of lactational pharmacokinetic study in the mouse, which is important for species comparison and extrapolation.

Developmental exposure of laboratory animals to higher levels of ATR (35–200 mg/kg) results in various adverse effects ranging from suppression of postnatal development to full-litter resorption (Narotsky et al., 2001; Rooney et al., 2003; Rayner et al., 2005). Of note, perinatal exposure of rodents to environmentally-relevant low doses of ATR causes neurobehavioral deficits (≥1 μg/kg) and structural brain changes (100 μg/kg) in the offspring (Giusi et al., 2006; Belloni et al., 2011), suggesting that the developing brain might be particularly sensitive to ATR. In terms of the effects of ATR's main metabolite DACT on the developing nervous system, in vivo studies do not exist at this point. However, our recent in vitro study suggested that DACT is less potent than ATR. Nevertheless, high concentrations of DACT disrupt dopaminergic neuron morphological differentiation (Lin et al., 2013a). The studies described above highlight the potential of adverse effects of ATR overexposure on the developing fetus and neonate, the brain in particular. However, these studies do not correlate adverse effects with estimations of fetal or neonatal target tissue concentrations of ATR or its metabolites.

Risk assessment of ATR in sensitive subpopulations, including fetuses and infants, is limited by the scarcity of human pharmacokinetic data. Physiologically based pharmacokinetic (PBPK) models in rodents are useful tools that can aid the process because they can perform route-to-route, species, and dose extrapolations, as well as dose–response analysis. Fetal and/or neonatal rodent PBPK models have been developed for several other xenobiotics (Corley et al.,

2003; Lu et al., 2012); these models facilitate the risk assessment of developmental exposure to these chemicals. At present, PBPK models for ATR are available for adult male rats (Timchalk et al., 1990; McMullin et al., 2003; McMullin et al., 2007b) and mice (Lin et al., 2011), but not for rodent dams, fetuses, or neonates. In order to improve our understanding of potential adverse effects due to developmental ATR exposure by providing fetal and neonatal tissue dosimetry for ATR and its metabolites, while taking advantage of very recent pharmacokinetic data from rat dams exposed to ATR during gestation and/or lactation (Fraites et al., 2011), we sat out to develop PBPK models for ATR describing its kinetic behavior in rodent dams, fetuses, and neonates.

Methods

Model development

Data source for model calibration

The data used to calibrate the gestational and lactational models for ATR are from two independent studies, performed by the same group (Fraites et al., 2011). In study 1, pregnant Sprague Dawley rats were treated with ATR (5 or 25 mg/kg) by daily oral gavage from gestational day (GD) 14 to GD20. Two hours after the last dosing on GD20, maternal plasma, tissues (the brain and 4th mammary gland), and fetuses were collected. Fetuses were analyzed on a per whole fetus basis. In study 2, Sprague Dawley rats were treated with the same ATR dosages from GD14 to postnatal day (PND) 10. Pups were not dosed directly with ATR, i.e., postnatal exposure was only lactational. Approximately 2 h after the last dosing on PND10, plasma and tissues from dams (the brain and 4th mammary gland) and pups (the brain), as well as neonatal intragastric milk samples were collected. All samples were analyzed for concentrations of ATR and its metabolites using a LC/MS method (Fraites et al., 2011) modified

from Ross and Filipov (2006) and Ross et al. (2009). Only the 5 mg/kg data sets from study 1 and study 2 were used to calibrate the gestational and lactational models, respectively. The units of relevant data used in their study were retained in our PBPK models, i.e., "ng/mL (μg/L)" for plasma concentration, "ng/g (μg/kg)" for tissue or milk concentration, "ng/mL ∗ h" for area under plasma concentration curve, and "ng/g ∗ h" for area under tissue or milk concentration curve.

Software for model development

AcslX simulation software (Version 2.5, Aegis Technologies Group, Inc., Huntsville, AL) was used to develop the gestational and lactational PBPK models and to run all the simulations. Model codes can be obtained upon request from the corresponding author. Growth equations for pregnancy and lactation and values for parameters simulated with TABLE functions are provided in Appendix C (Tables C1–C12).

Gestational model structure

The gestational model was composed of four sub-models for ATR, and its metabolites DE, DIP, and DACT (Fig. 5.1). Each sub-model consisted of 8 compartments: blood, brain, liver, kidney, mammary gland, placenta, fetus, and rest of body. All compartments were well-mixed and flow-limited (McMullin et al., 2007b; Lin et al., 2011). Twelve fetuses per litter were modeled based on the average litter size reported in Fraites et al. (2011). All fetuses from a single litter were modeled as one large aggregated fetal compartment for simplicity (Yoon et al., 2009a; Loccisano et al., 2012).

Pregnant rats

Absorption

Oral uptake of ATR was simulated using a two-compartment model as described and explained in detail in our adult ATR PBPK model (Lin et al., 2011) with some modifications (Fig. 5.1). First, to accommodate repeated daily exposure paradigm, the PULSE function was used, as shown in the following equations:

Exposure = PULSE(0, 24, Tlen) * PULSE(DS, Tsim, Doff)……(5.1)

RDose = (Dose/Tlen) * Exposure……..(5.2)

where Tlen is the length of each exposure, h (here, as oral gavage exposure duration is very short, Tlen was set at 0.001 h); DS represents the initiation time of oral gavage, h; Tsim is the total simulation time or the end simulation time, h; Doff is the duration of exposure, h; Dose represents the amount of ATR that is given to the rat, μg; RDose is the rate of oral exposure to ATR, μg/h; Exposure represents the exposure paradigm, unitless. Taking advantage of these equations, the present model can be used for simulation of variable exposure durations by modifying the DS, Tsim, or Doff. The second modification involved the absorption rate constants which were body weight$^{0.25}$ ($BW^{0.25}$)-scaled to accommodate the changing BW during gestation and to enhance the model's potential extrapolation capability across species similar to another PBPK modeling study (Fisher et al., 2011). For example, the gastric absorption rate constant K1 (h^{-1}) was scaled as follows:

$K1 = K1C/BW^{0.25}$……..(5.3)

where K1C is the gastric absorption rate constant after $BW^{0.25}$ scaling, $kg^{0.25}$/h. The third modification was the incorporation of fecal elimination from the intestinal compartment, with K4 (h^{-1}) representing the fecal elimination rate constant. This modification was included to better

recapitulate the pharmacokinetic process of ATR and was described based on the following evidence: (1) 18–20% of the radioactivity was recovered in the feces of rats orally exposed to ^{14}C-atrazine (^{14}C-ATR; 1.5 or 30 mg/kg; Bakke et al., 1972; Timchalk et al., 1990) and (2) intestinal metabolism of ATR by rodent enterocytes does not take place (Lin et al., 2011).

Metabolism

The description of ATR metabolism was based on earlier PBPK models in adult rodents (Timchalk et al., 1990; McMullin et al., 2003; McMullin et al., 2007b; Lin et al., 2011) with some modifications to accommodate potential differences between single and multiple exposures due to ATR's autoinduction metabolism (Hanioka et al., 1998b, 1999a; Islam et al., 2002; Dong et al., 2009; Abass et al., 2012). For example, for the current model, the maximal metabolic rate of ATR to DE was described as follows:

$$VmaxcATR\_DE\_current = VmaxcATR\_DE + VmaxcATR\_DE * Kincreasefactor \quad (5.4)$$

where VmaxcATR_DE is the initial maximal metabolic rate for naïve female rats, $\mu g/(h * kg^{0.75})$; Kincreasefactor represents the extent of net increase of metabolic rate, which is exposure dependent, unitless; VmaxcATR_DE_current is the actual maximal metabolic rate on specific day of exposure, $\mu g/(h * kg^{0.75})$.

Elimination

Due to lack of urine data in Fraites et al. (2011) and the similarity of plasma ATR/metabolite profiles between rats and mice (Brzezicki et al., 2003; Ross and Filipov, 2006; Ross et al., 2009), the description of urine elimination of ATR or its metabolites was primarily based on the adult mouse model (Lin et al., 2011) and adult mouse experimental data (Ross et al., 2009). Urine elimination of ATR metabolites was modeled using a first-order elimination process with some adjustments, whereas urine elimination of ATR itself is negligible

(Ross et al., 2009) and it was not included in the model. Changes involving the urine elimination rate constants were similar to the changes of absorption rate constants, i.e., the rate constants were $BW^{0.75}$-scaled. It has been reported that urine volume of pregnant and non-pregnant rats differs (Churchi-l et al., 1980; Atherton et al., 1982). In order to recapitulate urine elimination characteristics of the pregnant rat more precisely and enhance the model's extrapolation capability, the TABLE function was used to model the dynamic changes of urine volume during gestation based on the data in Atherton et al. (1982). As a result, the current urine elimination rate constant of ATR's metabolites, such as DACT, was described as follows:

$$Kurine3C\_current = Kurine3C * Urineflowfactor \quad (5.5)$$

where Kurine3C is the urine elimination rate constant of DACT for the non-pregnant rat, $/(h * kg^{0.75})$; Urineflowfactor represents the fold change of urine volume for the pregnant rat defined by the TABLE function, unitless (Table C1, Appendix C); Kurine3C_current is the actual urine elimination rate constant of DACT for the pregnant rat on particular GD, $/(h * kg^{0.75})$.

Plasma, red blood cell and tissue binding

Mathematical descriptions of the binding characteristics of ATR and DACT with plasma proteins and red blood cells (RBC) were based on Lin et al. (2011). Taking into account recent evidence that both ATR and DACT bind to brain proteins (Dooley et al., 2010; Fakhouri et al., 2010), a code, based on Yoon et al. (2009a), describing the binding characteristics of ATR and DACT with brain proteins was incorporated into the model. Due to potential greater sensitivity of the fetus to ATR, in order to better evaluate the fetal dosimetry of ATR and its main metabolite DACT, equations describing the binding of ATR and DACT with fetal tissue proteins were also added to the model (Yoon et al., 2009a). All binding was assumed to be reversible,

with a specific binding capacity (BMaxTissue) and association and dissociation rate constants (KaTissue and KdTissue, respectively) that are tissue- and chemical-specific. Due to lack of direct evidence that ATR and DACT bind to other adult tissues and in order to avoid over complexity in the coding, binding with other tissues was not considered. In the DE and DIP sub-models, protein binding was not considered because no data for it are available.

Fetuses

Fetal exposure to ATR and its metabolites was through the placenta. Placental transfer was described as a bidirectional transfer process between maternal and fetal plasma. At present, there is no direct evidence that ATR or its metabolites pass through the placenta via an active transport mechanism. Therefore, placental bidirectional transfer was described as a simple diffusion process with first-order rate constants (KtransinC and KtransoutC, respectively, $L/h/kg^{0.75}$), similar to the approach by Fisher et al. (1989) and Loccisano et al. (2012). The distribution of ATR and its metabolites throughout the fetus was assumed to be flow-limited and fetal metabolism of ATR, DE or DIP was considered negligible. In the rationale for the latter, the following was considered: (1) the major P450 isoforms that are responsible for ATR metabolism in the rat are CYP1A1/2, CYP2B1/2, CYP2D1, and CYP2E1 (Hanioka et al., 1998b, 1999a) and (2) the mRNA and protein levels of these P450 isoforms in the fetal rat liver at late gestation (GD17, 18, or 20) are either undetectable or 4- to 90-fold less than those in the neonate (PND 1; Ejiri et al., 2005; Czekaj et al., 2006).

Lactational model structure

The lactational model was composed of eight sub-models for ATR, DE, DIP, and DACT in the dam and pup, respectively (Fig. 5.2). Each maternal sub-model consisted of 6 flow-limited compartments (blood, brain, liver, kidney, mammary gland, and rest of body), whereas each

neonatal sub-model contained 5 flow-limited compartments (blood, brain, liver, kidney, and rest of body). Twelve pups per litter were modeled based on the average litter size and the fact that ATR (<100 mg/kg) exposure results in insignificant (<3%) loss of pups during lactation (Fraites et al., 2011).

Lactating rats

Lactating rats retained all of the basic features used to describe kinetic characteristics of ATR and its metabolites in pregnant rats. The only difference is that urine elimination rate constants for lactating rats were assumed to be the same as non-pregnant rats because urine flow rate (μL/min) throughout lactation is similar to urine flow rate in non-pregnant rats (Arthur and Green, 1983).

Neonatal rats

Neonates were exposed to ATR and its metabolites only through milk. Oral absorption of ATR or its metabolites via milk and their transfer into pups' liver, such as Rmilkpup for ATR, were described as follows:

Rmilkpup = Frac * Rmilk/N……(5.6)

where Frac is the degree of fractional uptake, unitless; Rmilk is the rate of incorporation of ATR from mammary gland into milk, μg/h; N is litter size, unitless. The basic features used to describe the distribution, plasma, RBC, or brain tissue binding, metabolism and elimination in dams were retained in the neonatal sub-models. Neonatal metabolism was taken into account because the expression of P450s is markedly increased after birth and P450 activity is also moderately elevated postnatally (Henderson, 1971; Lucier et al., 1979; Imaoka et al., 1991; Watanabe et al., 1993). For example, the neonatal metabolism of ATR to DE was described as follows:

VmaxATR_DEpup = VmaxATR_DE * Kneomet * Kneomet2 * KliverR……..(5.7)

where VmaxATR_DEpup is the maximal metabolic rate of ATR to DE in the pup, μg/h; VmaxATR_DE is the maximal metabolic rate of ATR to DE in the naïve female rat, μg/h; Kneomet is the age-dependent changing ratio of P450 content (nmol/g liver tissue) in neonates (Watanabe et al., 1993) compared to adult rats and was described using a TABLE function, unitless (Table C2, Appendix C); Kneomet2 is the age-dependent changing ratio of P450 activity in neonates compared to adult female rats (Henderson, 1971; Lucier et al., 1979) and was described using a TABLE function, unitless (Table C3, Appendix C); KliverR is the age-dependent changing ratio of the absolute liver weight for the neonate compared to adult female rats (Mirfazaelian and Fisher, 2007), unitless (Table C4, Appendix C). Even though neonates were exposed to ATR for 11 days (Fraites et al., 2011) and ATR exposure increases the expression and activity of P450s, due to the facts that (1) the model-derived absorbed dose of ATR by the pup (on average 0.000002 mg/day) is far (~700,000-fold) less than the administered dose to the dam (5 mg/kg: 1.375 mg/day for a 0.275 kg dam) and (2) ATR concentrations in neonatal plasma/brain were undetectable or below the limit of quantification (Fraites et al., 2011), the auto-inducing metabolism caused by repeated daily ATR exposure in the neonate was considered negligible and was not incorporated in the lactational model. Neonatal rats do not urinate spontaneously until 2–3 weeks after birth and they normally depend on the dam's licking to provoke micturition reflexively. The neonate's urine, in turn, is re-ingested by the dam from licking neonates (Capek and Jelinek, 1956; Friedman et al., 1981). Hence, neonatal urine elimination was also incorporated and described with the same approach used for the dam (Loccisano et al., 2012). However, because the model-derived absorbed dose of DACT by the pup (on average 0.0012 mg/day [0.008 μmol/day]) is much (~800-fold) smaller than the

administered dose of ATR to the dam (5 mg/kg: 0.9315 mg/day [6.4 μmol/day] for a 0.275 kg dam) and the PND0-10 cumulative amount of urinary DACT in the pup (~0.013 mg) is also greatly (~570-fold) lower than in the dam (~7.4 mg), this additional input of DACT from neonatal urine to dams' gut, which only occurs at early lactation, was assumed negligible. Therefore, this process was not incorporated into the maternal sub-models.

Model parameterization

Physiological parameters

Dynamic changes in maternal/fetal/neonatal organ/tissue volumes, tissue growth, and blood flow rates associated with gestation and lactation were described mathematically based on existing models for the same strain of rats (Sprague Dawley) at similar age (Yoon et al., 2009a, b; Loccisano et al., 2012). Values and equations of physiological parameters are provided in Table 5.1 or in Appendix C (Tables C1–C12) along with the references they were obtained from or based on.

Chemical-specific parameters

To the extent possible, chemical-specific parameters used in the adult male mouse (Lin et al., 2011) and the latest adult male rat (McMullin et al., 2007b) models were utilized in the current gestational and lactational models. Changes and re-estimations required for pregnancy, lactation, fetal, or neonatal growth are described in the text below and all values are provided in Table 5.2. All chemical-specific parameters for the dam in the gestational and lactational models are identical.

Pregnant/lactating rats

Uptake and elimination

Initially, we turned off fecal elimination (set K4 = 0) and incorporated the absorption rate constants (5 mg/kg; K1 = 0.3, K2 = 1, and K3 = 0.01) from the adult male mouse model (Lin et al., 2011). Simulation showed that 79% of the administered ATR is absorbed within 72 h after the last dosing, which is consistent with previous pharmacokinetic studies in rats with similar dose levels (1.5 or 30 mg/kg; Bakke et al., 1972; Timchalk et al., 1990). Next, we turned on fecal elimination, estimated the fecal elimination rate constant, and slightly adjusted the intestinal absorption rate constant (K3) to fit the data that approximately 18–20% of administered ATR was excreted via feces 72 h after single oral dosing (Bakke et al., 1972; Timchalk et al., 1990). Urine elimination rate constants were estimated by visually fitting the maternal plasma data from Fraites et al. (2011). All rate constants were scaled to maternal body weight ($BW^{0.25}$ or $BW^{0.75}$, as appropriate; Table 5.2).

Partition coefficients

Based on published PCs for the liver and the body used for adult male rats (McMullin et al., 2007b), which are all equal/close to 1 (Table C13, Appendix C), initially, we set the values for PCs of ATR and its metabolites for all compartments to be 1 and slightly adjusted the gestational model PCs for the brain and mammary gland by visual fitting to the 5 mg/kg data set from study 1 (Fraites et al., 2011). We also incorporated the newly available PCs for ATR in the rat liver and brain determined using a negligible depletion solid-phase microextraction method (Tremblay et al., 2012) into the model. These experimental PCs were very close to our estimated PCs and the overall simulation did not change significantly. In the final model, the experimental PCs (Tremblay et al., 2012) were used whenever possible. In addition, we estimated

ATR/metabolites PCs for the liver, brain and muscle using published algorithms (Poulin and Krishnan, 1995; Poulin and Theil, 2000) and calculated PCs of ATR/metabolites for the brain, mammary gland, fetus, and milk using the single time point tissue/plasma concentration ratio method (C_{tissue}/C_{plasma}) reported in Lin et al. (2011) and Fisher et al. (2011). Because algorithm-predicted PCs of ATR in the liver (9.45) and brain (12.21) are more than 10-fold higher than experimentally-determined values (0.69 and 0.73, respectively) and the algorithm-predicted PC values were, in 15% of 269 chemicals or drugs, more than 4-fold different from corresponding mean experimental values (Poulin and Theil, 2000; Tremblay et al., 2012), we opted to use experimental PCs. PCs derived from different methods/studies were compared and the result is provided in Appendix C (Table C13).

Plasma, RBC and tissue binding

The estimations of plasma, RBC and brain protein binding parameters were based on the adult male mouse model (Lin et al., 2011), with all necessary unit changes made i.e., μmol vs. μg, and /(h ∗ μmol) vs. /(h ∗ μg); these estimations are described in more detail in Table 5.2. Binding was calibrated to meet the criterion that, on average, 26% (18% to 37%) of plasma ATR and DACT were protein-bound (Lu et al., 1998).

Metabolism

Similar to the adult rodent PBPK models (McMullin et al., 2007b; Lin et al., 2011), we initially incorporated the in vitro metabolic rate constants of ATR to DE, and ATR to DIP determined using rat liver microsomes (Hanioka et al., 1999b) and the estimated metabolic rate constants of DE to DACT, and DIP to DACT for adult mice (Lin et al., 2011) into the current gestational and lactational rat models. The result was an overestimation of ATR and underestimation of ATR's metabolite levels in the plasma. Next, we increased ATR's initial

metabolic rates up to 3-fold of the in vitro metabolic rates as recommended by earlier modeling studies (Lipscomb et al., 1998; Kramer et al., 2001; Lin et al., 2011); the model still overestimated plasma ATR concentration and underestimated plasma concentrations of ATR metabolites. Thereafter, we took into account ATR's autoinduction metabolism and estimated the auto-inducing profile (Kincreasefactor) based on the extent of increase in the protein/mRNA expression or activity of major ATR metabolizing P450 isoforms or total P450 content in (1) rats (Hanioka et al., 1998b; Islam et al., 2002) exposed to ATR for 3 days (increased protein levels and activity of CYP1A1/2 and CYP2B/1 by 1.4- to 2.8-fold), (2) human hepatocytes (Abass et al., 2012) exposed to ATR for 24 h (increased mRNA levels and enzyme activity of CYP1A2, CYP2A6 [3–12 fold], CYP2B6 and CYP3A4 [1.2–3.5 fold]), and (3) zebrafish (Dong et al., 2009) exposed to ATR for 5–25 days (increased total P450s by up to 5-fold on day 10). P450 expression and induction profile in mammals and fish exposed to xenobiotics (e.g., TCDD, PCBs, and dexamethasone) are similar (Hahn, 1998; Tseng et al., 2005; Jonsson et al., 2007; Goldstone et al., 2010). Based on the above, we hypothesized that dam's ATR metabolism increases gradually, perhaps linearly, during the first 10 days of exposure, and reaches the greatest level on day 11. After longer exposure (≥11 days), ATR's metabolism reaches a plateau. In support of our hypothesis, a recent study showed that the activity of the major ATR metabolizing enzyme, CYP1A1/2, remained increased (56%) after 28-day oral exposure to ATR (200 mg/kg) of male rats (Pogrmic-Majkic et al., 2012). However, there is no available evidence as to whether or when ATR metabolism in rodents returns to basal levels. Considering the possibility that increased expression and activity of P450s upon short-term ATR exposure may also increase the metabolism of DE and DIP to DACT, we also incorporated relevant code (Kincreasefactor1 and Kincreasefactor2 for DE and DIP, respectively) in the models. Based on these assumptions,

Kincreasefactor was calibrated to 40% increase per exposure/day within the first 10-day exposure period followed by a plateau. Kincreasefactor1 and Kincreasefactor2 were set by visual fitting to the 5 mg/kg data sets from studies 1 and 2 (Fraites et al., 2011) to values of 0 and 1 for the gestational and lactational model, respectively (Table 5.2). These adjustments resulted in adequate simulation of plasma levels of ATR and its metabolites. Time-course for ATR autoinduction metabolism is shown in Fig. C1 (Appendix C).

Fetuses

Placental transfer

Initially, placental transfer of ATR, DE, DIP, and DACT was simulated with a single bidirectional rate constant for each chemical (i.e., KtransinC = KtransoutC = 1 L/h/kg$^{0.75}$ for all chemicals). The model was able to adequately predict fetal concentrations of these chemicals with their PCs in the fetus set as 1.6, 1, 1.1, and 1.2 for ATR, DE, DIP, and DACT, respectively. However, these PC values were close to, but different from our a priori assumption that all PCs, unless data exist, are/will be 1 as in the earlier adult rat model (McMullin et al., 2007b). Next, because fetal concentrations of these chemicals were slightly higher than their respective levels in maternal plasma (Fraites et al., 2011), we tried setting their PCs in the fetus to 1 while using asymmetric placental transfer rate constants (Clewell et al., 2003; Clewell et al., 2008; Loccisano et al., 2012). These rate constants were estimated by fitting the maternal plasma and fetal concentration data set (5 mg/kg dose group) from study 1 (Fraites et al., 2011) and were further calibrated to meet the criteria that the simulated placental transfer rates for each chemical are within the range of blood flow rates for several richly perfused organs, such as the brain, liver and kidney (the calculated clearance terms in units of L/h or L/h/kg$^{0.75}$ are provided in Table C14, Appendix C). Since transfer of nutrients and other substances, including xenobiotics, through the

placenta increases as gestation progresses (Rosso, 1975; Schneider, 1991) and is proportional to fetal size, placental transfer parameters in the current model were scaled by fetal $BW^{0.75}$ (Yoon et al., 2009a). In addition, we compared our estimated placental transfer rates with that of other lipophilic non-persistent xenobiotics, such as the pesticide chlorpyrifos (Lowe et al., 2009), and found that they are comparable.

Tissue binding for the fetus

There is no detailed information on the binding characteristics of ATR or DACT with fetal tissue proteins. Hence, binding parameters (i.e., maximal binding capacities and dissociation rate constants) for the fetus were set to be equal to those used for the maternal brain based on their similar protein composition and blood flow (Waehneldt and Shooter, 1973; Girard et al., 1983; Engle and Lemons, 1986; Brown et al., 1997; Dowell and Kauer, 1997; Yoon et al., 2009a). Specifically, the total protein content of adult rat brain is 8–10% of wet weight and the protein concentrations in the fetus during late gestation are around 10% of wet weight (ranging from 5.6% to 16.3% throughout gestation; Waehneldt and Shooter, 1973; Engle and Lemons, 1986). In terms of blood flow, in rats, the blood flow to the adult brain and to the fetus during late gestation is 0.164 and 0.155 L/h, respectively (Girard et al., 1983; Brown et al., 1997; Dowell and Kauer, 1997; Yoon et al., 2009a); the corresponding values in humans are 48.64 and 56.32 L/h, respectively (Yoon et al., 2011). The association rate constants were estimated by visually fitting to fetal concentration data set (5 mg/kg dose group) from study 1 (Fraites et al., 2011), and were calibrated such that the percentage of bound ATR/DACT in the fetus is close to that in the maternal plasma, i.e., 26% (Lu et al., 1998).

Milk

Lactational transfer

Description of mammary gland/milk transfer of ATR and its metabolites was initially based on a flow-limited process similar to that of trichloroethylene (Fisher et al., 1990). Assumption was made that maternal blood supply perfusing the mammary tissue is in intimate contact with the milk, i.e., mammary tissue and milk were considered as a single compartment with uniform xenobiotic amount, concentration, and PC (Lee et al., 2007). However, this assumption is inconsistent with the data used for our model development that mammary tissue and milk ATR levels are approximately 3-fold different from each other (Fraites et al., 2011). Therefore, the first approach was abandoned. Fisher et al. (1990) also proposed an alternative approach and used it to describe lactational transfer of trichloroacetic acid, assuming its movement across mammary tissue into the milk compartment is a diffusion-limited process. By using this method, 8 additional chemical-specific parameters (milk/mammary PCs and permeability area across products from mammary tissue to milk for ATR and its metabolites) were needed, and all these parameters had to be estimated. After incorporating these additional estimated parameters, our model properly predicted milk levels of ATR and its metabolites, but greatly underestimated their neonatal plasma and brain levels. Due to its sub-optimal performance and to avoid increasing the complexity and variability of the model, this second approach was also abandoned. Yoon et al. (2009b) developed a third approach in their lactational model for manganese in which manganese's transfer from mammary gland to milk was described as a diffusion process, with a first-order clearance process. A similar approach was used in their earlier models describing the lactational transfer of another herbicide, 2,4-dichlorophenoxyacetic acid, and 16 theoretical test compounds with a wide range of chemical properties, including

some possessing similar chemical properties to ATR (i.e., milk concentration is lower than maternal plasma level; Yoon and Barton, 2008). By using this method, our lactational model accurately predicted neonatal plasma, brain, and milk data. Therefore, this method was used in the final lactational model. In brief, a "virtual" milk compartment was added to the lactational model. This compartment has no formal volume, but carries chemicals to the pups with a variable milk production rate (implemented in acslX with a TABLE function) over the lactation period; the amount of milk produced was assumed to be equal to the amount consumed by the pups with no delay between production and ingestion (Yoon and Barton, 2008; Yoon et al., 2009b). Free ATR or its metabolites in the mammary gland were transferred into the milk through a diffusion process described by a first-order clearance (KmilkC, L/h/kg$^{0.75}$); it was also assumed that milk ATR/metabolites do not diffuse back into the blood perfusing the mammary tissue (Yoon and Barton, 2008; Yoon et al., 2009b). The clearance rate constants for ATR and its metabolites were estimated by fitting them to the milk data (5 mg/kg dose group) from study 2 (Fraites et al., 2011). No residual milk volume was considered, and milk concentrations were determined by dividing the rates of incorporation of these chemicals from mammary gland into milk (Rmilk, μg/h) by the milk production rates (KLac, L/h; Yoon and Barton, 2008; Yoon et al., 2009b).

Pups

Pups' suckling rate was set equal to the dam's milk production rate (Yoon et al., 2009b). Degree of fractional uptake was assumed to be 100% due to newborn's immature gastrointestinal tract (Xu, 1996). PCs used for the dam were utilized for the pup. Description of plasma, RBC and tissue binding with ATR or DACT for the pup was the same as for the dam. Urine elimination rate constants for pups were set equal to those for non-pregnant rats.

Dose extrapolation

After calibration of the models with the 5 mg/kg data set, the models were applied to the higher dose condition (25 mg/kg). The gestational and lactational model simulations were compared with the experimental data sets (25 mg/kg) from studies 1 and 2, respectively (Fraites et al., 2011).

Model evaluation: validation and species extrapolation

Gestational model

Gestational model's performance was evaluated with data sets not used in model calibration, from study 3 (a separate study, distinct from studies 1 and 2) in Fraites et al. (2011). In study 3, pregnant Sprague Dawley rats were exposed to ATR (5 or 25 mg/kg) from GD18 to GD20 by daily oral gavage and sample collection and analyses were similar to study 1 (Fraites et al., 2011). To further evaluate the gestational model and test its cross-species extrapolation capacity, a pharmacokinetic study with ATR was conducted in pregnant C57BL/6 mice.

Pharmacokinetic study with ATR in pregnant C57BL/6 mice

Chemicals and reagents. ATR (98.9% purity), DE (99.5%), DIP (98%), DACT (96%), and simazine (99%) were purchased from Chem Service (West Chester, PA). For LC–MS, stock solutions (10 mM) of ATR, DE, DIP, and simazine (used as internal standard) were prepared in ethanol, and DACT (50 mM) was dissolved in DMSO. All LC–MS solvents were from Fisher (Fair Lawn, NJ).

Animals and study design. Time-pregnant (copulatory plug positive = GD0) C57BL/6 mice (9–12 months old, 28.0 ± 1.1 g, Taconic, Hudson, NY) were housed individually with water and food available ad libitum under constant temperature (22 °C) on a 12-h light/dark cycle in an AAALAC accredited facility throughout the study. All animal procedures were in

accordance with the Animal Welfare Act and the Guide for the Care and Use of Laboratory Animals (NIH, 2011) and were approved in advance by the Institutional Animal Care and Use Committee (IACUC) of the University of Georgia. Mice were dosed by daily oral gavage with corn oil vehicle or 5 mg/kg ATR (5 mL/kg) from GD12 to GD18, based on the dose level and exposure paradigm of the rat pharmacokinetic study (Fraites et al., 2011) used for model development. At 2 or 6 h after the last dosing on GD18, subgroups of mice were euthanized and maternal plasma, brain, liver, placenta and fetuses were harvested. All samples were frozen on dry ice and stored at −80 °C until analysis. Prior to freezing, fetuses were extensively washed in sterile PBS.

Sample preparation and analytical procedure. The procedure for analyzing ATR and its metabolites in mouse tissues was adapted from Ross et al. (2009). Briefly, mouse tissues (liver, brain and placenta) were accurately weighed and Dounce homogenized in 4:1 (v/v) acetonitrile:aqueous acetic acid (0.1% v/v; 2.0 mL of extraction solvent per 60 mg tissue), followed by sonication (4 × 10 s pulses, 30 min on ice between pulses; Branson Sonifier 250, Branson Ultrasonics, Danbury, CT). Homogenates were stored at −20 °C for at least 30 min, followed by centrifugation (10,500 ×*g*, 20 min, 4 °C) to remove insoluble material. Supernatants were filtered (0.45 μm) and a 2-mL aliquot added to a plastic microfuge tube containing internal standard (simazine, 1.25 nmol). Extracts were dried in a SpeedVac centrifuge for 4.5 h at 40 °C and the residues were redissolved in 19:1 (v/v) 0.1% acetic acid/methanol (200 μL), microfuge filtered (0.22 μm), and injected (10 μL) onto a LC–MS/MS system.

Whole fetuses were homogenized in aqueous acetic acid (0.1% v/v) as a 15% (w/v) mixture using a Waring high-speed blender (2 × 15 s bursts). The homogenate was filtered through glass wool and an aliquot (400 μL) transferred to a microcentrifuge tube containing 1.6-

mL ice-cold acetonitrile and internal standard (simazine, 1.25 nmol). Samples were stored at −20 °C for 30 min. After centrifugation (10,500 ×*g*, 20 min, 4 °C), the supernatants were filtered (0.45 μm), and an aliquot (2 mL) was transferred to clean microcentrifuge tubes and dried on SpeedVac for 4.5 h at 40 °C. The residues were redissolved in 19:1 (v/v) 0.1% acetic acid/methanol (200 μL), microfuge filtered (0.22 μm), and injected (10 μL) onto the LC–MS/MS system.

Analysis of plasma was performed by procedures developed in our previous study (Ross et al., 2009). In brief, plasma (250-μL aliquots) was added to a microcentrifuge tube and mixed with 1-mL ice-cold acetonitrile containing internal standard (simazine, 1.25 nmol). Samples were stored at −20 °C for 30 min, followed by centrifugation at 16,000 ×*g* (15 min, 4 °C). Supernatants were dried in a SpeedVac and the residues redissolved in 19:1 (v/v) 0.1% acetic acid/methanol (200 μL), microfuge filtered (0.22 μm), and injected (10 μL) onto the LC–MS/MS system.

ATR and its major metabolites in tissue and plasma extracts were analyzed using a UPLC–MS/MS system (Waters Acquity UPLC interfaced with a Thermo Quantum Access Max triple quadrupole mass spectrometer). Briefly, analytes were injected onto a Phenomenex Gemini C6-phenyl column (100 × 2 mm) containing a guard column, and eluted with the following linear gradient solvent system: 0 min (95% A, 5% B), 1 min (95% A, 5% B), 17.5 min (34% A, 66% B), 20 min (5% A, 95% B), 22 min (5% A, 95% B), 25 min (95% A, 5% B), held for 5 min before next injection. Solvent A was 0.1% acetic acid in water and solvent B was 0.1% acetic acid in methanol; flow rate, 0.3 mL/min. The SRMs for analytes were: DACT (146 > 79), DIP (174 > 79), DE (188 > 104), simazine (202 > 174), and ATR (216 > 174). SRMs were segmented during the chromatographic run to enhance sensitivity. All mass spectrometric parameters were

optimized by direct infusion of authentic standards of each analyte into the mass spectrometer. Calibration curves were prepared by spiking known quantities of each analyte into matrix (liver or plasma obtained from control naive mice) and extracted for LC–MS/MS analysis in the manner described above.

Gestational model extrapolation from rats to mice

Scaling of the physiological changes during pregnancy from rats to mice was based on O'Flaherty et al. (1992). The BW of a pregnant mouse on GD0 was set as 28.0 g based on the measured average value in current study. The BW of an individual fetus at the end of gestation (at the time of delivery) was set as 1.34 g based on an earlier mouse gestational PBPK model (Terry et al., 1995). Mouse-specific metabolic rates of ATR to DE/DIP and DE/DIP to DACT and urine elimination rates of ATR's metabolites were from our adult male mouse model (Lin et al., 2011) as female-specific data are not available. The other chemical-specific parameters used in the present gestational rat model were employed to model the kinetics of ATR in pregnant mice.

Lactational model

The lactational model was evaluated with data sets from Stoker and Cooper (2007). In Stoker and Cooper (2007), lactating Wistar rat dams were exposed to ^{14}C-ATR (2 or 4 mg/rat) by oral gavage on PND3; 2.5 h after maternal exposure, the pups (10 pups/litter) were allowed to nurse for 30 min. At the end of the nursing period, radioactivity of ^{14}C-chlorotriazine residues was measured in neonatal stomach and brain. The same physiological and chemical-specific parameters used in the present model were employed to simulate the kinetics of ^{14}C-chlorotriazines in Wistar rats (Stoker and Cooper, 2007).

The criteria for a validated model were based on WHO guidelines (WHO, 2010), i.e., the simulations are generally within a factor of two of the measured values. Sensitivity analyses were performed for both models and are discussed elsewhere in the manuscript and in Appendix C.

Model applications

Daily internal dose metrics

As a measure of the internal dose metric, the average daily (24-h cumulative) AUCs for concentrations of ATR or DACT in the maternal and neonatal plasma and tissues, fetuses, and in the milk were calculated by dividing their respective total AUCs during the gestational or lactational exposure period by the number of exposure days (Gargas et al., 2000b; Yoon et al., 2011). These dose metrics were used to compare internal exposures to ATR or DACT between (1) pregnant rats and fetuses (gestational model), (2) shorter and longer exposures (3-day vs. 7-day; gestational model), (3) lactating rats and neonates (lactational model), and (4) fetuses and neonates (gestational and lactational models).

Comparison of model-derived gestational carryover and lactational exposure estimates

The gestational model was run for 22 days [GD22 coincides with PND0 regardless of actual date of parturition as defined in Fraites et al. (2011)], and the end of simulation values at the beginning of GD22 for each ATR dose were predicted and utilized as the PND0 parameter values for the lactational model. To examine the effects of gestational carryover and lactational exposure on neonatal dosimetry separately, the gestational and lactational models were run and the neonatal plasma/brain DACT dosimetry was predicted under several hypothetical scenarios: (1) gestational exposure only (GD14-21 or GD0-21), (2) lactational exposure only (PND0-10 or PND0-21), and (3) combined gestational and lactational exposure (GD14 to PND10 or GD0 to

PND21). These exposure paradigms were chosen based on literature where experimental data are available (GD14 to PND10; Fraites et al., 2011) or to mimic environmental exposures encompassing the entire gestation and/or lactation.

Results

Model calibration

Gestational model

Model predictions of maternal plasma, maternal tissue and fetal concentrations of ATR and its metabolites at 2 h after the last dosing on GD20 were compared to measured data in pregnant rats dosed orally with 5 mg/kg ATR from GD14 to GD20 (Fraites et al., 2011). Results for ATR and its major metabolite DACT are shown in Fig. 5.3A, while results for the intermediate metabolites (DE and DIP) are provided in Appendix C (Fig. C2). Overall, the model slightly overestimated (within a factor of 2) maternal plasma ATR levels, but it accurately predicted maternal plasma levels of its metabolites, as well as maternal brain, mammary gland, and fetal concentrations of both ATR and its metabolites. Model-predicted time-course of maternal plasma and fetal ATR/DACT concentrations are shown in Fig. 5.4A. Model simulations suggest that peak maternal plasma or fetal concentrations of ATR and DACT occur at 0.5–1 and 2–3 h after dosing, respectively; thereafter, ATR concentrations decrease rapidly, while DACT concentrations remain at relatively high levels up until 6 h post dosing. Daily maximum concentrations of ATR in the maternal plasma or in the fetus decrease gradually as exposure proceeds; daily maximum DACT levels remain relatively constant throughout the entire exposure period. These data indicate that the autoinduction metabolism of ATR mainly affects the time-course kinetics of ATR and it has smaller effect on the kinetics of DACT.

Lactational model

Model simulations of maternal and neonatal plasma and tissue, as well as milk concentrations of ATR and its metabolites 2 h post dosing on PND10 were compared to measured levels following oral dam exposure to 5 mg/kg ATR from GD14 to PND10 (Fraites et al., 2011). Results for ATR and DACT are shown in Fig. 5.3B and results for DE and DIP are given in Appendix C (Fig. C3). All model predictions were in good agreement with the experimental data, except for a slight (within a factor of 2) overestimation of mammary gland ATR concentration. For the neonatal plasma and brain concentrations of ATR, DE and DIP, the model predictions are not given because their levels were close to, or below, detection limits (Fraites et al., 2011). Model-predicted time-course of maternal plasma and neonatal ATR/DACT concentrations are shown in Fig. 5.4B. Of note, at the same dose (5 mg/kg), the model-predicted concentrations of ATR in maternal plasma were consistently lower following 19 days of exposure (GD14 to PND10; Fig. 5.4B) compared to 7-day exposure (GD14-20; Fig. 5.4A), but the model-predicted levels of DACT were relatively higher following longer ATR exposure, likely due to ATR autoinduction metabolism producing more DACT, which is consistent with the experimental data of Fraites et al. (2011).

Dose extrapolation

The gestational and lactational models were calibrated with 5 mg/kg data sets and then were extrapolated to the higher dose (25 mg/kg). As shown in Fig. 5.3A, gestational model-predicted maternal plasma/tissue and fetal concentrations of ATR and DACT at 2 h after the last dosing on GD20 are consistent with the experimental data from Fraites et al. (2011) across both dose levels. Similarly, the lactational model adequately predicted maternal plasma/tissue, milk, and neonatal plasma/brain concentrations of ATR and/or DACT at 2 h after the last dosing on

PND10 reported in Fraites et al. (2011) at both dose levels, except a slight overestimation (within a factor of 2) of maternal plasma ATR level at 25 mg/kg (Fig. 5.3B).

Model evaluation

Gestational model

Evaluation with Sprague Dawley rat data from study 3 in Fraites et al. (2011). The model estimates of maternal plasma, maternal brain, mammary gland and fetal concentrations of ATR and DACT at 2 h after the last dosing on GD20 were compared to measured levels from study 3 (Fraites et al., 2011). As shown in Table 5.3, there was a very good agreement between simulated and measured data of ATR or DACT concentrations in all the tissues at both doses, except an underestimation (~3-fold) of fetal ATR concentration at 25 mg/kg. As mentioned in the Methods section, fetal P450-mediated metabolism is very low (Ejiri et al., 2005; Czekaj et al., 2006). Hence, the underestimation of fetal ATR level may be due to saturation of fetal metabolism of ATR, resulting in a higher tendency towards accumulation of ATR in the fetus at the higher dose (25 mg/kg).

Evaluation with C57BL/6 mouse data. Measured concentrations of ATR and DACT in maternal plasma/brain, placenta and fetuses at 2 or 6 h after the last dosing on GD18 were compared to model predictions (Table 5.4). Overall, the model fairly accurately predicted maternal plasma/tissue concentrations of ATR at both 2 and 6 h (within 2.5–3 fold) and it did an even better job in predicting ATR levels in the fetus at both time points, highlighting the fact that the model properly describes the placental transfer of ATR. The model also accurately estimated the levels of the predominant ATR metabolite DACT in all maternal plasma/tissues at both time points, but it overestimated (~ 10-fold) DACT's levels in the fetus. This overestimation (discussed elsewhere in the manuscript) may be due to the different fetus collection procedures,

i.e., the fetuses were extensively washed in PBS before freezing in current study, which may have resulted in the loss of the unbound DACT fraction because DACT (logKow = 0.11) is more polar and less lipophilic than ATR (logKow = 2.75; Noble, 1993; Kaune et al., 1998).

Lactational model

Evaluation with Wistar rat data from Stoker and Cooper (2007). Measured levels of ^{14}C-chlorotriazines in neonatal stomach milk (a surrogate for milk in the mammary gland) and brain were compared to model-simulated levels of DACT [a predominant component of chlorotriazines, i.e., 91–93% of total chlorotriazines in milk and 93–97% of total chlorotriazines in neonatal brain (Fraites et al., 2011)] and are shown in Table 5.5. The lactational model slightly underestimated the neonatal brain ^{14}C-chlorotriazine levels (around 2-fold), but the predicted milk DACT levels agreed with the measured ^{14}C-chlorotriazine levels across the two doses (2 or 4 mg ^{14}C-ATR/rat dam). The slight underestimation of neonatal brain dosimetry may be due to (1) the longer sucking deprivation period [2.5 vs. 1.5 h; a known factor that reliably increases subsequent sucking and milk intake in rat pups (Brake et al., 1982)] and/or (2) the lower number of pups per litter (10 vs. 12; Stoker and Cooper, 2007; Fraites et al., 2011).

Sensitivity analysis

Sensitivity analysis revealed that the fetus PCs, ATR metabolism, urine elimination of DACT, and placental transfer rates (Table A15) were important parameters for determining fetal ATR/DACT levels, while neonatal brain DACT levels were highly sensitive to its neonatal brain PC, milk clearance, neonatal urine elimination, and neonatal uptake rate parameters (Table A16).

Model applications

Comparison of model-derived maternal and fetal exposure estimates

The average daily ATR/DACT AUCs in maternal plasma/tissues and in whole fetus in the two gestational exposure paradigms (study 1: GD14–20; study 3: GD18–20) at the 5 mg/kg dose were predicted and used to compare maternal and fetal exposures to ATR and DACT (Fig. 5.5A). Maternal plasma and tissues and the fetus have different ATR/metabolite exposure profiles. For example, the levels of ATR in maternal plasma and brain are very close, indicating that ATR can readily pass the blood–brain barrier. In the mammary gland, the internal ATR dose is approximately 3.5-fold higher than maternal plasma or brain level, indicating a favorable partitioning of ATR into the mammary gland during late stages of gestation. Compared to the dam, fetal ATR level is close to maternal plasma or brain level, which suggests that ATR can readily diffuse through the blood–placenta barrier and reach the fetus. On the other hand, DACT levels in the mammary gland are 50% less than maternal plasma DACT. Interestingly, fetal DACT is somewhat higher than maternal plasma DACT. Collectively, these model predictions suggest that both ATR and DACT can diffuse through the blood–placenta barrier efficiently.

Comparison of model-derived shorter and longer exposure estimates

As shown in Fig. 5.5A, the average daily AUC for ATR in the maternal plasma or the fetus after a 7-day exposure is on average 26% less than after a 3-day exposure; the average daily AUC for DACT in the maternal plasma or the fetus after a 7-day exposure is about 15% higher than after a 3-day exposure. These results suggest that internal DACT AUC dosimetry increases gradually as exposure continues, likely because of increased metabolism of ATR resulting in more DACT production, whereas AUC dosimetry for ATR decreases as ATR multi-day dosing proceeds.

Comparison of model-derived fetal and neonatal exposure estimates

Based on the gestational and lactational model simulations (Fig. 5.5), we conclude that fetal internal exposures to ATR and DACT are around 1500- and 2.5-fold higher than neonatal exposures, respectively, provided that pregnant and lactating rats are exposed to the same external dose of ATR (5 mg/kg). These data suggest that in utero exposures to ATR and DACT (especially ATR) may be of greater concern than lactational exposures.

Comparison of model-derived gestational carryover and lactational exposure estimates

In study 2 from Fraites et al. (2011), neonates were exposed to ATR and its metabolites both in utero (GD14-21) and via breast milk (PND0-10). Under this exposure scenario, neonatal plasma or brain ATR, DE, DIP (data not shown), or DACT (Figs. 5.6A, C, solid lines) levels were decreased postnatally, suggesting that gestational carryover contributes to neonatal dosimetry. To examine the extent of the effects of gestational carryover, we turned off gestational or lactational exposure separately, and ran the models as if dams were exposed to ATR only during gestation (GD14–21; Figs. 5.6A, C, dash lines) or only during lactation (PND0–10; Figs. 5.6A, C, dotted lines). We found that the effects of gestational carryover on ATR, DE, DIP, and DACT levels in neonates last up to 1 h, 10 h, 5 h, and 9.5 days postnatally, respectively. Thereafter, gestational-only exposure neonatal plasma/brain ATR/DE/DIP/DACT levels were below current limits of quantification (Fraites et al., 2011). These data indicate that gestational carryover of DACT plays an important role in neonatal plasma or tissue dosimetry up until mid-lactation.

To mimic a more realistic environmental exposure situation, we ran the models assuming that fetuses/neonates are exposed to ATR and its metabolites throughout the entire gestation and/or lactation (Figs. 5.6B, D). The model simulations suggest that gestational carryover of

DACT affects neonatal dosimetry up to PND9.5, and it is independent of the length of gestational exposure (GD14–21 vs. GD0–21), indicating that it is mainly the exposure during late gestation that contributes to gestational carryover. To examine the effects on neonatal plasma/brain dosimetry between continuous (GD0 to PND21; Figs. 5.6B, D) and partial (GD14 to PND10; Figs. 5.6A, C) perinatal exposures, we compared the neonatal plasma/brain DACT AUC from PND0 to PND10 ($AUC_{PND0–10}$) between exposure scenarios and found that they are almost identical, indicating that exposure during early pregnancy (i.e., GD0–13) doesn't contribute to neonatal dosimetry. In lactational-only exposure scenario (PND0–21), we compared the neonatal plasma/brain DACT AUC between PND0–10 ($AUC_{PND0–10}$) and PND11–21 ($AUC_{PND11–21}$), and found that the extent of neonatal exposure to DACT during the first half of lactation is almost five-fold higher than exposure to DACT during the second half of lactation. This result indicates that early lactation (in terms of exposure mainly to DACT) may be a susceptible period during lactational-only exposure to ATR.

Discussion

The present PBPK models properly describe placental/lactational transfer and tissue distribution of ATR and its metabolites in pregnant, lactating, fetal and neonatal rats; rat-based models also extrapolate well to mice. Model predictions indicate that (1) the fetus is exposed to both ATR and its major metabolite DACT at levels similar to their maternal plasma levels, with DACT's levels being much higher than ATR, (2) the nursing neonate is exposed primarily to DACT at levels around one-third of maternal plasma levels, while lactational exposure to ATR is minimal, and (3) gestational carryover of DACT greatly affects neonatal dosimetry, especially during the first half of lactation. Thus, in terms of developmental exposure to ATR and/or its metabolites, exposure during pregnancy and early lactation may be of particular concern. Based

on our mouse study, it appears that about 10% of the DACT that reaches the fetus is tissue-bound.

Values of the PCs used in the present models range from 0.5 to 1, except the PC for ATR in the mammary gland (PM = 5). Because ATR is a relatively lipophilic compound (logKow = 2.75; Noble, 1993), its mammary gland PC is expected to change in response to dynamic changes in lipid composition. Among the possible reasons for the relatively high mammary gland PC may be increases in mammary gland size, blood flow, and lipid stores during pregnancy and/or lactation (Hanwell and Linzell, 1973; Rosso et al., 1981; Pujol et al., 2006). This life stage-dependent chemical partitioning property has been observed with other chemicals, such as PCBs, which have mammary gland PC 8-fold higher than that in the liver of lactating rats (Lee et al., 2007). On the other hand, the mammary gland PCs of DE, DIP and DACT are not as high as that of ATR, probably due to their lower lipophilicity, i.e., the logKow values are 1.51, 1.12 and 0.11 for DE, DIP and DACT, respectively (Noble, 1993; Kaune et al., 1998).

Metabolic rates of ATR in repeated exposures are higher than the corresponding in vitro values (Hanioka et al., 1999b) or the estimated single exposure in vivo values. One possible reason is the physiological changes occurring during pregnancy and/or lactation. However, normal pregnancy is generally associated with a small decrease in total rodent liver P450 content and/or activity (He et al., 2005; He et al., 2007; Koh et al., 2011). Specifically, the expression of major ATR metabolizing P450 isoforms (i.e., CYP2B2, CYP2D1, CYP2E1) in female rats is moderately decreased during late gestation (He et al., 2005), indicating that the increased ATR metabolism is unlikely due to physiological factors. A more likely reason for the increased metabolic rates is ATR autoinduction metabolism, as discussed in detail in the Methods section. Other pesticides (e.g., pyrethroids and chlorpyrifos) and certain drugs (e.g., carbamazepine and

voriconazole) can increase their own metabolism or the metabolism of other compounds that are substrates for the same P450s (Scheyer et al., 1994; Roffey et al., 2003; Das et al., 2008; Yang et al., 2009; Casabar et al., 2010). PBPK model-predicting changes in metabolism due to P450 induction have also been implemented for other chemicals, such as PCBs (Sasso et al., 2012), TCDD (Andersen et al., 1997; Emond et al., 2006), and methylene chloride (Thomas et al., 1996). Of note, ATR induces the expression and activity of several P450s in human hepatocytes (Abass et al., 2012), indicating potential human relevance of this finding. However, some details about ATR autoinduction metabolism remain uncertain. Thus, the detailed ATR autoinduction metabolism profile, especially in chronic low-dose rodent exposures and in humans, needs to be developed.

By using mouse-specific parameters, the present gestational model properly predicted measured mouse plasma/tissue ATR/DACT concentrations at 2 time points, validating the model in mice and suggesting that it could be used for species extrapolation, including as a foundation for extrapolating to humans. Of note, in our mouse study, the measured ATR/DACT concentrations in the placenta are similar to those in maternal plasma. Within the context of ATR pharmacokinetic studies, this is the first report of ATR/metabolite concentrations in the placenta. These novel results are in agreement with data from pregnant rats (Fraites et al., 2011) where ATR/DACT concentrations in the whole unwashed fetus are similar to those in maternal plasma and suggest that fetuses are exposed to a placental compartment where levels of ATR/DACT are comparable to their maternal plasma levels. Consistent with our finding, other pesticides, such as chlorpyrifos, pass the placenta efficiently and reach the fetus (Salama et al., 1993; Abdel-Rahman et al., 2002). While the species extrapolation of the model across two different time points was validated with our in vivo mouse study, there are uncertainties in the model

parameters describing urine elimination of DACT in rat dams and pups due to the lack of rat urine data and the lack of complete detailed time-course data for model calibration. To improve the robustness of the present models, more detailed pharmacokinetic studies are warranted to capture the time-course kinetics of ATR and DACT in both maternal and neonatal plasma and urine.

Based on our measured mouse fetal ATR/DACT levels and the model simulations, it seems that around 10% of the DACT that reaches the fetus is fetal-tissue bound, suggesting that the fetus has low capacity/affinity to bind DACT. This may be because fetal hemoglobin's higher oxygen binding affinity (Adachi et al., 1997) and the more polar nature of DACT. In addition, the accurate predictions of ATR levels in the washed mouse fetus suggest that most fetal ATR is fetal-tissue bound. While fetal ATR is much lower than fetal DACT levels, its toxicological importance cannot be completely overlooked. For example, binding of ATR to growth hormone-releasing hormone receptor results in inhibition of growth hormone gene transcription in neonatal rat pituitary cells exposed to environmentally-relevant levels of ATR (Fakhouri et al., 2010). In terms of DACT, it binds multiple proteins involving energy regulation and cellular defense in the brain of adult ATR-exposed rats (Dooley et al., 2010); the toxicological consequence of the DACT-adducted proteins remains to be elucidated. The lower fetal tissue binding of DACT might result in higher availability of free DACT that can cross the immature fetal blood–brain barrier and affect brain development. In addition, the period of exposure also contributes to the reported greater vulnerability of the developing nervous system to ATR (Giusi et al., 2006; Belloni et al., 2011), especially when the exposure coincides with key brain developmental processes (Rice and Barone, 2000), such as neuronal differentiation, which is affected by both ATR and DACT (Lin et al., 2013a). Further studies that measure the fetal target

tissue bound fraction of ATR or DACT and, importantly, determine the toxicological significance of the binding will be helpful in refining the gestational PBPK model and elucidating the mechanisms of ATR's developmental neurotoxicity.

The mechanism behind the rapid placental transfer of ATR/metabolites is unclear. Placental transfer of chemicals can be influenced by numerous factors, including chemical properties, placental characteristics, maternal, and fetal factors (Poulsen et al., 2009). In this regard, the relative lipophilicity of ATR and its metabolites (Noble, 1993) may contribute to their rapid placental transfer. Moreover, ATR, DE, DIP, and DACT are all weak bases and the pH gradient between the maternal and embryonic plasma may trap ionized forms of these chemicals in the slightly more acidic embryonic compartment (Rogers and Kavlock, 2001). Also, the ability of ATR and DACT to bind to plasma, RBC, or tissue proteins (Lu et al., 1998; Dooley et al., 2006; Dooley et al., 2007; Dooley et al., 2008; Dooley et al., 2010; Fakhouri et al., 2010) and the lack of elimination pathways in the fetal compartment may favor partitioning of these chemicals into the placenta-fetal unit. In addition, it cannot be ruled out that their placental transfer is mediated via an active transport process by placental membrane transporters, such as ATP-binding cassette (ABC) transporters. Although their involvement in the placental transport of ATR/metabolites is unknown at this time, a recent study showed that ATR induces expression of an ABC transporter (*ZmMRP1*) in corn (Pang et al., 2012). As placental transfer rate parameters are important for determining fetal ATR or DACT levels, future studies characterizing this process by using in vitro or in vivo approaches, such as in Prouillac and Lecoeur (2010), are needed.

Based on the lactational model simulations, neonatal exposure to ATR via milk consumption is minimal. This may be due to the rapid metabolism of ATR in dams [the plasma

half-lives of ATR (3-50 mg/kg) range from 0.7 to 2.9 h (EPA, 2011)], the low milk transfer of ATR (Fraites et al., 2011), or the increased metabolism of ATR during early postnatal life (Lucier et al., 1979; Watanabe et al., 1993). The large contribution of gestational DACT carryover to its neonatal dosimetry is likely attributable to DACT's relatively longer half-life [4.8–42 h at ATR doses from 5 to 250 mg/kg (Ross et al., 2009)]. Its abundance and ability to bind plasma, RBC and tissue proteins may also play a role (Dooley et al., 2006; Dooley et al., 2007; Dooley et al., 2010). Model predictions also indicate that neonatal brain DACT AUC during the first half of lactation is 4.6-fold higher than during the second half. In rodents, DACT is excreted primarily via the urine (Ross et al., 2009). Hence, possible reasons for the higher neonatal brain DACT dosimetry during early lactation may be smaller bladder capacity and immature voiding of rat pups during the first 10 PNDs (Zvarova and Zvara, 2012). Also, as the pups grow, body and brain volumes increase and milk consumption rate (L/h/kg) decreases (Yoon et al., 2009b). As milk is the only source of DACT, their exposure (neonatal brain DACT AUC) will likely decrease, especially during late lactation. Because neonatal brain DACT levels are highly sensitive to milk clearance rate parameters, further studies assessing the transfer of ATR and its metabolites into milk could be used to refine the lactational model.

To demonstrate how the present models can aid risk assessment of developmental exposure to ATR, the linked model was run across a wide dose range (0.00000001–100,000 μg/kg [0.00001–100 mg/kg]) for a literature-based exposure scenario (GD14–PND21) and the levels of several internal dose metrics (average daily AUCs of maternal plasma/fetal/neonatal brain DACT) were predicted (Fig. 5.7). Dosimetry of DACT was chosen because DACT, the predominant metabolite of ATR, is readily detected in ATR-exposed rodents or humans (Barr et al., 2007; Ross et al., 2009; Chevrier et al., 2011; Fraites et al., 2011);

neonatal plasma/tissue levels of ATR are too low to be detected with current methodology even in pups born to rodent dams exposed to relatively high doses of ATR (Fraites et al., 2011). The regression equations for each internal dose metrics are also given, along with the estimated environmental/occupational exposure levels (Gammon et al., 2005), points of departure observed from studies in rats (EPA, 2003), and external doses to the dam at which certain adverse developmental effects in the offspring were observed (Rooney et al., 2003; Giusi et al., 2006; Belloni et al., 2011). These equations correlate fetal/neonatal brain dosimetry with maternal plasma dosimetry well. Thus, in terms of exposure assessment, once exposure duration is known, appropriate equations can be created and utilized to predict fetal/neonatal target organ exposure based on maternal data, as demonstrated in Fig. 5.5A and Fig. 5.5B for gestational and lactational exposures, respectively. This is particularly important because (1) in epidemiology or biomonitoring studies involving pregnant/lactating women, the available data are almost exclusively from maternal blood or urine (Chevrier et al., 2011; Woodruff et al., 2011) and (2) in rodent studies, while the external dose to the dam is known, usually no information is available on the fetal/neonatal dose (Giusi et al., 2006; Belloni et al., 2011). From a regulatory perspective, the occupational exposure levels and the current guideline values (LOAEL and NOAEL), which are based on rodent studies, are all higher than the external dose that results in behavioral deficits in a developmental exposure paradigm in rodents (Belloni et al., 2011); on the other hand, the estimated environmental exposure levels are substantially lower than the lowest (Belloni et al., 2011) external dose associated with adverse neurodevelopmental outcome in rodents. Thus, from a gestational/lactational exposure point of view and assuming ATR dosimetry is comparable between rodents and humans, the risk of ATR overexposure in occupational, but not environmental, settings may be underestimated by current guidelines; additional studies, using

relevant exposure routes/scenarios, are necessary to determine whether developmental exposure guidelines for ATR need to be revised. To address potential species differences of ATR dosimetry between rodents and humans and to aid human risk assessment, the dose metrics associated with the critical external doses observed in rodent studies (Rooney et al., 2003; Giusi et al., 2006; Belloni et al., 2011) could be employed to predict oral human equivalent exposure doses by extrapolating the present rat models to humans (Gargas et al., 2000b, a; Crowell et al., 2011). However, to do that, more data are needed, including: (1) the potential ATR autoinduction metabolism profile in humans (human tissues), (2) pharmacokinetic data of pregnant/lactating/fetal/neonatal rodents receiving long-term low-dose ATR with intermittent high-dose acute challenges (spikes), a more realistic human exposure paradigm (Lozier et al., 2012), and (3) detailed plasma/urinary data from pregnant/lactating women with known recent exposure to ATR.

In conclusion, we have successfully developed gestational and lactational PBPK models for ATR in rats and extrapolated one of them to mice. These models can now be used to predict fetal or neonatal target organ (i.e., brain) dosimetry of ATR and its metabolites. Model predictions will provide insights into designing early life toxicity and pharmacokinetic studies and interpreting study findings. These models can be used as a framework for developing gestational and lactational PBPK models for other chlorotriazine herbicides. As more human biological monitoring data becomes available, these models can ultimately be scaled up to humans and help risk assessment of ATR in sensitive subpopulations, such as pregnant women, fetuses and neonates.

Conflict of interest statement

The authors declare that there are no conflicts of interest.

Disclaimer

The findings and conclusions in this report are those of the author(s) and do not necessarily represent the official position of the U.S. Food and Drug Administration. Mention of trade names is not an endorsement of any commercial product.

Acknowledgements

The experimental data used for model calibration was based on Fraites et al. (2011). We thank all the authors because this work was essential for our publication. We also wish to acknowledge Drs. K. Barry Delclos, Xiaoxia Yang, and Frederick Beland, National Center for Toxicological Research, Food and Drug Administration, Jefferson, AR, for critically reviewing this manuscript. Our interactions with Dr. Sheppard A. Martin, Neurotoxicology Branch, Toxicity Assessment Division, National Health and Environmental Effects Research Laboratory, Office of Research and Development, U.S. Environmental Protection Agency, Research Triangle Park, NC, with whom we had helpful methodological discussions, are also greatly appreciated.

Table 5.1. Physiological parameters for pregnant rats, fetuses, lactating rats and pups used in the PBPK modeling process.

Parameter	Values chosen	Sources
Pregnant rats		
Body weight (BW, kg)	0.24-0.38[c]	Clewell et al. (2003), Yoon et al. (2009a)
Cardiac output index (QCC, L/h/kg)	24.56-21.6[c]	Dowell and Kauer (1997), Yoon et al. (2009a)
Tissue volumes (fraction of initial BW)		
Liver (VLC, unitless)	0.0366	Brown et al. (1997)
Brain (VBRC, unitless)	0.0057	Brown et al. (1997)
Kidney (VKC, unitless)	0.0073	Brown et al. (1997)
Tissue volumes (fraction of BW)		
Blood[a] (VbloodC, unitless)	0.074	Brown et al. (1997)
Plasma[a] (VplasmaC, unitless)	0.047	Altman and Dittmer (1971), Brown et al. (1997), Clewell et al. (2003)
Red blood cells[a] (VrbcC, unitless)	0.027	Altman and Dittmer (1971), Brown et al. (1997), Clewell et al. (2003)
Tissue volumes (changing during pregnancy)		
Mammary gland (VM, L)	0.0024-0.013[c]	Hanwell and Linzell (1973), Rosso et al. (1981), Yoon et al. (2009a)
Fat (VF, L)[b]	0.017-0.024[c]	Naismith et al. (1982), Brown et al. (1997), Yoon et al. (2009a)
Placenta (Vpla, L)	0-0.0167[c]	O'Flaherty et al. (1992), Clewell et al. (2003), Yoon et al. (2009a)
Blood flows (fraction of initial cardiac output)		
Liver (QLC, unitless)	0.2408	Brown et al. (1997)
Brain (QBRC, unitless)	0.02	Brown et al. (1997)
Kidney (QKC, unitless)	0.141	Brown et al. (1997)
Blood flows (changing during pregnancy)		
Mammary gland (QM, L/h)	0.012-0.064[c]	Hanwell and Linzell (1973), Clewell et al. (2003), Yoon et al. (2009a)
Placenta (Qpla, L/h)	0-1.42[c]	O'Flaherty et al. (1992), Clewell et al. (2003), Yoon et al. (2009a)

[a] The fractional volumes of blood, plasma or red blood cells were assumed to remain constant across life stages.

[b] The fat was not described as a separate compartment in the gestational model. Fat volume was included for the purpose of calculating maternal BW only.

[c] These values represent the range of changes during gestation or lactation. Refer to the Appendix C for the values of these and other parameters (i.e., Urineflowfactor, Kneomet, Kneomet2, and KliverR) simulated with TABLE functions and growth equations for gestation and lactation (Tables C1-C12).

Table 5.1 (continued). Physiological parameters for pregnant rats, fetuses, lactating rats and pups used in the PBPK modeling process.

Parameter	Values chosen	Sources
Fetuses		
Body weight for individual fetus (V1fetus, kg)	0-0.0068[c]	Sikov and Thomas (1970), Yoon et al. (2009a)
Cardiac output index (QCCfetus, L/h/kg)	22.8	Girard et al. (1983), Yoon et al. (2009a)
Lactating rats		
Body weight (BW, kg)	0.257-0.292[c]	Shirley (1984), Yoon et al. (2009b)
Cardiac output index (QCC, L/h/kg)	29.5-48.8[c]	Hanwell and Linzell (1973), Dowell and Kauer (1997), Yoon et al. (2009b)
Tissue volumes (fraction of postnatal BW)		
Brain (VBRC, unitless)	0.0057	Brown et al. (1997)
Tissue volumes (fraction of BW)		
Liver (VLC, unitless)	0.0376-0.0524[c]	Hanwell and Linzell (1973), Yoon et al. (2009b)
Kidney (VKC, unitless)	0.0073-0.008[c]	Hanwell and Linzell (1973)
Mammary gland (VMC, unitless)	0.049-0.054[c]	Hanwell and Linzell (1973), Rosso et al. (1981), Yoon et al. (2009b)
Blood flows (fraction of cardiac output)		
Liver (QLC, unitless)	0.2408-0.3853[c]	Hanwell and Linzell (1973), Yoon et al. (2009b)
Brain (QBRC, unitless)	0.02	Brown et al. (1997)
Kidney (QKC, unitless)	0.141-0.1008[c]	Hanwell and Linzell (1973)
Mammary gland (QMC, unitless)	0.09-0.13[c]	Hanwell and Linzell (1973), Yoon et al. (2009b)
Milk suckling rate (L/h/kg, individual pup)	0.0216-0.0073[c]	Mirfazaelian and Fisher (2007), Yoon and Barton (2008), Yoon et al. (2009b)
Growing pups		
Body weight (BWpup, kg)	0.0067-0.057[c]	Mirfazaelian and Fisher (2007)
Cardiac output (QCpup, L/h)	0.3-2.03[c]	Rodriguez et al. (2007a)
Tissue volumes (actual volume)		
Liver (VLpup, L)	0.00034-0.0021[c]	Mirfazaelian and Fisher (2007)
Brain (VBRpup, L)	0.00021-0.0015[c]	Mirfazaelian and Fisher (2007)
Kidney (VKpup, L)	0.000075-0.00031[c]	Mirfazaelian and Fisher (2007)
Tissue blood flows (fraction of cardiac output)		
Liver (QLCpup, unitless)	0.045-0.128[c]	Stulcová (1977), Yoon et al. (2009b)
Brain (QBRCpup, unitless)	0.093-0.046[c]	Stulcová (1977), Yoon et al. (2009b)
Kidney (QKCpup, unitless)	0.015-0.0764[c]	Stulcová (1977), Loccisano et al. (2012)

Table 5.2. Chemical-specific parameters used for the development of gestational and lactational PBPK models of ATR in rats.

Parameter	Description	ATR	DE	DIP	DACT	Sources
Absorption[a]						
K1C ($kg^{0.25}$/h)	Gastric absorption rate constant scalar	0.2	-	-	-	Ross et al. (2009), Lin et al. (2011)
K2C ($kg^{0.25}$/h)	Gastric-emptying rate constant scalar	0.7	-	-	-	Ross et al. (2009), Lin et al. (2011)
K3C ($kg^{0.25}$/h)	Intestinal absorption rate constant scalar	0.018[b]	-	-	-	Estimated based on Bakke et al. (1972), Timchalk et al. (1990) and Lin et al. (2011)
PCs for the dam						
PL[a]	Liver:blood PC	0.69*	1^	1^	1^	*: Tremblay et al. (2012) ; ^: McMullin et al. (2007b)
PBR[a]	Brain:blood PC	0.73*	0.5^[c]	0.5^[c]	0.9^[c]	*: Tremblay et al. (2012); ^: estimated based on Fraites et al. (2011)
PK[a]	Kidney:blood PC	1	1	1	1	McMullin et al. (2007b)
PM	Mammary gland:blood PC	5^[c]	1*	1*	0.8^[c]	*:McMullin et al. (2007b); ^: estimated based on Fraites et al. (2011)
PP	Placenta:blood PC	1	1	1	1	McMullin et al. (2007b)
Poth[a]	Other tissue:blood PC	1	1	1	1	McMullin et al. (2007b)
Plasma protein binding[a]						
BmaxC (μg/kg)	Maximal binding capacity scalar	601.78[d]	-	-	15974.84[d]	Ross et al. (2009), Lin et al. (2011)
Ka (/(μg*h))	Association rate constant	0.05[e]	-	-	0.002[e]	Lu et al. (1998), Lin et al. (2011)
Kd (/h)	Dissociation rate constant	1[f]	-	-	1[f]	Lin et al. (2011)

- Indicates parameter not included in the models.

[a] Parameters assumed to be the same in pregnant/lactating rats and pups.

[b] These parameters were estimated based on the data from Bakke et al. (1972) and Timchalk et al. (1990) as described in Lin et al. (2011).

[c] Data set at 5 mg/kg in study 1 (ATR exposure: GD14-20) from Fraites et al. (2011) was used to estimate these parameters by visual fitting.

[d] Data set at 250 mg/kg from Ross et al. (2009) was used to estimate these parameters as described in Lin et al. (2011).

[e] Data set from Lu et al. (1998) was used to estimated these parameters by visual fitting as described in Lin et al. (2011).

[f] Assigned default value as described in Lin et al. (2011).

[g] Initial maximal metabolic rates in pregnant or lactating rats. Refer to the Methods section for detailed description of these parameters.

[h] Kincreasefactor, Kincreasefactor1 and Kincreasefactor2 represent autoinduction metabolism factors for ATR, DE and DIP, respectively. Refer to the Methods section and Fig. C1 (Appendix C) for detailed description of these parameters.

[i] Data set at 5 mg/kg in study 2 (ATR exposure: GD14 - PND10) from Fraites et al. (2011) was used to estimated these parameters by visual fitting.

Table 5.2 (continued). Chemical-specific parameters used for the development of gestational and lactational PBPK models of ATR in rats.

Parameter	Description	ATR	DE	DIP	DACT	Sources
Red blood cell binding[a]						
BmaxC (μg/kg)	Maximal binding capacity scalar	12725.71[d]	-	-	1228296.45[d]	Ross et al. (2009), Lin et al. (2011)
Ka (/(μg*h))	Association rate constant	0.01[e]	-	-	0.0002[e]	Lu et al. (1998), Lin et al. (2011)
Kd (/h)	Dissociation rate constant	1[f]	-	-	1[f]	Lin et al. (2011)
Brain tissue binding[a]						
BmaxC (μg/kg)	Maximal binding capacity scalar	284.71[d]	-	-	7503.1[d]	Ross et al. (2009), Lin et al. (2011)
Ka (/(μg*h))	Association rate constant	0.6[e]	-	-	0.02[e]	Lu et al. (1998), Lin et al. (2011)
Kd (/h)	Dissociation rate constant	1[f]	-	-	1[f]	Lin et al. (2011)
Metabolism						
VmaxcATR_DE (μg/h/kg$^{0.75}$)	Maximal metabolic rate from ATR to DE	35925.33[g]	-	-	-	Lipscomb et al. (1998), Hanioka et al. (1999b), Kramer et al. (2001), Lin et al. (2011)
VmaxcATR_DIP (μg/h/kg$^{0.75}$)	Maximal metabolic rate from ATR to DIP	388265.62[g]	-	-	-	Lipscomb et al. (1998), Hanioka et al. (1999b), Kramer et al. (2001), Lin et al. (2011)
Vmaxc1 (μg/h/kg$^{0.75}$)	Maximal metabolic rate from DE to DACT	-	2626.82[g]	-	-	Ross et al. (2009), Lin et al. (2011)
Vmaxc2 (μg/h/kg$^{0.75}$)	Maximal metabolic rate from DIP to DACT	-	-	7291.2[g]	-	Ross et al. (2009), Lin et al. (2011)
KmATR_DE (μg/L)[a]	Michaelis-Menten constant	9598.21	-	-	-	Hanioka et al. (1999b), Lin et al. (2011)
KmATR_DIP (μg/L)[a]	Michaelis-Menten constant	10870.78	-	-	-	Hanioka et al. (1999b), Lin et al. (2011)
Km1 (μg/L)[a]	Michaelis-Menten constant	-	2439.19	-	-	McMullin et al. (2007b), Lin et al. (2011)
Km2 (μg/L)[a]	Michaelis-Menten constant	-	-	2256.8	-	McMullin et al. (2007b), Lin et al. (2011)
Kincreasefactor	Auto-induction metabolism profile	0.0-4.0[h]	0.0-1.0[h]	0.0-1.0[h]	-	Hanioka et al. (1998b), Islam et al. (2002), Dong et al. (2009), Abass et al. (2012)

Table 5.2 (continued). Chemical-specific parameters used for the development of gestational and lactational PBPK models of ATR in rats.

Parameter	Description	ATR	DE	DIP	DACT	Sources
Elimination[a]						
KurineC (/(h*kg$^{0.75}$))	Urine elimination rate constant scalar	-	1[c]	0.5[c]	14[c]	Estimated based on Fraites et al. (2011)
K4C (kg$^{0.25}$/h)	Fecal elimination rate constant scalar	0.006[b]	-	-	-	Estimated based on Bakke et al. (1972), Timchalk et al. (1990) and Lin et al. (2011)
Placental transfer						
KtransinC (L/h/kg$^{0.75}$)	Diffusion rate constant scalar from maternal placenta to fetal venous blood	1.1[c]	1.1[c]	1.2[c]	1.4[c]	Estimated based on Fraites et al. (2011)
KtransoutC (L/h/kg$^{0.75}$)	Diffusion rate constant scalar from fetal arterial blood to maternal placenta	1[c]	1[c]	1[c]	1[c]	Estimated based on Fraites et al. (2011)
PCs for the fetus						
Pfetus	Fetus:blood PC	1	1	1	1	McMullin et al. (2007b)
Whole fetal tissue binding						
BmaxC (µg/kg)	Maximal binding capacity scalar	284.71	-	-	7503.1	Assumed equal to the maternal brain
Ka (/(µg*h))	Association rate constant	0.15[e]	-	-	0.006[e]	Lu et al. (1998), Lin et al. (2011)
Kd (/h)	Dissociation rate constant	1[f]	-	-	1[f]	Lin et al. (2011)
Milk clearance						
Kmilkc (L/h/kg$^{0.75}$)	Diffusional clearance from mammary gland tissue into milk	0.0035[i]	0.0035[i]	0.0035[i]	0.0035[i]	Estimated based on Fraites et al. (2011)
Neonatal absorption						
Frac (%)	Fractional absorption	100	100	100	100	Xu (1996)

Table 5.3. Gestational model predicted and measured concentrations of ATR/DACT in maternal plasma, tissues and fetuses[a].

	ATR		DACT	
Tissue	Simulated	Experimental	Simulated	Experimental
5 mg/kg				
Maternal plasma	5.2[b]	2.9 ± 0.8	705.3[b]	980.0 ± 88.6
Maternal brain	3.4[b]	2.8 ± 0.9	546.5[b]	776.7 ± 96.5
Mammary gland	22.5[b]	15.2 ± 5.1	409.0[b]	466.7 ± 71.5
Whole fetus	5.2[b]	4.3 ± 0.9	750.7[b]	1094.2 ± 70.5
25 mg/kg				
Maternal plasma	25.7[b]	37.3 ± 9.5	3465.8[b]	3333.3 ± 540.1
Maternal brain	16.9[b]	31.0 ± 4.3	2702.1[b]	2700.0 ± 561.3
Mammary gland	112.9[b]	210.0 ± 44.2	2030.5[b]	1763.3 ± 660.0
Whole fetus	26.2	77.9 ± 14.5	3693.5[b]	4070.0 ± 582.5

[a] Pregnant Sprague Dawley rats were exposed to ATR (5 or 25 mg/kg) from GD18 to GD20 by daily oral gavage. Experimental data (means ± SEM) are from Study 3 in Fraites et al. (2011). Data represent concentrations at 2 h after last dosing on GD20. Unit: ng/g or ng/ml.

[b] Indicates that simulated values are within two-fold range of the experimental data.

Table 5.4. Gestational model predicted and measured concentrations of ATR/DACT in the mouse dam plasma/tissues and whole fetus[a].

	ATR		DACT	
	Simulated	Experimental	Simulated	Experimental
Plasma				
2 h	3.58[b]	6.88 ± 5.54	164.62[b]	140.15 ± 38.91
6 h	1.90	0.65 ± 0.30	64.94[b]	88.45 ± 31.08
Brain				
2 h	2.55[b]	9.89 ± 6.76	143.84[b]	130.12 ± 37.03
6 h	1.36[b]	2.81 ± 0.59	56.43[b]	99.99 ± 35.13
Placenta				
2 h	3.45[b]	7.70 ± 3.61	160.82[b]	102.02 ± 20.81
6 h	1.79[b]	2.39 ± 0.47	61.13[b]	76.40 ± 34.20
GD18 fetus				
2 h	4.46[b]	5.53 ± 3.24	250.08	15.48 ± 1.86
6 h	2.04[b]	1.95	88.96	17.82

[a] C57BL/6 mouse dams were exposed to vehicle or ATR (5 mg/kg) by daily oral gavage from GD12 to GD18. Levels of ATR/metabolites were analyzed by LC-MS/MS as described in the Methods section. Experimental data are expressed as means ± SEM and represent concentrations at 2 or 6 h after the last dosing on GD18. Unit: ng/g or ng/ml. Concentrations in the vehicle-treated dam were below limits of quantification and are not shown.

[b] Indicates that simulated values are within two-fold range of the experimental data.

Table 5.5. Lactational model predicted and measured levels of DACT/^{14}C-chlorotriazines in milk and neonatal brain.

	Milk concentration[b] (ng/g)		Neonatal brain				Neonatal brain/milk concentration ratio	
			Concentration (ng/g)		% of administered dose			
Treatment[a]	Simulated[c]	Experimental[d]	Simulated[c]	Experimental[d]	Simulated[c]	Experimental[d]	Simulated[c]	Experimental[d]
2 mg ^{14}C-ATR	524.24[ef]	658 ± 370	4.68[e]	13 ± 0.2	0.000095[e]	0.00022 ± 0.00004	0.009[e]	0.020
4 mg ^{14}C-ATR	1050.36[ef]	1172 ± 650	9.38[e]	20 ± 0.2	0.000096[e]	0.00018 ± 0.00001	0.009[e]	0.017

[a] Lactating Wistar rats (mean BW ± SEM: 0.3055 ± 0.002 kg) were exposed to ^{14}C-ATR (2 or 4 mg/rat) on PND3 by oral gavage (Stoker and Cooper, 2007).

[b] Neonatal stomach contents were used as a surrogate for milk in Stoker and Cooper (2007).

[c] Simulated levels for DACT.

[d] Measured levels (means ± SD) for ^{14}C-chlorotriazines (Stoker and Cooper, 2007).

[e] Indicates that simulated values are within two-fold range of the experimental data.

[f] Indicates that simulated values are within the SD of the experimental data.

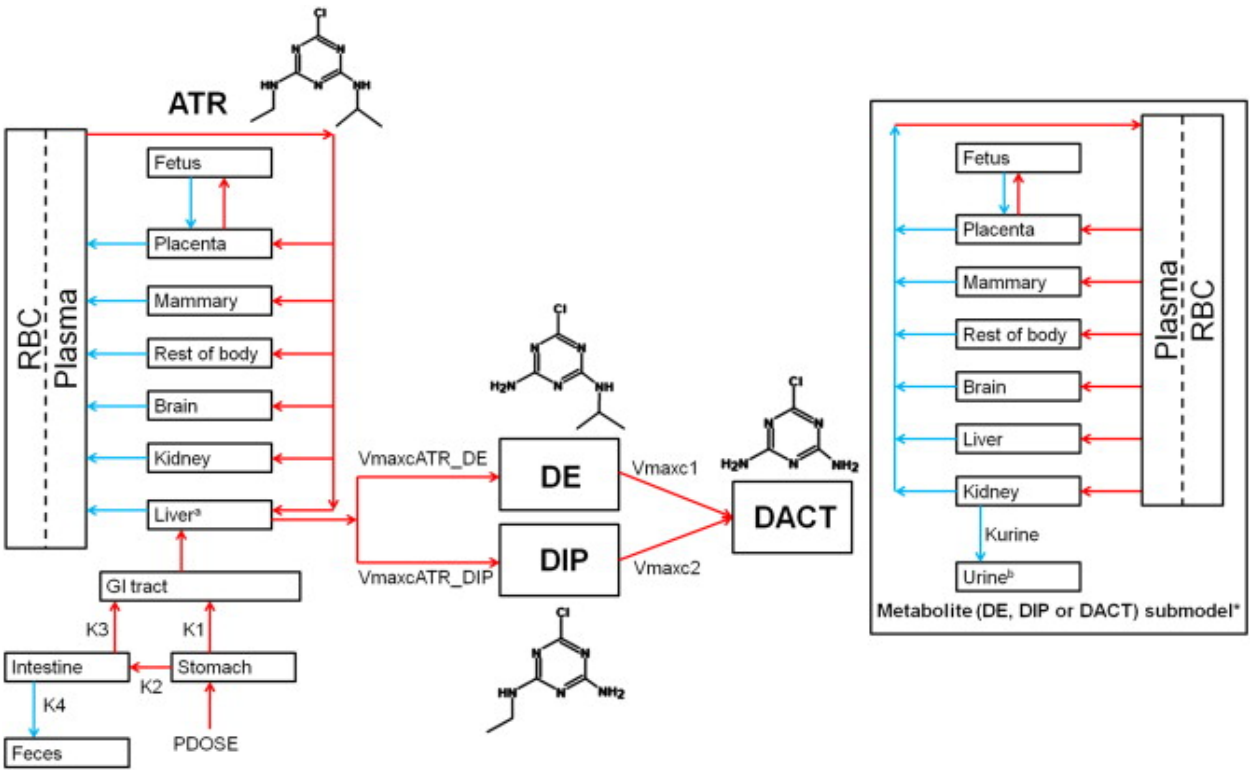

Figure 5.1. A schematic diagram for a gestational PBPK model of ATR (atrazine) in the pregnant rat. ATR's major metabolites are: DE (desethylatrazine), DIP (desisopropylatrazine), and DACT (didealkylatrazine). The fetus is modeled as a single compartment. *The inset on the right shows the submodel for DACT; the submodels for DE and DIP are identical to DACT's submodel except that they do not include RBC or plasma protein binding in the blood compartment. The chemical structures of ATR, DE, DIP, and DACT are also included in the figure. [a] and [b] highlight representative novel modeling algorithms used in the present model: ([a]) exposure dependent P450-mediated autoinduction metabolism of ATR, DE and DIP in the liver compartment and ([b]) gestational stage-dependent urine elimination of metabolites. VmaxcATR_DE, VmaxcATR_DIP, Vmaxc1, and Vmaxc2 represent maximal metabolic rates from ATR to DE, from ATR to DIP, from DE to DACT, and from DIP to DACT, respectively, in naïve rats.

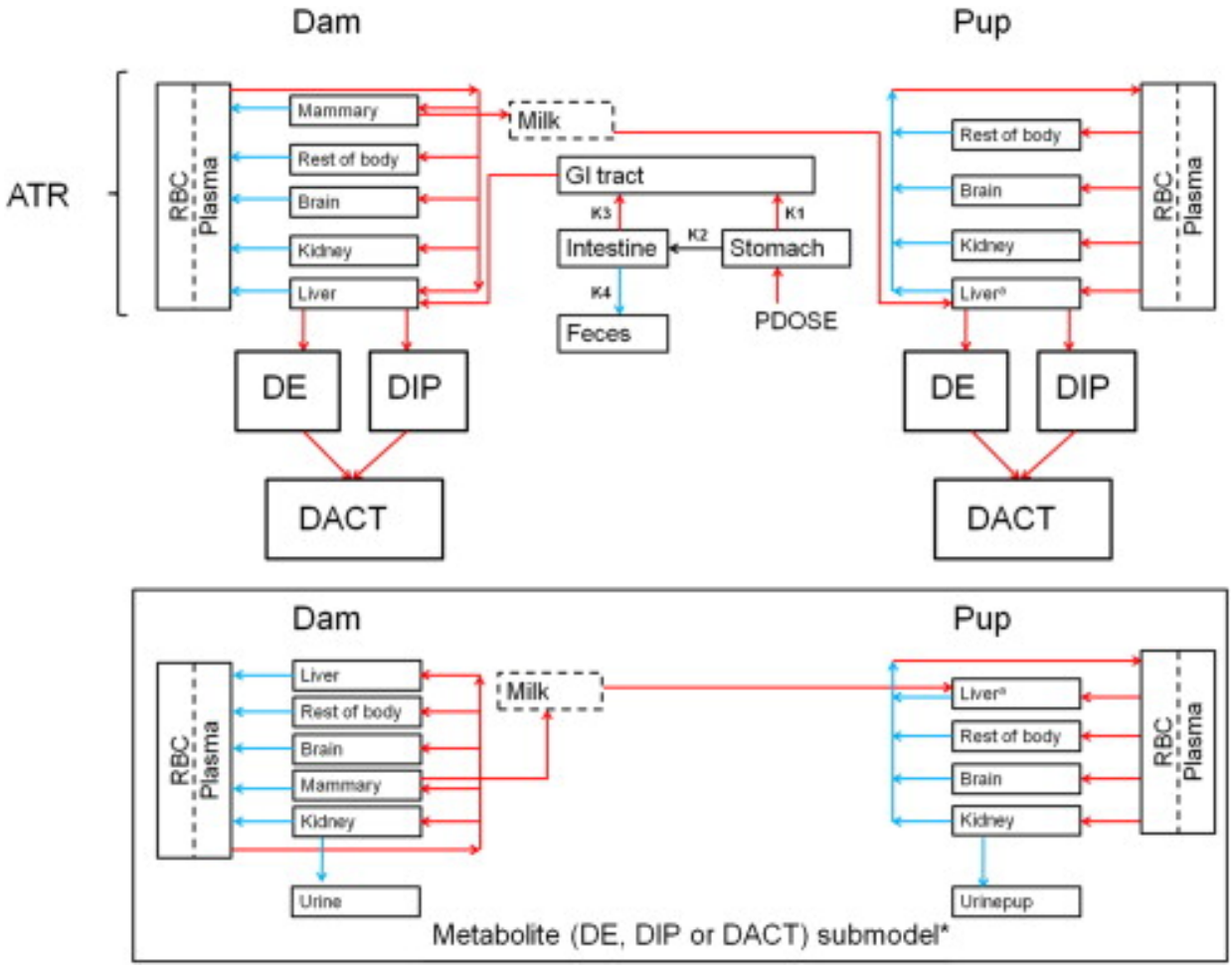

Figure 5.2. A schematic diagram for a lactational PBPK model of ATR (atrazine) in the lactating rat and pups. ATR's major metabolites are: DE (desethylatrazine), DIP (desisopropylatrazine), and DACT (didealkylatrazine). Only the dam is dosed directly (oral gavage); both ATR and its metabolites are transferred to the pup through milk. *The inset on the bottom shows the submodel for DACT; the submodels for DE and DIP are identical to DACT's submodel except that they do not include RBC or plasma protein binding in the blood compartment. For chemical structures of ATR, DE, DIP, and DACT, refer to Figure 5.1. [a] highlights representative novel modeling algorithms used in the present model, i.e., neonatal age-dependent P450-mediated metabolism of ATR, DE and DIP in the neonatal liver compartment.

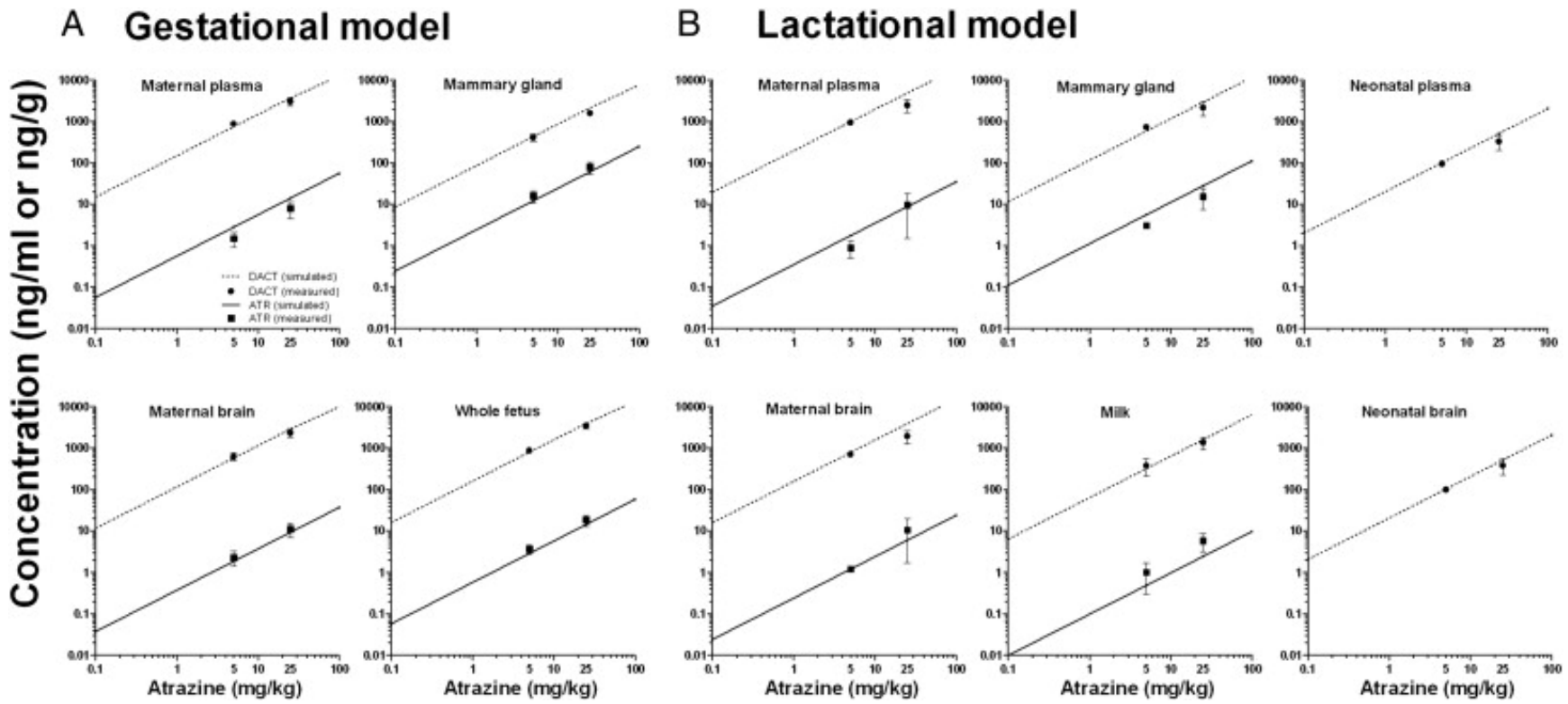

Figure 5.3. Comparison of model predictions (ATR: solid lines; DACT: dotted lines) and measured concentrations (Fraites et al., 2011) of ATR (■, means ± SEM) and DACT (●, means ± SEM) in the whole fetus, milk, or maternal/neonatal plasma/tissues following maternal exposure to ATR (5 or 25 mg/kg) by daily oral gavage from GD14 to GD20 (A) or from GD14 to PND10 (B). Data represent concentrations at 2 h after the last dosing.

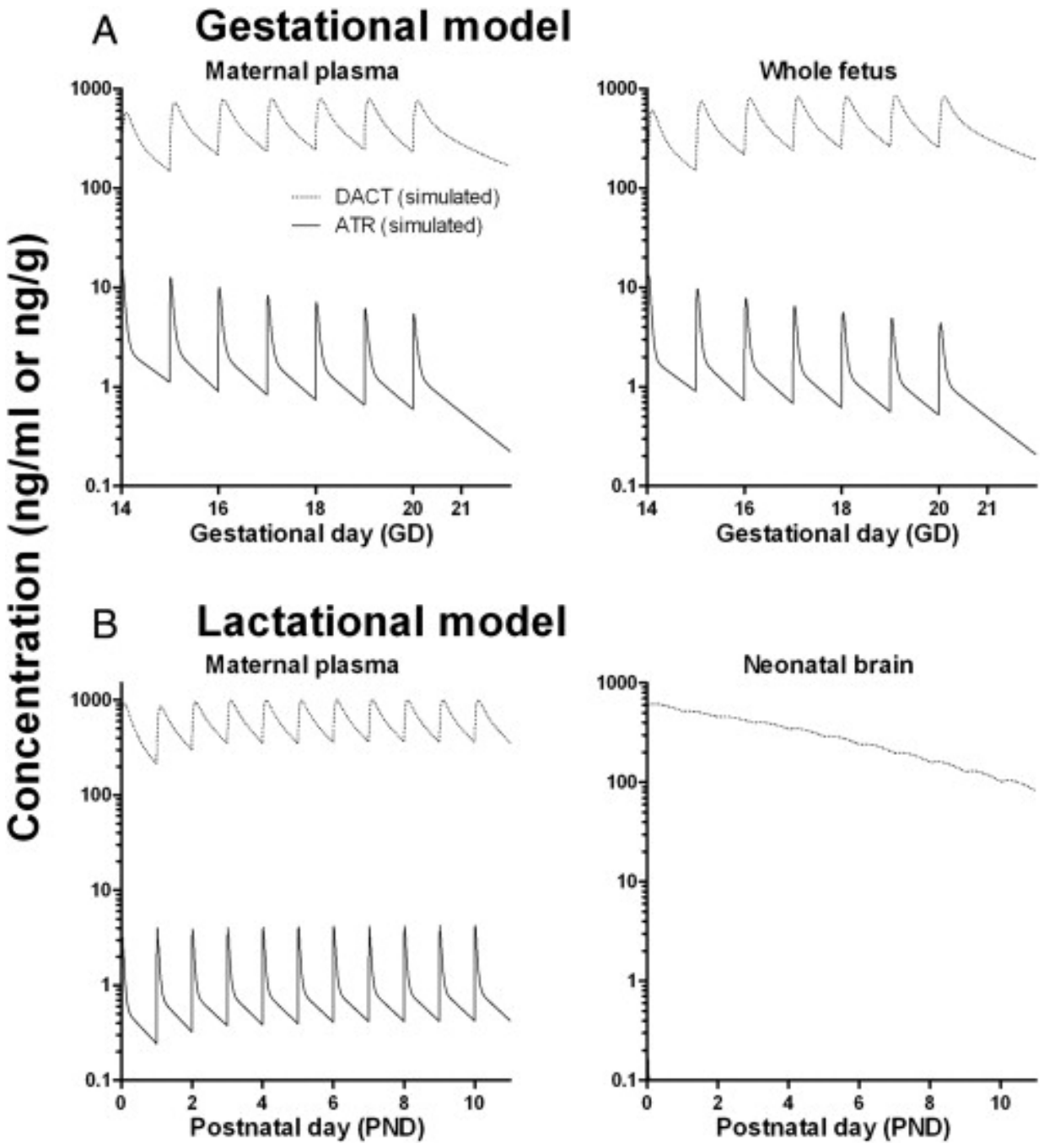

Figure 5.4. Model-predicted concentrations of ATR (solid lines) and DACT (dotted lines) in maternal plasma, whole fetus, or neonatal brain following maternal exposure to ATR (5 mg/kg) by daily oral gavage from GD14 to GD20 (A) or from GD14 to PND10 (B).

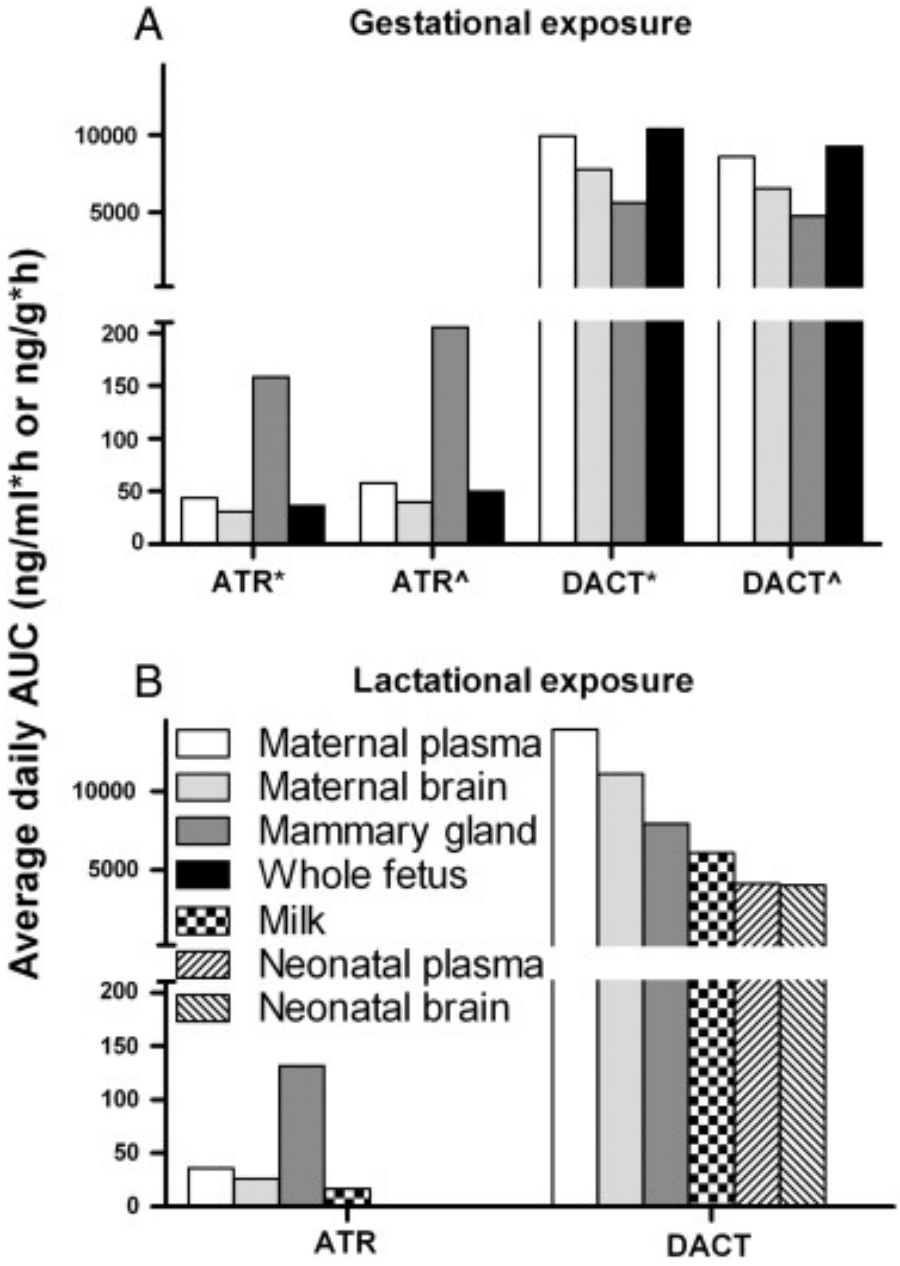

Figure 5.5. Comparison of model-derived estimates between maternal and fetal/neonatal exposures to ATR or DACT in a 7-day (*: GD14–20; A), a 3-day (^: GD18–20; A) or an 11-day (PND0–10; B) oral ATR (5 mg/kg) exposure paradigms. Bars represent simulated average daily AUCs of ATR or DACT concentrations in maternal plasma, maternal brain, mammary gland, whole fetus, milk, neonatal plasma or neonatal brain during respective exposure periods. AUC: area under the concentration curve.

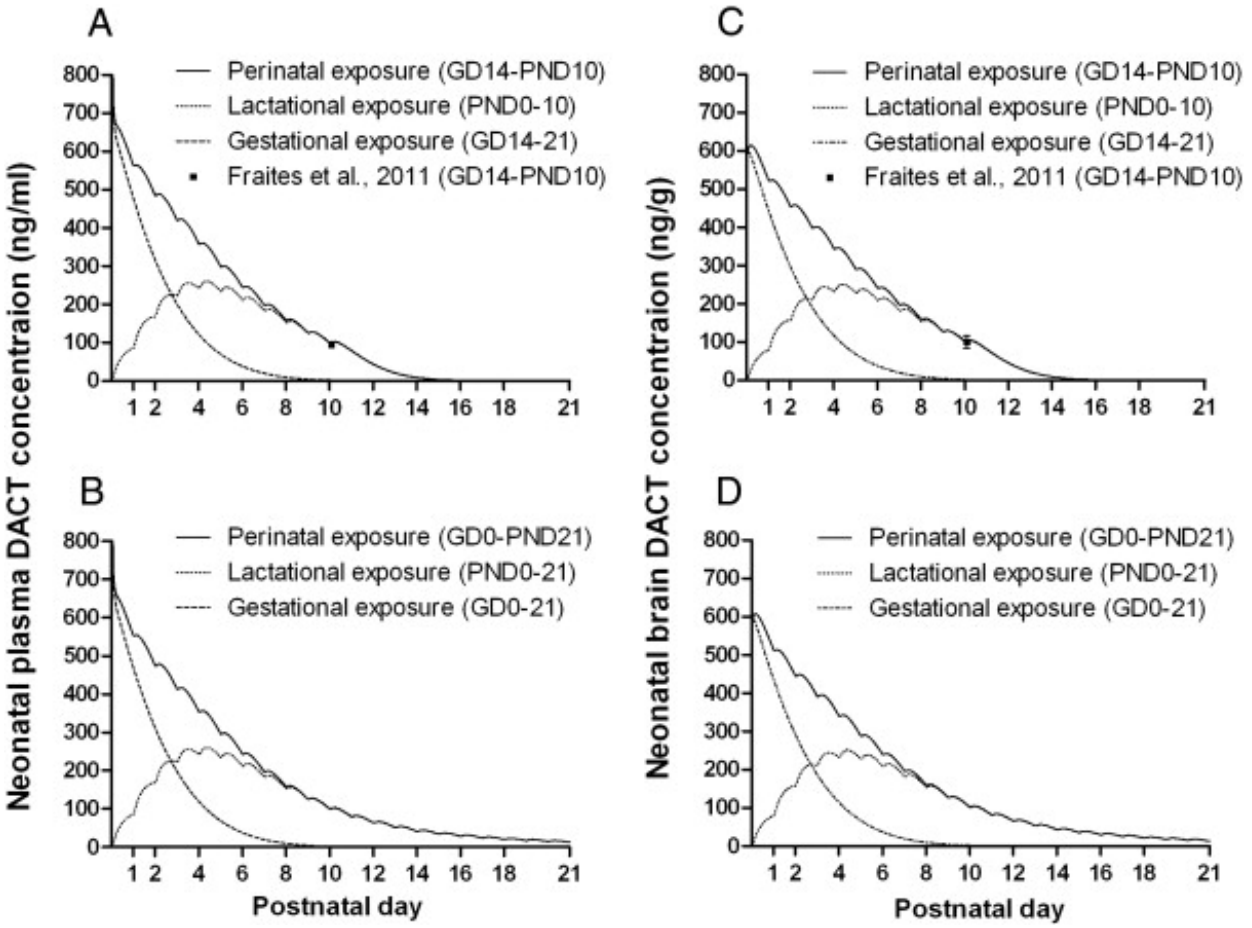

Figure 5.6. Comparison of model-derived gestational carryover and lactational exposure estimates. Solid lines represent simulated neonatal plasma (A, B) and brain (C, D) concentrations of DACT following maternal exposure to ATR (5 mg/kg) by daily oral gavage from GD14 to PND10 (A, C) or from GD0 to PND21 (B, D). Solid symbols (■, means ± SEM; Fraites et al., 2011) represent measured levels at 2 h after the lasting dosing on PND10 (A, C) after a 19-day exposure (GD14–PND10). Dash lines represent simulated gestational carryover from dams exposed to ATR (5 mg/kg) GD14–21 (A, C), or GD0–21 (B, D). Dotted lines represent simulated levels from dams exposed to ATR (5 mg/kg) PND0–10 (A, C), or PND0–21 (B, D).

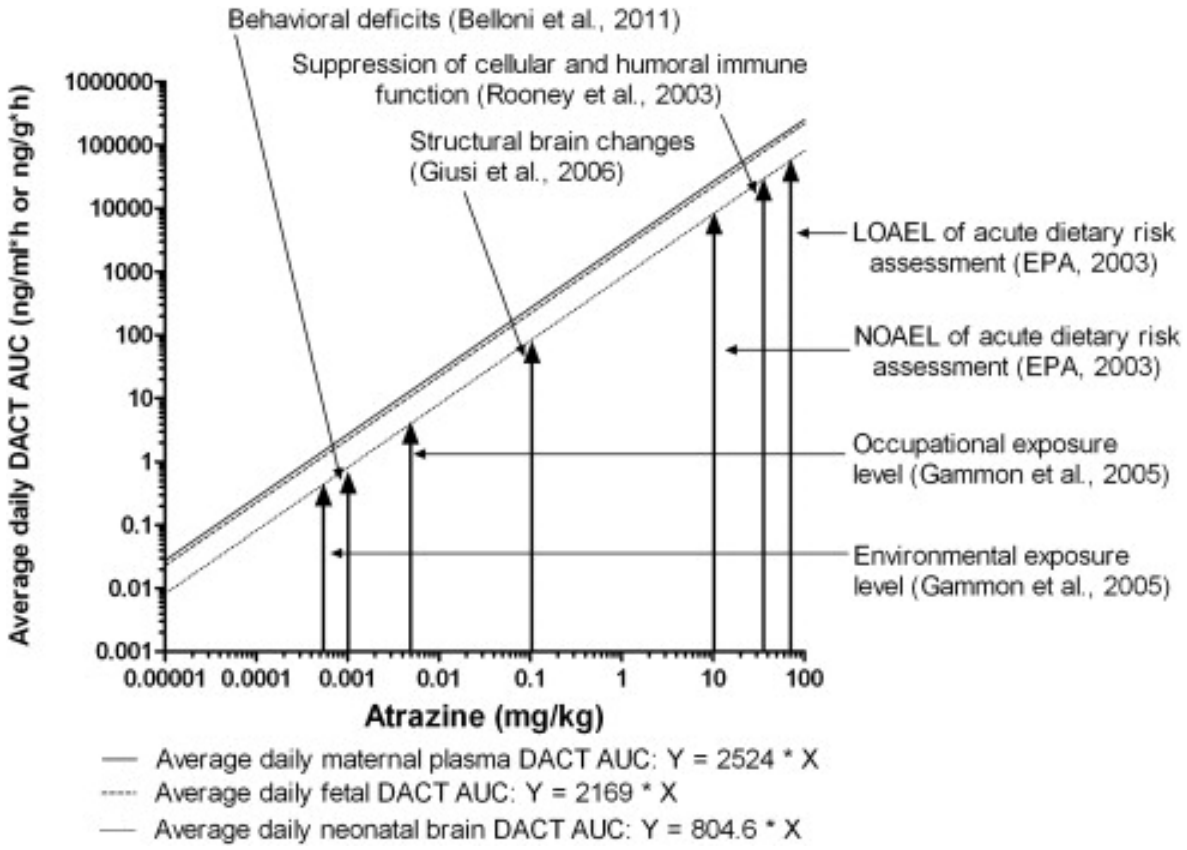

Figure 5.7. Simulations of dose-dependent average daily DACT AUCs in maternal plasma (solid line), whole fetus (dashed line), and neonatal brain (dotted line) at external doses to the dam ranging from 0.00001 to 100 mg/kg (0.00000001 to 100,000 μg/kg) given from GD14 to PND21. The exposure paradigm was chosen to resemble paradigms used in selected developmental rodent toxicity studies [GD14–PND21: Giusi et al. (2006), Belloni et al. (2011); GD10 to PND23: Rooney et al. (2003)]. Arrows represent estimated environmental/occupational exposure levels (Gammon et al., 2005), rodent studies-based points of departure (LOAEL and NOAEL) for acute dietary risk assessment (EPA, 2003), or LOAELs for different adverse effects from selected rodent studies. Regression equations for the three dose metrics of interest are also included on the figure. LOAEL: lowest observed adverse effect level; NOAEL: no observed adverse effect level; AUC: area under the concentration curve.

CHAPTER 6

DIFFERENTIATION STATE-DEPENDENT EFFECTS OF IN VITRO EXPOSURE TO ATRAZINE OR ITS METABOLITE DIAMINOCHLOROTRIAZINE IN A DOPAMINERGIC CELL LINE[1]

[1] Lin, Z., Dodd, C.A., Filipov, N.M. 2013. Life Sciences. 92(1):81-90. Reprinted here with permission of the publisher.

Abstract

Aims: This study sought to determine the impact of in vitro exposure to the herbicide atrazine (ATR) or its major mammalian metabolite diaminochlorotriazine (DACT) on dopaminergic cell differentiation.

Main methods: N27 dopaminergic cells were exposed for 24 or 48 h to ATR or DACT (12–300 μM) and their effects on cell viability, ATP levels, ADP:ATP ratio and differentiation markers, such as soma size and neurite outgrowth, were assessed.

Key findings: Overall, intracellular ATP levels and soma size (decreased by ATR at ≥ 12 μM; 48 h) were the two parameters most sensitive to ATR exposure in undifferentiated and differentiating dopaminergic cells, respectively. At the morphological level, ATR, but not DACT, increased the percentage of morphologically abnormal undifferentiated N27 cells. On the other hand, exposure to DACT (300 μM; 48 h), but not ATR, increased the ADP:ATP ratio regardless of the differentiation state and it moderately disrupted thin neurite outgrowth. Only the highest concentration of ATR or DACT (300 μM) was cytotoxic after a longer exposure (48 h) and undifferentiated N27 cells were the least sensitive to the cytotoxic effects of ATR or DACT.

Significance: Our results suggest that the energy perturbation and morphological disruption of dopaminergic neuronal differentiation induced by ATR and, to a lesser extent, DACT, may be associated with reported neurological deficits caused by developmental ATR exposure in rodents.

Keywords: Atrazine, Diaminochlorotriazine (DACT), Chlorotriazine herbicides, Dopaminergic neuron differentiation, N27 cells

Introduction

Atrazine (ATR), a chlorotriazine herbicide, is frequently found in ground, surface, and municipal water due to its widespread use and relative persistence (ATSDR, 2003; Battaglin et al., 2009). Human exposure to this herbicide is a concern as ATR or its metabolites have been detected in the urine of pesticide applicators and their families (Barr et al., 2007; Curwin et al., 2007).

In animal studies, excessive exposure to ATR has negative effects on immune (Filipov et al., 2005), reproductive (Cooper et al., 2007), and nervous systems (Coban and Filipov, 2007; Bardullas et al., 2011). In the nervous system, the basal ganglia dopamine (DA) circuitries are ATR targets. For example, oral exposure to ATR in rodents produces neurobehavioral changes that are accompanied by a decrease in striatal DA levels (Bardullas et al., 2011) and it decreases nigral and ventral tegmental DA (tyrosine hydroxylase [TH] positive) neurons (Coban and Filipov, 2007). ATR also disrupts DA homeostasis in catecholaminergic PC12 cells (Das et al., 2000), rat striatal slices (Filipov et al., 2007) and striatal synaptic vesicles (Hossain and Filipov, 2008).

ATR and its major mammalian metabolite, diaminochlorotriazine (DACT), can cross the placenta and have been detected in newborn rat pups born to orally exposed dams (Fraites et al., 2011). Following oral exposure to ATR, DACT levels are much higher than ATR in the fetus and in the brains of pups, rat dams (Fraites et al., 2011), or adult male mice (Ross et al., 2009).

Recent studies suggest that ATR is a developmental neurotoxicant. Thus, prenatal exposure to ATR is associated with fetal growth restriction in humans (Chevrier et al., 2011). In rodents, perinatal exposure from gestational day (GD) 14 through postnatal day (PND) 21 causes structural brain changes and related neurobehavioral deficits in the offspring (Giusi et al.,

2006; Belloni et al., 2011), suggesting that ATR affects neurodevelopment. Moreover, the developing nervous system is particularly sensitive to ATR as doses of ATR ineffective in adult rodents are neurotoxic in a developmental exposure paradigm (Giusi et al., 2006; Belloni et al., 2011). However, effects of ATR on DA neuron development have not yet been investigated.

In the present in vitro study, we investigated the effects of ATR and DACT on dopaminergic neuronal differentiation, which is a critical part in neuron development. For our analysis, we chose ATR/DACT concentrations based on earlier studies in PC12 cells (Das et al., 2000, 2001) or striatal slices (Filipov et al., 2007) and on fetal levels of DACT or ATR observed in a rat developmental exposure paradigm (Fraites et al., 2011). We selected the N27 cell line, an immortalized TH-positive neuronal line derived from rat mesencephalic tissue at the peak of DA neuron generation (E12; Prasad et al., 1994). These cells have been used extensively for studies of DA toxicants, including pesticides (Peng et al., 2004; Saminathan et al., 2011). Moreover, undifferentiated N27 cells can easily be differentiated, yielding morphological and functional characteristics of post-mitotic DA neurons (Prasad et al., 1998; Clarkson et al., 1999), making this cell line a useful model for examination of ATR's effects on dopaminergic cell differentiation.

Materials and methods

Chemicals and reagents

Atrazine, 2-chloro-4-(ethylamine)-6-(isopropylamine)-s-triazine (ATR; lot # 421-55A, purity: 98.9%) and diaminochlorotriazine, 2-chloro-4,6-diamino-1,3,5-triazine (DACT; lot # 404-99A, purity: 96.7%) were purchased from Chem Service, Inc. (West Chester, PA, USA). A 75-mM stock of ATR was prepared in absolute ethanol, and a 300-mM stock of DACT was prepared in dimethyl sulfoxide (DMSO). Fetal bovine serum (FBS) was from Atlanta Biologicals

(Lawrenceville, GA, USA); dibutyryl adenosine 3′,5′-cyclic monophosphate (DB-cAMP) was from Biolog (Hayward, CA, USA) and was dissolved in sterile PBS (100-mM stock). The RPMI 1640 medium and the other cell culture-related chemicals were purchased from Invitrogen (Grand Island, NY, USA). All other chemicals, unless specified, were obtained from Sigma (Saint Louis, MO, USA).

Cell culture

Undifferentiated N27 dopaminergic cells were maintained in RPMI 1640 medium containing 10% FBS, 1 mM Na-pyruvate, 1 mM non-essential amino acids, 250 ng/ml fungizone, 100 units/ml penicillin, 100 μg/ml streptomycin, 50 μM 2-mercaptoethanol, 2 mM glutamax and 7.5% $NaHCO_3$ (complete RPMI medium) in a humidified atmosphere of 5% CO_2/95% air at 37 °C. After overnight (16–24 h) culture, medium was changed to low serum (2% FBS) RPMI or N-2 supplemented serum-free RPMI (N-2 RPMI) and exposures were initiated for the undifferentiated N27 cells (Fig. 6.1). To induce cell differentiation, cells were treated with 2 mM DB-cAMP in N-2 RPMI medium for 48 h (Clarkson et al., 1999). Differentiating N27 cells were treated with ATR or DACT during this 48 h period (Fig. 6.1). After the 48 h differentiation induction period, the N27 cells were considered differentiated and medium was changed to DB-cAMP-free N-2 RPMI medium for exposure to ATR or DACT of differentiated cells (Fig. 6.1).

Treatment

Undifferentiated, differentiating and differentiated N27 dopaminergic cells at a density of 0.1×10^6 cells/ml were plated in 96-well (100-μl cell suspension/well) or 12-well (1000-μl cell suspension/well) plates and exposed to vehicle (0.4% ethanol for ATR or 0.1% DMSO for DACT), 12, 60, or 300 μM ATR or DACT for 24 or 48 h. Staurosporine (10 μM; 6 h) or Triton

X-100 (Triton; 0.1%; 1 or 15 min) served as positive controls (Zhang and Bhavnani, 2006; Seo and Seo, 2009). Ninety-six well plates were used for measurements of cell viability, ATP levels and ADP:ATP ratio; 12-well plates were used for all morphological analyses.

Cell viability

Cell viability was determined using the Quick Cell Proliferation assay kit from Biovision (Mountain View, CA, USA) following the manufacturer's instructions. The assay is based on the cleavage of the tetrazolium salt WST-1 to a formazan dye by cellular mitochondrial dehydrogenases. After 24- or 48-h treatment with ATR or DACT, WST-1 (dissolved in Electro Coupling Solution, 10 µl/well) was added, cells were incubated at 37 °C for 2 h, and shaken thoroughly for 1–2 min. Next, 1% SDS (10 µl/well) was added to stop the reaction and cells were shaken for another 1–2 min. Absorbance was measured using an Epoch microtiter plate reader (BioTek Instruments, Inc., Winooski, VT, USA) at 440 nm. The percentage of viable cells in each treatment was determined relative to respective vehicle controls.

ATP level and ADP:ATP ratio

Intracellular ATP level and the ADP:ATP ratio were measured using the luciferase-based ApoGlow assay kit (Lonza, Rockland, ME, USA) according to the manufacturer's instructions. Following exposure to ATR or DACT, ATP releasing reagent (100 µl/well) was added to each well 8 min before measuring luminescence using a BioTek Synergy 4 multi-modal microplate reader (Winooski, VT, USA). First, a 1-s integrated reading (Reading A) was taken immediately after microinjection of ATP monitoring reagent (50 µl/well). After a 10-min delay, ADP converting reagent (50 µl/well) was microinjected, followed by a 1-s integrated reading (Reading B). After another 5-min delay, a final 1-s integrated reading (Reading C) was taken. The ADP:ATP ratio was calculated from measurements of A, B, and C as follows: (C−B) /A.

Morphological analysis

Morphological analysis was based on relevant literature that examined neurite outgrowth of differentiated PC12 cells (Das et al., 2004; Ito et al., 2011) and differentiation characteristics of N27 cells (Prasad et al., 1998). Morphologically identifiable undifferentiated and differentiating N27 dopaminergic cells were photographed with 25–50 cells per view (2 views/well) using a phase-contrast inverted microscope (Axiovert 35, Zeiss, Oberkochen, Germany) linked to a SPOT RT Color camera (Diagnostic Instruments Inc., Sterling Heights, MI, USA) at 10 × magnification. All morphological analyses were done using ImageJ software (Version 1.4.3.67, NIH) by an evaluator blinded to treatment.

Parameters measured for undifferentiated cells included soma size and the percentage of normal or abnormal cells. Normal undifferentiated cells were defined as cells with at least one short neurite, while abnormal undifferentiated cells were defined as cells without any neurites. The average of two views per well was used for statistical analysis.

Differentiating cells were analyzed for the following parameters: (1) total neurite number, (2) thin neurite number, (3) total length of all thin neurites, (4) average length per thin neurite, and (5) soma size of cells with at least one thin neurite. A neurite was defined as a process that was longer than one diameter of the soma, and was classified as either thick or thin, with the diameter of thin neurites being at least 2-fold less than that of thick neurites (Craske et al., 2005; Kohno et al., 2005). Neurite number was determined by counting neurites in 25 randomly selected cells, with the entire soma and neurites (thick and thin [if present]) clearly identifiable. These 25 cells accounted for approximately 65% of all cells in each view. Total thin neurite length was equal to the sum of all thin neurite lengths measured in 10 randomly selected cells

with at least one thin neurite per cell, while the average length per thin neurite was determined by dividing this sum to the total number of thin neurites.

The percentage of differentiated and undifferentiated cells within the 48-h differentiation time period was determined by counting 25 randomly selected cells. Differentiating cells that possessed at least one thin neurite were labeled as differentiated, while cells without neurites or with few short, typically thick, neurites were defined as undifferentiated (Prasad et al., 1998). The percentages of differentiated cells and undifferentiated cells were calculated from the total number of cells. All raw data that were originally in unit of pixel were converted to unit of μm based on a calibration image.

Statistics

All data are expressed as means ± SEM and were analyzed by ANOVA (SigmaStat 2.03, SPSS Inc., Chicago, IL, USA). If significance was detected by ANOVA ($p \leq 0.05$) then the Student–Newman–Keuls multiple comparison *post hoc* test was used to evaluate the differences between treatments with significance level set at $\alpha = 0.05$. If at the same concentration and exposure time effects of both ATR and DACT were significant, i.e., cell viability and intercellular ATP level data, efficacies between ATR and DACT were compared using Student's *t*-test.

Results

Effects of ATR or DACT on cell viability

Exposure of up to 300 μM ATR or DACT for 24 h was not cytotoxic to N27 cells, regardless of the differentiation stage (Fig. 6.2A). After 48 h, exposure to 300 μM ATR decreased cell viability by 25.0%, 44.3%, and 43.3% in undifferentiated, differentiating, and differentiated N27 cells, respectively (Fig. 6.2B). DACT, at the same concentration and exposure

time (300 μM; 48 h) resulted in significantly decreased viability only in cells that were differentiating (15.7%) or differentiated (10.4%; Fig. 6.2B), but its effects on cell viability of both differentiating and differentiated cells were smaller than the effects of 300 μM ATR (Fig. 6.2B). These results indicate that in terms of cytotoxicity only the highest (300 μM) ATR/DACT concentrations were cytotoxic (48 h) and that differentiating and differentiated N27 cells are relatively more sensitive than undifferentiated N27 cells to ATR or DACT, with ATR being more efficacious than DACT. As expected, cell viability was substantially decreased by the positive controls regardless of differentiation stage (Fig. 6.2).

Effects of ATR or DACT on intracellular ATP level

For ATR, 24 h exposure to only the highest (300 μM) concentration significantly decreased intracellular ATP levels (data not shown). However, while 24 h exposure to lower concentrations of ATR or DACT did not affect ATP levels in N27 cells at any differentiation stage, longer exposure (48 h) to ATR at concentrations as low as 12 μM dose-dependently decreased ATP levels in undifferentiated cells (Fig. 6.3A). Similar to 24 h, at 48 h, ATP levels in differentiating and differentiated cells were only decreased at the highest level of ATR (300 μM; Fig. 6.3A). For DACT, a significant decrease in ATP was detected at the highest concentration for all cell types regardless of exposure time (24 h: not shown; 48 h: Fig. 6.3A). At the same concentration and exposure time (300 μM; 48 h), ATR consistently had greater effect than DACT on ATP levels in N27 cells independent of differentiation stage (Fig. 6.3A). These data suggest that, in terms of intracellular ATP level, undifferentiated cells are more sensitive to ATR than differentiating and differentiated cells and that, compared to DACT, ATR is more potent in undifferentiated cells and more efficacious in differentiating and differentiated cells. As

anticipated, positive control (staurosporine, Triton) treatments decreased ATP levels and increased ADP:ATP ratio in cells at all differentiation stages (Fig. 6.3).

Effects of ATR or DACT on ADP:ATP ratio

ATR exposure for either 24 (data not shown) or 48 h (Fig. 6.3B) did not alter ADP:ATP ratio in any of the cell types. The absence of ATR's effects on the ADP:ATP ratio, together with its significant effects on intracellular ATP levels, suggests that ATR exposure mainly arrests proliferation and/or growth of N27 cells. However, DACT exposure at the highest level (300 μM) for 48 h significantly increased ADP:ATP ratios of undifferentiated, differentiating, and differentiated N27 cells (Fig. 6.3B), indicating that longer exposure to a high concentration of DACT may be apoptotic in N27 cells regardless of differentiation stage.

Effects of ATR or DACT on soma size

ATR exposure (300 μM) for 24 or 48 h significantly decreased the average soma size of undifferentiated N27 cells (from 732.85 ± 46.67 and 740.72 ± 16.82 μm^2/cell in vehicle-treated groups to 572.13 ± 6.45 and 508.84 ± 15.72 μm^2/cell in ATR-treated cells, respectively; Fig. 6.5A). The decrease in soma size was greater after 48 h and is illustrated in Fig. 6.4A. In differentiating cells, ATR exposure produced a dose- and time-dependent decrease in soma size. Effects were seen at ≥ 60 μM after 24 h and at concentrations as low as 12 μM after 48 h (Fig. 6.5B). DACT exposure (12–300 μM) up to 48 h had no effect on soma size in either cell type (Fig. 6.5). Representative images illustrating the decrease in soma size of differentiating cells by ATR, but not DACT, are shown on Fig. 6.4B. Collectively, the soma size data indicate that ATR, but not DACT, disrupts N27 cell differentiation by inhibiting soma size enlargement.

Effects of ATR or DACT on the percentage (%) of normal and abnormal undifferentiated N27 cells

Exposure to ATR (300 μM) for 24 h produced a significant decrease in the % of normal and a significant increase in the % of abnormal undifferentiated N27 cells (Fig. 6.6A). These changes were also present with ≥ 60 μM ATR following longer exposure (48 h; Fig. 6.6B). In contrast, DACT exposure (12–300 μM) up to 48 h had no effects on the % of normal and abnormal cells undifferentiated (Fig. 6.6). A representative image illustrating the effects of ATR and the lack of effect of DACT is shown on Fig. 6.4A.

Effects of ATR or DACT on the number of total and thin neurites in differentiating N27 cells

Exposure to ATR (12–300 μM) up to 48 h did not affect the number of total or thin neurites in differentiating cells (24 h: data not shown; 48 h: Table 6.1). After 24 h exposure to DACT, there was a trend toward a decrease in the number of total and thin neurites (data not shown) that became significant for the number of thin neurites at 48 h (Table 6.1), but the effect was a threshold-like and lacked dose-dependency. This effect of DACT on neurite formation suggests that prolonged exposure to DACT might have mild effects on N27 cell differentiation by inhibiting thin neurite formation.

Effects of ATR or DACT on the total and average thin neurite lengths in differentiating N27 cells

There were no significant alterations of total or average thin neurite length in differentiating cells exposed to ATR (12–300 μM) up to 48 h (24 h: data not shown; 48 h: Table 6.1). For DACT, there was an overall trend towards a significant decrease in the average length per thin neurite following 48 h exposure ($p = 0.06$; Table 6.1), indicating a potential modest

inhibitory effect of DACT on thin neurite extension in differentiating N27 cells. Representative images illustrate the lack of ATR effect and the effect of DACT on thin neurite length (Fig. 6.4B).

Effects of ATR or DACT on the percentage (%) of differentiated and undifferentiated cells in differentiating N27 cells

Exposure of differentiating N27 cells to ATR or DACT (12–300 μM) for 24 h did not change the % of differentiated and undifferentiated N27 cells (Fig. 6.7A). However, longer exposure (48 h) to 300 μM ATR resulted in a significant decrease in the % of differentiated cells and a significant increase in the % of undifferentiated cells suggesting a possible delay in differentiation caused by a high level of ATR, which may have also been associated with the cytotoxicity observed by this concentration of ATR (Fig. 6.7B). DACT only exhibited a trend ($p = 0.07$) towards this effect.

Discussion

The major findings of the present study are: (1) intracellular ATP levels and soma size are the two most sensitive parameters affected by ATR exposure in undifferentiated and differentiating dopaminergic cells, respectively; (2) prolonged exposure to high concentration of DACT may induce apoptosis of dopaminergic cells regardless of differentiation state; (3) during the process of differentiation, ATR and DACT affect dopaminergic neuron morphology differentially. Collectively, these findings suggest that the energy perturbation and morphological disruption of dopaminergic neuronal differentiation induced by ATR and, to a lesser extent, DACT may be involved in the developmental neurotoxicity associated with ATR.

The most prominent effect of ATR exposure in undifferentiated dopaminergic cells was a decrease of intracellular ATP levels, which was significant at levels as low as 12 μM. This result

indicates that ATR may affect the ability of mitochondria to produce ATP as mitochondria are the main generators of intracellular ATP (Chang and Reynolds, 2006). Effects of ATR on mitochondria in other cell types have been reported. Thus, ATR, at concentrations similar to the ones used in our study, inhibited mitochondrial function by: (1) disrupting mitochondrial membrane potential in grass carp snout epidermis-derived ZC-7901 cells (Liu et al., 2006), (2) binding to F1F0-ATP synthase in isolated human sperm and isolated rat liver mitochondria (Hase et al., 2008), and (3) decreasing expression of a key enzyme, acyl-CoA dehydrogenase, involved in fatty acid β oxidation for ATP generation in the mitochondria in *Xenopus laevis* (Zaya et al., 2011). Decreased intracellular ATP content and ultrastructural alterations of mitochondria were also observed in liver and muscle cells of rats chronically exposed to ATR via the drinking water (Lim et al., 2009). Collectively, our data and these studies suggest that ATR exposure decreases intracellular ATP levels of dopaminergic neurons probably by affecting the mitochondrial ability to produce ATP.

The greater vulnerability of undifferentiated cells to ATR exposure in terms of intracellular ATP levels is likely due to the enhanced energy demands of dividing cells (Vander Heiden et al., 2009). In addition, it has been reported that energy production in undifferentiated embryonic stem cells and proliferating cells is less efficient than corresponding differentiating and differentiated cells due to low mitochondrial mass, reduced number of mitochondria and heavy reliance on aerobic glycolysis (Vander Heiden et al., 2009; Armstrong et al., 2010; Prigione et al., 2010). Because undifferentiated cells' energy demands are elevated and their ATP production is less efficient, it is not that surprising that undifferentiated dopaminergic cells were more sensitive to ATR-induced alterations in intracellular ATP. Of note, the threshold concentration of 12 μM is well below the concentrations of ATR reported to cause cytotoxicity

to dopaminergic cells, which typically range from 200 to 300 μM (Das et al., 2000; Abarikwu et al., 2011a; Abarikwu et al., 2011b; and our current study). The enhanced susceptibility of undifferentiated cells and the lower threshold suggest the possible presence of a critical window of vulnerability for developmental exposure to ATR, i.e., the potential damage would be greatest if exposure occurs between GD 6 and GD 10.5 in mice (GD 12 in rats) at the start of DA neuron development and before DA neurons become post-mitotic (Prakash and Wurst, 2006), corresponding to the middle stage of the first trimester of pregnancy in humans (Almqvist et al., 1996), particularly from GD 40 to GD 45 (Clancy et al., 2007).

Another important target of ATR exposure in undifferentiated dopaminergic cells was cell morphology, i.e., ATR increased the percentage of morphologically abnormal cells and decreased the soma size, with the former effect being dose-dependent. These morphological changes could also have, in part, resulted from the energy perturbation caused by ATR because disruption of ATP homeostasis has been associated with failure of maintenance of cellular morphology in various cell types, including brain cells (Jurkowitz-Alexander et al., 1992; Lee et al., 2002).

Interestingly, DACT appears to be far less potent than ATR in disrupting intracellular ATP levels, but it also uniquely elevates the ADP:ATP ratio, albeit only at the highest concentration. The degree of which ATP level and the ADP:ATP ratio are altered can correlate with the type of cell death that is initiated (Bradbury et al., 2000). The decrease in ATP and the corresponding increase in ADP:ATP ratio we saw with 300 μM DACT (48 h) suggests that longer exposure to a high level of DACT induces N27 cell apoptosis regardless of differentiation state. The fact that high level DACT is likely to induce apoptosis in dopaminergic neurons is important in light of the reports that DACT is the metabolite most often detected in human urine

(Barr et al., 2007), and that DACT levels in the brain of ATR-treated adult mice and in the whole fetus, as well as developing brain of pups delivered from ATR-exposed rat dams, are 20- to 200-fold higher than ATR levels (Ross et al., 2009; Fraites et al., 2011).

Contrary to the apparent apoptotic effects of high concentrations of DACT, even the highest concentration of ATR (300 μM), which was cytotoxic, did not increase the ADP:ATP ratio. In light of the very substantial effects of ATR on cellular ATP, a very intriguing and virtually unexplored possibility for the cytotoxicity caused by high levels of ATR is via necroptosis (Vandenabeele et al., 2010). If the cellular demise is via necroptosis, true apoptotic alterations such as caspase activation and increased ADP:ATP ratio, may not be observed, but the cells, including neuronal cells (Fukui et al., 2012), experience rapid depletion of cellular ATP.

In differentiating dopaminergic neurons, the most sensitive parameter to ATR exposure is soma size, which was dose-dependently decreased at levels as low as 12 μM. These data indicate that ATR disrupts dopaminergic neuron differentiation primarily by inhibiting soma growth. Soma size enlargement and neurite outgrowth are morphological characteristics indicative of dopaminergic neuron maturation (Clarkson et al., 1999). The soma size effective concentration (12 μM) is 25-fold lower than the effective concentration (300 μM) causing cytotoxicity, indicating that ATR mainly affects dopaminergic neuronal growth and differentiation, rather than survival. In rodents, dopaminergic neuronal soma growth primarily occurs postnatally, i.e., dopaminergic neuronal soma size on PND 14 is close to adult level, and is approximately 5-fold higher than that on GD 17 (Lieb et al., 1996). Thus, these results suggest that an additional potential sensitive window of the dopaminergic system to ATR exposure may be within the first

two postnatal weeks in rodents, which corresponds to the middle stage of the second trimester of pregnancy in humans, particularly from GD 110 to GD 155 (Clancy et al., 2007).

DACT, on the other hand, appears to affect the differentiation process by moderately reducing thin neurite formation, but only at the highest concentration (300 μM) after longer exposure (48 h). In light of the facts that DACT is the major mammalian metabolite of ATR and the maximal plasma concentrations of ATR and DACT ranged 0.6–2.8 and 2.8–109.8 μM in mice or rats exposed to single oral dose of ATR (5–250 mg/kg; Brzezicki et al., 2003; Ross and Filipov, 2006; Ross et al., 2009), respectively, the contribution of DACT, perhaps through a different mechanism, to the in vivo effects of ATR on dopaminergic neuronal differentiation should not be discounted. Together, the disruption of dopaminergic neuron maturation and the cytotoxic effects induced by both ATR and DACT could decrease the number of functionally mature dopaminergic neurons, ultimately contributing to the extensive neurodegenerative alterations and neurobehavioral deficits, such as altered motor and cognitive functions observed after developmental rodent exposure to ATR (Giusi et al., 2006; Belloni et al., 2011). Overall, our data indicate that ATR and, to a lesser extent, DACT affect neuronal differentiation and that the dopaminergic system may be particularly sensitive to ATR during defined developmental windows. Whether or not ATR affects dopaminergic neuronal differentiation in vivo and at longer exposures to levels lower than 12 μM in vitro remains to be determined.

Consistent with our results, in vitro exposure to other dopaminergic toxicants such as the pesticides chlorpyrifos, parathion and dieldrin, has been demonstrated to disrupt dopaminergic neuron differentiation by either affecting soma growth, decreasing neurite outgrowth, or both (Das and Barone, 1999; Slotkin et al., 2007). *In utero* exposure to another developmental neurotoxicant, ethanol, decreases soma size and inhibits neurite outgrowth of dopaminergic

neurons of substantia nigra pars compacta in rats (Shetty et al., 1993). The effects of these neurotoxicants on dopaminergic neuron differentiation may ultimately contribute to the dopamine-related behavioral deficits observed in rodents exposed to them during development (Olson et al., 1980; Ricceri et al., 2006; Schneider et al., 2011).

The concentrations used in this study are comparable to those used in previous studies and their relevancy to high levels of ATR exposure in farmers, pesticide applicators, and others in the vicinity of ongoing pesticide application, including pregnant women has been discussed (Das et al., 2000; Filipov et al., 2007). Additionally, ATR or its metabolites have been detected in urine samples from the general (nonfarm) population of pregnant women in northwest France up to 3 years after ATR was banned in Europe (Chevrier et al., 2011), indicating significant environmental exposure to ATR. Of note, environmental exposure to ATR in humans during pregnancy is associated with various birth defects such as small-for-gestation-age and pre-term delivery (Ochoa-Acuña et al., 2009; Chevrier et al., 2011). The relationship between these epidemiological findings and dopaminergic abnormalities in adulthood is not well studied in human cohorts, but, nevertheless, a fairly large imaging study suggests that besides various hemorrhagic lesions, the most common pathology in the brains of pre-term infants is basal ganglia abnormalities (Dyet et al., 2006). In rodents, exposure to environmentally relevant low doses of ATR during nervous system development causes structural and neurobehavioral alterations, including in the striatum and of motor behavior (Giusi et al., 2006; Belloni et al., 2011). Overall, our data support the notion that a developing fetus might be at a greater risk for DA toxicity caused by ATR overexposure.

Conclusions

Our results indicate that the energy perturbation and the morphological disruption of dopaminergic neuronal differentiation induced by ATR and, to a lesser extent, DACT, may be involved in the mechanism of developmental neurotoxicity of this herbicide. The existence of differentiation state-associated targets most sensitive to ATR indicates that the dopaminergic circuitries might be particularly vulnerable to ATR during defined developmental windows. Accordingly, excessive exposure to ATR during pregnancy may be of particular concern.

Conflict of interest statement

The authors declare that there are no conflicts of interest.

Acknowledgments

The authors wish to thank Dr. Zhen Fang Fu, Department of Pathology, College of Veterinary Medicine, University of Georgia, for the access to the imaging system used for morphological analysis, and Mrs. Irina I. Georgieva, Department of Physiology and Pharmacology, College of Veterinary Medicine, University of Georgia, for providing skillful technical assistance.

Table 6.1. Neurite number and thin neurite length of differentiating N27 cells.

	Control	12 μM	60 μM	300 μM
ATR, 48 h				
Total neurite number	47.72±1.52	47.35±1.54	48.94±1.50	48.11±1.32
Thin neurite number	35.09±0.74	35.46±1.00	36.44±1.14	37.39±1.71
Total thin neurite length (μm)	870.16±52.00	828.98±35.36	848.64±13.78	853.89±21.46
Average length per thin neurite (μm)	46.71±1.52	43.67±1.36	44.51±0.63	44.75±1.42
DACT, 48 h				
Total neurite number	49.13±1.35	45.17±1.47	47.00±1.23	45.98±1.34
Thin neurite number[a]	37.26±1.01	32.17±1.60[b]	34.17±1.38	32.33±1.44[c]
Total thin neurite length (μm)	863.34±35.61	743.80±32.23	786.75±41.46	783.29±35.68
Average length per thin neurite[d] (μm)	46.58±1.09	45.39±1.49	42.96±1.01	42.17±1.38

[a] Indicates overall ANOVA $p \leq 0.05$.

[b] Indicates $p = 0.06$ vs. control.

[c] Indicates $p \leq 0.05$ vs. control.

[d] Indicates overall ANOVA $p = 0.06$.

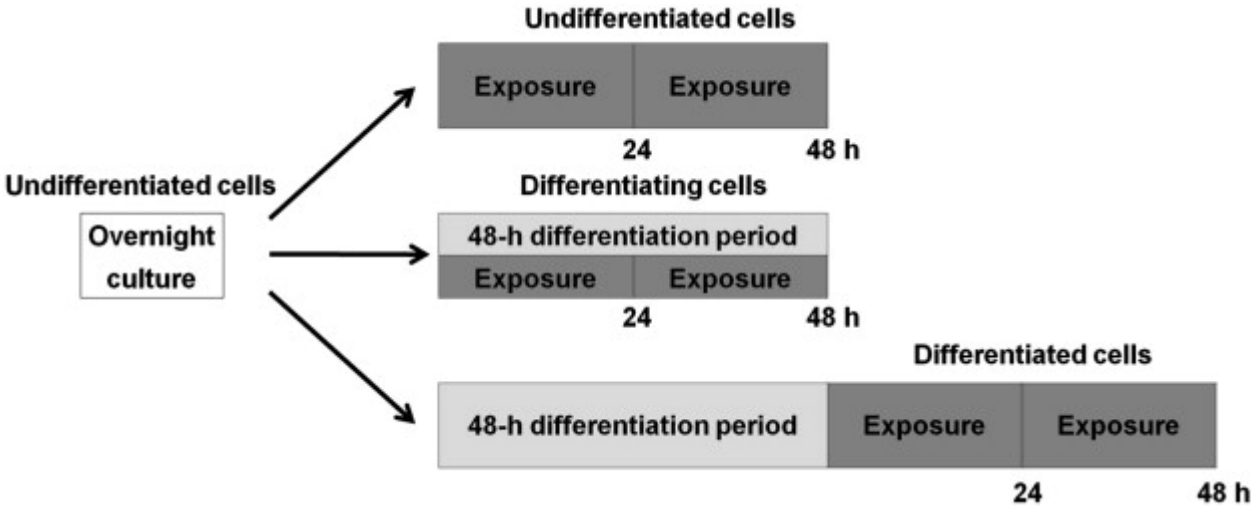

Figure 6.1. Experimental design and a timeline. Undifferentiated, differentiating, or differentiated N27 dopaminergic cells were exposed to 0 (vehicle), 12, 60, or 300 μM atrazine (ATR) or its major mammalian metabolite diaminochlorotriazine (DACT) for 24 or 48 h.

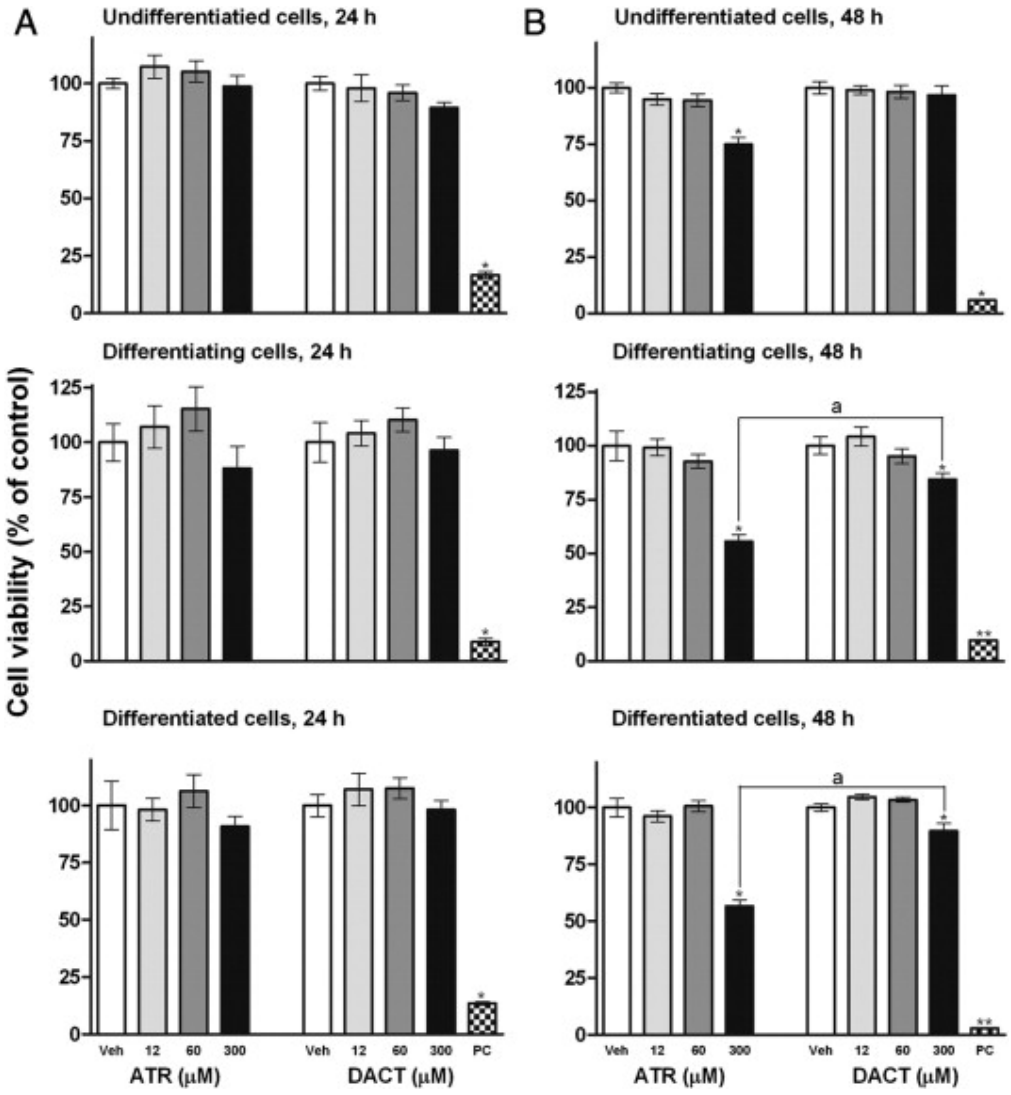

Figure 6.2. Cell viability of undifferentiated, differentiating, and differentiated N27 dopaminergic cells exposed to vehicles (Veh), ATR, or DACT for 24 (A) or 48 h (B). The number of viable cells is represented as percentage (%) of control. Positive controls (PC): 10 μM staurosporine for 6 h (undifferentiated and differentiating, 24 h), 0.1% Triton for 1 min (differentiated, 24 h), or 0.1% Triton for 15 min (all cells; 48 h). * and ** indicate significant effects of ATR, DACT, or positive controls ($p \leq 0.05$). Means not sharing the same number of asterisks are significantly different ($p \leq 0.05$). [a] indicates significant difference between ATR and DACT ($p \leq 0.05$).

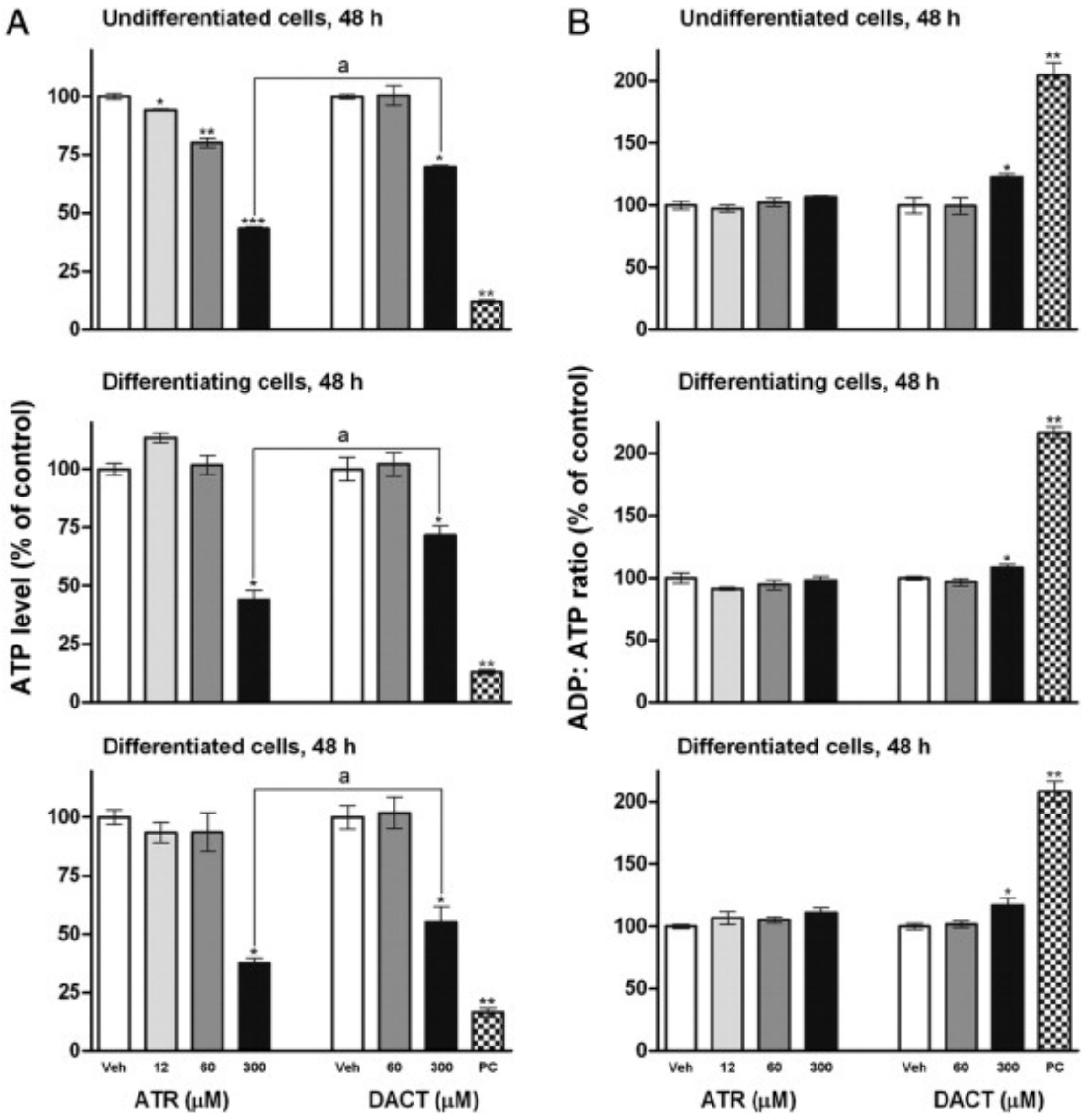

Figure 6.3. Intracellular ATP level (A) and ADP:ATP ratio (B) in undifferentiated, differentiating, and differentiated N27 dopaminergic cells exposed to vehicles (Veh), ATR, DACT for 48 h, or to positive control (PC: 0.1% Triton) for 15 min. ATP level and ADP:ATP ratio are represented as percentage (%) of control. * and ** indicate significant effects of ATR, DACT, or positive control ($p \leq 0.05$). Means not sharing the same number of asterisks are significantly different ($p \leq 0.05$). [a] indicates significant difference between ATR and DACT ($p \leq 0.05$).

Figure 6.4. Representative pictures of undifferentiated (A) and differentiating (B) N27 dopaminergic cells exposed to vehicles, ATR or DACT (300 μM) for 24 or 48 h. Panel A: arrowheads mark somas, as well as all the cells without neurites in a given field (abnormal cells); short arrows mark a representative cell with one or two short neurites (shorter than one diameter of soma size) in a given field (normal cells); long arrows mark a representative cell with at least one long neurite (longer than one diameter of soma size) in a given field (normal cells). Panel B: arrowheads mark somas; thick arrows mark regular thick neurites; thin arrows mark thin neurites. Each representative field is from a representative image of each treatment group and cell type.

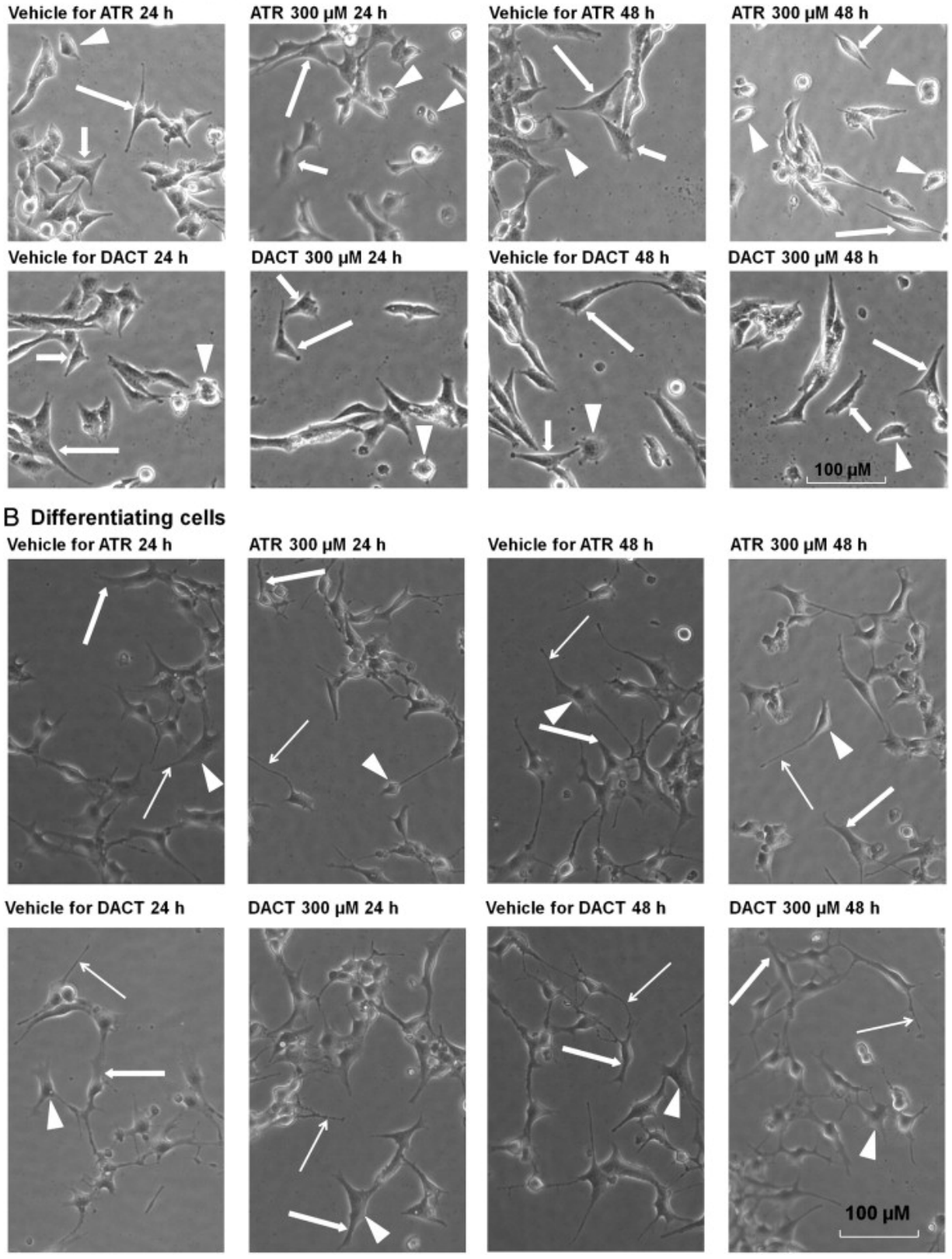
A Undifferentiated cells
Vehicle for ATR 24 h
ATR 300 μM 24 h
Vehicle for ATR 48 h
ATR 300 μM 48 h
Vehicle for DACT 24 h
DACT 300 μM 24 h
Vehicle for DACT 48 h
DACT 300 μM 48 h
100 μM
B Differentiating cells
Vehicle for ATR 24 h
ATR 300 μM 24 h
Vehicle for ATR 48 h
ATR 300 μM 48 h
Vehicle for DACT 24 h
DACT 300 μM 24 h
Vehicle for DACT 48 h
DACT 300 μM 48 h
100 μM

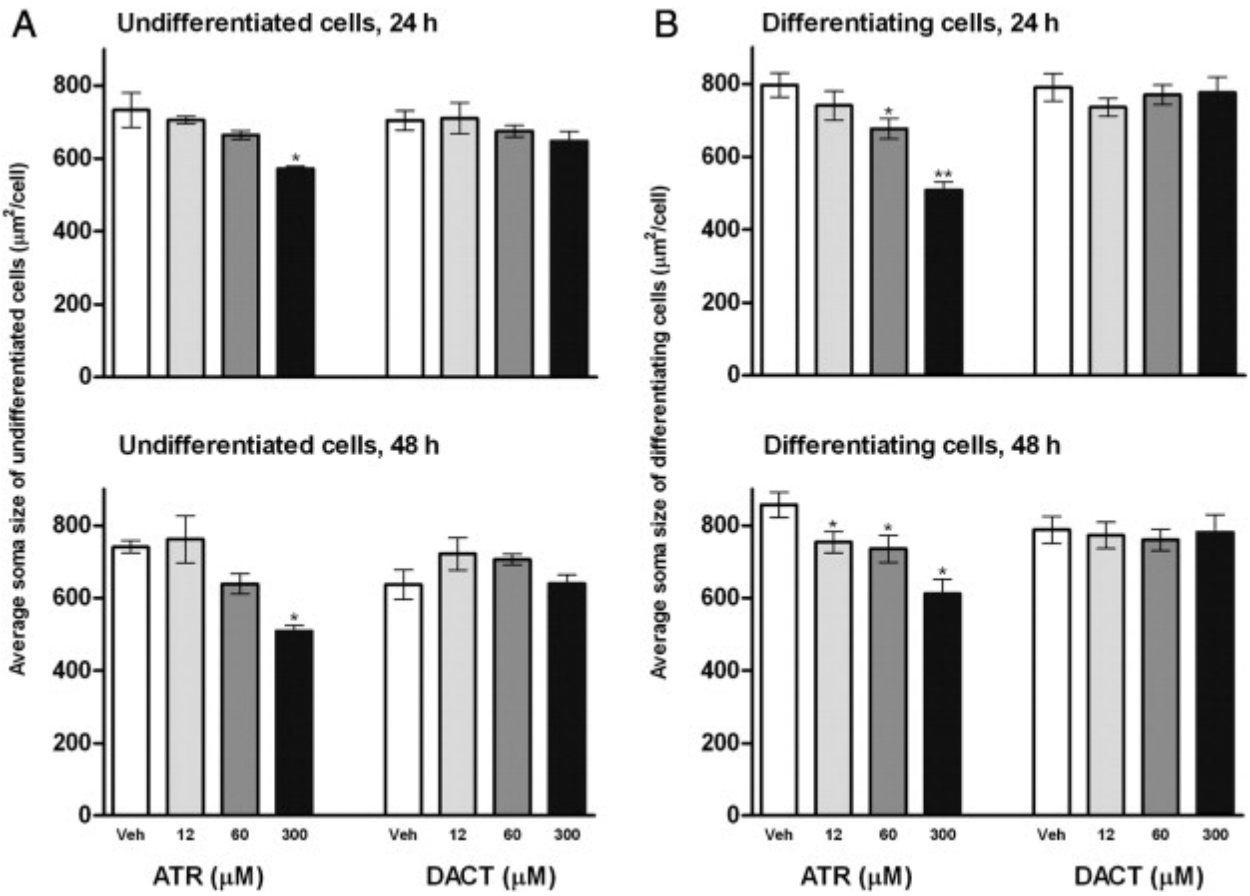

Figure 6.5. Average soma size of undifferentiated (A) and differentiating (B) N27 dopaminergic cells exposed to vehicles (Veh), ATR or DACT for 24 or 48 h. * and ** indicate a significant effect of ATR ($p \leq 0.05$). Means not sharing the same number of asterisks are significantly different ($p \leq 0.05$).

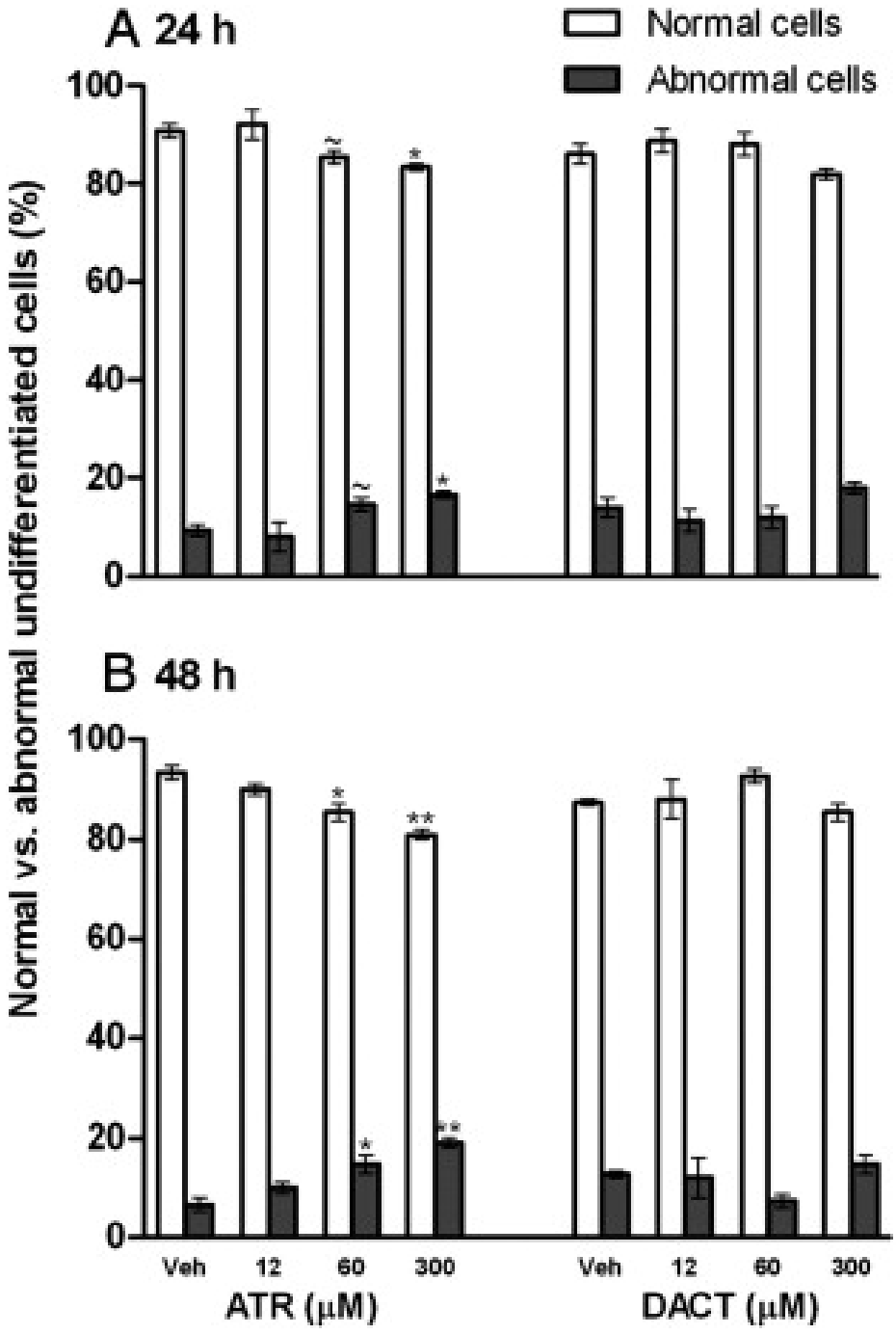

Figure 6.6. Percentage (%) of normal and abnormal undifferentiated N27 dopaminergic cells exposed to vehicles (Veh), ATR or DACT for 24 (A) or 48 h (B). * and ** indicate a significant effect of ATR ($p \leq 0.05$). ~ indicates $p = 0.07$. Means not sharing the same number of asterisks are significantly different ($p \leq 0.05$).

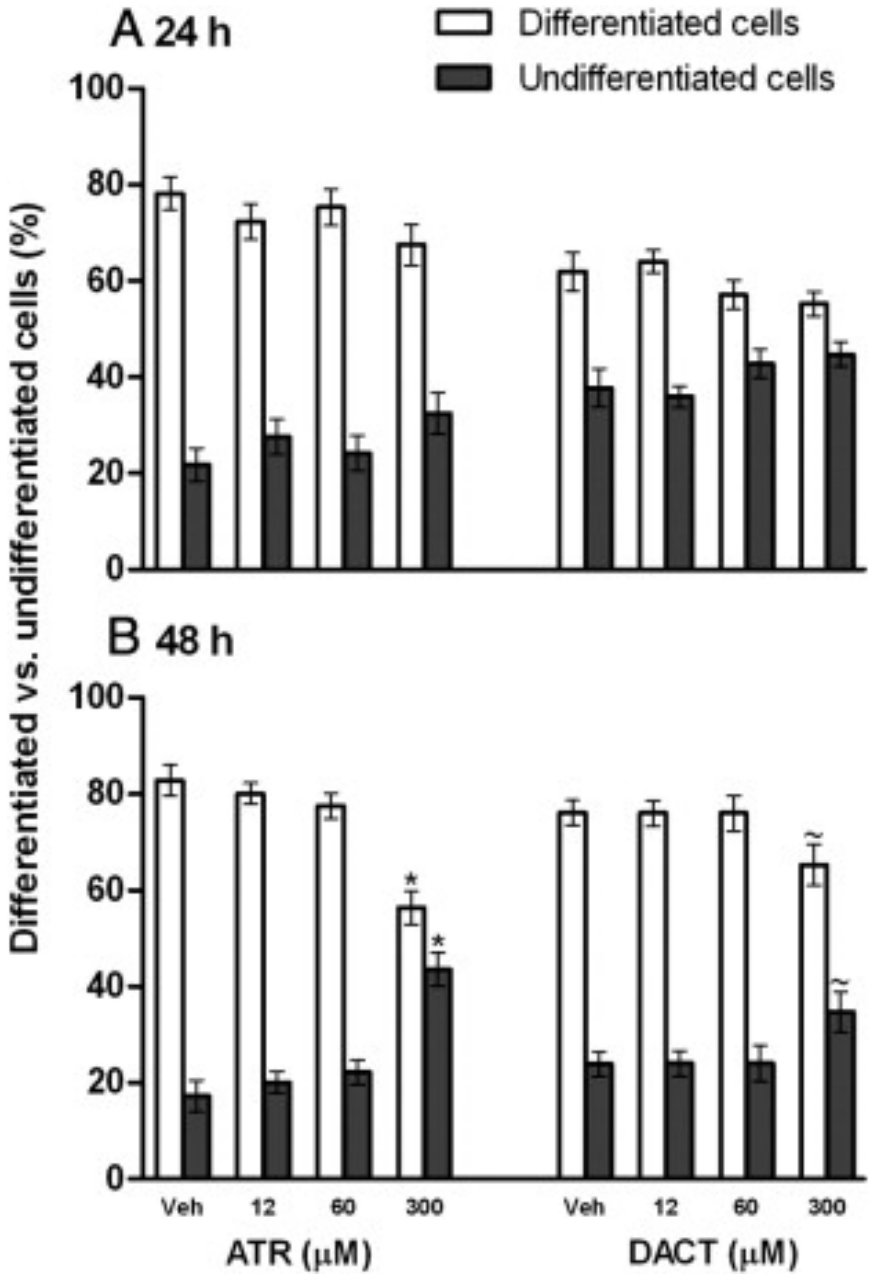

Figure 6.7. Percentage (%) of differentiated and undifferentiated N27 dopaminergic cells exposed to vehicles (Veh), ATR or DACT for 24 (A) or 48 h (B) during differentiation induced by DB-cAMP. * indicates a significant effect of ATR ($p \leq 0.05$). ~ indicates $p = 0.07$.

CHAPTER 7

GESTATIONAL AND LACTATIONAL EXPOSURE TO ATRAZINE VIA THE DRINKING WATER CAUSES SPECIFIC BEHAVIORAL DEFICITS AND SELECTIVELY ALTERS MONOAMINERGIC SYSTEMS IN C57BL/6 MOUSE DAMS, JUVENILE AND ADULT OFFSPRING[1]

[1] Lin, Z., Dodd, C.A., Xiao, S., Krishna, S., Ye, X., Filipov, N.M. To be submitted to *Toxicological Sciences*.

Abstract

Atrazine (ATR) is one of the most frequently detected pesticides in the US water supply. The present study aimed to investigate neurobehavioral and neurochemical effects of ATR in C57BL/6 mouse offspring and dams exposed to environmentally-relevant dose of ATR (3 mg/L) via the drinking water from gestational day 6 to postnatal day (PND) 23. Behavioral tests included open field, pole, grip strength, novel object recognition (NOR), forced swim, and/or marble burying tests. Maternal weight gain and offspring (PND21, 35, and 70) body/brain weights were not affected by ATR. However, ATR-treated dams exhibited hyperactivity and decreased NOR performance. ATR-exposed juvenile offspring (PND35) were hyperactive (males and females), spent more time immobile in the forced swim test (males), and buried more marbles (females). In adult offspring (PND70), the only behavioral change was a sex-specific (females) decreased NOR performance by ATR. Neurochemically, ATR increased striatal dopamine (DA) in dams and juvenile offspring (males and females), but not in adult offspring. Additionally, ATR decreased serotonin in the perirhinal cortex of female adult offspring. These results suggest that perinatal exposure to low concentrations of ATR targets the nigrostriatal DA pathway in dams and offspring, alters motor and cognitive behaviors of dams, induces sex-selective changes involving motor and emotional functions in juvenile offspring, and decreases cognitive ability of female adult offspring, which may be associated with altered serotonin homeostasis in the perirhinal cortex. These findings suggest that ATR exposure during gestation and lactation may be detrimental to the nervous system of both offspring and dams.

Keywords: Atrazine, Pesticides, Dopamine, Behavior, Developmental neurotoxicity

Introduction

Atrazine (ATR) is a widely used chlorotriazine herbicide and a ubiquitous water contaminant (ATSDR, 2003). The primary route of human exposure is via drinking ATR-contaminated water. In areas of heavy ATR use, such as the Midwestern US, ATR concentrations in the drinking water and surface water could reach up to 34 and 224 μg/L, respectively, which greatly exceed the current maximum contaminant level for the US (3 μg/L; ATSDR, 2003; Mosquin et al., 2012). ATR and/or its metabolites are commonly detected in urine samples from pesticides applicators, their families, and the general population, including from pregnant women (Curwin et al., 2007; Chevrier et al., 2011). ATR/metabolites residues are also detected in umbilical cord plasma samples from residentially exposed urban population (Whyatt et al., 2003) and in breast milk samples from a general population (Balduini et al., 2003), highlighting the potential of adverse health impact of ATR-contaminated drinking water during the highly vulnerable gestational and lactational periods.

Animal studies have shown that exposure to relatively high amounts of ATR (≥10 mg/kg) targets the brain monoaminergic systems, especially the nigrostriatal dopamine (DA) system, resulting in a range of cellular, molecular, and behavioral abnormalities (Coban and Filipov, 2007; Bardullas et al., 2011; Lin et al., 2013b; Rodriguez et al., 2013). For example, short-term (4-10 days) ATR (125-250 mg/kg) exposure induces hypoactivity, object recognition memory deficits, and anxiety-like behavior that are accompanied with altered DA and serotonin (5-HT) homeostasis in the striatum and prefrontal cortex in adult mice (Lin et al., 2013b); short-term (14 days) ATR (125-250 mg/kg) exposure also decreases striatal DA and reduces substantia nigral and ventral tegmental area (VTA) DA (tyrosine hydroxylase [TH] positive) neurons in juvenile mice (Coban and Filipov, 2007). However, effects on monoamine systems and associated

behaviors following exposure to lower, environmentally-relevant concentrations of ATR during sensitive periods, such as gestation and lactation, have not been investigated.

It has been shown that gestational and/or lactational exposure to higher doses of ATR (100 mg/kg) delays vaginal opening and mammary gland development in the offspring (Rayner et al., 2004). On the other hand, oral exposure to environmentally-relevant lower amounts of ATR during pregnancy and lactation alters motor activity (≥0.001 mg/kg) in juvenile offspring and causes extensive neurodegenerative alterations (0.1 mg/kg) in cortical, striatal, hippocampal hypothalamic areas of adult offspring (Giusi et al., 2006; Belloni et al., 2011), suggesting that the developing nervous system is particularly sensitive to ATR and that some effects are only observed/still present in adulthood. Environmental exposure to ATR during pregnancy in humans has been associated with various adverse birth outcomes, such as preterm birth (Ochoa-Acuña et al., 2009). One of the most common pathologies in the brains of preterm infants is basal ganglia abnormalities (Dyet et al., 2006), suggesting a possible epidemiological correlate between developmental ATR exposure and basal ganglia disorders.

The developing nervous system has greater sensitivity than the fully developed one to a number of toxicants, including heavy metals and pesticides; this increased sensitivity is attributed not only to the presence of an immature blood-brain barrier, but also to the complex temporal and regional emergence of critical developmental processes (e.g, proliferation, differentiation; Rice and Barone, 2000). Our recent study (Lin et al., 2013a) suggests that ATR affects dopaminergic neuronal differentiation in vitro and that the developing dopaminergic system may be particularly vulnerable to ATR when dopaminergic neurons are undifferentiated, e.g., from gestational day (GD) 6 to GD10.5 in mice (Prakash and Wurst, 2006). However,

developmental neurotoxicity studies for ATR exposure that includes this sensitive window have not been reported.

In line with the main human exposure route and considering the lack of neurobehavioral and neurochemical data associated with gestational and lactational ATR exposure on dams and offspring, this study aimed to determine the effects of drinking water exposure to an environmentally-relevant concentration of ATR (3 mg/L) from GD6 to postnatal day (PND) 23 on monoamine-relevant behavior and neurochemistry in dams, juvenile and adult offspring. For behavioral analyses, we chose the following tests: open filed, pole, grip strength, marble burying, novel object recognition (NOR), and forced swim tests (FST). These tests are commonly used to evaluate motor, emotional, cognitive functions of rodents and have been shown to be, at least in part, related to the normal function of brain regions receiving rich monoaminergic innervations, including the prefrontal cortex, nucleus accumbens, striatum, perirhinal cortex, and hippocampus (Antunes and Biala, 2012; Malkova et al., 2012). These regions were collected for analysis of monoamine levels in order to reveal potential neurochemical substrates associated with ATR-induced behavioral changes.

Materials and methods

Animals and chemicals

Adult male C57BL/6 breeder mice (2-6 months old, 29.3 ± 1.4 g) and female C57BL/6 mice (2-6 months old, 21.7 ± 0.4 g Taconic, Hudson, NY) were housed with water and food available ad libitum under constant temperature (22 ºC) on a 12:12 (Light:Dark) h ligh cycle in an AAALAC accredited facility throughout the study. Female mice were housed in pairs until mating. For breeding, two virgin female mice were placed with one male breeder overnight and removed next morning at lights-on. Pregnancy was identified by the appearance of a vaginal plug

on the following morning (Fraites et al., 2011); pregnant mice were designated as GD1 and were randomly assigned to control or treated groups. Mice with confirmed pregnancies were housed individually. All animal procedures were conducted according to the latest NIH guidelines and were approved in advance by the Institutional Animal Care and Use Committee (IACUC) of the University of Georgia.

Atrazine (98.9% purity) was purchased from Chem Service (West Chester, PA). All chemicals (i.e., $NaH_2PO_4H_2O$, octyl sodium sulfate, EDTA disodium salt, triethylamine, and methanol) for the mobile phase used for HPLC analysis (described below) were purchased from Thermo Fisher (Fair Lawn, NJ). Ethanol was purchased from Decon Labs, Inc. (King of Prussia, PA). All other chemicals, including HPLC standards, unless specified, were obtained from Sigma (Saint Louis, MO, USA).

Exposure solution preparation and exposure paradigm

ATR-containing drinking water solutions were prepared by dilution of a 50-mM stock solution of ATR (10784.5 mg/L; in absolute ethanol) in deionized water. For the control water solution, a volume of ethanol equal to the largest amount added to the test water solutions was added (0.028% v/v in the developmental study). This ethanol concentration is more than 100-fold less than the lowest concentration (3% v/v) reported to cause developmental neurotoxicity in rodents in a perinatal exposure paradigm (Tattoli et al., 2001). Mice drank the ATR- or vehicle-containing water solutions ad libitum; fresh water solutions were prepared weekly and the water bottles were changed and weighted weekly.

In a pilot dose-finding study, limited number (n=3/group) of pregnant mice was exposed to ATR via drinking water at a concentration of 0 (vehicle control), 0.03, 3, or 30 mg/L from GD6 to PND23. The dosage levels were selected based on the OECD (Organization for

Economic Cooperation and Development) developmental neurotoxicity study guidelines (OECD, 2007). Thus, the highest dose (30 mg/L) aimed to produce some maternal and/or fetal/neonatal toxicity, and was lower than the solubility limit of ATR in water (34.7 mg/L; ATSDR, 2003). The lowest dose (0.03 mg/L) was based on the highest level (0.034 mg/L) in the Midwestern US drinking water (Mosquin et al., 2012). The medium dose (3 mg/L) was around 10-fold higher than maximum level (0.224 mg/L) in Midwestern US surface water (ATSDR, 2003). This dose aimed to demonstrate a dose-response relationship and was selected by taking an uncertainty factor of 10 to account for species differences between rodents and humans (Lang et al., 1996). This medium dose was also in line with the oral dose (0.1 mg/kg/day) reported to cause developmental neurotoxicity in mice (Giusi et al., 2006; Belloni et al., 2011), allowing cross-study comparisons. In this pilot study, all three dams in the highest dose group (30 mg/L) aborted around GD17, while all three dams in the medium dose group (3 mg/L) delivered normal litters in a timely manner (GD20±1) and cared for their litters similar to control dams. Hence, the main developmental study focused only on the 3 mg/L ATR exposure level.

In the developmental study, timed-pregnant C57BL/6 mice (10/group) were exposed to vehicle or 3 mg/L ATR via drinking water from GD6 to PND23-24. The experimental timeline is depicted in Fig. 7.1 and is also described in further detail in the Methods section below.

Observations and tissue collection of dams, juvenile and adult offspring

Health status observations and dam inspection for parturition to determine the time of delivery were made twice daily (A.M. and P.M.). The day of parturition was designated as PND0. All pregnant mice were allowed to deliver spontaneously and nursed their pups until PND23-24. Maternal body weights, food and water consumptions were recorded weekly. Mean actual ATR exposure (mg/kg/day) was determined by multiplying the concentration of ATR in

the water (mg/L) by the relative water consumption volume (L/kg/day) for each animal and it is reported later in the text.

Health observations on all pups were performed daily and on PND6, the litter size for each litter was recorded. Mean litter size for control and ATR-exposed dams was 5.9 ± 0.6 and 6.6 ± 0.6, respectively, and they were not different from each other ($p = 0.44$). Similarly, the female:male (f:m) sex ratios (49:51 and 47:53 for control and ATR-treated groups, respectively) were not affected ($p = 0.95$) by the ATR treatment. Two pups (one male and one female) per litter were weighted and sacrificed on PND21-22 (thereafter designated PND21); the remaining pups were weighted and weaned on PND23-24 (thereafter designated PND23) when dams were sacrificed (one day after a 2-day behavioral analysis [Fig. 7.1]). Juvenile (PND35-36; thereafter designated PND35) and adult (PND70-71; thereafter designated PND70) offspring were also subjected to a 2-day behavioral analysis (Fig. 7.1) and sacrificed 24 h after completion of the behavioral tests. Brain tissues from all animals (dams, PND21, PND35, and PND70) were collected and processed similar to Coban and Filipov (2007). At the time of brain collection, body weights, brain, liver, spleen, thymus, uterus, ovary, and/or testis weights were also measured.

Behavioral analysis of dams, juvenile and adult offspring

Open field test (dams, juvenile and adult offspring)

Motor activity was measured in dams (PND21, prior to weaning), juvenile (PND35) and adult (PND70) offspring using an open field test as in Lin et al. (2013b). Briefly, each mouse was individually monitored for 30 min in an open arena (l × w × h: 25 × 25 × 40 cm, divided into 16 square grids; Coulbourn Instruments, Whitehall, PA) with Limelight video tracking software (Actimetrics, Wilmette, IL). Parameters evaluated included: (1) total distance traveled (cm) and

number of crossings, analyzed per 5 minute interval; (2) number of rearing during the first 5 min; and (3) time spent in the periphery or center, analyzed per 5 min interval (Lin et al., 2013b).

Pole test (dams, juvenile and adult offspring)

Motor coordination was evaluated via a pole test (Lin et al., 2013b). In brief, mice were gently placed head-up on top of a vertical metal pole with a gauze-wrapped rough surface. The maximum time allowed for turning was 60 sec and the maximum total time per trial was 120 sec. A total of 4 trials were conducted for each mouse with a 3-5 min resting period between each trial. The average time to turn, time to descend, and total time spent on the pole for all 4 trials were used for statistical analysis (Lin et al., 2013b).

Grip strength test (dams, juvenile and adult offspring)

Neuromuscular function was evaluated by measuring forelimb grip strength using a mouse-specific strength gauge (Bioseb, France) as in Lin et al. (2013b). The maximum grip strength was recorded in Newtons [N]. For each mouse, 4 measurements (1 min apart) were taken to obtain an average value, which was used for statistical analysis.

Novel object recognition test (NOR; dams and adult offspring)

Memory function was assessed using a NOR based on Lin et al. (2013b). Mice were habituated to the open arena for 30 min while conducting the open field test. One day later, mice were placed in the arena for 5 min with two identical objects. After a 1-h rest period in their home cages, mice were placed back into the arena for 5 min with one familiar object and one novel object. The order of objects and object location was randomized. To prevent the use of odor cues, the objects and the arenas were always thoroughly cleaned between sessions with 0.4% Roccal-D Plus (Pfizer Inc., New York, NY). The number approaching the novel (N1) vs. the familiar object (N2) was counted using the Limelight video tracking software. The novelty

preference was determined by comparing the percentage of the number of approaches towards the familiar vs. the novel object. The novelty preference index (NPI) was calculated based on Lin et al. (2013b).

Forced swim test (FST; dams, juvenile and adult offspring)

The FST was conducted according to Lin et al. (2013b). Briefly, mice were gently placed in a cylindrical container (d × h: 18 × 25 cm) filled approximately with 3 L tap water (29 ± 1 ºC) and allowed to swim for 15 min. Fresh water and clean container were used for every mouse. The Limelight video tracking software was used to score the total time spent swimming vs. immobile and the number of climbings by an experimenter blinded to treatment groups as in Lin et al. (2013b).

Marble burying test (juvenile and adult offspring)

Anxiety-like behavior was assessed using a marble burying test as described by Malkova et al. (2012) with minor modifications. Clean testing cages (l × w × h: 40.5 × 20.5 × 18.5 cm) were filled with a 4-cm layer of pine bedding (American Wood Fibers, Columbia, MD). Animals were habituated to these cages for 10 min and then returned to their home cages. Twenty blue glass marbles (supplier 1 cm diameter) were gently laid on the top of the bedding, equidistant from each other in a 4 × 5 arrangement. After a 40-min resting period, animals were placed back into the testing cages and the number of marbles at least two-thirds covered by bedding material in 10 min was counted (Malkova et al., 2012). New bedding and clean marbles were used for each animal.

Neurochemistry of dams, juvenile and adult offspring

Tissue collection from the different brain regions subject to this investigation and determination of monoamines and their metabolites were performed as described in our earlier

studies (Coban and Filipov, 2007; Lin et al., 2013b) with minor modifications. Briefly, micropunches from the prefrontal cortex, nucleus accumbens, striatum, hippocampus (1.5 mm in diameter), and perirhinal cortex (0.75 mm in diameter) were collected from 500-μm thick frozen sections, placed in centrifuge tubes containing 100 μL (50 μL for perirhinal cortex) of 0.2 N perchloric acid, sonicated, and centrifuged (13200 g at 4 ºC for 10 min). An aliquot (20 μL) of the supernatant was injected into HPLC for determination of: (1) DA and its metabolites: DOPAC (3,4-dihydroxyphenylacetic acid), HVA (homovanillic acid) or 3-MT (3-methoxytyramine), (2) 5-HT and its metabolite 5-HIAA (5-hydroxyindoleacetic acid), or (3) NE (norepinephrine) and its metabolite MHPG (3-methoxy-4-hydroxyphenylglycol) with electrochemical detection method. The analytes were separated on a C_{18}, 5 μm base deactivated reverse-phase column (4.6 mm × 25 cm; Supelco, Sigma) using an isocratic flow rate of 0.5 mL/min. The mobile phase and Electrochemical Detector (Waters 2465; Waters Co., Milford, MA) settings were the same as in Lin et al. (2013b). The results were analyzed with Empower chromatographic software (Waters Co.), and normalized on a per mg protein basis. Protein digestion and concentration determination were based on our earlier protocols (Coban and Filipov, 2007; Lin et al., 2013b).

Statistics

Data were analyzed with dam or (as appropriate) litter as the experimental unit using SigmaStat 2.03 (SPSS Inc., Chicago, IL) and presented as means ± SEM. Three independent replications of the experiments were performed with an average of three animals/treatment/time point. Data were initially subjected to two-way (treatment × experiment) analysis of variance (ANOVA), except the marble burying test, nucleus accumbens and perirhinal cortex neurochemistry data, which were available only from the third experiment. There were no

statistical differences between the different experiments ($P > 0.05$) for body/organ weight, food/water consumption, and behavioral data; these data within the same treatment and time point were pooled for analyses using one-way ANOVA, unless specifically mentioned below. The offspring body/organ weights data were analyzed by a two-way ANOVA to determine the effects of an additional factor, sex. The open field test data were analyzed within sex (as appropriate) by a two-way ANOVA to determine the effect of an additional factor, interval (5-min time period), on horizontal and location parameters. Student's t-test was used to compare the difference between approaching the familiar vs. the novel object in the NOR within each treatment group. Neurochemistry data were analyzed within sex (as appropriate) by a two-way (treatment × experiment) ANOVA. If significance was detected by ANOVA ($p \leq 0.05$) then the Fisher's LSD multiple comparison post hoc test (two-tailed) was used to evaluate the differences between treatments with significance level set at $\alpha = 0.05$.

Results

Food/water consumption and calculated ATR exposure level (dams)

Overall, as expected, food and water consumption increased in both control and ATR-treated groups throughout gestation and lactation (Table 7.1); there were no significant differences ($p \geq 0.12$) between control and ATR-treated groups in the amount of food and water consumed. Calculated maternal ATR exposure levels increased over time as a result of the increased water consumption, ranging from 0.694 (the first week of exposure) to 2.204 mg/kg/day (the last week of exposure), with an average exposure level of 1.4 mg/kg/day.

Effects of drinking water ATR exposure during gestation and lactation on body weights and general health status

Drinking water ATR (3 mg/L) exposure from GD6 to PND23 did not cause overt toxicity to the dams, juvenile or adult offspring: the dam's and offspring's weight gain or the general health status and appearance of the ATR-exposed dams and their offspring were not different from controls (Tables D1 and D2, Appendix D). In addition, no significant changes were found in the absolute or relative weights of selected organs, including the brain, liver, spleen, thymus, ovary, uterus, and/or testis in dams, juvenile or adult offspring between treatment groups, except a trend towards an increase ($p = 0.1$) of the adult offspring's relative spleen weight (Tables D1 and D2, Appendix D). As expected, there were significant sex differences in the body weights ($p \leq 0.001$) of juvenile and adult offspring, with males being heavier than females, as well as in the relative brain weights of juvenile offspring and the relative brain/spleen/thymus weights of adult offspring, which were lower in males than in females ($p \leq 0.01$, Table D2, Appendix D).

Dam behavior

In the open field test, ATR-treated dams had increased number of crossings ($p \leq 0.001$; data not shown) and distance traveled ($p \leq 0.05$) per 5 min interval, spent less time in the periphery and longer time in the center of the open field arenas ($p \leq 0.05$; Fig. 7.2). On the other hand, during the first 5 min exploration period, the number of rearings ($p = 0.723$; Fig. 7.2) was not different between control and ATR-exposed animals.

In the NOR test, control dams, as expected, displayed novel object bias by showing higher percentage (63%) in the number of approaches towards the novel object ($p \leq 0.001$; Fig. 7.3). On the contrary, there was no difference in the number of approaches towards the novel vs. the familiar object for the ATR-treated dams ($p = 0.822$), indicating decreased novelty

preference by ATR. If these data are expressed as NPI, ATR exposure resulted in a decreased NPI in ATR-treated dams ($p \leq 0.05$; data not shown).

No significant differences were found in the pole, grip strength and FST tests between control and ATR-treated dams ($p \geq 0.12$; Figs. D1 and D2, Appendix D).

Juvenile offspring behavior

The distance traveled per 5 min interval in the open field test was increased in ATR-treated male ($p \leq 0.01$) and female ($p \leq 0.001$) juvenile offspring (Fig. 7.4); while the number of crossings per 5 min interval was also elevated in ATR-exposed female ($p \leq 0.001$) offspring, but not in males ($p = 0.498$; data not shown). On the other hand, no significant alterations were found in the number of rearings during the first 5 min ($p = 0.77$) and in the time spent in the center or periphery of the arenas ($p = 0.87$) between control and ATR-treated groups in male juveniles (Fig. 7.4). In the female juveniles, a non-significant trend ($p = 0.09$) towards increased time in the center and decreased time in the periphery was observed.

The forelimb grip strength was not affected by ATR in both male and female juvenile offspring ($p \geq 0.26$, Fig. D3, Appendix D). In addition, ATR exposure did not affect the performance of male juvenile offspring in the pole test ($p \geq 0.33$), but ATR-treated female juvenile offspring exhibited trends towards decreases in the time to turn ($p = 0.09$) and in the time to descend ($p = 0.10$), and a significant decrease of the total time ($p \leq 0.05$, Fig. 7.5). Similarly, ATR-treated female juveniles buried higher number of marbles than control animals in the marble burying test ($p \leq 0.05$, Fig. 7.6); while the marble burying behavior was not altered by ATR in male juveniles ($p = 0.63$).

In the FST, ATR exposure significantly decreased the time spent swimming, reduced the number of climbings, and increased the time spent immobile in male juvenile offspring ($p \leq 0.05$, Fig. 7.7); no alterations were observed in the female juvenile offspring ($p \geq 0.37$).

Adult offspring behavior

As shown in Fig. 7.8, the ATR-treated adult males, similar to control males and females, exhibited higher number of approaches towards the novel object ($p \leq 0.01$). However, this novel object preference was absent in the ATR-treated females, i.e., they had equal number of approaches towards the familiar vs. the novel object ($p = 0.69$), suggesting a sex-dependent (female-only) object recognition memory deficits.

As shown in Figs. D4-D7 (Appendix D), no significant differences were observed in the open field, pole, grip, FST, and marble burying tests between control and ATR-treated groups in both male and female adult offspring ($p \geq 0.23$). However, in the marble burying test, males buried more marbles than females ($p \leq 0.05$; Fig. D7, Appendix D).

Dam neurochemistry

In the dam, striatal levels of DA ($p \leq 0.01$) and its metabolites DOPAC, HVA, and 3-MT ($p \leq 0.05$) were significantly increased by ATR, but ATR did not affect striatal 5-HT/5-HIAA levels ($p \geq 0.41$, Table 7.2). In the nucleus accumbens, ATR exposure resulted in a trend towards a decrease of DA ($p = 0.06$), significantly decreased HVA ($p \leq 0.01$) and 3-MT ($p \leq 0.05$), but it did not alter 5-HT or NE homeostasis ($p \geq 0.17$; Table D3, Appendix D). In addition, a decrease of 5-HT ($p \leq 0.05$) in the prefrontal cortex and a decrease of NE ($p \leq 0.05$) in the perirhinal cortex were observed, but ATR did not change the levels of other selected monoamines in these two regions ($p \geq 0.28$, Table D3, Appendix D). In the dam's hippocampus, the only significant effect was an increase of HVA ($p \leq 0.05$, Table D3, Appendix D).

Juvenile offspring neurochemistry

In both male and female juveniles, striatal levels of DA were increased by ATR ($p \leq 0.01$), but DA's metabolites DOPAC, HVA, and 3-MT, as well as striatal 5-HT homeostasis were not changed ($p \geq 0.29$, Table 7.2). In the prefrontal cortex and hippocampus, no significant changes of monoamines or their metabolites were found ($p \geq 0.15$, Table D4, Appendix D).

Adult offspring neurochemistry

In the striatum of adult offspring, ATR exposure did not alter the levels of DA and its metabolites DOPAC and HVA in both males and females ($p \geq 0.20$), but there was an increase in the level of the DA's metabolite 3-MT in females ($p \leq 0.05$, Table 7.2). Additionally, striatal 5-HT homeostasis was not affected by ATR in both males and females ($p \geq 0.09$).

In the nucleus accumbens, DA's metabolite 3-MT was decreased by ATR in males ($p \leq 0.05$); whereas 5-HT's metabolite 5-HIAA ($p \leq 0.01$) was increased by ATR in females (Table D5, Appendix D). In the prefrontal cortex, the only significant change was a decrease of DA in males ($p \leq 0.001$); in the perirhinal cortex, the only significant alterations were decreased levels of DA's metabolite DOPAC ($p \leq 0.05$) and of 5-HT ($p \leq 0.05$) in females (Table D5, Appendix D). No significant differences between ATR-exposed and control mice were observed in the hippocampal monoamine levels of adult offspring ($p \geq 0.12$, Table D5, Appendix D).

Discussion

This study provides evidence that maternal exposure to low drinking water concentrations of ATR induces multiple behavioral abnormalities involving motor, emotional, and/or cognitive functions in both dams and offspring. Notably, the ATR-induced behavioral changes in the offspring are time-dependent and occur in a sex- and behavioral domain-specific manner. These behavioral alterations are associated with widespread perturbation on brain

monoamine homeostasis that is, in some cases, age- and sex-specific. In the context of ATR neurotoxicity studies, the current exposure paradigm as well as the findings on the behavioral and the associated neurochemical effects in dams and offspring are novel.

One of the major findings from this study is that exposure to low drinking water concentrations of ATR (3 mg/L, on average 1.4 mg/kg) during gestation and lactation decreases object recognition memory function in dams and adult female offspring. This finding is consistent with earlier studies that found short-term ATR (≥25 mg/kg) exposure reduces the NOR performance of adult male mice (Lin et al., 2013b) and that adult mouse offspring from dams orally exposed to ATR from GD14 to PND21 exhibit altered memory function assessed by a passive avoidance test, with the effects being greater on females (Belloni et al., 2011). Thus, ATR's effects on the offspring's cognitive function may be delayed and sex-specific. The perirhinal cortex plays an important role in object recognition memory (Antunes and Biala, 2012). The female-only adult offspring effect of ATR on 5-HT (75% decrease) levels in the perirhinal cortex and the decreased NE in perirhinal cortex of dams may, in part, account for the observed NOR memory deficits in female adult offspring and dams, suggesting the perirhinal cortex as a novel target of ATR. Besides the perirhinal cortex, object recognition memory also engages the prefrontal cortex, nucleus accumbens, and the hippocampus (Nelson et al., 2010; Preston and Eichenbaum, 2013). Therefore, the decreased DA in nucleus accumbens and reduced 5-HT in the prefrontal cortex may also contribute to the memory deficits in ATR-treated dams, indicating that ATR might affect the memory processes at multiple levels. Furthermore, it has been shown that ATR exposure from GD14 to PND21 induces dimorphic neuropathology by targeting the frontoparietal cortical and striatal areas in a sex-independent manner while affecting the hippocampus and hypothalamus only in adult female offspring (Giusi et al., 2006). These

sex-specific effects of ATR on brain structure may also contribute to the sex-selective effect of ATR on the adult offspring's object recognition memory.

Another major finding from this study is that ATR exposure causes hyperactivity in the dam and in male and female juvenile offspring, but in the offspring this effect is transient and does not persist into adulthood. This finding is in line with earlier studies that found chronic (1 year) dietary exposure to ATR (10 mg/kg) increases locomotor activity in male rats (Bardullas et al., 2011) and oral exposure to ATR (0.001 mg/kg) from GD14 to PND16 increases exploratory behavior in an open field test in male and female juvenile (PND16) mouse offspring (Belloni et al., 2011). On the other hand, exposure to high doses of ATR (100-250 mg/kg) results in hypoactivity (Lin et al., 2013b; Rodriguez et al., 2013) that lasts up to 5 days in adult male rodents (Rodriguez et al., 2013). These findings suggest that ATR exposure consistently disrupts motor function, regardless of the sex, physiological status, or exposure paradigm. The direction of this effect may be dose- and time-dependent. As the nigrostriatal DA system participates in motor control (Schultz, 2007), the increased striatal DA in dams and juvenile offspring, and the lack of effects on striatal DA in adult offspring may be responsible for the increased motor activity in dams and juvenile offspring, and the unchanged adult offspring's motor activity. This finding agrees with previous studies that demonstrated ATR-induced alterations on motor activity are accompanied with altered striatal DA homeostasis in adult male rodents (Lin et al., 2013b; Rodriguez et al., 2013). The finding that the effect of ATR on the striatal DA level is transient agrees with our earlier study that short-term (14-day) oral ATR exposure disrupts striatal DA homeostasis temporarily (within 1 week after exposure; ≥125 mg/kg), but it causes an apparent persistent loss of DA neurons in the substantial nigra, probably due to compensatory restoration of striatal tissue DA levels by the surviving DA neurons (Coban and Filipov, 2007).

In agreement with the transient hyperactivity, ATR-treated juvenile females exhibited less turning and total time in the pole test, which may also be attributed to increased striatal DA (striatal DA content has been shown to be a sensitive indicator of pole test performance; Matsuura et al., 1997). The pole test results are also suggestive of ATR-induced anxiety-like behavior in juvenile females. Consistent with this possibility, ATR-exposed juvenile females, but not males, buried more marbles in the marble burying test, indicating female offspring-specific increased anxiety-like behavior (Kobayashi et al., 2008). On the other hand, in juvenile males, ATR exposure increased the time spent immobile in the FST, suggesting increased depressive-like behavior (Kobayashi et al., 2008). These sex-specific effects on emotional function did not persist into adulthood. In line with our findings, sex-dependent effects on anxiety/depression have also been observed in offspring of rodents exposed to other toxicants (e.g., methylmercury and chlorpyrifos) during gestation and/or lactation, with females responding with anxiety-like behavior (Ricceri et al., 2006) and males responding with depressive-like behavior (Onishchenko et al., 2007).

Anxiety and depression disorders are known to be associated with abnormalities of monoamine systems (Ressler and Nemeroff, 2000). However, except increased striatal DA, there were no other changes in the monoamine levels in the striatum, prefrontal cortex and hippocampus of ATR-treated juvenile offspring. These results imply that there may be other brain regions and/or neurotransmitter pathways targeted by ATR. Alternatively, ATR's effects on gonadal hormones (Cooper et al., 1996; Friedmann, 2002), may contribute to/be responsible for these sex-specific effects. For example, pubertal hormones play an important role in the development and control of sexually dimorphic brain and behaviors (Sisk and Zehr, 2005). Ovarian hormones, such as estrogen, are associated with anti-anxiety effects (Palanza, 2001);

while testosterone is related to anti-depressive-like behavior in rodents (Frye and Walf, 2009). In this regard, ATR exposure has been shown to decrease serum estrogen, increase progesterone (Cooper et al., 1996), and reduce testosterone levels in rats (Friedmann, 2002). These sex-specific effects of ATR on gonadal hormones may, in part, account for its sex-selective effects on the emotional function in juvenile offspring, but this remains to be investigated.

Recent pharmacokinetic studies suggest that following gestational and/or lactational rodent exposure to ATR via the oral route (5 or 25 mg/kg), the fetus is exposed to ATR and its metabolites at levels similar to maternal plasma levels, and the neonate is mainly exposed to ATR's major metabolite DACT at levels one third of maternal plasma level (Fraites et al., 2011; Lin et al., 2013c). Both ATR and DACT can bind to brain tissue proteins (Dooley et al., 2010; Fakhouri et al., 2010) and ATR adduction can cause protein dysfunction (Fakhouri et al., 2010). Moreover, both ATR and DACT can disrupt morphological differentiation of dopaminergic neurons in vitro (Lin et al., 2013a). Therefore, the observed behavioral abnormalities in the adult offspring long after exposure has been terminated may be because ATR and DACT directly affect major nervous system developmental processes, such as neuronal differentiation.

Among the behavioral tests used in current study, the novelty preference in the NOR was abolished in ATR-treated dam and adult female offspring, while changes in other behavioral tests were more modest or transient in nature, suggesting that NOR may be more sensitive to ATR than the other behavioral tests. Neurochemically, striatal DA homeostasis was altered in dams, male and female juvenile offspring; other endpoints were changed either in dams or in offspring, suggesting that the most consistent neurochemical endpoint affected by drinking water ATR

exposure is striatal DA. These data from the current perinatal study agree with earlier studies in adult rodents (Bardullas et al., 2011; Lin et al., 2013b; Rodriguez et al., 2013).

Compared to the two existing rodent developmental neurotoxicity studies with ATR in which exposure route was oral gavage and exposure duration was from GD14 to PND21 (Giusi et al., 2006; Belloni et al., 2011), the present study used an environmentally-relevant drinking water exposure route (Mosquin et al., 2012). Our exposure duration included the early period (GD6-13) of nervous system development when neuronal cells are undifferentiated (Prakash and Wurst, 2006) because this period may be particularly vulnerable to ATR (Lin et al., 2013a). The dose was also carefully chosen by considering the maximum surface water concentration in Midwestern US (ATSDR, 2003) and including an uncertainty factor of 10 to account for the species differences between rodents and humans (Lang et al., 1996). Overall, by using human-relevant novel exposure paradigm, the present study suggests that ATR exposure during gestation and lactation may be detrimental to the nervous system of both dams and offspring.

Conclusions

Our results indicate that maternal exposure to low drinking water concentrations of ATR induces multiple behavioral abnormalities in the dam and offspring. These behavioral alterations are associated with perturbation of brain monoamine homeostasis in a brain region- and, in some cases, sex- and time-specific manner. As an example, alterations of monoamine levels in the perirhinal cortex may be involved in the ATR-induced object recognition memory deficits, suggesting perirhinal cortex as a potential novel target of ATR. The finding that ATR exposure results in delayed effects on cognitive function and long-term effects on monoamine systems in the offspring suggests that developmental ATR exposure may increase vulnerability to neurodegenerative diseases involving monoamine system dysfunction later in life. The finding

that ATR causes sex-specific behavioral changes in the offspring suggests that ATR overexposure may be a contributing environmental factor to the development of sex-biased neurodevelopmental disorders.

Conflict of interest statement

The authors declare that there are no conflicts of interest.

Acknowledgments

The authors thank Ms. Rong Li and Mr. Fei Zhao from Department of Physiology and Pharmacology, College of Veterinary Medicine, University of Georgia, Athens, GA, for providing skillful technical assistance.

Table 7.1. Food/water consumption and calculated ATR exposure levels of the dams[a].

	Food[b] (g/kg/day)		Water[b] (mL/kg/day)		ATR intake[b]
	Control	3 mg/kg ATR	Control	3 mg/kg ATR	(mg/kg/day)
GD6-12	187.066 ± 4.540	179.461 ± 10.837	263.912 ± 17.708	231.376 ± 9.890	0.694 ± 0.0296
GD13-19	214.667 ± 6.821	219.236 ± 9.893	258.111 ± 16.437	241.805 ± 7.987	0.725 ± 0.0239
GD20-PND6	281.678 ± 10.558	273.082 ± 17.873	354.216 ± 27.481	327.750 ± 20.324	0.983 ± 0.0610
PND7-13	435.427 ± 26.179	476.267 ± 33.125	560.119 ± 44.924	541.664 ± 31.596	1.625 ± 0.0949
PND14-20	422.180 ± 35.030	473.949 ± 39.667	687.626 ± 56.781	708.702 ± 41.371	2.126 ± 0.124
PND21-23	ND	ND	686.278 ± 64.333	734.581 ± 49.631	2.204 ± 0.149

[a] When food/water consumption could not be determined for an animal during a given interval (due to food/water spillage, obvious erroneous value, etc.), group-mean values were calculated for that interval using the available data. There were no significant differences ($p \geq 0.12$) between control and ATR-treated groups in the food and water consumption at any time interval. ND, not determined. Data are presented as means ± SEM.

[b] Food, water, and ATR intake dose are expressed on a mg/kg basis based on the maternal/dam body weight only, i.e., pup's consumption, which may have been substantial during the second half of their pre-weaning postnatal life was not considered.

Table 7.2. Concentrations of monoamines and their metabolites in the striatum of mouse dams, juvenile and adult offspring exposed to ATR from GD6 to PND23[a].

	DA	DOPAC	HVA	3-MT	5-HT	5-HIAA
Dams						
Vehicle	180.10 ± 6.20	16.63 ± 0.62	11.65 ± 0.51	13.26 ± 0.90	1.26 ± 0.16	1.04 ± 0.12
3 mg/L ATR	**205.75 ± 6.30***	**18.70 ± 0.65***	**13.67 ± 0.52***	**16.08 ± 0.88***	1.09 ± 0.17	1.19 ± 0.12
Juvenile males						
Vehicle	122.51 ± 2.83	14.41 ± 0.62	11.79 ± 0.59	12.62 ± 1.15	1.17 ± 0.24	1.14 ± 0.07
3 mg/L ATR	**136.79 ± 3.30***	14.13 ± 0.72	12.81 ± 0.69	14.04 ± 1.34	0.98 ± 0.28	1.25 ± 0.08
Juvenile females						
Vehicle	132.61 ± 2.77	14.13 ± 0.83	11.99 ± 0.41	14.24 ± 1.35	1.62 ± 0.28	1.25 ± 0.12
3 mg/L ATR	**145.78 ± 2.59***	15.22 ± 0.80	12.31 ± 0.39	14.69 ± 1.30	1.38 ± 0.27	1.23 ± 0.12
Adult males						
Vehicle	195.49 ± 7.79	16.35 ± 0.38	14.18 ± 1.22	14.79 ± 1.14	1.56 ± 0.16	1.28 ± 0.11
3 mg/L ATR	180.19 ± 7.79	15.82 ± 0.38	13.75 ± 1.22	14.90 ± 1.14	1.84 ± 0.16	1.57 ± 0.11
Adult females						
Vehicle	175.83 ± 11.88	15.99 ± 1.37	14.35 ± 0.89	14.40 ± 1.33	2.11 ± 0.35	1.71 ± 0.06
3 mg/L ATR	174.99 ± 9.58	17.75 ± 1.11	14.55 ± 0.72	**19.19 ± 1.07***	2.54 ± 0.28	1.65 ± 0.05

[a] Data represent means ± SEM; unit: ng/mg protein. DA: dopamine; DOPAC: dihydroxyphenylacetic acid; HVA: homovanillic acid; 3-MT: 3-methoxytyramine; 5-HT: serotonin; 5-HIAA: 5-hydroxyindoleacetic acid.

* Different from control group ($p \leq 0.05$).

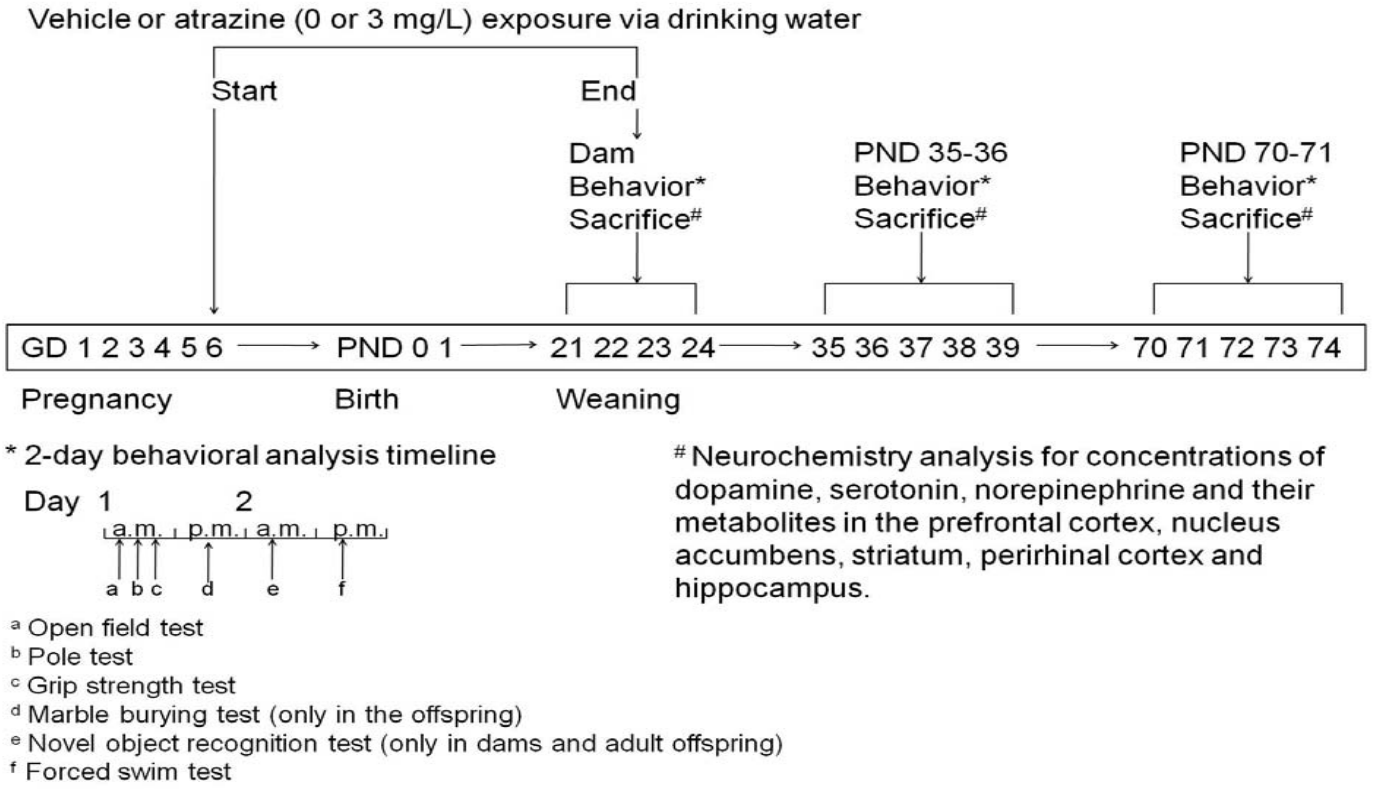

Figure 7.1. Experimental design and a timeline for the current study. Pregnant C57BL/6 mice were exposed to vehicle or 3 mg/L atrazine (ATR) via drinking water from GD6 to PND23-24. Dams (PND21-22), juvenile (PND35-36) and adult (PND70-71) offspring were subjected to a 2-day behavioral analysis, followed by tissue collections 1-2 days after completion of behavioral tests. Selected brain regions were collected for monoamine neurochemistry analysis with HPLC.

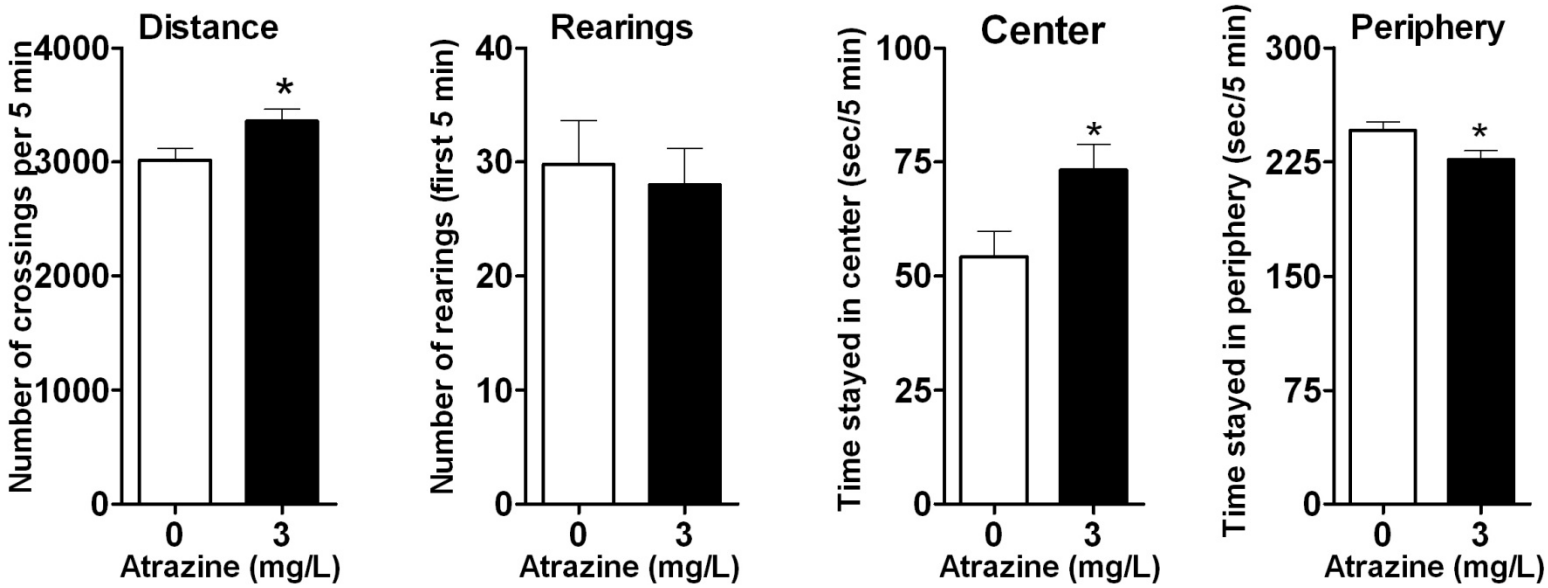

Figure 7.2. Effects of drinking water atrazine (ATR) exposure from gestational day 6 to postnatal day 21-22 on locomotor activity in an open field test in mouse dams. * Indicates significant difference from the control group ($p \leq 0.05$). Data are expressed as means ± SEM.

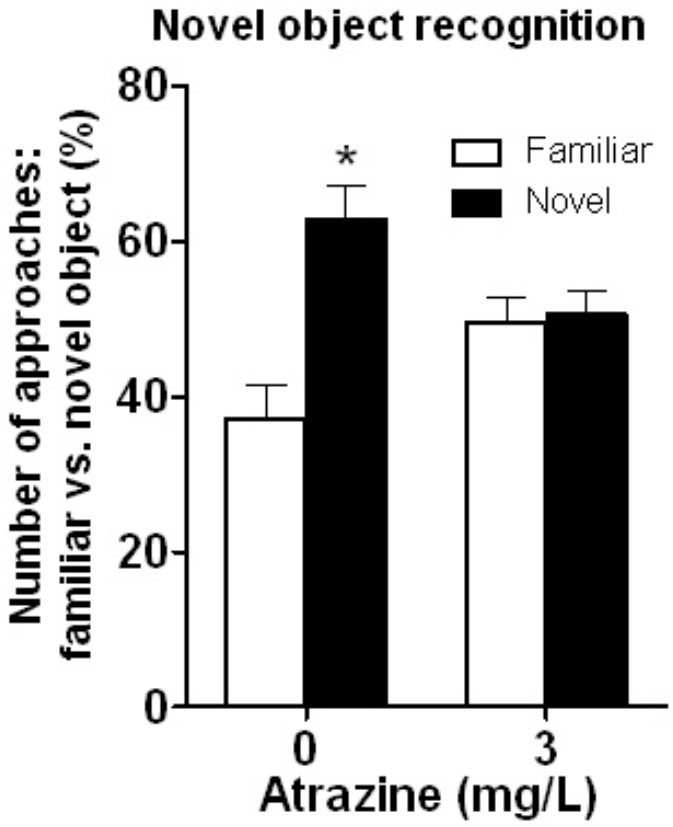

Figure 7.3. Effects of drinking water atrazine (ATR) exposure from gestational day 6 to postnatal day 22-23 on the number of approaches towards a familiar vs. a novel object (%) in a novel object recognition test in mouse dams. * Indicates significant difference between the novel and the familiar within a treatment group ($p \leq 0.05$). Data are expressed as means ± SEM.

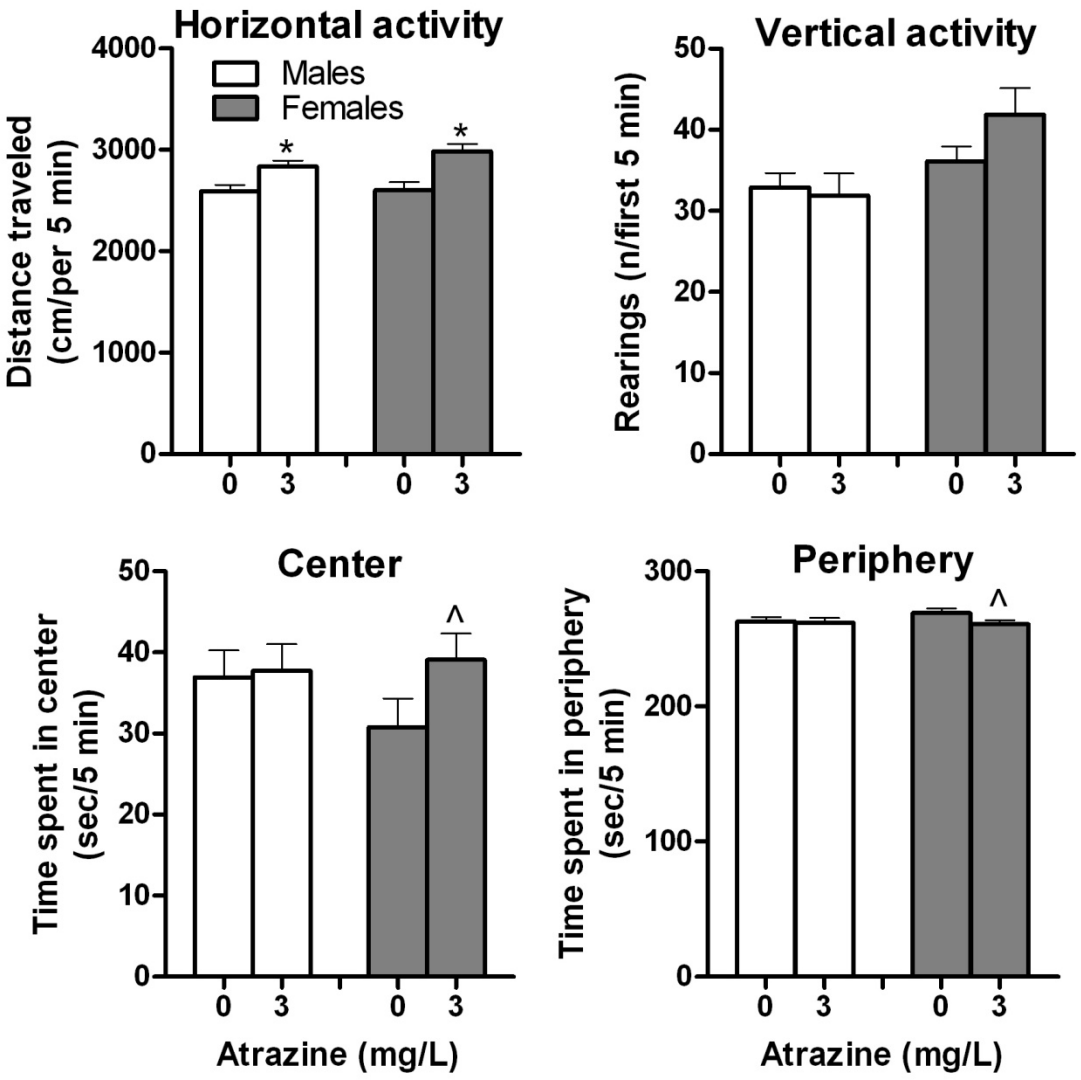

Figure 7.4. Effects of drinking water atrazine (ATR) exposure from gestational day 6 to postnatal day 23-24 on the locomotor activity in an open field test in juvenile mouse offspring. * Indicates significant difference from the control group ($p \leq 0.05$). ^ Indicates a trend towards significant difference from the control group ($p \leq 0.10$). Data are expressed as means ± SEM.

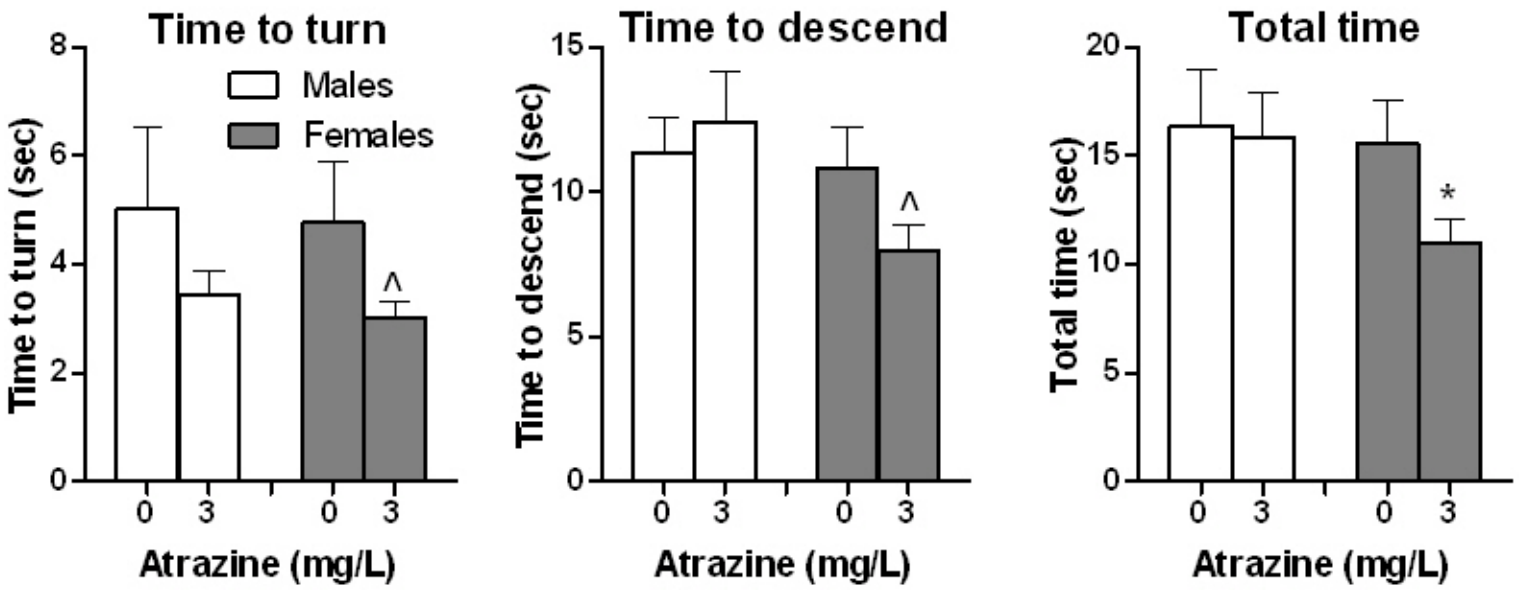

Figure 7.5. Effects of drinking water atrazine (ATR) exposure from gestational day 6 to postnatal day 23-24 on the time to turn, time to descend, and total time spent in a pole test in juvenile mouse offspring. * Indicates significant difference from the control group ($p \leq 0.05$). ^ Indicates a trend towards significant difference from the control group ($p \leq 0.10$). Data are expressed as means ± SEM.

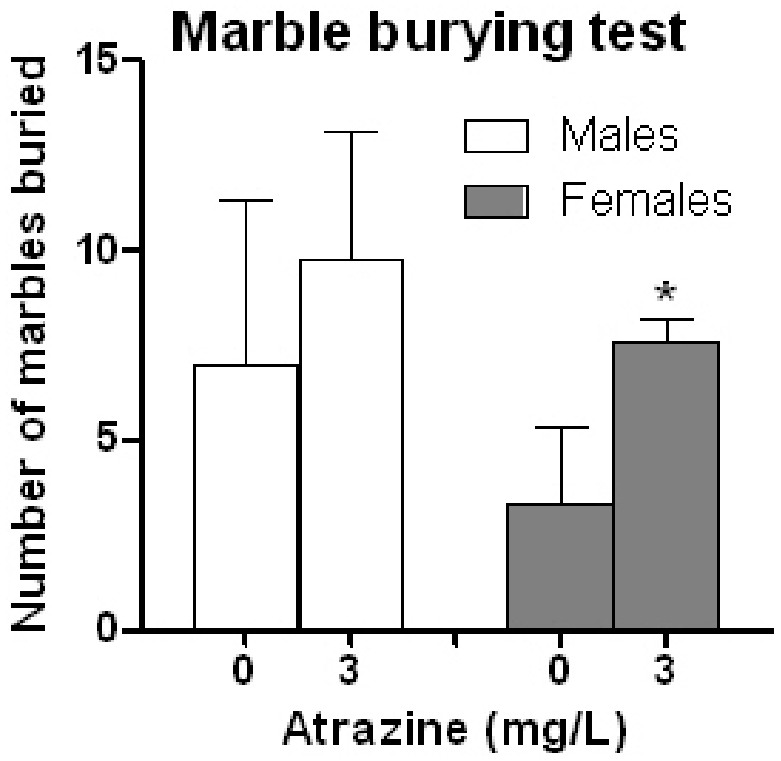

Figure 7.6. Effects of drinking water atrazine (ATR) exposure from gestational day 6 to postnatal day 23-24 on the number of marbles buried in a marble burying test in juvenile mouse offspring. * Indicates significant difference from the control group ($p \leq 0.05$). Data are expressed as means ± SEM.

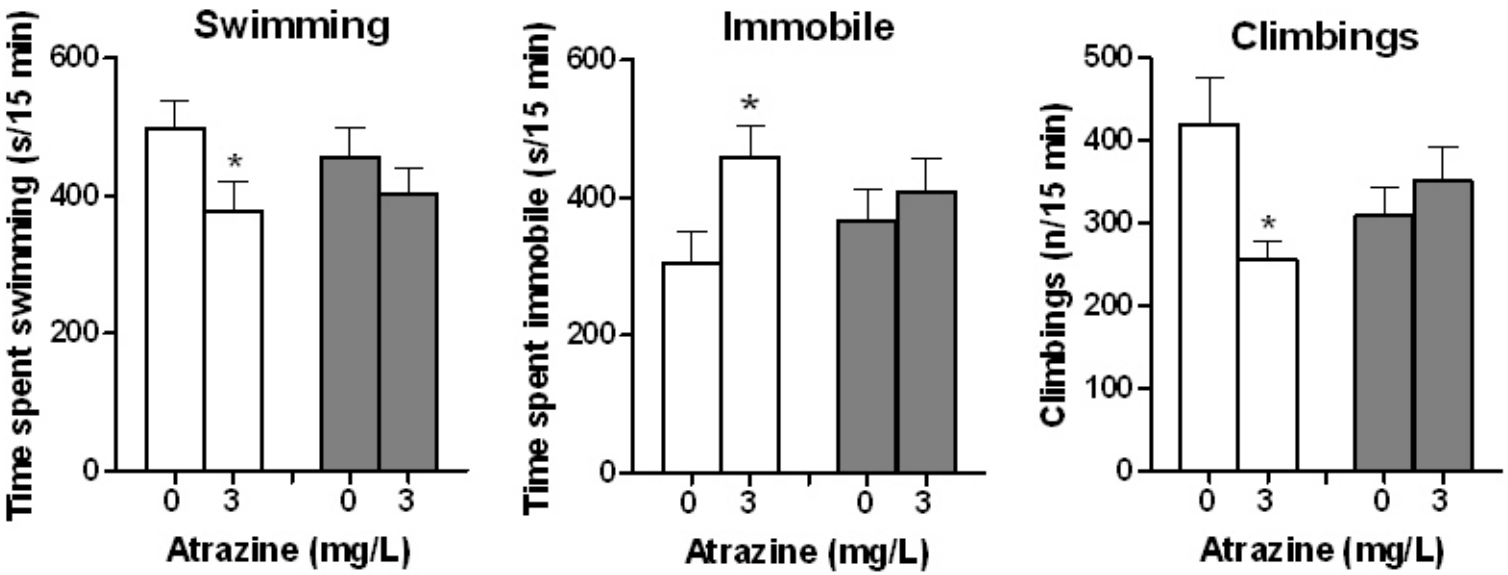

Figure 7.7. Effects of drinking water atrazine (ATR) exposure from gestational day 6 to postnatal day 23-24 on the time spent swimming, time spent immobile, and the number of climbings in a forced swim test in juvenile mouse offspring. * Indicates significant difference from the control group ($p \leq 0.05$). Data are expressed as means ± SEM.

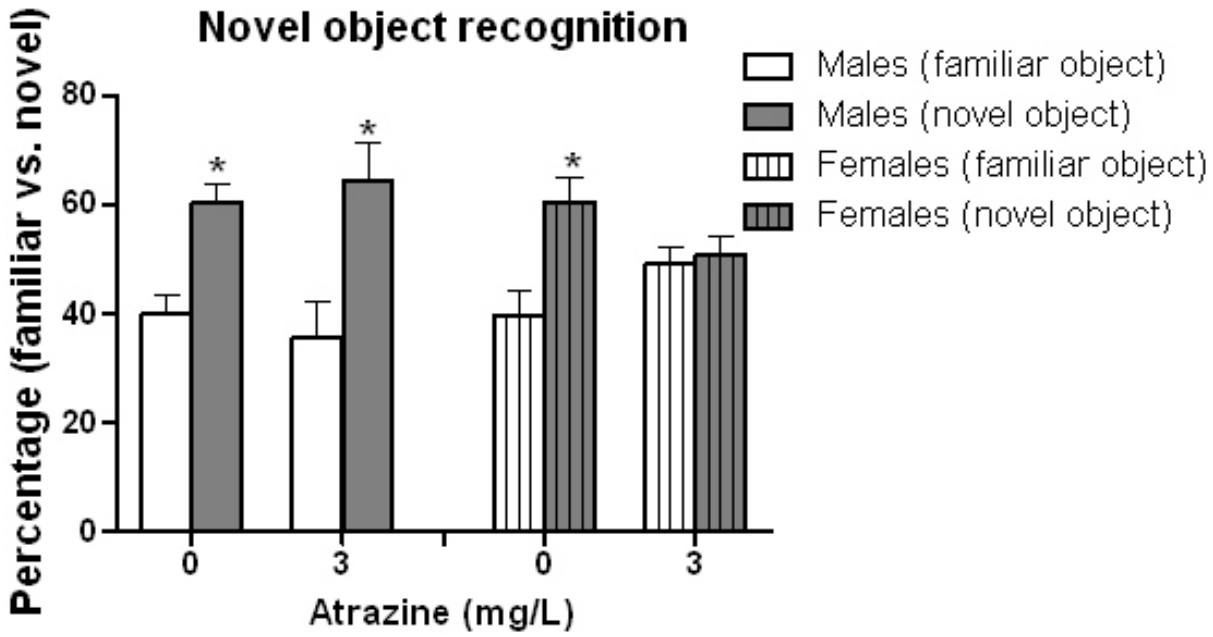

Figure 7.8. Effects of drinking water atrazine (ATR) exposure from gestational day 6 to postnatal day 23-24 on the number of approaches towards a familiar vs. a novel object (%) in a novel object recognition test in adult mouse offspring. * Indicates significant difference between the novel and the familiar within a treatment group of each sex ($p \leq 0.05$). Data are expressed as means ± SEM.

CHAPTER 8

OVERALL DISCUSSION, CONCLUSIONS, AND FUTURE DIRECTIONS

Overall discussion

Excessive ATR exposure, especially to sensitive subpopulations, is a public concern in many countries, including the US, where this herbicide is still extensively used; the concern is because of its ubiquitous presence in the environment, i.e., water supplies, soil, sediments and ATR's reported multiple organ toxicities. Available experimental scientific evidence and quantitative tools for ATR's toxicity are insufficient in many aspects. As a result, the proper risk assessment for this herbicide is yet to be done. The goals of this dissertation project were to determine the neurotoxic effects of ATR exposure during different life stages and to develop PBPK models for ATR; together, the newly obtained experimental and modeling data provides vital information that can be used to improve the lifespan risk assessment to human health that is associated with ATR overexposure.

To accomplish these goals, five Specific Aims were conducted. Aim 1 determined the effects of short-term exposure to occupationally-relevant doses of ATR on multiple behaviors and associated neurochemistry in adult male mice. Aim 2 developed a PBPK model for ATR in adult male mice. Aim 3 constructed PBPK models for ATR in rat dams, fetuses, and neonates. Aim 4 determined the effects of ATR and its main metabolite DACT on dopaminergic neuron differentiation in vitro. Aim 5 evaluated the neurobehavioral and neurochemical effects of exposure to an environmentally-relevant low concentration of ATR during gestation and lactation via the drinking water in mouse dams and offspring. Major accomplishments, novel

findings, implications, and conclusions from the completion of these Specific Aims can be summarized as follows.

One of the major findings from this research is that ATR exposure disrupts the nigrostriatal DA pathway, resulting in altered striatal DA homeostasis and motor function. Whether adult mice were orally exposed for a short-term to occupationally-relevant higher doses of ATR or the exposure to ATR was via the drinking water to environmentally-relevant lower concentrations during the vulnerable gestational and lactational periods, striatal DA homeostasis and motor activity were altered in adults and juveniles irrespective of sex. These findings are consistent with previous studies reporting that long-term (1-year, dietary) or short-term (2-week, intraperitoneal injections or oral gavage) exposures to occupationally relevant higher doses of ATR (≥10 mg/kg) alter striatal DA and motor activity in adult male rats (Bardullas et al., 2011; Rodriguez et al., 2013) and juvenile male mice (Coban and Filipov, 2007). Thus, in spite of the differences in exposure routes, duration, and doses, available studies, including ours, consistently suggest that the nigrostriatal DA pathway is a sensitive ATR target. Moreover, our developmental study suggests that the effects of ATR on the nigrostriatal DA pathway and the associated motor function while being sex-independent, are observed at much lower exposure levels when the exposure is during the vulnerable (Rice and Barone, 2000) gestational and lactational periods when the nervous system is developing.

Besides targeting the nigrostriatal DA pathway, we found that ATR exposure also targets other monoamine pathways, namely 5-HT and NE. This novel finding implies that the neurological effects of ATR are not restricted to a specific neural pathway and ATR may cause extensive perturbation on multiple neural circuitries. Notably, altered 5-HT and NE homeostasis was observed not only in adult male mice exposed to higher doses of ATR for 10 days, but also

in adult female offspring and dams exposed to low-level drinking water ATR during gestation and lactation. This finding suggests that developmental low-dose ATR exposure can cause long-term effects on 5-HT and NE systems in adult female offspring.

In line with ATR's effects on 5-HT and NE systems, another novel finding from this research is that ATR exposure decreases object recognition memory in adult male mice exposed to higher doses of ATR for short-term, as well as in adult female offspring and dams exposed to low-dose ATR from GD6 to PND23. This finding is consistent with earlier studies that found long-term (1 year) dietary exposure to a higher dose of ATR (10 mg/kg) affects spatial memory in male adult rats (evaluated by a non-delayed random foraging test; Bardullas et al., 2011) and that perinatal (GD14-PND21) low-dose ATR (0.1 mg/kg) exposure alters memory function in adult mice (assessed by a passive avoidance test), with the effects being greater on the females (Belloni et al., 2011). Thus, the effects of developmental ATR exposure on the offspring's cognitive function may be delayed and sex-specific. Moreover, ATR-induced memory deficits may be attributed to its effects on the 5-HT and/or NE circuitries, as discussed before. Of note, we found that memory function of adult male mice is affected by ATR at doses that do not change motor activity and the selected brain monoamine indices in Aim 1. These data signify that ATR may target other brain regions or neurotransmitter pathways. This hypothesis was confirmed in Aim 5, in which we found developmental ATR exposure decreases memory function in adult female offspring that is associated with decreased 5-HT in the perirhinal cortex, suggesting the perirhinal cortex as a potential novel target of ATR. In terms of other neural circuitries, the hippocampus-dependent cholinergic and glutaminergic systems, which play important roles in memory function (Preston and Eichenbaum, 2013), might be potential targets. For example, developmental exposure to other pesticides causes object recognition memory

deficits that are accompanied by decreased acetylcholine esterase activity (N'Go et al., 2013) and reduced levels of NMDA type of glutamate receptors in the hippocampus of rodents (Win-Shwe et al., 2013). In this regard, ATR exposure decreases the activity and mRNA expression of brain acetylcholine esterase in fish (Xing et al., 2010a; Xing et al., 2010b).

ATR's effects on emotional function have not been reported before. In our studies, we found that (1) high-dose short-term ATR exposure causes anxiety-like behavior in adult male mice and (2) low-dose maternal ATR exposure induces anxiety-like behavior in juvenile female mice and depressive-like behavior in juvenile male mice; these effects are not persistent into adulthood. These results suggest that ATR exposure can disrupt emotional function, with the effects on the offspring being sex-specific and perhaps, transient. Emotional disorders are known to be associated with abnormalities of monoamine systems (Ressler and Nemeroff, 2000). Therefore, the observed extensive perturbation on DA, 5-HT, and/or NE homeostasis in adult male mice in Aim 1 may be involved in ATR-induced anxiety-like behavior. However, in ATR-treated juvenile offspring, except increased striatal DA, there were no other changes in the monoamine levels in the striatum, prefrontal cortex and hippocampus. These results imply that there may be other target brain regions or other mechanisms, such as ATR's effects on hormone levels (Cooper et al., 1996; Friedmann, 2002) that may contribute to these sex-specific effects; this remains to be investigated.

While the mechanisms of ATR's developmental neurotoxicity are largely unknown, our research suggests that both ATR and DACT affect DA neuron differentiation, with ATR primarily inhibiting soma growth dose-dependently and DACT moderately affecting neurite outgrowth only at high doses. These effects may, in part, contribute to the observed developmental neurotoxicity. Soma size enlargement and neurite outgrowth are not specific to

DA neuron differentiation, but are typical characteristics of neuronal development (Gruol and Franklin, 1987; Clarkson et al., 1999). Therefore, it is possible that ATR and DACT also affect differentiation of other neuronal cell types, such as serotonergic and adrenergic neurons, which need to be investigated in future studies. The ontogeny of nervous system developmental events, including proliferation, migration, differentiation, synaptogenesis, myelination, and apoptosis, is interrelated and overlapped (Rice and Barone, 2000). Hence, it is possible that perturbation of neuronal proliferation and differentiation caused by ATR and DACT will also disrupt other related developmental events, such as migration. The potential effects of ATR and DACT on other developmental processes need to be determined in future studies.

The PBPK models for ATR in adult male mice, as well as in rat dams, fetuses, and neonates properly describe the plasma and brain dosimetry of ATR and its metabolites across a wide dose range (5-250 mg/kg). Successful simulation of ATR kinetics in the brain across the lifespan implies that these models can be used to predict the brain dosimetry of ATR and its metabolites associated with the observed adult/developmental neurotoxicity of ATR from this research and from other studies (Giusi et al., 2006; Coban and Filipov, 2007; Belloni et al., 2011; Rodriguez et al., 2013), which together can be used to establish brain-specific dose-response relationship, a key component in the risk assessment process. However, it should be cautious to apply the present model to predict the brain concentrations of ATR in rodents following long-term exposure. This is because the present models were calibrated based on data from mice exposed to a single dose of ATR (Ross et al., 2009) and from rat dams exposed to ATR for short-term (3-19 days; Fraites et al., 2011). Nevertheless, our gestational and lactational PBPK models have properly simulated ATR autoinduction metabolism profile following short-term exposures (3-19 days), which has implications in humans because it also occurs in humans

(Abass et al., 2012). In order to more precisely describe ATR metabolism in humans, the dose- and time-dependency of ATR autoinduction metabolism, especially in long-term low-dose exposures, needs to be determined in future studies.

Compared to existing ATR PBPK models in adult rats (Timchalk et al., 1990; McMullin et al., 2003; McMullin et al., 2007b), a unique feature of our models is that they have been successfully extrapolated to one different species, either from mice to rats or from rats to mice. This suggests that our models can be used to conduct species extrapolation. Thus, our models provide a valuable foundation for developing ATR PBPK models in humans across the lifespan in the future.

Another major contribution from the adult mouse PBPK model is the description of dose-dependent oral absorption characteristics of ATR, i.e., the absorption rate for lower doses (≤5 mg/kg) is around 2-fold higher than that of higher doses (≥25 mg/kg). The low-dose specific absorption rate has been incorporated into the gestational and lactational models, in which model simulations correlated with measured data (Fraites et al., 2011) very well. This finding has important implications in future modeling studies in humans. To be more specific, the absorption rate of environmentally-relevant low doses of ATR, which are usually much lower than 5 mg/kg, may be greater than the 5-mg/kg-specific absorption rate. This possibility should be considered in modeling low-dose exposure in humans.

The gestational and lactational model simulation results indicate that ATR exposure during pregnancy results in much higher amounts of ATR and its metabolites in the developing brain than exposure during lactation. These results are important because nervous system development timelines are different from rodents and humans. Specifically, it occurs from GD6 to 3-4 weeks postnatally in rodents and mainly during pregnancy (gestational week 3.5 to 40) in

humans (Rice and Barone, 2000). Hence, if rodent dams and human mothers are exposed to similar amount of ATR throughout nervous system development, the developing nervous system in the offspring of humans may be more vulnerable to the effects of ATR than in rodents because it may receive much greater amounts of ATR and its metabolite. Thus, when extrapolating developmental neurotoxicity data of ATR from rodents to humans, the species difference in the dosimetry of ATR and its metabolites in the developing brain should be considered.

From the point of exposure assessment, the adult mouse model successfully simulates the urinary dosimetry of ATR's metabolites across a wide dose range. This suggests that, once the exposure type, i.e., ATR, is known, the adult model can be used to predict internal/external exposure via reverse dosimetry analysis. In addition, the gestational and lactational model simulation results provide useful information about the relationship between maternal and fetal/neonatal dosimetry. Thus, these models can help predict fetal and neonatal brain dosimetry based on maternal exposure information.

Conclusions

The novel findings from Aim 1 are that short-term exposure to occupationally-relevant doses of ATR induces multiple behavioral abnormalities involving motor, cognitive and emotional functions and that ATR targets monoamine pathways. These findings greatly improve our understanding of the potential neurotoxicity following short-term high-dose ATR exposures. Our results may improve risk assessment of ATR, because the LOAEL for the altered NOR performance (25 mg/kg) in Aim 1 is almost 3-fold lower than the current EPA LOAEL (70 mg/kg), which is based on ATR's adverse effects on the reproductive and endocrine systems.

The PBPK model for ATR in adult male mice in Aim 2 properly describe the plasma, brain, and urine dosimetry of ATR and its metabolites DE, DIP and DACT across a wide dose

range. This model increases our understanding of ATR kinetic behavior in adult animals. The model simulation results and the observed neurotoxicity data from Aim 1 can be used to establish brain-specific dose-response relationship. The description of urinary dosimetry of ATR's metabolites indicates that the model can be applied to exposure assessment. This model has been extrapolated from mice to rats, suggesting it as a foundation for scaling to humans.

PBPK models for ATR in dams, fetuses, and neonates in Aim 3 accurately simulate the plasma and tissue dosimetry of ATR and its metabolites DE, DIP, and DACT following gestational and/or lactational exposures. These models improve our understanding of placental/lactational transfer and kinetic behavior of ATR and its metabolites in the fetus and neonate. These models can be used to predict fetal and neonatal brain dosimetry based on maternal exposure information, which can greatly improve exposure assessment in the fetus and neonate in biomonitoring studies. Model simulation results together with observed developmental neurotoxicity of ATR in Aim 5 can be used to establish developing brain-specific dose-response curves. They can also help design early life toxicity and pharmacokinetic studies, as well as interpret study findings. These models provide a framework for developing gestational and lactational PBPK models for other chlorotriazine herbicides, and can be used as a foundation for extrapolating to humans.

The results in Aim 4 suggest that both ATR and DACT affect DA neuron differentiation, with ATR primarily inhibiting soma growth and DACT moderately decreasing neurite outgrowth. These findings may in part account for the observed developmental neurotoxicity of ATR. Moreover, we found that intracellular ATP levels and soma size are the most sensitive parameters to ATR in undifferentiated and differentiating DA cells, respectively. These results imply that the DA circuitries might be particularly vulnerable to ATR during defined

developmental windows. Also, they can help interpret the toxicological significance of gestational and lactational PBPK model simulations results and the design of future developmental neurotoxicity studies of ATR.

Aim 5 demonstrated that exposure to environmentally-relevant low doses of ATR during gestation and lactation induce multiple behavioral changes involving motor, cognitive, and/or emotional functions in the mouse dam and offspring. These behavioral alterations are associated with disruption of brain monoamine homeostasis in a brain region-specific manner. The findings that ATR causes delayed effects on cognitive function and long-term effects on monoamine systems in the offspring suggest that developmental ATR exposure may increase vulnerability to neurodegenerative disorders of monoamine systems later in life. The finding that ATR induces sex-selective behavioral changes in the offspring suggests that ATR overexposure may be a contributing factor to the development of sex-biased neurodevelopmental disorders.

Collectively, this dissertation work provides occupationally- and environmentally-relevant experimental and modeling evidence about ATR's neurotoxicity across the lifespan. This research identified multiple novel nervous system-related targets for ATR, i.e., novel neural circuitries (i.e., 5-HT and NE pathways), brain regions (e.g., perirhinal cortex), and behavioral domains (i.e., cognition and emotion). In addition, the PBPK modeling part of this dissertation substantially increases our understanding of the kinetic behavior of ATR in the body, especially its placental and lactational transfer characteristics and target (brain) tissue levels of ATR and its major mammalian metabolites. Together, the findings from this research can aid the hazard identification, dose-response relationship establishment, and exposure assessment of this widely used herbicide.

Future directions

The present short-term high-dose exposure study revealed two novel behavioral targets of ATR. In order to make these findings more relevant to the general population, future studies could use a long-term low-dose drinking water exposure paradigm. Besides the behavioral tests used in this study, additional tests that assess other behavioral domains, such as learning ability, spatial memory, and sensory function should be considered in future studies. Because this work suggests that object recognition memory may be the most sensitive behavioral endpoint of ATR, future studies investigating the underlying mechanisms are warranted. Specifically, prefrontal cortex, perirhinal cortex and hippocampus have been shown to play critical roles in the object recognition memory (Preston and Eichenbaum, 2013). Future studies using more sensitive analytical method, such as microdialysis, to determine extracellular levels of monoamines in these regions following ATR exposure are recommended. The physiological actions of monoamines are mediated by their respective receptors, so it is necessary to determine the expression and activity of monoamine receptors in ATR's target brain regions in the future.

The present in vivo developmental neurotoxicity study serves as a starting point for the establishment of ATR developmental neurotoxicity dose-response relationship. Future studies could apply the present study design and include two or more lower doses. The effects of ATR exposure during gestation and lactation on maternal care behavior should also be evaluated in the future, as it is related to offspring behavior. The present in vitro developmental neurotoxicity study suggests potential existence of defined developmental windows that are most vulnerable to ATR. Therefore, future animal studies using multiple different developmental exposure paradigms to identify the most sensitive period to ATR are needed. The present in vitro study suggests that both ATR and DACT affect morphological differentiation of dopaminergic

neurons. However, the mechanisms of ATR-induced soma shrinkage and DACT-induced neurite outgrowth inhibition remain to be investigated. As nervous system development encompasses multiple processes, the effects of ATR and its metabolites on the other critical developmental events, such as migration, synaptogenesis, and myelination, deserve further investigation.

The gestational and lactational PBPK models provide valuable information about ATR's kinetic behavior in rodent dams, fetuses, and neonates. In order to further optimize these models, future pharmacokinetic studies for ATR in rodent dams, fetuses, and neonates should include multiple time points to determine the concentration time-course of ATR/metabolites in the plasma and tissues. The maternal and neonatal urine samples should also be collected. Besides pharmacokinetic data, more information about ATR's mode of action is needed. For example, the protein-bound fraction of ATR and DACT in the brain or in the whole fetus and the functional consequences of ATR- or DACT-protein adduction need to be determined. Partition coefficients for ATR and its metabolites in various tissues, especially in the whole fetus and milk, need to be measured using experimental methods (Tremblay et al., 2012). The present PBPK models of ATR in rodents across the lifespan provide a foundation for scaling to humans. However, to develop models in humans, more data are needed, such as pharmacokinetic data of rodents receiving long-term low-dose drinking water ATR with intermittent high-dose acute challenges and detailed plasma/urinary data from humans with known recent exposure to ATR.

In summary, the present dissertation research demonstrated that an integrative evaluation approach synthesizing experimental and PBPK modeling studies provides comprehensive information that advances our understanding of ATR neurotoxicity and kinetic behavior, which can be used to improve its risk assessment. However, there are still important data gaps in this field that need to be addressed in the future.

REFERENCES

Abarikwu SO, Adesiyan AC, Oyeloja TO, Oyeyemi MO, Farombi EO. Changes in sperm characteristics and induction of oxidative stress in the testis and epididymis of experimental rats by a herbicide, atrazine. Arch Environ Contam Toxicol 2010;58:874-82.

Abarikwu SO, Farombi EO, Kashyap MP, Pant AB. Kolaviron protects apoptotic cell death in PC12 cells exposed to Atrazine. Free Radic Res 2011a;45:1061-73.

Abarikwu SO, Farombi EO, Pant AB. Biflavanone-kolaviron protects human dopaminergic SH-SY5Y cells against atrazine induced toxic insult. Toxicol In Vitro 2011b;25:848-58.

Abass K, Lamsa V, Reponen P, Kublbeck J, Honkakoski P, Mattila S, et al. Characterization of human cytochrome P450 induction by pesticides. Toxicology 2012;294:17-26.

Abbas R, Fisher JW. A physiologically based pharmacokinetic model for trichloroethylene and its metabolites, chloral hydrate, trichloroacetate, dichloroacetate, trichloroethanol, and trichloroethanol glucuronide in B6C3F1 mice. Toxicol Appl Pharmacol 1997;147:15-30.

Abdel-Rahman AA, Blumenthal GM, Abou-Donia SA, Ali FA, Abdel-Monem AE, Abou-Donia MB. Pharmacokinetic profile and placental transfer of a single intravenous injection of [(14)C]chlorpyrifos in pregnant rats. Arch Toxicol 2002;76:452-9.

Adachi K, Konitzer P, Pang J, Reddy KS, Surrey S. Amino acids responsible for decreased 2,3-biphosphoglycerate binding to fetal hemoglobin. Blood 1997;90:2916-20.

Adams NH, Hodgson E, Levi PE. In vitro studies of the metabolism of atrazine, simazine, and terbutryn in several vertebrate species. J Agric Food Chem 1990;38:1411-7.

Ademola JI, Sedik LE, Wester RC, Maibach HI. In vitro percutaneous absorption and metabolism in man of 2-chloro-4-ethylamino-6-isopropylamine-s-triazine (atrazine). Arch Toxicol 1993;67:85-91.

Alcaro A, Huber R, Panksepp J. Behavioral functions of the mesolimbic dopaminergic system: an affective neuroethological perspective. Brain Res Rev 2007;56:283-321.

Allen NE, Schwarzel AK, Canning CG. Recurrent falls in Parkinson's disease: a systematic review. Parkinsons Dis 2013;2013:906274.

Almqvist PM, Akesson E, Wahlberg LU, Pschera H, Seiger A, Sundstrom E. First trimester development of the human nigrostriatal dopamine system. Exp Neurol 1996;139:227-37.

Altman PL, Dittmer DS. Volume of blood in tissue: Vertebrates. Respiration and Circulation. Bethesda, MD: Federation of American Societies for Experimental Biology; 1971. p. 383-7.

Andersen ME. Development of physiologically based pharmacokinetic and physiologically based pharmacodynamic models for applications in toxicology and risk assessment. Toxicol Lett 1995;79:35-44.

Andersen ME, Birnbaum LS, Barton HA, Eklund CR. Regional hepatic CYP1A1 and CYP1A2 induction with 2,3,7,8-tetrachlorodibenzo-p-dioxin evaluated with a multicompartment geometric model of hepatic zonation. Toxicol Appl Pharmacol 1997;144:145-55.

Antunes M, Biala G. The novel object recognition memory: neurobiology, test procedure, and its modifications. Cogn Process 2012;13:93-110.

Armstrong L, Tilgner K, Saretzki G, Atkinson SP, Stojkovic M, Moreno R, et al. Human induced pluripotent stem cell lines show stress defense mechanisms and mitochondrial regulation similar to those of human embryonic stem cells. Stem Cells 2010;28:661-73.

Arthur SK, Green R. Renal function during lactation in the rat. J Physiol 1983;334:379-93.

Atherton JC, Dark JM, Garland HO, Morgan MR, Pidgeon J, Soni S. Changes in water and electrolyte balance, plasma volume and composition during pregnancy in the rat. J Physiol 1982;330:81-93.

ATSDR. Potential for human exposure. In: Toxicological profile for atrazine. Atlanta: U.S. Agency for Toxic Substances and Disease Registry; 2003. p. 129-60.

Bakke JE, Larson JD, Price CE. Metabolism of atrazine and 2-hydroxyatrazine by the rat. J Agric Food Chem 1972;20:602-7.

Baldi I, Lebailly P, Mohammed-Brahim B, Letenneur L, Dartigues JF, Brochard P. Neurodegenerative diseases and exposure to pesticides in the elderly. Am J Epidemiol 2003;157:409-14.

Balduini L, Matoga M, Cavalli E, Seilles E, Riethmuller D, Thomassin M, et al. Triazinic herbicide determination by gas chromatography-mass spectrometry in breast milk. J Chromatogr B Analyt Technol Biomed Life Sci 2003;794:389-95.

Bardullas U, Giordano M, Rodriguez VM. Chronic atrazine exposure causes disruption of the spontaneous locomotor activity and alters the striatal dopaminergic system of the male Sprague-Dawley rat. Neurotoxicol Teratol 2011;33:263-72.

Bardullas U, Limon-Pacheco JH, Giordano M, Carrizales L, Mendoza-Trejo MS, Rodriguez VM. Chronic low-level arsenic exposure causes gender-specific alterations in locomotor activity, dopaminergic systems, and thioredoxin expression in mice. Toxicol Appl Pharmacol 2009;239:169-77.

Barr DB, Panuwet P, Nguyen JV, Udunka S, Needham LL. Assessing exposure to atrazine and its metabolites using biomonitoring. Environ Health Perspect 2007;115:1474-8.

Battaglin WA, Furlong ET, Burkhardt MR, Peter CJ. Occurrence of sulfonylurea, sulfonamide, imidazolinone, and other herbicides in rivers, reservoirs and ground water in the Midwestern United States, 1998. Sci Total Environ 2000;248:123-33.

Battaglin WA, Rice KC, Focazio MJ, Salmons S, Barry RX. The occurrence of glyphosate, atrazine, and other pesticides in vernal pools and adjacent streams in Washington, DC, Maryland, Iowa, and Wyoming, 2005-2006. Environ Monit Assess 2009;155:281-307.

Baudry A, Mouillet-Richard S, Launay JM, Kellermann O. New views on antidepressant action. Curr Opin Neurobiol 2011;21:858-65.

Belloni V, Dessi-Fulgheri F, Zaccaroni M, Di Consiglio E, De Angelis G, Testai E, et al. Early exposure to low doses of atrazine affects behavior in juvenile and adult CD1 mice. Toxicology 2011;279:19-26.

Berry C, La Vecchia C, Nicotera P. Paraquat and Parkinson's disease. Cell Death Differ 2010;17:1115-25.

Bjorkman S. Reduction and lumping of physiologically based pharmacokinetic models: prediction of the disposition of fentanyl and pethidine in humans by successively simplified models. J Pharmacokinet Pharmacodyn 2003;30:285-307.

Bradbury DA, Simmons TD, Slater KJ, Crouch SP. Measurement of the ADP:ATP ratio in human leukaemic cell lines can be used as an indicator of cell viability, necrosis and apoptosis. J Immunol Methods 2000;240:79-92.

Brake SC, Sager DJ, Sullivan R, Hofer M. The role of intraoral and gastrointestinal cues in the control of sucking and milk consumption in rat pups. Dev Psychobiol 1982;15:529-41.

Bretveld RW, Thomas CM, Scheepers PT, Zielhuis GA, Roeleveld N. Pesticide exposure: the hormonal function of the female reproductive system disrupted? Reprod Biol Endocrinol 2006;4:30.

Brown RP, Delp MD, Lindstedt SL, Rhomberg LR, Beliles RP. Physiological parameter values for physiologically based pharmacokinetic models. Toxicol Ind Health 1997;13:407-84.

Brown TP, Rumsby PC, Capleton AC, Rushton L, Levy LS. Pesticides and Parkinson's disease--is there a link? Environ Health Perspect 2006;114:156-64.

Brzezicki JM, Andersen ME, Cranmer BK, Tessari JD. Quantitative identification of atrazine and its chlorinated metabolites in plasma. J Anal Toxicol 2003;27:569-73.

Buchholz BA, Fultz E, Haack KW, Vogel JS, Gilman SD, Gee SJ, et al. HPLC-accelerator MS measurement of atrazine metabolites in human urine after dermal exposure. Anal Chem 1999;71:3519-25.

Campbell A, Holstege D, Swezey R, Medina-Cleghorn D. Detoxification of molinate sulfoxide: comparison of spontaneous and enzmatic glutathione conjugation using human and rat liver cytosol. J Toxicol Environ Health A 2008;71:1338-47.

Cannon JR, Tapias V, Na HM, Honick AS, Drolet RE, Greenamyre JT. A highly reproducible rotenone model of Parkinson's disease. Neurobiol Dis 2009;34:279-90.

Capek K, Jelinek J. The development of the control of water metabolism. I. The excretion of urine in young rats. Physiol Bohemoslov 1956;5:91-6.

Casabar RC, Das PC, Dekrey GK, Gardiner CS, Cao Y, Rose RL, et al. Endosulfan induces CYP2B6 and CYP3A4 by activating the pregnane X receptor. Toxicol Appl Pharmacol 2010;245:335-43.

Catenacci G, Barbieri F, Bersani M, Ferioli A, Cottica D, Maroni M. Biological monitoring of human exposure to atrazine. Toxicol Lett 1993;69:217-22.

Catenacci G, Colli G, Verni P, Barisano A. Environmental and biologic monitoring of atrazine exposure at a formulating plant. G Ital Med Lav Ergon 2002;24:35-42.

Chang DT, Reynolds IJ. Mitochondrial trafficking and morphology in healthy and injured neurons. Prog Neurobiol 2006;80:241-68.

Chen N, Aleksa K, Woodland C, Rieder M, Koren G. Ontogeny of drug elimination by the human kidney. Pediatr Nephrol 2006;21:160-8.

Chevreuil M, Garmouma M, Teil MJ, Chesterikoff A. Occurrence of organochlorines (PCBs, pesticides) and herbicides (triazines, phenylureas) in the atmosphere and in the fallout from urban and rural stations of the Paris area. Sci Total Environ 1996;182:25-37.

Chevrier C, Limon G, Monfort C, Rouget F, Garlantezec R, Petit C, et al. Urinary biomarkers of prenatal atrazine exposure and adverse birth outcomes in the PELAGIE birth cohort. Environ Health Perspect 2011;119:1034-41.

Churchi-l SE, Bengele HH, Alexander EA. Sodium balance during pregnancy in the rat. Am J Physiol 1980;239:R143-8.

Clancy B, Finlay BL, Darlington RB, Anand KJ. Extrapolating brain development from experimental species to humans. Neurotoxicology 2007;28:931-7.

Clarkson ED, Edwards-Prasad J, Freed CR, Prasad KN. Immortalized dopamine neurons: A model to study neurotoxicity and neuroprotection. Proc Soc Exp Biol Med 1999;222:157-63.

Clewell HJ, 3rd, Gentry PR, Gearhart JM, Covington TR, Banton MI, Andersen ME. Development of a physiologically based pharmacokinetic model of isopropanol and its metabolite acetone. Toxicol Sci 2001;63:160-72.

Clewell RA, Kremer JJ, Williams CC, Campbell JL, Jr., Andersen ME, Borghoff SJ. Tissue exposures to free and glucuronidated monobutylyphthalate in the pregnant and fetal rat following exposure to di-n-butylphthalate: evaluation with a PBPK model. Toxicol Sci 2008;103:241-59.

Clewell RA, Merrill EA, Yu KO, Mahle DA, Sterner TR, Mattie DR, et al. Predicting fetal perchlorate dose and inhibition of iodide kinetics during gestation: a physiologically-based pharmacokinetic analysis of perchlorate and iodide kinetics in the rat. Toxicol Sci 2003;73:235-55.

Coban A, Filipov NM. Dopaminergic toxicity associated with oral exposure to the herbicide atrazine in juvenile male C57BL/6 mice. J Neurochem 2007;100:1177-87.

Cooper RL, Laws SC, Das PC, Narotsky MG, Goldman JM, Lee Tyrey E, et al. Atrazine and reproductive function: mode and mechanism of action studies. Birth Defects Res B Dev Reprod Toxicol 2007;80:98-112.

Cooper RL, Stoker TE, Goldman JM, Parrish MB, Tyrey L. Effect of atrazine on ovarian function in the rat. Reprod Toxicol 1996;10:257-64.

Cooper RL, Stoker TE, Tyrey L, Goldman JM, McElroy WK. Atrazine disrupts the hypothalamic control of pituitary-ovarian function. Toxicol Sci 2000;53:297-307.

Corley RA, Bartels MJ, Carney EW, Weitz KK, Soelberg JJ, Gies RA, et al. Development of a physiologically based pharmacokinetic model for ethylene glycol and its metabolite, glycolic Acid, in rats and humans. Toxicol Sci 2005;85:476-90.

Corley RA, Mast TJ, Carney EW, Rogers JM, Daston GP. Evaluation of physiologically based models of pregnancy and lactation for their application in children's health risk assessments. Crit Rev Toxicol 2003;33:137-211.

Corrigan FM, Wienburg CL, Shore RF, Daniel SE, Mann D. Organochlorine insecticides in substantia nigra in Parkinson's disease. J Toxicol Environ Health A 2000;59:229-34.

Corsini E, Sokooti M, Galli CL, Moretto A, Colosio C. Pesticide induced immunotoxicity in humans: a comprehensive review of the existing evidence. Toxicology 2013;307:123-35.

Costa LG. Current issues in organophosphate toxicology. Clin Chim Acta 2006;366:1-13.

Costa LG, Giordano G, Guizzetti M, Vitalone A. Neurotoxicity of pesticides: a brief review. Front Biosci 2008;13:1240-9.

Costello S, Cockburn M, Bronstein J, Zhang X, Ritz B. Parkinson's disease and residential exposure to maneb and paraquat from agricultural applications in the central valley of California. Am J Epidemiol 2009;169:919-26.

Cragin LA, Kesner JS, Bachand AM, Barr DB, Meadows JW, Krieg EF, et al. Menstrual cycle characteristics and reproductive hormone levels in women exposed to atrazine in drinking water. Environ Res 2011;111:1293-301.

Craske ML, Fivaz M, Batada NN, Meyer T. Spines and neurite branches function as geometric attractors that enhance protein kinase C action. J Cell Biol 2005;170:1147-58.

Crowell SR, Henderson WM, Kenneke JF, Fisher JW. Development and application of a physiologically based pharmacokinetic model for triadimefon and its metabolite triadimenol in rats and humans. Toxicol Lett 2011;205:154-62.

Cummings AM, Rhodes BE, Cooper RL. Effect of atrazine on implantation and early pregnancy in 4 strains of rats. Toxicol Sci 2000;58:135-43.

Curwin BD, Hein MJ, Sanderson WT, Striley C, Heederik D, Kromhout H, et al. Urinary pesticide concentrations among children, mothers and fathers living in farm and non-farm households in iowa. Ann Occup Hyg 2007;51:53-65.

Czekaj P, Wiaderkiewicz A, Wiaderkiewicz R, Palasz A. Expression of constitutive and inducible cytochromes P450 in fetal and newborn rat liver. Polish J of Environ Stud 2006;15:699-708.

Das KP, Barone S, Jr. Neuronal differentiation in PC12 cells is inhibited by chlorpyrifos and its metabolites: is acetylcholinesterase inhibition the site of action? Toxicol Appl Pharmacol 1999;160:217-30.

Das KP, Freudenrich TM, Mundy WR. Assessment of PC12 cell differentiation and neurite growth: a comparison of morphological and neurochemical measures. Neurotoxicol Teratol 2004;26:397-406.

Das PC, Cao Y, Rose RL, Cherrington N, Hodgson E. Enzyme induction and cytotoxicity in human hepatocytes by chlorpyrifos and N,N-diethyl-m-toluamide (DEET). Drug Metabol Drug Interact 2008;23:237-60.

Das PC, McElroy WK, Cooper RL. Differential modulation of catecholamines by chlorotriazine herbicides in pheochromocytoma (PC12) cells in vitro. Toxicol Sci 2000;56:324-31.

Das PC, McElroy WK, Cooper RL. Alteration of catecholamines in pheochromocytoma (PC12) cells in vitro by the metabolites of chlorotriazine herbicide. Toxicol Sci 2001;59:127-37.

Das PC, McElroy WK, Cooper RL. Potential mechanisms responsible for chlorotriazine-induced alterations in catecholamines in pheochromocytoma (PC12) cells. Life Sci 2003;73:3123-38.

Davis LK, Murr AS, Best DS, Fraites MJ, Zorrilla LM, Narotsky MG, et al. The effects of prenatal exposure to atrazine on pubertal and postnatal reproductive indices in the female rat. Reprod Toxicol 2011;32:43-51.

de Lau LM, Breteler MM. Epidemiology of Parkinson's disease. Lancet Neurol 2006;5:525-35.

den Hollander B, Rozov S, Linden AM, Uusi-Oukari M, Ojanpera I, Korpi ER. Long-term cognitive and neurochemical effects of "bath salt" designer drugs methylone and mephedrone. Pharmacol Biochem Behav 2013;103:501-9.

Denovan LA, Lu C, Hines CJ, Fenske RA. Saliva biomonitoring of atrazine exposure among herbicide applicators. Int Arch Occup Environ Health 2000;73:457-62.

Dong X, Zhu L, Wang J, Xie H, Hou X, Jia W. Effects of atrazine on cytochrome P450 enzymes of zebrafish (Danio rerio). Chemosphere 2009;77:404-12.

Dooley GP, Ashley AK, Legare ME, Handa RJ, Hanneman WH. Proteomic analysis of diaminochlorotriazine (DACT) adducts in three brain regions of Wistar rats. Toxicol Lett 2010;199:17-21.

Dooley GP, Hanneman WH, Carbone DL, Legare ME, Andersen ME, Tessari JD. Development of an immunochemical detection method for atrazine-induced albumin adducts. Chem Res Toxicol 2007;20:1061-6.

Dooley GP, Prenni JE, Prentiss PL, Cranmer BK, Andersen ME, Tessari JD. Identification of a novel hemoglobin adduct in Sprague Dawley rats exposed to atrazine. Chem Res Toxicol 2006;19:692-700.

Dooley GP, Reardon KF, Prenni JE, Tjalkens RB, Legare ME, Foradori CD, et al. Proteomic analysis of diaminochlorotriazine adducts in wistar rat pituitary glands and LbetaT2 rat pituitary cells. Chem Res Toxicol 2008;21:844-51.

Dowell RT, Kauer CD. Maternal hemodynamics and uteroplacental blood flow throughout gestation in conscious rats. Methods Find Exp Clin Pharmacol 1997;19:613-25.

Dyet LE, Kennea N, Counsell SJ, Maalouf EF, Ajayi-Obe M, Duggan PJ, et al. Natural history of brain lesions in extremely preterm infants studied with serial magnetic resonance imaging from birth and neurodevelopmental assessment. Pediatrics 2006;118:536-48.

Echobicon DJ. Toxic effects of pesticides. In: Casarett and Doull's Toxicology. The Basic Science of Poisons. Ed: C. D. Klaassen. McGraw-Hill, New York. 2001;763-810.

Ejiri N, Katayama K, Doi K. Induction of cytochrome P450 isozymes by phenobarbital in pregnant rat and fetal livers and placenta. Exp Mol Pathol 2005;78:150-5.

Eldridge JC, Fleenor-Heyser DG, Extrom PC, Wetzel LT, Breckenridge CB, Gillis JH, et al. Short-term effects of chlorotriazines on estrus in female Sprague-Dawley and Fischer 344 rats. J Toxicol Environ Health 1994a;43:155-67.

Eldridge JC, Tennant MK, Wetzel LT, Breckenridge CB, Stevens JT. Factors affecting mammary tumor incidence in chlorotriazine-treated female rats: hormonal properties, dosage, and animal strain. Environ Health Perspect 1994b;102 Suppl 11:29-36.

Emond C, Birnbaum LS, DeVito MJ. Use of a physiologically based pharmacokinetic model for rats to study the influence of body fat mass and induction of CYP1A2 on the pharmacokinetics of TCDD. Environ Health Perspect 2006;114:1394-400.

Engle WA, Lemons JA. Composition of the fetal and maternal guinea pig throughout gestation. Pediatr Res 1986;20:1156-60.

EPA. Interim Reregistration Eligibility Decision for Atrazine. Case No. 0062, U.S. Environmental Protection Agency, Washington, DC. Available at URL: http://www.epa.gov/oppsrrd1/REDs/atrazine_ired.pdf. 2003. p. 12-73.

EPA. Re-Evaluation of Human Health Effects of Atrazine: Review of Cancer Epidemiology, Non-cancer Experimental Animal and In vitro Studies and Drinking Water Monitoring Frequency. U.S. Environmental Protection Agency, Washington, DC. Available at URL: http://www.regulations.gov/#!documentDetail;D=EPA-HQ-OPP-2011-0399-0080. 2011. p. 72-107.

Evans MV, Andersen ME. Sensitivity analysis of a physiological model for 2,3,7,8-tetrachlorodibenzo-p-dioxin (TCDD): assessing the impact of specific model parameters on sequestration in liver and fat in the rat. Toxicol Sci 2000;54:71-80.

Evans MV, Dowd SM, Kenyon EM, Hughes MF, El-Masri HA. A physiologically based pharmacokinetic model for intravenous and ingested dimethylarsinic acid in mice. Toxicol Sci 2008;104:250-60.

Fakhouri WD, Nunez JL, Trail F. Atrazine binds to the growth hormone-releasing hormone receptor and affects growth hormone gene expression. Environ Health Perspect 2010;118:1400-5.

Filipov NM, Pinchuk LM, Boyd BL, Crittenden PL. Immunotoxic effects of short-term atrazine exposure in young male C57BL/6 mice. Toxicol Sci 2005;86:324-32.

Filipov NM, Stewart MA, Carr RL, Sistrunk SC. Dopaminergic toxicity of the herbicide atrazine in rat striatal slices. Toxicology 2007;232:68-78.

Fisher JW, Twaddle NC, Vanlandingham M, Doerge DR. Pharmacokinetic modeling: prediction and evaluation of route dependent dosimetry of bisphenol A in monkeys with extrapolation to humans. Toxicol Appl Pharmacol 2011;257:122-36.

Fisher JW, Whittaker TA, Taylor DH, Clewell HJ, 3rd, Andersen ME. Physiologically based pharmacokinetic modeling of the pregnant rat: a multiroute exposure model for

trichloroethylene and its metabolite, trichloroacetic acid. Toxicol Appl Pharmacol 1989;99:395-414.

Fisher JW, Whittaker TA, Taylor DH, Clewell HJ, 3rd, Andersen ME. Physiologically based pharmacokinetic modeling of the lactating rat and nursing pup: a multiroute exposure model for trichloroethylene and its metabolite, trichloroacetic acid. Toxicol Appl Pharmacol 1990;102:497-513.

Fleming L, Mann JB, Bean J, Briggle T, Sanchez-Ramos JR. Parkinson's disease and brain levels of organochlorine pesticides. Ann Neurol 1994;36:100-3.

Foradori CD, Hinds LR, Hanneman WH, Handa RJ. Effects of atrazine and its withdrawal on gonadotropin-releasing hormone neuroendocrine function in the adult female Wistar rat. Biol Reprod 2009a;81:1099-105.

Foradori CD, Hinds LR, Hanneman WH, Legare ME, Clay CM, Handa RJ. Atrazine inhibits pulsatile luteinizing hormone release without altering pituitary sensitivity to a gonadotropin-releasing hormone receptor agonist in female Wistar rats. Biol Reprod 2009b;81:40-5.

Foradori CD, Hinds LR, Quihuis AM, Lacagnina AF, Breckenridge CB, Handa RJ. The differential effect of atrazine on luteinizing hormone release in adrenalectomized adult female Wistar rats. Biol Reprod 2011;85:684-9.

Foradori CD, Zimmerman AD, Hinds LR, Zuloaga KL, Breckenridge CB, Handa RJ. Atrazine Inhibits Pulsatile Gonadotropin-Releasing Hormone (GnRH) Release Without Altering GnRH Messenger RNA or Protein Levels in the Female Rat. Biol Reprod 2013;88:1-7.

Fraites MJ, Cooper RL, Buckalew A, Jayaraman S, Mills L, Laws SC. Characterization of the hypothalamic-pituitary-adrenal axis response to atrazine and metabolites in the female rat. Toxicol Sci 2009;112:88-99.

Fraites MJ, Narotsky MG, Best DS, Stoker TE, Davis LK, Goldman JM, et al. Gestational atrazine exposure: effects on male reproductive development and metabolite distribution in the dam, fetus, and neonate. Reprod Toxicol 2011;32:52-63.

Friedman MI, Bruno JP, Alberts JR. Physiological and behavioral consequences in rats of water recycling during lactation. J Comp Physiol Psychol 1981;95:26-35.

Friedmann AS. Atrazine inhibition of testosterone production in rat males following peripubertal exposure. Reprod Toxicol 2002;16:275-9.

Frye CA, Walf AA. Depression-like behavior of aged male and female mice is ameliorated with administration of testosterone or its metabolites. Physiol Behav 2009;97:266-9.

Fukui M, Choi HJ, Zhu BT. Rapid generation of mitochondrial superoxide induces mitochondrion-dependent but caspase-independent cell death in hippocampal neuronal cells that morphologically resembles necroptosis. Toxicol Appl Pharmacol 2012;262:156-66.

Gammon DW, Aldous CN, Carr WC, Jr., Sanborn JR, Pfeifer KF. A risk assessment of atrazine use in California: human health and ecological aspects. Pest Manag Sci 2005;61:331-55.

García MÁ, Santaeufemia M, Melgar MJ. Triazine residues in raw milk and infant formulas from Spanish northwest, by a diphasic dialysis extraction. Food Chem Toxicol 2012;50:503-10.

Gargas ML, Tyler TR, Sweeney LM, Corley RA, Weitz KK, Mast TJ, et al. A toxicokinetic study of inhaled ethylene glycol ethyl ether acetate and validation of a physiologically

based pharmacokinetic model for rat and human. Toxicol Appl Pharmacol 2000a;165:63-73.

Gargas ML, Tyler TR, Sweeney LM, Corley RA, Weitz KK, Mast TJ, et al. A toxicokinetic study of inhaled ethylene glycol monomethyl ether (2-ME) and validation of a physiologically based pharmacokinetic model for the pregnant rat and human. Toxicol Appl Pharmacol 2000b;165:53-62.

Gatto NM, Cockburn M, Bronstein J, Manthripragada AD, Ritz B. Well-water consumption and Parkinson's disease in rural California. Environ Health Perspect 2009;117:1912-8.

Geisler A, Endo S, Goss KU. Partitioning of polar and non-polar neutral organic chemicals into human and cow milk. Environ Int 2011;37:1253-8.

Gentry PR, Covington TR, Mann S, Shipp AM, Yager JW, Clewell HJ, 3rd. Physiologically based pharmacokinetic modeling of arsenic in the mouse. J Toxicol Environ Health A 2004;67:43-71.

Gianessi LP, Marcelli MB. Pesticide Use in U.S. Crop Production: 1997 National Summary Report. National Center for Food and Agricultural Policy, Washington, DC. 2000.

Gianessi LP, Reigner NP. The value of herbicides in U.S. crop production. Weed Technol 2007;21:559-66.

Gilliom RJ. Pesticides in U.S. streams and groundwater. Environ Sci Technol 2007;41:3408-14.

Ginsberg G, Hattis D, Russ A, Sonawane B. Pharmacokinetic and pharmacodynamic factors that can affect sensitivity to neurotoxic sequelae in elderly individuals. Environ Health Perspect 2005;113:1243-9.

Girard H, Klappstein S, Bartag I, Moll W. Blood circulation and oxygen transport in the fetal guinea pig. J Dev Physiol 1983;5:181-93.

Giusi G, Facciolo RM, Canonaco M, Alleva E, Belloni V, Dessi'-Fulgheri F, et al. The endocrine disruptor atrazine accounts for a dimorphic somatostatinergic neuronal expression pattern in mice. Toxicol Sci 2006;89:257-64.

Goldstone JV, McArthur AG, Kubota A, Zanette J, Parente T, Jonsson ME, et al. Identification and developmental expression of the full complement of Cytochrome P450 genes in Zebrafish. BMC Genomics 2010;11:643.

Gordon JA, Hen R. The serotonergic system and anxiety. Neuromolecular Med 2004;5:27-40.

Govantes F, Garcia-Gonzalez V, Porrua O, Platero AI, Jimenez-Fernandez A, Santero E. Regulation of the atrazine-degradative genes in Pseudomonas sp. strain ADP. FEMS Microbiol Lett 2010;310:1-8.

Grube A, Donaldson D, Kiely T, Wu L. Pesticides industry sales and usage 2006 and 2007 market estimates. U.S. Environmental Protection Agency, Washington, DC. http://www.epa.gov/opp00001/pestsales/07pestsales/market_estimates2007.pdf. 2011. p. 1-33.

Gruol DL, Franklin CL. Morphological and physiological differentiation of Purkinje neurons in cultures of rat cerebellum. J Neurosci 1987;7:1271-93.

Hahn ME. The aryl hydrocarbon receptor: a comparative perspective. Comp Biochem Physiol C Pharmacol Toxicol Endocrinol 1998;121:23-53.

Hall LL, Fisher HL, Sumler MR, Monroe RJ, Chernoff N, Shah PV. Dose response of skin absorption in young and adult rats. In: S. Z. Mansdorf, R. Sager, and A. P. Nielsen, editors. Performance of Protective Clothing: Second Symposium. Philadelphia: American Society for Testing and Materia; 1988. p. 177-94.

Hanioka N, Jinno H, Kitazawa K, Tanaka-Kagawa T, Nishimura T, Ando M, et al. In vitro biotransformation of atrazine by rat liver microsomal cytochrome P450 enzymes. Chem Biol Interact 1998a;116:181-98.

Hanioka N, Jinno H, Tanaka-Kagawa T, Nishimura T, Ando M. Changes in rat liver cytochrome P450 enzymes by atrazine and simazine treatment. Xenobiotica 1998b;28:683-98.

Hanioka N, Jinno H, Tanaka-Kagawa T, Nishimura T, Ando M. In vitro metabolism of chlorotriazines: characterization of simazine, atrazine, and propazine metabolism using liver microsomes from rats treated with various cytochrome P450 inducers. Toxicol Appl Pharmacol 1999a;156:195-205.

Hanioka N, Jinno H, Tanaka-Kagawa T, Nishimura T, Ando M. In vitro metabolism of simazine, atrazine and propazine by hepatic cytochrome P450 enzymes of rat, mouse and guinea pig, and oestrogenic activity of chlorotriazines and their main metabolites. Xenobiotica 1999b;29:1213-26.

Hanwell A, Linzell JL. The time course of cardiovascular changes in lactation in the rat. J Physiol 1973;233:93-109.

Hase Y, Tatsuno M, Nishi T, Kataoka K, Kabe Y, Yamaguchi Y, et al. Atrazine binds to F1F0-ATP synthase and inhibits mitochondrial function in sperm. Biochem Biophys Res Commun 2008;366:66-72.

Hata T, Itoh E, Nishikawa H. Behavioral characteristics of SART-stressed mice in the forced swim test and drug action. Pharmacol Biochem Behav 1995;51:849-53.

Hata T, Nishikawa H, Itoh E, Watanabe A. Depressive state with anxiety in repeated cold-stressed mice in forced swimming tests. Jpn J Pharmacol 1999;79:243-9.

Hatcher JM, Pennell KD, Miller GW. Parkinson's disease and pesticides: a toxicological perspective. Trends Pharmacol Sci 2008;29:322-9.

He XJ, Ejiri N, Nakayama H, Doi K. Changes in cytochrome P450 isozymes (CYPs) protein levels during lactation in rat liver. Exp Mol Pathol 2005;79:224-8.

He XJ, Yamauchi H, Suzuki K, Ueno M, Nakayama H, Doi K. Gene expression profiles of drug-metabolizing enzymes (DMEs) in rat liver during pregnancy and lactation. Exp Mol Pathol 2007;83:428-34.

Henderson PT. Metabolism of drugs in rat liver during the perinatal period. Biochem Pharmacol 1971;20:1225-32.

Hessel PA, Kalmes R, Smith TJ, Lau E, Mink PJ, Mandel J. A nested case-control study of prostate cancer and atrazine exposure. J Occup Environ Med 2004;46:379-85.

Hiller-Sturmhöfel S, Swartzwelder HS. Alcohol's effects on the adolescent brain: what can be learned from animal models. Alcohol Res Health 2005;28:213-21.

Hines CJ, Deddens JA, Lu C, Fenske R, Striley CA. Mixed-effect models for evaluating multiple measures of atrazine exposure among custom applicators. J Occup Environ Hyg 2006;3:274-83.

Hines RN, McCarver DG. The ontogeny of human drug-metabolizing enzymes: phase I oxidative enzymes. J Pharmacol Exp Ther 2002;300:355-60.

Hoebel BG, Avena NM, Rada P. An accumbens dopamine-acetylcholine system for approach and avoidance. In: A. J. Elliot, editor. Handbook of approach and avoidance motivation. New York: Taylor & Francis Group; 2008. p. 89-108.

Hoppin JA, Umbach DM, London SJ, Alavanja MC, Sandler DP. Chemical predictors of wheeze among farmer pesticide applicators in the Agricultural Health Study. Am J Respir Crit Care Med 2002;165:683-9.

Hossain MM, Filipov NM. Alteration of dopamine uptake into rat striatal vesicles and synaptosomes caused by an in vitro exposure to atrazine and some of its metabolites. Toxicology 2008;248:52-8.

Hotchkiss MG, Best DS, Cooper RL, Laws SC. Atrazine does not induce pica behavior at doses that increase hypothalamic-pituitary-adrenal axis activation and cause conditioned taste avoidance. Neurotoxicol Teratol 2012;34:295-302.

Hui X, Wester RC, Maibach HI. Pharmacokinetics of [^{14}C]-atrazine in rhesus monkeys, single-dose intravenous and oral administration. Toxicological & Environmental Chemistry 2011;93:370-82.

Imaoka S, Fujita S, Funae Y. Age-dependent expression of cytochrome P-450s in rat liver. Biochim Biophys Acta 1991;1097:187-92.

Islam MO, Hara M, Miyake J. Induction of P-glycoprotein, glutathione-S-transferase and cytochrome P450 in rat liver by atrazine. Environ Toxicol Pharmacol 2002;12:1-6.

Ito Y, Kimura T, Nam K, Katoh A, Masuzawa T, Kishida A. Effects of vibration on differentiation of cultured PC12 cells. Biotechnol Bioeng 2011;108:592-9.

Jablonowski ND, Koppchen S, Hofmann D, Schaffer A, Burauel P. Persistence of 14C-labeled atrazine and its residues in a field lysimeter soil after 22 years. Environ Pollut 2009;157:2126-31.

Jeyaratnam J. Acute pesticide poisoning: a major global health problem. World Health Stat Q 1990;43:139-44.

Jonsson ME, Orrego R, Woodin BR, Goldstone JV, Stegeman JJ. Basal and 3,3',4,4',5-pentachlorobiphenyl-induced expression of cytochrome P450 1A, 1B and 1C genes in zebrafish. Toxicol Appl Pharmacol 2007;221:29-41.

Joo H, Choi K, Hodgson E. Human metabolism of atrazine. Pesticide Biochem Physiol 2010;98:73-9.

Jurkowitz-Alexander MS, Altschuld RA, Hohl CM, Johnson JD, McDonald JS, Simmons TD, et al. Cell swelling, blebbing, and death are dependent on ATP depletion and independent of calcium during chemical hypoxia in a glial cell line (ROC-1). J Neurochem 1992;59:344-52.

Kamel F. Epidemiology. Paths from pesticides to Parkinson's. Science 2013;341:722-3.

Karrow NA, McCay JA, Brown RD, Musgrove DL, Guo TL, Germolec DR, et al. Oral exposure to atrazine modulates cell-mediated immune function and decreases host resistance to the B16F10 tumor model in female B6C3F1 mice. Toxicology 2005;209:15-28.

Kaune A, Brüggemann R, Kettrup A. High-performance liquid chromatographic measurement of the 1-octanol–water partition coefficient of s-triazine herbicides and some of their degradation products. J Chromatogr A 1998;805:119-26.

Kearns GL, Abdel-Rahman SM, Alander SW, Blowey DL, Leeder JS, Kauffman RE. Developmental pharmacology--drug disposition, action, and therapy in infants and children. N Engl J Med 2003;349:1157-67.

Kiely T, Donaldson D, Grube A. Pesticides industry sales and usage 2000 and 2001 market estimates. U.S. Environmental Protection Agency, Wanshington, DC. http://www.epa.gov/opp00001/pestsales/01pestsales/market_estimates2001.pdf. 2004. p. 1-33.

Kniewald J, Jakominic M, Tomljenovic A, Simic B, Romac P, Vranesic D, et al. Disorders of male rat reproductive tract under the influence of atrazine. J Appl Toxicol 2000;20:61-8.

Kobayashi T, Hayashi E, Shimamura M, Kinoshita M, Murphy NP. Neurochemical responses to antidepressants in the prefrontal cortex of mice and their efficacy in preclinical models of anxiety-like and depression-like behavior: a comparative and correlational study. Psychopharmacology (Berl) 2008;197:567-80.

Koh KH, Xie H, Yu AM, Jeong H. Altered cytochrome P450 expression in mice during pregnancy. Drug Metab Dispos 2011;39:165-9.

Kohno K, Kawakami T, Hiruma H. Effects of soluble laminin on organelle transport and neurite growth in cultured mouse dorsal root ganglion neurons: difference between primary neurites and branches. J Cell Physiol 2005;205:253-61.

Kolpin DW, Barbash JE, Gilliom RJ. Occurrence of pesticides in shallow groundwater of the United States: initial results from the National Water-Quality Assessment Program. Environ Sci Technol 1998;32:558-66.

Konradsen F. Acute pesticide poisoning--a global public health problem. Dan Med Bull 2007;54:58-9.

Kramer HJ, Drenth H, vandenBerg M, Seinen W, DeJongh J. Physiologically based pharmacokinetic model for tetrachlorobenzyltoluenes in rat: comparison of in vitro and in vivo metabolic rates. Toxicol Sci 2001;63:22-8.

Krutz LJ, Shaner DL, Zablotowicz RM. Enhanced degradation and soil depth effects on the fate of atrazine and major metabolites in Colorado and Mississippi soils. J Environ Qual 2010;39:1369-77.

Lang D, Criegee D, Grothusen A, Saalfrank RW, Bocker RH. In vitro metabolism of atrazine, terbuthylazine, ametryne, and terbutryne in rats, pigs, and humans. Drug Metab Dispos 1996;24:859-65.

Laws SC, Hotchkiss M, Ferrell J, Jayaraman S, Mills L, Modic W, et al. Chlorotriazine herbicides and metabolites activate an ACTH-dependent release of corticosterone in male Wistar rats. Toxicol Sci 2009;112:78-87.

Leavens TL, Borghoff SJ. Physiologically based pharmacokinetic model of methyl tertiary butyl ether and tertiary butyl alcohol dosimetry in male rats based on binding to alpha2u-globulin. Toxicol Sci 2009;109:321-35.

LeBaron HM, MacFarland JE, Burnside OC. The Triazine Herbicides 50 Years Revolutionizing Agriculture. Amsterdam: Elsevier; 2008. p. 1-44.

Lee SK, Chung SM, Lee MY, Lee JY, Bae ON, Chung JH. The roles of ATP and calcium in morphological changes and cytotoxicity induced by 1,4-benzoquinone in platelets. Biochim Biophys Acta 2002;1569:159-66.

Lee SK, Ou YC, Andersen ME, Yang RS. A physiologically based pharmacokinetic model for lactational transfer of PCB 153 with or without PCB 126 in mice. Arch Toxicol 2007;81:101-11.

Li Y, Li S, Wei C, Wang H, Sui N, Kirouac GJ. Changes in emotional behavior produced by orexin microinjections in the paraventricular nucleus of the thalamus. Pharmacol Biochem Behav 2010;95:121-8.

Lieb K, Andersen C, Lazarov N, Zienecker R, Urban I, Reisert I, et al. Pre- and postnatal development of dopaminergic neuron numbers in the male and female mouse midbrain. Brain Res Dev Brain Res 1996;94:37-43.

Lim S, Ahn SY, Song IC, Chung MH, Jang HC, Park KS, et al. Chronic exposure to the herbicide, atrazine, causes mitochondrial dysfunction and insulin resistance. PLoS One 2009;4:e5186.

Lin Z, Dodd CA, Filipov NM. Differentiation state-dependent effects of in vitro exposure to atrazine or its metabolite diaminochlorotriazine in a dopaminergic cell line. Life Sci 2013a;92:81-90.

Lin Z, Dodd CA, Filipov NM. Short-term atrazine exposure causes behavioral deficits and disrupts monoaminergic systems in male C57BL/6 mice. Neurotoxicol Teratol 2013b;39C:26-35.

Lin Z, Fisher JW, Ross MK, Filipov NM. A physiologically based pharmacokinetic model for atrazine and its main metabolites in the adult male C57BL/6 mouse. Toxicol Appl Pharmacol 2011;251:16-31.

Lin Z, Fisher JW, Wang R, Ross MK, Filipov NM. Estimation of placental and lactational transfer and tissue distribution of atrazine and its main metabolites in rodent dams, fetuses, and neonates with physiologically based pharmacokinetic modeling. Toxicol Appl Pharmacol 2013c;273:140-58.

Lipscomb JC, Fisher JW, Confer PD, Byczkowski JZ. In vitro to in vivo extrapolation for trichloroethylene metabolism in humans. Toxicol Appl Pharmacol 1998;152:376-87.

Litteljohn D, Mangano E, Shukla N, Hayley S. Interferon-gamma deficiency modifies the motor and co-morbid behavioral pathology and neurochemical changes provoked by the pesticide paraquat. Neuroscience 2009;164:1894-906.

Liu XM, Shao JZ, Xiang LX, Chen XY. Cytotoxic effects and apoptosis induction of atrazine in a grass carp (Ctenopharyngodon idellus) cell line. Environ Toxicol 2006;21:80-9.

Loccisano AE, Campbell JL, Jr., Butenhoff JL, Andersen ME, Clewell HJ, 3rd. Evaluation of placental and lactational pharmacokinetics of PFOA and PFOS in the pregnant, lactating, fetal and neonatal rat using a physiologically based pharmacokinetic model. Reprod Toxicol 2012;33:468-90.

Lotharius J, Brundin P. Pathogenesis of Parkinson's disease: dopamine, vesicles and alpha-synuclein. Nat Rev Neurosci 2002;3:932-42.

Lowe ER, Poet TS, Rick DL, Marty MS, Mattsson JL, Timchalk C, et al. The effect of plasma lipids on the pharmacokinetics of chlorpyrifos and the impact on interpretation of blood biomonitoring data. Toxicol Sci 2009;108:258-72.

Lozier MJ, Curwin B, Nishioka MG, Sanderson W. Determinants of atrazine contamination in the homes of commercial pesticide applicators across time. J Occup Environ Hyg 2012;9:289-97.

Lu C, Anderson LC, Morgan MS, Fenske RA. Salivary concentrations of atrazine reflect free atrazine plasma levels in rats. J Toxicol Environ Health A 1998;53:283-92.

Lu C, Holbrook CM, Andres LM. The implications of using a physiologically based pharmacokinetic (PBPK) model for pesticide risk assessment. Environ Health Perspect 2010;118:125-30.

Lu G, Abduljalil K, Jamei M, Johnson TN, Soltani H, Rostami-Hodjegan A. Physiologically-based Pharmacokinetic (PBPK) Models for Assessing the Kinetics of Xenobiotics during Pregnancy: Achievements and Shortcomings. Curr Drug Metab 2012;13:695-720.

Lucier GW, Lui EM, Lamartiniere CA. Metabolic activation/deactivation reactions during perinatal development. Environ Health Perspect 1979;29:7-16.

Lundholm K, Ekman L, Edstrom S, Karlberg I, Jagenburg R, Schersten T. Protein synthesis in liver tissue under the influence of a methylcholanthrene-induced sarcoma in mice. Cancer Res 1979;39:4657-61.

Magnelli L, Fibbi G, Caldini R, Pucci M, Del Rosso M. Inhibition of spontaneous growth and induced differentiation of murine erythroleukaemia cells by paraquat and atrazine. Food Chem Toxicol 1989;27:125-8.

Malkova NV, Yu CZ, Hsiao EY, Moore MJ, Patterson PH. Maternal immune activation yields offspring displaying mouse versions of the three core symptoms of autism. Brain Behav Immun 2012;26:607-16.

Martignoni M, Groothuis GM, de Kanter R. Species differences between mouse, rat, dog, monkey and human CYP-mediated drug metabolism, inhibition and induction. Expert Opin Drug Metab Toxicol 2006;2:875-94.

Matsuura K, Kabuto H, Makino H, Ogawa N. Pole test is a useful method for evaluating the mouse movement disorder caused by striatal dopamine depletion. J Neurosci Methods 1997;73:45-8.

McCarver DG, Hines RN. The ontogeny of human drug-metabolizing enzymes: phase II conjugation enzymes and regulatory mechanisms. J Pharmacol Exp Ther 2002;300:361-6.

McMullin TS, Andersen ME, Nagahara A, Lund TD, Pak T, Handa RJ, et al. Evidence that atrazine and diaminochlorotriazine inhibit the estrogen/progesterone induced surge of luteinizing hormone in female Sprague-Dawley rats without changing estrogen receptor action. Toxicol Sci 2004;79:278-86.

McMullin TS, Andersen ME, Tessari JD, Cranmer B, Hanneman WH. Estimating constants for metabolism of atrazine in freshly isolated rat hepatocytes by kinetic modeling. Toxicol In Vitro 2007a;21:492-501.

McMullin TS, Brzezicki JM, Cranmer BK, Tessari JD, Andersen ME. Pharmacokinetic modeling of disposition and time-course studies with [14C]atrazine. J Toxicol Environ Health A 2003;66:941-64.

McMullin TS, Hanneman WH, Cranmer BK, Tessari JD, Andersen ME. Oral absorption and oxidative metabolism of atrazine in rats evaluated by physiological modeling approaches. Toxicology 2007b;240:1-14.

Medinsky MA, Valentine JL. Toxicokinetics. In: C. D. Klaassen, editor. Casarett and Doull's Toxicology: The Basic Science of Poisons. sixth ed. New York: McGraw-Hill; 2001. p. 225-38.

Middlemore-Risher ML, Buccafusco JJ, Terry AV, Jr. Repeated exposures to low-level chlorpyrifos results in impairments in sustained attention and increased impulsivity in rats. Neurotoxicol Teratol 2010;32:415-24.

Miller G, Neilan M, Chia R, Gheryani N, Holt N, Charbit A, et al. ENU mutagenesis reveals a novel phenotype of reduced limb strength in mice lacking fibrillin 2. PLoS One 2010;5:e9137.

Mirfazaelian A, Fisher JW. Organ growth functions in maturing male Sprague-Dawley rats based on a collective database. J Toxicol Environ Health A 2007;70:1052-63.

Mirfazaelian A, Kim KB, Anand SS, Kim HJ, Tornero-Velez R, Bruckner JV, et al. Development of a physiologically based pharmacokinetic model for deltamethrin in the adult male Sprague-Dawley rat. Toxicol Sci 2006;93:432-42.

Mirfazaelian A, Kim KB, Lee S, Kim HJ, Bruckner JV, Fisher JW. Organ growth functions in maturing male Sprague-Dawley rats. J Toxicol Environ Health A 2007;70:429-38.

Montgomery KC. The relation between fear induced by novel stimulation and exploratory behavior. J Comp Physiol Psychol 1955;48:254-60.

Morley KC, Gallate JE, Hunt GE, Mallet PE, McGregor IS. Increased anxiety and impaired memory in rats 3 months after administration of 3,4-methylenedioxymethamphetamine ("ecstasy"). Eur J Pharmacol 2001;433:91-9.

Mosquin P, Whitmore RW, Chen W. Estimation of upper centile concentrations using historical atrazine monitoring data from community water systems. J Environ Qual 2012;41:834-44.

Munger R, Isacson P, Hu S, Burns T, Hanson J, Lynch CF, et al. Intrauterine growth retardation in Iowa communities with herbicide-contaminated drinking water supplies. Environ Health Perspect 1997;105:308-14.

N'Go P, Azzaoui F, Soro P, Samih M, Ahami A, Najimi M, et al. Developmental effects of malathion exposure on recognition memory and spatial learning in males Wistar rats. J Behav Brain Sci 2013;3:331-40.

Naismith DJ, Richardson DP, Pritchard AE. The utilization of protein and energy during lactation in the rat, with particular regard to the use of fat accumulated in pregnancy. Br J Nutr 1982;48:433-41.

Narotsky MG, Best DS, Guidici DL, Cooper RL. Strain comparisons of atrazine-induced pregnancy loss in the rat. Reprod Toxicol 2001;15:61-9.

Nelson AJ, Thur KE, Marsden CA, Cassaday HJ. Dissociable roles of dopamine within the core and medial shell of the nucleus accumbens in memory for objects and place. Behav Neurosci 2010;124:789-99.

NIH. Guide for the care and use of laboratory animals: eighth edition. National Research Council, Washington, D.C. 2011. p. 1-220.

Noble A. Partition coefficients (n-octanol—water) for pesticides. J Chromatogr A 1993;642:3-14.

Nowak P, Dabrowska J, Bortel A, Izabela B, Kostrzewa RM, Brus R. Prenatal cadmium and ethanol increase amphetamine-evoked dopamine release in rat striatum. Neurotoxicol Teratol 2006;28:563-72.

NTP. National Toxicology Program Report on the Immunotoxicity of Atrazine (CAS no. 1912-24-9) in Female B6C3F1 Mice (IMM94002). National Institute of Environmental Health Sciences, Research Triangle Park, NC. 1994.

O'Flaherty EJ, Scott W, Schreiner C, Beliles RP. A physiologically based kinetic model of rat and mouse gestation: disposition of a weak acid. Toxicol Appl Pharmacol 1992;112:245-56.

O'Shea M, Singh ME, McGregor IS, Mallet PE. Chronic cannabinoid exposure produces lasting memory impairment and increased anxiety in adolescent but not adult rats. J Psychopharmacol 2004;18:502-8.

Ochoa-Acuña H, Frankenberger J, Hahn L, Carbajo C. Drinking-water herbicide exposure in Indiana and prevalence of small-for-gestational-age and preterm delivery. Environ Health Perspect 2009;117:1619-24.

OECD-FAO. Organisation for Economic Co-operation and Development, Food and Agricultural Organization of the United Nations Agricultural Outlook, 2007-2016. OECD Publications, France, 87 pp. No. 8853.2007.

OECD. Organization for Economic Cooperation and Development (OECD) Guidelines for the Testing of Chemicals. Test No. 426: Developmental Neurotoxicity Study. OECD Environment Directorate, Paris, France. 2007.

Olson KL, Boush GM, Matsumura F. Pre- and postnatal exposure to dieldrin: Persistent stimulatory and behavioral effects. Pestic Biochem Physiol 1980;13:20-33.

Onishchenko N, Tamm C, Vahter M, Hokfelt T, Johnson JA, Johnson DA, et al. Developmental exposure to methylmercury alters learning and induces depression-like behavior in male mice. Toxicol Sci 2007;97:428-37.

Page ME, Brown K, Lucki I. Simultaneous analyses of the neurochemical and behavioral effects of the norepinephrine reuptake inhibitor reboxetine in a rat model of antidepressant action. Psychopharmacology (Berl) 2003;165:194-201.

Palanza P. Animal models of anxiety and depression: how are females different? Neurosci Biobehav Rev 2001;25:219-33.

Pang S, Duan L, Liu Z, Song X, Li X, Wang C. Co-Induction of a Glutathione-S-transferase, a Glutathione Transporter and an ABC Transporter in Maize by Xenobiotics. PLoS One 2012;7:e40712.

Parron T, Requena M, Hernandez AF, Alarcon R. Association between environmental exposure to pesticides and neurodegenerative diseases. Toxicol Appl Pharmacol 2011;256:379-85.

Peng J, Mao XO, Stevenson FF, Hsu M, Andersen JK. The herbicide paraquat induces dopaminergic nigral apoptosis through sustained activation of the JNK pathway. J Biol Chem 2004;279:32626-32.

Perez VP, de Lima MN, da Silva RS, Dornelles AS, Vedana G, Bogo MR, et al. Iron leads to memory impairment that is associated with a decrease in acetylcholinesterase pathways. Curr Neurovasc Res 2010;7:15-22.

Perona MT, Waters S, Hall FS, Sora I, Lesch KP, Murphy DL, et al. Animal models of depression in dopamine, serotonin, and norepinephrine transporter knockout mice: prominent effects of dopamine transporter deletions. Behav Pharmacol 2008;19:566-74.

Perrier D, Gibaldi M. General derivation of the equation for time to reach a certain fraction of steady state. J Pharm Sci 1982;71:474-5.

Petit-Demouliere B, Chenu F, Bourin M. Forced swimming test in mice: a review of antidepressant activity. Psychopharmacology (Berl) 2005;177:245-55.

Pinchuk LM, Lee SR, Filipov NM. In vitro atrazine exposure affects the phenotypic and functional maturation of dendritic cells. Toxicol Appl Pharmacol 2007;223:206-17.

Pogrmic-Majkic K, Kaisarevic S, Fa S, Dakic V, Glisic B, Hrubik J, et al. Atrazine effects on antioxidant status and xenobiotic metabolizing enzymes after oral administration in peripubertal male rat. Environ Toxicol Pharmacol 2012;34:495-501.

Pommery J, Mathieu M, Mathieu D, Lhermitte M. Atrazine in plasma and tissue following atrazine-aminotriazole-ethylene glycol-formaldehyde poisoning. J Toxicol Clin Toxicol 1993;31:323-31.

Poulin P, Krishnan K. An algorithm for predicting tissue: blood partition coefficients of organic chemicals from n-octanol: water partition coefficient data. J Toxicol Environ Health 1995;46:117-29.

Poulin P, Theil FP. A priori prediction of tissue:plasma partition coefficients of drugs to facilitate the use of physiologically-based pharmacokinetic models in drug discovery. J Pharm Sci 2000;89:16-35.

Poulsen MS, Rytting E, Mose T, Knudsen LE. Modeling placental transport: correlation of in vitro BeWo cell permeability and ex vivo human placental perfusion. Toxicol In Vitro 2009;23:1380-6.

Prakash N, Wurst W. Development of dopaminergic neurons in the mammalian brain. Cell Mol Life Sci 2006;63:187-206.

Prasad KN, Carvalho E, Kentroti S, Edwards-Prasad J, Freed C, Vernadakis A. Establishment and characterization of immortalized clonal cell lines from fetal rat mesencephalic tissue. In Vitro Cell Dev Biol Anim 1994;30A:596-603.

Prasad KN, Clarkson ED, La Rosa FG, Edwards-Prasad J, Freed CR. Efficacy of grafted immortalized dopamine neurons in an animal model of parkinsonism: a review. Mol Genet Metab 1998;65:1-9.

Preston AR, Eichenbaum H. Interplay of hippocampus and prefrontal cortex in memory. Curr Biol 2013;23:R764-73.

Prigione A, Fauler B, Lurz R, Lehrach H, Adjaye J. The senescence-related mitochondrial/oxidative stress pathway is repressed in human induced pluripotent stem cells. Stem Cells 2010;28:721-33.

Prouillac C, Lecoeur S. The role of the placenta in fetal exposure to xenobiotics: importance of membrane transporters and human models for transfer studies. Drug Metab Dispos 2010;38:1623-35.

Pruett SB, Fan R, Zheng Q, Myers LP, Hebert P. Modeling and predicting immunological effects of chemical stressors: characterization of a quantitative biomarker for immunological changes caused by atrazine and ethanol. Toxicol Sci 2003;75:343-54.

Pruett SB, Fan R, Zheng Q, Schwab C. Patterns of immunotoxicity associated with chronic as compared with acute exposure to chemical or physical stressors and their relevance with regard to the role of stress and with regard to immunotoxicity testing. Toxicol Sci 2009;109:265-75.

Pujol E, Proenza AM, Roca P, Llado I. Changes in mammary fat pad composition and lipolytic capacity throughout pregnancy. Cell Tissue Res 2006;323:505-11.

Ramos A, Mormede P. Stress and emotionality: a multidimensional and genetic approach. Neurosci Biobehav Rev 1998;22:33-57.

Rayner JL, Enoch RR, Fenton SE. Adverse effects of prenatal exposure to atrazine during a critical period of mammary gland growth. Toxicol Sci 2005;87:255-66.

Rayner JL, Wood C, Fenton SE. Exposure parameters necessary for delayed puberty and mammary gland development in Long-Evans rats exposed in utero to atrazine. Toxicol Appl Pharmacol 2004;195:23-34.

Ressler KJ, Nemeroff CB. Role of serotonergic and noradrenergic systems in the pathophysiology of depression and anxiety disorders. Depress Anxiety 2000;12 Suppl 1:2-19.

Ricceri L, Venerosi A, Capone F, Cometa MF, Lorenzini P, Fortuna S, et al. Developmental neurotoxicity of organophosphorous pesticides: fetal and neonatal exposure to chlorpyrifos alters sex-specific behaviors at adulthood in mice. Toxicol Sci 2006;93:105-13.

Rice D, Barone S, Jr. Critical periods of vulnerability for the developing nervous system: evidence from humans and animal models. Environ Health Perspect 2000;108 Suppl 3:511-33.

Rinsky JL, Hopenhayn C, Golla V, Browning S, Bush HM. Atrazine exposure in public drinking water and preterm birth. Public Health Rep 2012;127:72-80.

Rodriguez CE, Mahle DA, Gearhart JM, Mattie DR, Lipscomb JC, Cook RS, et al. Predicting age-appropriate pharmacokinetics of six volatile organic compounds in the rat utilizing physiologically based pharmacokinetic modeling. Toxicol Sci 2007a;98:43-56.

Rodriguez VM, Limon-Pacheco JH, Mendoza-Trejo MS, Gonzalez-Gallardo A, Hernandez-Plata I, Giordano M. Repeated exposure to the herbicide atrazine alters locomotor activity and the nigrostriatal dopaminergic system of the albino rat. Neurotoxicology 2013;34:82-94.

Rodriguez VM, Thiruchelvam M, Cory-Slechta DA. Sustained exposure to the widely used herbicide atrazine: altered function and loss of neurons in brain monoamine systems. Environ Health Perspect 2005;113:708-15.

Rodriguez VM, Thiruchelvam M, Kochar J, Cory-Slechta DA. Atrazine exposure causes alterations in the nigrostriatal and mesostriatal systems in the rat. The Toxicologist (Supplement to Toxicological Sciences) 2007b;188:910 [Abstract].

Roecker R, Junges GM, de Lima DD, Delwing F, Wyse ATS, Cruz JN, et al. Prolonged acetylcholinesterase inhibition and impairment in object recognition memory in rats subjected to chronic hyperprolinemia. Biol Med 2012;4:126-33.

Roffey SJ, Cole S, Comby P, Gibson D, Jezequel SG, Nedderman AN, et al. The disposition of voriconazole in mouse, rat, rabbit, guinea pig, dog, and human. Drug Metab Dispos 2003;31:731-41.

Rogers JM, Kavlock RJ. Developmental toxicology. In: C. D. Klaassen, editor. Casarett and Doull's Toxicology: The Basic Science of Poisons, 6th edition: McGraw-Hill Medical Publishing Division; 2001. p. 351-86.

Rooney AA, Matulka RA, Luebke RW. Developmental atrazine exposure suppresses immune function in male, but not female Sprague-Dawley rats. Toxicol Sci 2003;76:366-75.

Ross MK, Filipov NM. Determination of atrazine and its metabolites in mouse urine and plasma by LC-MS analysis. Anal Biochem 2006;351:161-73.

Ross MK, Jones TL, Filipov NM. Disposition of the herbicide 2-chloro-4-(ethylamino)-6-(isopropylamino)-s-triazine (Atrazine) and its major metabolites in mice: a liquid chromatography/mass spectrometry analysis of urine, plasma, and tissue levels. Drug Metab Dispos 2009;37:776-86.

Rosso P. Changes in the transfer of nutrients across the placenta during normal gestation in the rat. Am J Obstet Gynecol 1975;122:761-6.

Rosso P, Keyou G, Bassi JA, Slusser WM. Effect of malnutrition during pregnancy on the development of the mammary glands of rats. J Nutr 1981;111:1937-41.

Rousseaux S, Hartmann A, Soulas G. Isolation and characterisation of new Gram-negative and Gram-positive atrazine degrading bacteria from different French soils. FEMS Microbiol Ecol 2001;36:211-22.

Rowe AM, Brundage KM, Barnett JB. Developmental immunotoxicity of atrazine in rodents. Basic Clin Pharmacol Toxicol 2008;102:139-45.

Rowe AM, Brundage KM, Schafer R, Barnett JB. Immunomodulatory effects of maternal atrazine exposure on male Balb/c mice. Toxicol Appl Pharmacol 2006;214:69-77.

Royl G, Balkaya M, Lehmann S, Lehnardt S, Stohlmann K, Lindauer U, et al. Effects of the PDE5-inhibitor vardenafil in a mouse stroke model. Brain Res 2009;1265:148-57.

Salama AK, Bakry NM, Abou-Donia MB. A review article on placental transfer of pesticides. J Occup Med Toxicol 1993;2:383-97.

Saminathan H, Asaithambi A, Anantharam V, Kanthasamy AG, Kanthasamy A. Environmental neurotoxic pesticide dieldrin activates a non receptor tyrosine kinase to promote pkcdelta-mediated dopaminergic apoptosis in a dopaminergic neuronal cell model. Neurotoxicology 2011;32:567-77.

Sass JB, Colangelo A. European Union bans atrazine, while the United States negotiates continued use. Int J Occup Environ Health 2006;12:260-7.

Sasso AF, Georgopoulos PG, Isukapalli SS, Krishnan K. Bayesian Analysis of a Lipid-Based Physiologically Based Toxicokinetic Model for a Mixture of PCBs in Rats. J Toxicol 2012;2012:895391.

Satsuma K. Complete biodegradation of atrazine by a microbial community isolated from a naturally derived river ecosystem (microcosm). Chemosphere 2009;77:590-6.

Scheyer RD, Cramer JA, Mattson RH. A pharmacodynamic approach to the estimate of carbamazepine autoinduction. J Pharm Sci 1994;83:491-4.

Schneider H. Placental transport function. Reprod Fertil Dev 1991;3:345-53.

Schneider ML, Moore CF, Adkins MM. The effects of prenatal alcohol exposure on behavior: rodent and primate studies. Neuropsychol Rev 2011;21:186-203.

Schultz W. Multiple dopamine functions at different time courses. Annu Rev Neurosci 2007;30:259-88.

Seo SR, Seo JT. Calcium overload is essential for the acceleration of staurosporine-induced cell death following neuronal differentiation in PC12 cells. Exp Mol Med 2009;41:269-76.

Shaw G. New evidence for association of pesticides with Parkinson Disease. Neurology Today 2011;11:1,16-21.

Shetty AK, Burrows RC, Phillips DE. Alterations in neuronal development in the substantia nigra pars compacta following in utero ethanol exposure: immunohistochemical and Golgi studies. Neuroscience 1993;52:311-22.

Shibayama H, Kotera T, Shinoda Y, Hanada T, Kajihara T, Ueda M, et al. Collaborative work on evaluation of ovarian toxicity. 14) Two- or four-week repeated-dose studies and fertility study of atrazine in female rats. J Toxicol Sci 2009;34 Suppl 1:SP147-55.

Shirley B. The food intake of rats during pregnancy and lactation. Lab Anim Sci 1984;34:169-72.

Sik A, van Nieuwehuyzen P, Prickaerts J, Blokland A. Performance of different mouse strains in an object recognition task. Behav Brain Res 2003;147:49-54.

Sikov MR, Thomas JM. Prenatal growth of the rat. Growth 1970;34:1-14.

Simic B, Kniewald J, Kniewald Z. Effects of atrazine on reproductive performance in the rat. J Appl Toxicol 1994;14:401-4.

Singh M, Sandhir R, Kiran R. Effects on antioxidant status of liver following atrazine exposure and its attenuation by vitamin E. Exp Toxicol Pathol 2011;63:269-76.

Sinha J, Reyes SJ, Gallivan JP. Reprogramming bacteria to seek and destroy an herbicide. Nat Chem Biol 2010;6:464-70.

Sisk CL, Zehr JL. Pubertal hormones organize the adolescent brain and behavior. Front Neuroendocrinol 2005;26:163-74.

Slotkin TA, MacKillop EA, Ryde IT, Tate CA, Seidler FJ. Screening for developmental neurotoxicity using PC12 cells: comparisons of organophosphates with a carbamate, an organochlorine, and divalent nickel. Environ Health Perspect 2007;115:93-101.

Smidt MP, Smits SM, Burbach JP. Molecular mechanisms underlying midbrain dopamine neuron development and function. Eur J Pharmacol 2003;480:75-88.

Solari M, Paquin J, Ducharme P, Boily M. P19 neuronal differentiation and retinoic acid metabolism as criteria to investigate atrazine, nitrite, and nitrate developmental toxicity. Toxicol Sci 2010;113:116-26.

Speed HE, Blaiss CA, Kim A, Haws ME, Melvin NR, Jennings M, et al. Delayed reduction of hippocampal synaptic transmission and spines following exposure to repeated subclinical doses of organophosphorus pesticide in adult mice. Toxicol Sci 2012;125:196-208.

Squillace PJ, Scott JC, Moran MJ, Nolan BT, Kolpin DW. VOCs, pesticides, nitrate, and their mixtures in groundwater used for drinking water in the United States. Environ Sci Technol 2002;36:1923-30.

Staats DA, Fisher JW, Connolly RB. Gastrointestinal absorption of xenobiotics in physiologically based pharmacokinetic models. A two-compartment description. Drug Metab Dispos 1991;19:144-8.

Stoker TE, Cooper RL. Distribution of 14C-atrazine following an acute lactational exposure in the Wistar rat. Reprod Toxicol 2007;23:607-10.

Stoker TE, Laws SC, Guidici DL, Cooper RL. The effect of atrazine on puberty in male wistar rats: an evaluation in the protocol for the assessment of pubertal development and thyroid function. Toxicol Sci 2000;58:50-9.

Stranahan AM, Arumugam TV, Cutler RG, Lee K, Egan JM, Mattson MP. Diabetes impairs hippocampal function through glucocorticoid-mediated effects on new and mature neurons. Nat Neurosci 2008;11:309-17.

Stulcová B. Postnatal development of cardiac output distribution measured by radioactive microspheres in rats. Biol Neonate 1977;32:119-24.

Suckow MA, Danneman P, Brayton C. The Laboratory MOUSE, CRC Press, Boca Raton London New York Washington, D.C. 2001.

Swan SH. Semen quality in fertile US men in relation to geographical area and pesticide exposure. Int J Androl 2006;29:62-8; discussion 105-8.

Swan SH, Kruse RL, Liu F, Barr DB, Drobnis EZ, Redmon JB, et al. Semen quality in relation to biomarkers of pesticide exposure. Environ Health Perspect 2003;111:1478-84.

Sweeney LM, Gargas ML, Strother DE, Kedderis GL. Physiologically based pharmacokinetic model parameter estimation and sensitivity and variability analyses for acrylonitrile disposition in humans. Toxicol Sci 2003;71:27-40.

Tadeo JL. Analysis of pesticides in food and environmental samples, CRC Press, Boca Raton, FL. 2008. p. 151-318.

Tanner CM, Kamel F, Ross GW, Hoppin JA, Goldman SM, Korell M, et al. Rotenone, paraquat, and Parkinson's disease. Environ Health Perspect 2011;119:866-72.

Tanner CM, Ottman R, Goldman SM, Ellenberg J, Chan P, Mayeux R, et al. Parkinson disease in twins: an etiologic study. JAMA 1999;281:341-6.

Tattoli M, Cagiano R, Gaetani S, Ghiglieri V, Giustino A, Mereu G, et al. Neurofunctional effects of developmental alcohol exposure in alcohol-preferring and alcohol-nonpreferring rats. Neuropsychopharmacology 2001;24:691-705.

Taylor TN, Greene JG, Miller GW. Behavioral phenotyping of mouse models of Parkinson's disease. Behav Brain Res 2010;211:1-10.

Terry KK, Elswick BA, Welsch F, Conolly RB. Development of a physiologically based pharmacokinetic model describing 2-methoxyacetic acid disposition in the pregnant mouse. Toxicol Appl Pharmacol 1995;132:103-14.

Thiruchelvam M, Richfield EK, Baggs RB, Tank AW, Cory-Slechta DA. The nigrostriatal dopaminergic system as a preferential target of repeated exposures to combined paraquat and maneb: implications for Parkinson's disease. J Neurosci 2000;20:9207-14.

Thomas RS, Yang RS, Morgan DG, Moorman MP, Kermani HR, Sloane RA, et al. PBPK modeling/Monte Carlo simulation of methylene chloride kinetic changes in mice in relation to age and acute, subchronic, and chronic inhalation exposure. Environ Health Perspect 1996;104:858-65.

Timchalk C, Dryzga MD, Langvardt PW, Kastl PE, Osborne DW. Determination of the effect of tridiphane on the pharmacokinetics of [14C]-atrazine following oral administration to male Fischer 344 rats. Toxicology 1990;61:27-40.

Timchalk C, Kousba AA, Poet TS. An age-dependent physiologically based pharmacokinetic/pharmacodynamic model for the organophosphorus insecticide chlorpyrifos in the preweanling rat. Toxicol Sci 2007;98:348-65.

Timchalk C, Poet TS. Development of a physiologically based pharmacokinetic and pharmacodynamic model to determine dosimetry and cholinesterase inhibition for a binary mixture of chlorpyrifos and diazinon in the rat. Neurotoxicology 2008;29:428-43.

Timchalk C, Poet TS, Kousba AA. Age-dependent pharmacokinetic and pharmacodynamic response in preweanling rats following oral exposure to the organophosphorus insecticide chlorpyrifos. Toxicology 2006;220:13-25.

Tornero-Velez R, Mirfazaelian A, Kim KB, Anand SS, Kim HJ, Haines WT, et al. Evaluation of deltamethrin kinetics and dosimetry in the maturing rat using a PBPK model. Toxicol Appl Pharmacol 2010;

Tremblay RT, Kim D, Fisher JW. Determination of tissue to blood partition coefficients for nonvolatile herbicides, insecticides, and fungicides using negligible depletion solid-phase microextraction (nd-SPME) and ultrafiltration. J Toxicol Environ Health A 2012;75:288-98.

Trentacoste SV, Friedmann AS, Youker RT, Breckenridge CB, Zirkin BR. Atrazine effects on testosterone levels and androgen-dependent reproductive organs in peripubertal male rats. J Androl 2001;22:142-8.

Tsai CH, Lin PH, Troester MA, Rappaport SM. Formation and removal of pentachlorophenol-derived protein adducts in rodent liver under acute, multiple, and chronic dosing regimens. Toxicol Sci 2003;73:26-35.

Tseng HP, Hseu TH, Buhler DR, Wang WD, Hu CH. Constitutive and xenobiotics-induced expression of a novel CYP3A gene from zebrafish larva. Toxicol Appl Pharmacol 2005;205:247-58.

Ugazio G, Bosio A, Burdino E, Ghigo L, Nebbia C. Lethality, hexobarbital narcosis and behavior in rats exposed to atrazine, bentazon or molinate. Res Commun Chem Pathol Pharmacol 1991;74:349-61.

Vandenabeele P, Galluzzi L, Vanden Berghe T, Kroemer G. Molecular mechanisms of necroptosis: an ordered cellular explosion. Nat Rev Mol Cell Biol 2010;11:700-14.

Vander Heiden MG, Cantley LC, Thompson CB. Understanding the Warburg effect: the metabolic requirements of cell proliferation. Science 2009;324:1029-33.

Victor-Costa AB, Bandeira SM, Oliveira AG, Mahecha GA, Oliveira CA. Changes in testicular morphology and steroidogenesis in adult rats exposed to Atrazine. Reprod Toxicol 2010;

Vidair CA. Age dependence of organophosphate and carbamate neurotoxicity in the postnatal rat: extrapolation to the human. Toxicol Appl Pharmacol 2004;196:287-302.

Villanueva CM, Durand G, Coutte MB, Chevrier C, Cordier S. Atrazine in municipal drinking water and risk of low birth weight, preterm delivery, and small-for-gestational-age status. Occup Environ Med 2005;62:400-5.

Waehneldt TV, Shooter EM. A comparison of the protein composition of the brains of four rodents. Brain Res 1973;57:361-71.

Wallace M, Frankfurt M, Arellanos A, Inagaki T, Luine V. Impaired recognition memory and decreased prefrontal cortex spine density in aged female rats. Ann N Y Acad Sci 2007;1097:54-7.

Watanabe J, Asaka Y, Kanamura S. Postnatal development and sublobular distribution of cytochrome P-450 in rat liver: a microphotometric study. J Histochem Cytochem 1993;41:397-400.

Weber GJ, Sepulveda MS, Peterson SM, Lewis SS, Freeman JL. Transcriptome alterations following developmental atrazine exposure in zebrafish are associated with disruption of neuroendocrine and reproductive system function, cell cycle, and carcinogenesis. Toxicol Sci 2013;132:458-66.

Weiss B. Vulnerability of children and the developing brain to neurotoxic hazards. Environ Health Perspect 2000a;108 Suppl 3:375-81.

Weiss B. Vulnerability to pesticide neurotoxicity is a lifetime issue. Neurotoxicology 2000b;21:67-73.

Weiss JM, Goodman PA, Losito BG, Corrigan S, Charry JM, Bailey WH. Behavioral depression produced by an uncontrollable stressor: Relationship to norepinephrine, dopamine, and serotonin levels in various regions of rat brain. Brain Res Rev 1981;3:167-205.

West AP. Neurobehavioral studies of forced swimming: the role of learning and memory in the forced swim test. Prog Neuropsychopharmacol Biol Psychiatry 1990;14:863-77.

Wetzel LT, Luempert LG, 3rd, Breckenridge CB, Tisdel MO, Stevens JT, Thakur AK, et al. Chronic effects of atrazine on estrus and mammary tumor formation in female Sprague-Dawley and Fischer 344 rats. J Toxicol Environ Health 1994;43:169-82.

WHO. Characterization and application of physiologically based pharmacokinetic models in risk assessment. World Health Organization, Geneva, Switzerland. 2010. p. 21-37.

Whyatt RM, Barr DB, Camann DE, Kinney PL, Barr JR, Andrews HF, et al. Contemporary-use pesticides in personal air samples during pregnancy and blood samples at delivery among urban minority mothers and newborns. Environ Health Perspect 2003;111:749-56.

Win-Shwe TT, Nakajima D, Ahmed S, Fujimaki H. Impairment of novel object recognition in adulthood after neonatal exposure to diazinon. Arch Toxicol 2013;87:753-62.

Winneke G. Developmental aspects of environmental neurotoxicology: lessons from lead and polychlorinated biphenyls. J Neurol Sci 2011;308:9-15.

Woodruff TJ, Zota AR, Schwartz JM. Environmental chemicals in pregnant women in the United States: NHANES 2003-2004. Environ Health Perspect 2011;119:878-85.

Xing H, Han Y, Li S, Wang J, Wang X, Xu S. Alterations in mRNA expression of acetylcholinesterase in brain and muscle of common carp exposed to atrazine and chlorpyrifos. Ecotoxicol Environ Saf 2010a;73:1666-70.

Xing H, Li S, Wang Z, Gao X, Xu S, Wang X. Histopathological changes and antioxidant response in brain and kidney of common carp exposed to atrazine and chlorpyrifos. Chemosphere 2012;88:377-83.

Xing H, Wang J, Li J, Fan Z, Wang M, Xu S. Effects of atrazine and chlorpyrifos on acetylcholinesterase and carboxylesterase in brain and muscle of common carp. Environ Toxicol Pharmacol 2010b;30:26-30.

Xu RJ. Development of the newborn GI tract and its relation to colostrum/milk intake: a review. Reprod Fertil Dev 1996;8:35-48.

Yang D, Wang X, Chen YT, Deng R, Yan B. Pyrethroid insecticides: isoform-dependent hydrolysis, induction of cytochrome P450 3A4 and evidence on the involvement of the pregnane X receptor. Toxicol Appl Pharmacol 2009;237:49-58.

Yi LT, Li YC, Pan Y, Li JM, Xu Q, Mo SF, et al. Antidepressant-like effects of psoralidin isolated from the seeds of Psoralea Corylifolia in the forced swimming test in mice. Prog Neuropsychopharmacol Biol Psychiatry 2008;32:510-9.

Yoon M, Barton HA. Predicting maternal rat and pup exposures: how different are they? Toxicol Sci 2008;102:15-32.

Yoon M, Nong A, Clewell HJ, 3rd, Taylor MD, Dorman DC, Andersen ME. Evaluating placental transfer and tissue concentrations of manganese in the pregnant rat and fetuses after inhalation exposures with a PBPK model. Toxicol Sci 2009a;112:44-58.

Yoon M, Nong A, Clewell HJ, 3rd, Taylor MD, Dorman DC, Andersen ME. Lactational transfer of manganese in rats: predicting manganese tissue concentration in the dam and pups from inhalation exposure with a pharmacokinetic model. Toxicol Sci 2009b;112:23-43.

Yoon M, Schroeter JD, Nong A, Taylor MD, Dorman DC, Andersen ME, et al. Physiologically based pharmacokinetic modeling of fetal and neonatal manganese exposure in humans: describing manganese homeostasis during development. Toxicol Sci 2011;122:297-316.

Zaya RM, Amini Z, Whitaker AS, Ide CF. Exposure to atrazine affects the expression of key genes in metabolic pathways integral to energy homeostasis in Xenopus laevis tadpoles. Aquat Toxicol 2011;104:254-62.

Zhang J, Fitsanakis VA, Gu G, Jing D, Ao M, Amarnath V, et al. Manganese ethylene-bis-dithiocarbamate and selective dopaminergic neurodegeneration in rat: a link through mitochondrial dysfunction. J Neurochem 2003;84:336-46.

Zhang Y, Bhavnani BR. Glutamate-induced apoptosis in neuronal cells is mediated via caspase-dependent and independent mechanisms involving calpain and caspase-3 proteases as well as apoptosis inducing factor (AIF) and this process is inhibited by equine estrogens. BMC Neurosci 2006;7:49.

Zheng Q, Olivier K, Won YK, Pope CN. Comparative cholinergic neurotoxicity of oral chlorpyrifos exposures in preweanling and adult rats. Toxicol Sci 2000;55:124-32.

Zimmerman LJ, Valentine HL, Valentine WM. Characterization of S-(N,N-Dialkylaminocarbonyl)cysteine Adducts and Enzyme Inhibition Produced by Thiocarbamate Herbicides in the Rat. Chem Res Toxicol 2004;17:258-67.

Zvarova K, Zvara P. Urinary bladder function in conscious rat pups: a developmental study. Am J Physiol Renal Physiol 2012;302:F1563-8.

APPENDIX A

SUPPLEMENTARY DATA FOR CHAPTER 3

Table A1. Concentrations[a] of monoamines or their metabolites in the striatum of mice exposed to ATR (0-250 mg/kg) for 10 days.

Group	DOPAC	DOPAC/DA	3-MT	5-HT	5-HIAA/5-HT
Control	14.29 ± 0.94	0.07 ± 0.01	12.13 ± 0.61	2.70 ± 0.23	0.73 ± 0.04
5 mg/kg	15.24 ± 0.91	0.08 ± 0.01	12.14 ± 0.39	2.51 ± 0.28	0.75 ± 0.06
25 mg/kg	14.92 ± 0.84	0.08 ± 0.01	12.13 ± 0.37	2.55 ± 0.17	0.74 ± 0.04
125 mg/kg	16.93 ± 1.89	0.08 ± 0.01	12.73 ± 0.65	2.88 ± 0.14	1.02 ± 0.06
250 mg/kg	13.42 ± 0.50	0.06 ± 0.00	13.37 ± 0.36	3.09 ± 0.07	0.85 ± 0.04

[a] Data represent means ± SEM; unit: ng/mg protein. DA: dopamine; DOPAC: dihydroxyphenylacetic acid; 3-MT: 3-methoxytyramine; 5-HT: serotonin; 5-HIAA: 5-hydroxyindoleacetic acid.

Table A2. Concentrations[a] of monoamines and their metabolites in the prefrontal cortex and hippocampus of mice exposed to ATR (0-250 mg/kg) for 10 days.

Group	DA	DOPAC	HVA	5-HT	5-HIAA	NE	MHPG
Prefrontal cortex							
Control	0.81 ± 0.06	0.11 ± 0.01	0.37 ± 0.05	3.66 ± 0.23	1.33 ± 0.12	8.17 ± 0.28	1.70 ± 0.10
5 mg/kg	**1.16 ± 0.05***	0.16 ± 0.02	0.48 ± 0.05	3.53 ± 0.21	1.49 ± 0.06	8.66 ± 0.20	1.93 ± 0.24
25 mg/kg	0.91 ± 0.13	0.13 ± 0.02	0.38 ± 0.04	4.35 ± 0.39	1.44 ± 0.05	8.48 ± 0.45	1.91 ± 0.14
125 mg/kg	1.00 ± 0.08	**0.26 ± 0.04***	**1.06 ± 0.11***	4.03 ± 0.32	**1.85 ± 0.20***	**9.70 ± 0.43***	2.07 ± 0.11
250 mg/kg	0.82 ± 0.11	0.19 ± 0.04	**0.61 ± 0.08***	3.98 ± 0.51	1.48 ± 0.05	**9.26 ± 0.47***	2.05 ± 0.09
Hippocampus							
Control	0.87 ± 0.04	0.49 ± 0.07	0.31 ± 0.06	3.28 ± 0.53	2.78 ± 0.45	10.04 ± 1.34	1.47 ± 0.07
5 mg/kg	0.91 ± 0.06	0.51 ± 0.05	0.34 ± 0.05	3.30 ± 0.29	3.15 ± 0.25	10.27 ± 0.41	1.43 ± 0.14
25 mg/kg	0.94 ± 0.09	0.45 ± 0.02	0.30 ± 0.05	3.37 ± 0.44	2.94 ± 0.48	9.42 ± 0.88	1.58 ± 0.12
125 mg/kg	0.90 ± 0.05	0.51 ± 0.02	0.47 ± 0.08	3.32 ± 0.10	4.05 ± 0.38	10.27 ± 0.46	1.60 ± 0.12
250 mg/kg	0.89 ± 0.07	0.52 ± 0.03	0.36 ± 0.04	3.82 ± 0.27	3.71 ± 0.36	11.64 ± 0.73	**2.13 ± 0.08***

[a] Data represent means ± SEM; unit: ng/mg protein. DA: dopamine; DOPAC: dihydroxyphenylacetic acid; HVA: homovanillic acid; 5-HT: serotonin; 5-HIAA: 5-hydroxyindoleacetic acid; NE: norepinephrine; MHPG: 3-methoxy-4-hydroxyphenylglycol.

* Different from control group ($p \leq 0.05$).

APPENDIX B

SUPPLEMENTARY MATERIALS FOR CHAPTER 4

Supplementary data

Lists of abbreviations and key mass balance differential equations used in the model and the manuscript are presented below:

Chemical, compartment, and symbol abbreviations

Chemical abbreviations

ATR: atrazine

1: DE, desethyl atrazine

2: DIP, desisopropyl atrazine

3: DACT, didealkyl atrazine

Compartment abbreviations

L: liver, oxidative metabolism organ

BR: brain, a known target organ

K: kidney, main elimination organ

R: richly perfused tissue

S: slowly perfused tissue

Primary symbols

Rj: rate of change of chemicals in tissue j (μmol/h)

Aj: amount of chemicals in tissue j (μmol)

Cj: concentration of chemicals in tissue j (μM)

CVj: concentration of chemicals in vein of tissue j (μM)

Vj: volume of tissue j (l)

Qj: blood flow through tissue j (l/h)

Pj: tissue j plasma distribution/partition coefficient

Abbreviations used to represent parameters

Abbreviations for blood compartment

KaATRplasma: ATR and plasma protein (Albumin) second order association rate constant (/(h*μmol))

KdATRplasma: ATR-protein complex first order dissociation rate constant (h^{-1})

BMaxplasma: maximum binding capacity of ATR with plasma protein (μmol)

KaATRrbc: ATR and red blood cell (RBC) second order association rate constant (/(h*μmol))

KdATRrbc: ATR-RBC complex first order dissociation rate constant (h^{-1})

BMaxrbc: maximum binding capacity of ATR with RBC (μmol)

KaDACTplasma: DACT and plasma protein (Albumin) second order association rate constant (/(h*μmol))

KdDACTplasma: DACT-protein complex first order dissociation rate constant (h^{-1})

BMaxplasma3: maximum binding capacity of DACT with plasma protein (μmol)

KaDACTrbc: DACT and RBC second order association rate constant (/(h*μmol))

KdDACTrbc: DACT-RBC complex first order dissociation rate constant (h^{-1})

BMaxrbc3: maximum binding capacity of DACT with RBC (μmol)

Abbreviations for absorption

K1: gastric absorption rate constant (h^{-1})

K2: gastrointestinal (GI) transfer rate constant (h^{-1})

K3: intestinal absorption rate constant (h^{-1})

Abbreviations for metabolism

VmaxATR_DE: maximum rate of metabolism of ATR to DE in liver (μmol/h)

VmaxATR_DIP: maximum rate of metabolism of ATR to DIP in liver (μmol/h)

VmaxDEDACT: maximum rate of metabolism of DE to DACT in liver (μmol/h)

VmaxDIPDACT: maximum rate of metabolism of DIP to DACT in liver (μmol/h)

KmATR_DE: concentration of ATR at half the maximum rate of VmaxATR_DE (μmol/l)

KmATR_DIP: concentration of ATR at half the maximum rate of VmaxATR_DIP (μmol/l)

Km1: concentration of DE at half the maximum rate of VmaxDEDACT (μmol/l)

Km2: concentration of DIP at half the maximum rate of VmaxDIPDACT (μmol/l)

Abbreviations for elimination

Rurinei: elimination rate of DE, DIP or DACT through urine (μmol/h, i = 1, 2, or 3)

Aurinei: cumulative elimination amount of DE, DIP or DACT through urine (μmol, i = 1, 2, or 3)

Key differential equations

ATR sub-model

The rate of absorption of ATR from the lumen into the blood supply of the GI tract is described empirically using two-compartment model. The rates of change in the stomach and intestine are as follows:

RAST = -K2*AST-K1*AST ……...…(B1)

RAI = K2*AST-K3*AI……...(B2)

where AST and AI are the amount of ATR in stomach and intestine:

AST = Integ(RAST,Dose)……...(B3)

AI = Integ(RAI,0)……(B4)

The rate of absorption of ATR from the GI tract into the portal vein and then transported directly to the liver is:

RAO = K1*AST+K3*AI……..……(B5)

Blood compartment

The rate of change, amount and concentration of free ATR in the plasma:

RAPlasmaFree = QC*(CV - CPlasmaFree) +RARBCunbind-RARBCbind+ RAplasmaunbind-RAplasmabind……..…….(B6)

APlasmaFree = Integ(RAPlasmaFree,0.0)……..(B7)

CPlasmaFree = APlasmaFree/VPlasma……..(B8)

The rate of change, amount and concentration of plasma protein bound ATR in the blood:

RAPlasmabound = RAPlasmabind-RAPlasmaunbind……....(B9)

APlasmabound = Integ(RAPlasmabound,0)…….(B10)

CPlasmabound = APlasmabound/VPlasma……...(B11)

The rate of change, amount and concentration of RBC bound ATR in the blood:

RARBCbound = RARBCbind-RARBCunbind…….(B12)

ARBCbound = Integ(RARBCbound,0)……..…(B13)

CRBCbound = ARBCbound/VRBC…….(B14)

The amount and concentration of ATR in the blood:

Ablood = APlasmaFree + APlasmabound+ ARBCbound……..…(B15)

Cblood = Ablood/Vblood……..(B16)

The amount and concentration of ATR in the plasma:

Aplasma = APlasmaFree + APlasmabound……...(B17)

Cplasma = Aplasma/Vplasma……...(B18)

The rate of binding of plasma protein with ATR:

RAplasmabind = KaATRplasma*BMaxPlasmaRemain*AplasmaFree……(B19)

The rate of unbinding of plasma protein-ATR complex:

RAplasmaunbind = KdATRplasma*Aplasmabound…….(B20)

The rate of binding of RBC with ATR:

RARBCbind = KaATRrbc*BMaxRBCRemain*APlasmaFree…….(B21)

The rate of unbinding of RBC-ATR complex:

RARBCunbind = KdATRrbc*ARBCbound…….(B22)

The remaining maximum binding capacity of plasma protein with ATR:

BMaxPlasmaRemain = BMaxPlasma – Aplasmabound……...(B23)

The remaining maximum binding capacity of RBC with ATR:

BMaxRBCRemain = BMaxRBC – ARBCbound…….….(B24)

The concentration of ATR in the vein:

CV = (CVL*QL+CVBR*QBR+CVK*QK+CVS*QS+CVR*QR)/QC)……..(B25)

Liver compartment (All tissues are modeled as flow-limited compartments.)

RL = QL*(CPlasmaFree-CVL)+RAO-RATR_DEmet-RATR_DIPmet……...(B26)

AL = Integ(RL,0)……..……..…(B27)

CL = AL/VL……..(B28)

CVL = AL/(VL*PL)……..(B29)

Where RATR_DEmet and RATR_DIPmet correspond to oxidative metabolic rates of ATR to DE and DIP in liver:

RATR_DEmet = VmaxATR_DE*CVL/(KmATR_DE+CVL)…….(B30)

RATR_DIPmet = VmaxATR_DIP*CVL/(KmATR_DIP+CVL)…….(B31)

Brain compartment

RBR = QBR*(CPlasmaFree-CVBR)…….(B32)

ABR = Integ(RBR,0)…….(B33)

CBR = ABR/VBR…….(B34)

CVBR = ABR/(VBR*PBR)……..(B35)

For kidney, richly and slowly perfused tissue compartments, the differential equations are similar as those described the brain compartment with the letters ”K”, ”R” and ”S” substituting the letter “BR”, respectively.

DE sub-model

Blood compartment

CV1 = (CVL1*QL+CVBR1*QBR+CVR1*QR1+CVS1*QS)/QC)…….(B36)

Rblood1 = QC*(CV1-CA1)……..(B37)

Ablood1 = Integ(Rblood1,0)…….(B38)

CA1 = Ablood1/Vblood……(B39)

Liver compartment

RAL1 = QL*(CA1-CVL1)+RATR_DEmet-RDE_DACTmet……..….(B40)

AL1 = Integ(RAL1,0)……(B41)

CL1 = AL1/VL……..(B42)

CVL1 = AL1/(VL*PL1)……(B43)

Brain compartment

RABR1 = QBR*(CA1-CVBR1)……...(B44)

ABR1 = Integ(RABR1,0)……..(B45)

CBR1 = ABR1/VBR…….(B46)

CVBR1 = ABR1/(VBR*PBR1)……(B47)

For richly and slowly perfused tissue compartments, the differential equations are similar as those described the brain compartment with the letters ”R” and ”S” substituting the letter “BR”, respectively.

DIP sub-model

For DIP sub-model, the differential equations are the similar as DE’s sub-model with the number “2” substituting the number ”1”.

DACT sub-model

Blood compartment

Differential equations for DACT in the blood compartment are similar to those described the blood compartment in the ATR sub-model, with suffix “3” for each parameter to represent DACT.

Liver compartment

RL3 = QL*(CPlasmaFree3-CVL3)+RDE_DACTmet+RDIP_DACTmet……(B48)

AL3 = Integ(RL3,0)……...(B49)

CL3 = AL3/VL……..(B50)

CVL3 = AL3/(VL*PL3)……(B51)

Where RDE_DACTmet and RDIP_DACTmet correspond to oxidative metabolic rates of DE to DACT, and DIP to DACT in liver:

RDE_DACTmet = VmaxDEDACT*CVL1/(Km1+CVL1)……..(B52)

RDIP_DACTmet = VmaxDIPDACT*CVL2/(Km2+CVL2)……(B53)

Brain compartment

RBR3 = QBR*(CPlasmaFree3-CVBR3)……..(B54)

ABR3 = Integ(RBR3,0)…….(B55)

CBR3 = ABR3/VBR……..……(B56)

CVBR3 = ABR3/(VBR*PBR3)……(B57)

For kidney, richly and slowly perfused tissue compartments, the differential equations are similar as those described the brain compartment with the letters ”K”, ”R” and ”S” substituting the letter “BR”, respectively.

Conversion of the unit of metabolic rate constants from pmol/min/mg protein in Hanioka et al. (1999b) to µmol/h

Body weight of mice: 0.0253 kg (Ross et al., 2009)

Liver weight of mice: 0.0253 kg * 0.0549 = 1.38897 g (Brown et al., 1997)

The average amount of protein in the mouse liver is 192 mg protein /g wet liver weight (Lundholm et al., 1979).

Mouse liver protein weight: 1.38897 g * 192 mg protein /g = 266.68 mg liver protein

An example calculation is the ATR metabolism to DIP (Vmax = 805 pmol/min/mg protein):

805 pmol/min/mg protein * 60 mins * 266.68 liver protein/mouse = 12880644 pmol/h

12880644 pmol/h ÷ 1000000 = 12.88 µmol/h

Distribution coefficients (PCs)

Table B1. Distribution coefficients (PCs) for ATR and its Cl-TRIs in male C57BL/6 mice given four oral doses of ATR.

Distribution coefficient	250 mg/kg[a]	125 mg/kg	25 mg/kg	5 mg/kg[b]
ATR				
Liver	51.81	207.63	210.88	78.09
Brain	0.48	0.88	2.65	2.08
Kidney	14.79	65.89	106.48	125.36
DACT				
Liver	0.63	0.65	0.6	2.11
Brain	0.55	0.46	0.4	2.08
Kidney	0.29	0.38	0.58	1.83
DE				
Liver	1.89	1.21	5	5
DIP				
liver	0.42	0.82	2.13	6.4

[a] Distribution coefficients used in the development and evaluation of the mouse PBPK model for ATR. [b] Distribution coefficients used in the development of comparative simulations of the 5 mg/kg ATR dose kinetic behavior.

Comparisons of experimental and simulated AUCs of plasma concentrations of ATR and its Cl-TRIs

Table B2. Plasma concentration AUC for ATR and its Cl-TRIs in mice receiving four oral doses of ATR.

Compound	Dose (mg/kg)	Experimental result (h*μmol)	Simulated result (h*μmol)
ATR	250	10.27	11.08
	125	2.07	5.51
	25	0.57	1.1
	5[a]	0.69	0.28[a]
DE	250	38.53	22.77
	125	10.4	10.27
	25	2.03	1.91
	5[a]	0.92	0.47[a]
DIP	250	58.32	52.02
	125	13.32	19.33
	25	2.49	3.37
	5[a]	1.15	0.81[a]
DACT	250	1244.93	1376.96
	125	754.27	701.55
	25	144.29	142.52
	5[a]	18.46	38.37[a]

[a] By using 5 mg/kg-specific PCs based PBPK model, the plasma concentration AUCs for ATR, DE, DIP and DACT are 0.28, 0.49, 0.87, 33.35 h*μmol, respectively.

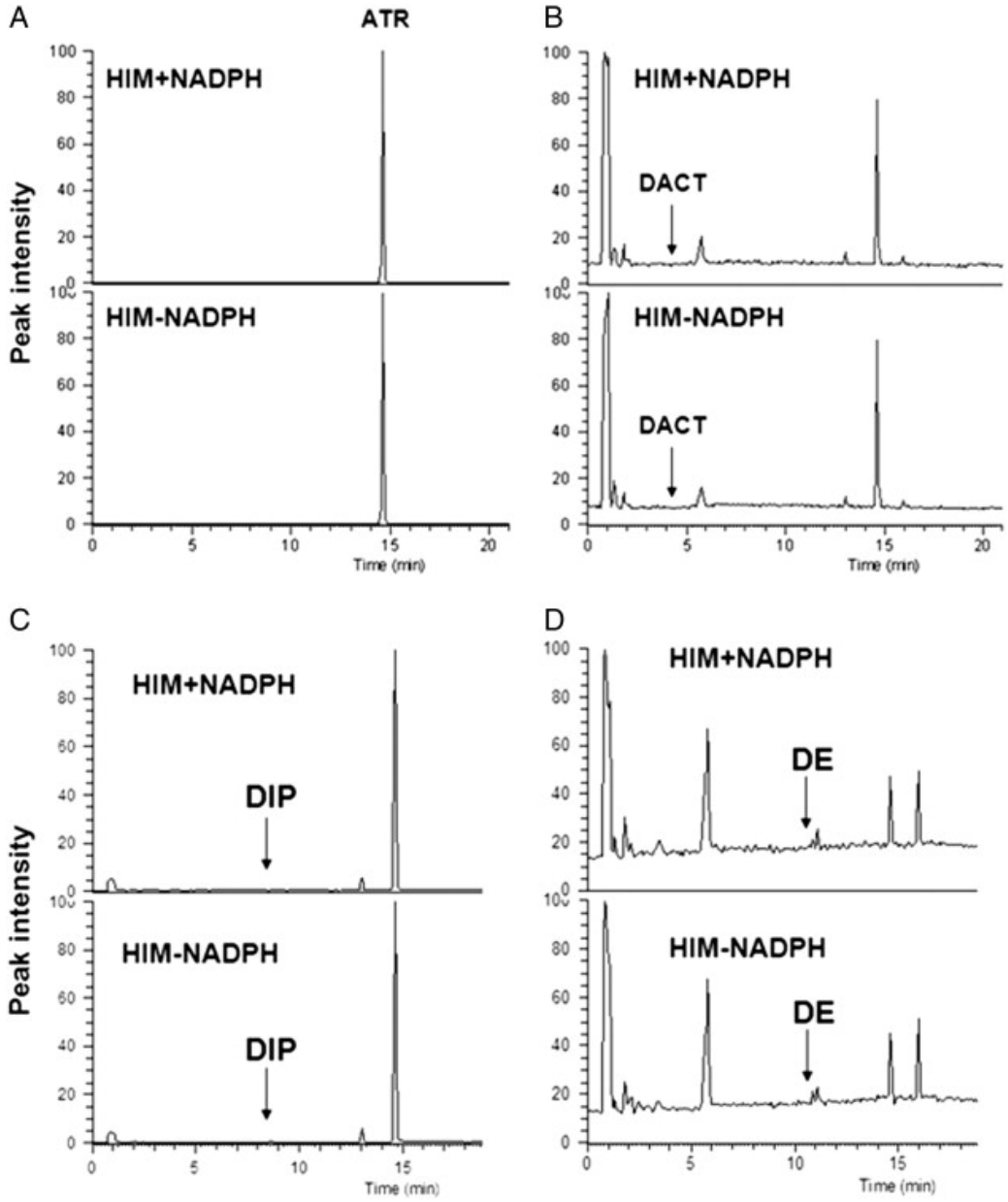

Figure B1. Lack of intestinal metabolism of atrazine (ATR). ATR was incubated with pooled human intestinal microsomes (HIM) ± NADPH in a total volume of 250 µl essentially as described previously for mouse liver microsomes (Ross and Filipov, 2006). No evidence for metabolism of ATR to DACT, DIP, or DE was observed in the LC-MS chromatograms, as evidenced from the lack of disappearance of ATR (A), or the production of DACT (B), DIP (C), and DE (D).

The PBPK model code (csl. file) for atrazine in adult male mice

```
PROGRAM
!September 16th,2009, to August 5th,2010
!ATR is metabolized to DE, DIP,
!DE and DIP are metabolized to DACT,
!Atrazine(ATR) is a 6 compartment model (blood, brain, liver, kidney, richly and slowly perfused tissues),
!Desethyl atrazine(DE) and desisopropyl atrazine(DIP) are 5 compartment models (brain, liver, richly and slowly perfused tissues)
!Didealkyl atrazine(DACT) is a 6 compartment model (blood, brain, liver, kidney, richly and slowly perfused tissues),
!All metabolites (DE, DIP and DACT) are excreted in urine.

        INITIAL
                ! code that is executed once at the beginning of a simulation run goes here
!Blood flow rate
CONSTANT QCC = 16.5!Cardiac output (L/h/kg0.75) (Brown et al., 1997, p. 454)
CONSTANT QLC = 0.161!Fraction of blood flow to liver (Brown et al., 1997, Table 23)
CONSTANT QBRC = 0.033!Fraction of blood flow to brain (Brown et al., 1997, Table 23)
CONSTANT QKC = 0.091!Fraction of blood flow to kidney (Brown et al., 1997, Table 23)

!Tissue volumes
CONSTANT BW = 0.0253!Body weight (kg) (Ross et al. 2009)
CONSTANT VLC = 0.0549!Fraction liver tissue (Brown et al., 1997, Table 4)
CONSTANT VBRC = 0.0165!Fraction brain tissue (Brown et al., 1997, Table 4)
CONSTANT VKC = 0.0167!Fraction kidney tissue (Brown et al., 1997, Table 4)
CONSTANT VbloodC = 0.049!Blood volume, fraction of BW (Brown et al., 1997, Table 21)

!Partition coefficients for ATR, unitless (All these PC values derive from area method at the highest dose - 250 mg/kg data.)
CONSTANT PL = 51.81!Liver:blood partition coefficient (caculated using area method)
CONSTANT PBR = 0.48!Brain:blood partition coefficient (caculated using area method)
CONSTANT PK =  14.15!Kidney:blood partition coefficient (caculated using area method)
CONSTANT PS = 0.48!Slowly perfused tissue:blood partition coefficient (set equal to brain)
CONSTANT PR = 51.81!Richly perfused tissue:blood partition coefficient (set equal to liver)
```

!Partition coefficients for DE, unitless (All these PC values derive from area method at the highest dose - 250 mg/kg data.)
CONSTANT PL1 = 1.89!Liver:blood partition coefficient (caculated using time point tissue plasma concentration ratio)
CONSTANT PBR1 = 0.48!Brain:blood partition coefficient (set equal to the PC of ATR in the brain)
CONSTANT PS1 = 0.48!Slowly perfused tissue:blood partition coefficient (set equal to brain)
CONSTANT PR1 = 1.89!Richly perfused tissue:blood partition coefficient (set equal to liver)

!Partition coefficients for DIP, unitless (All these PCs values derive from area method at the highest dose - 250 mg/kg data.)
CONSTANT PL2 = 0.42!Liver:blood partition coefficient (caculated using time point tissue plasma concentration ratio)
CONSTANT PBR2 = 0.48!Brain:blood partition coefficient (set equal to the PC of ATR in the brain)
CONSTANT PS2 = 0.48!Slowly perfused tissue:blood partition coefficient (set equal to brain)
CONSTANT PR2 = 0.42!Richly perfused tissue:blood partition coefficient (set equal to liver)

!Partition coefficients for DACT, unitless (All these PCs values derive from area method at the highest dose - 250 mg/kg data.)
CONSTANT PL3 = 0.63!Liver:blood partition coefficient (caculated using area method)
CONSTANT PBR3 = 0.55!Brain:blood partition coefficient (caculated using area method)
CONSTANT PK3 = 0.29!Kidney:blood partition coefficient (caculated using area method)
CONSTANT PS3 = 0.55!Slowly perfused tissue:blood partition coefficient (set equal to brain)
CONSTANT PR3 = 0.63!Richly perfused tissue:blood partition coefficient (set equal to liver)

!metabolic constants for ATR, ATR-->DE
!CONSTANT VmaxATR_DE = 8.86!4.43 umol/h Maximum velocity of metabolism of ATR to DE (umol/h) (Hanioka et al. 1999)
!(The in vitro value is 4.43. The present model uses 8.86. The in vivo metabolic rate is two fold of in vitro value, which is consistant with previous PBPK model of other compound. (Kramer et al., 2001)
CONSTANT VmaxcATR_DE = 139.667!69.83 Maximum velocity of metabolism of ATR to DE (umol/h/kg$^{0.75}$) (Hanioka et al. 1999) (Scalable to body weight)
CONSTANT KmATR_DE = 52.5!Michaelis-Menten constant (uM) (Hanioka et al. 1999)

!metabolic constants for ATR, ATR-->DIP
!CONSTANT VmaxATR_DIP = 25.76!12.88 Maximum velocity of metabolism of ATR to DIP (umol/h) (Hanioka et al. 1999)
!(The in vitro value is 12.88. The present model uses 25.76. The in vivo metabolic rate is two fold of in vitro value, which is consistant with previous PBPK model of other compound. (Kramer et al., 2001)

CONSTANT VmaxcATR_DIP = 406.074!203.04 Maximum velocity of metabolism of ATR to DIP (umol/h/kg$^{0.75}$) (Hanioka et al. 1999) (Scalable to body weight)
CONSTANT KmATR_DIP = 29.5! Michaelis-Menten constant (umol/l) (Hanioka et al. 1999)

!metabolic constants for DE-->DACT
CONSTANT Vmaxc1 = 14!6.598!39.598 Maximum velocity of metabolism of DE to DACT (umol/h/kg$^{0.75}$) (estimated)
CONSTANT Km1 = 13 !Michaelis-Menten constant (umol/l) (McMullin et al. 2007) (assume same as rat value)

!metabolic constants for DIP-->DACT
CONSTANT Vmaxc2 = 42!75.539 Maximum velocity of metabolism of DIP to DACT (umol/h/kg$^{0.75}$) (estimated)
CONSTANT Km2 = 13 !Michaelis-Menten constant (umol/l) (McMullin et al. 2007) (assume same as rat value)

!Plasma protein binding (approximately 26% (18% - 37%)) ATR bound to plasma protein
! Based on McMullin et al., 2003, 1.5% of total chlorotriazine was bound to red blood cells.
! We can figure out the amount of ATR-RBC complex, DACT-RBC complex, the concentration of DACT/ATR bound to RBC.
! The maximum binding capacity of DACT was ten fold to the calculated DACT-RBC complex concentration.
! The maximum binding capacity of ATR was ten fold to the calculated ATR-RBC complex.
! All the dissociation rate constants were assumed to be 1.
! The association rates were estimated by manually adjusting to meet the criteria that 26% of ATR/DACT bound to plasma protein and
! The simulated concentration of ATR-RBC or DACT-RBC is close to calculated concentration.

CONSTANT KaATRplasma = 180! ATR and plasma protein (Albumin) second order association rate constant, (/(umol*h)) (estimated)
CONSTANT KdATRplasma = 1! ATR-plasma protein complex first order dissociation rate constant, (/h) (fixed)
CONSTANT BMaxplasmac = 2.79!umol, maximal binding capacity of ATR with plasma protein (assumed, highest concentration of plasma ATR observed at the highest dose group - 250 mg/kg)

CONSTANT KaATRrbc = 720!ATR and RBC second order association rate constant, (/(umol*h)) (estimated)
CONSTANT KdATRrbc = 1! ATR-RBC complex first order dissociation rate constant, (/h) (fixed)
CONSTANT BMaxrbcc = 59!umol, maximum binding capacity of ATR with RBC (set to ten fold to the caculated concentration, round up to integer)

CONSTANT KaDACTplasma = 5!DACT and plasma protein (Albumin) second order association rate constant, (/(umol*h)) (estimated)
CONSTANT KdDACTplasma = 1!DACT-plasma protein complex first order dissociation rate constant, (/h) (fixed)
CONSTANT BMaxplasmac3 = 109.755!umol, maximum binding capacity of DACT with plasma protein (assumed, highest concentration of plasma DACT observed at the highest dose group - 250 mg/kg)

CONSTANT KaDACTrbc = 5!DACT and RBC second order association rate constant, (/(umol*h)) (estimated)
CONSTANT KdDACTrbc = 1! DACT-RBC complex first order dissociation rate constant, (/h) (fixed)
CONSTANT BMaxrbcc3 = 8439!umol, maximum binding capacity of DACT with RBC (set to ten fold to the caculated concentration, round up to integer)

! elimination constants
CONSTANT Kurine1 = 3 ! first order urinary elimination rate constant for DE (/hr) (estimated)
CONSTANT Kurine2 = 1.5 ! first order urinary elimination rate constant for DIP (/hr) (estimated)
CONSTANT Kurine3 = 20 ! first order urinary elimination rate constant for DACT (/hr) (estimated)

!Unit conversion from mg ATR to umol ATR: 1 mg = 4.64 umol
!1 mg=1000 ug;
!1000 ug/215.93 g/mol=4.64 umol;
!1 mg=4.64 umol
CONSTANT MWATR1 = 4.64 !Molecular weight of ATR (umol/mg)

CONSTANT PDose = 250 !oral dose (mg/kg)

! Oral absorption rate constant
CONSTANT K1 = 0.14!(Gastric absorption rate constant,estimated) (/h)
CONSTANT K2 = 1!(GI transfer rate constant,estimated) (/h)
CONSTANT K3 = 0.01!(Intestinal absorption rate constant,estimated) (/h)

```
!Scaled parameters
! Cardiac output and regional blood flow
QC = QCC*BW**0.75
QL = QLC*QC
QBR = QBRC*QC
QK = QKC*QC
QS = 0.24*QC-QBR
QR = 0.76*QC-QL-QK!(for ATR and DACT sub-models)
QR1 = 0.76*QC-QL!(for DE and DIP sub-models)

! Tissue volumes
VL = VLC*BW
VBR = VBRC*BW
VK = VKC*BW
VS = 0.82*BW-VBR
VR = 0.09*BW-VL-VK
VR1 = 0.09*BW-VL
Vblood = VbloodC*BW
Vplasma = VbloodC*BW*0.582 ! volume of plasma
Vrbc = VbloodC*BW*0.418 !(volume of RBC)

! Dosing
Dose = PDose*BW*MWATR1  !(umol)

!Metabolic parameters
VmaxATR_DE=VmaxcATR_DE*BW**0.75 !(umol/h)
VmaxATR_DIP=VmaxcATR_DIP*BW**0.75 !(umol/h)
VmaxDEDACT=Vmaxc1*BW**0.75 !(umol/h)
VmaxDIPDACT=Vmaxc2*BW**0.75 !(umol/h)
```

```
!plasma protein binding parameter
BMaxplasma = BMaxplasmac*Vplasma !Maximum binding capacity of ATR with plasma protein, umol
BMaxrbc = BMaxrbcc*VbloodC*BW*0.418 !Maximum binding capacity of ATR with RBC, umol

BMaxplasma3 = BMaxplasmac3*Vplasma !Maximum binding capacity of DACT with plasma protein, umol
BMaxrbc3 = BMaxrbcc3*VbloodC*BW*0.418 !Maximum binding capacity of DACT with RBC, umol

        END ! INITIAL

        DYNAMIC
                ALGORITHM IALG = 2
                NSTEPS    NSTP = 10
                MAXTERVAL MAXT = 1.0e9
                MINTERVAL MINT = 1.0e-9
                CINTERVAL CINT = 0.1

                DERIVATIVE

! ATR uptake from stomach to liver through
RAST = -K2*AST-K1*AST
AST = Integ(RAST,Dose)!(umol)
RAI = K2*AST-K3*AI
AI = Integ(RAI,0)
RAO = K1*AST+K3*AI
AAO = Integ(RAO,0)

!**************Model for ATR****************

!ATR in blood

RAPlasmaFree = QC*(CV - CPlasmaFree) +RARBCunbind-RARBCbind+ RAplasmaunbind-RAplasmabind
APlasmaFree = Integ(RAPlasmaFree,0.0)
```

```
CPlasmaFree = APlasmaFree/VPlasma
RAPlasmabound = RAPlasmabind-RAPlasmaunbind
APlasmabound = Integ(RAPlasmabound,0)
CPlasmabound = APlasmabound/VPlasma

RARBCbound = RARBCbind-RARBCunbind
ARBCbound = Integ(RARBCbound,0)
CRBCbound = ARBCbound/VRBC
Ablood = APlasmaFree + APlasmabound+ ARBCbound
Cblood = Ablood/Vblood
Aplasma = APlasmaFree + APlasmabound
Cplasma = Aplasma/Vplasma
AUCCplasma = Integ(Cplasma,0)


RAplasmabind = KaATRplasma*BMaxPlasmaRemain*AplasmaFree
RAplasmaunbind = KdATRplasma*Aplasmabound
RARBCbind = KaATRrbc*BMaxRBCRemain*APlasmaFree
RARBCunbind = KdATRrbc*ARBCbound

BMaxPlasmaRemain = BMaxPlasma - APlasmabound
BMaxRBCRemain = BMaxRBC - ARBCbound

CV = ((CVL*QL+CVBR*QBR+CVK*QK+CVS*QS+CVR*QR)/QC)

! Liver compartment
RL = QL*(CPlasmaFree-CVL)+RAO-RATR_DEmet-RATR_DIPmet
AL = Integ(RL,0)
CL = AL/VL
CVL = AL/(VL*PL)
```

```
!metabolism of ATR
RATR_DEmet = VmaxATR_DE*CVL/(KmATR_DE+CVL) !rate of metabolism of ATR to DE
AATR_DEmet = Integ(RATR_DEmet,0)
RATR_DIPmet = VmaxATR_DIP*CVL/(KmATR_DIP+CVL) !rate of metabolism of ATR to DIP
AATR_DIPmet = Integ(RATR_DIPmet,0)
AATRmet = AATR_DEmet+AATR_DIPmet !amount of ATR metabolized(umol)

! Brain compartment

RBR = QBR*(CPlasmaFree-CVBR)
ABR = Integ(RBR,0)
CBR = ABR/VBR
CVBR = ABR/(VBR*PBR)
AUCCBR = Integ(CBR,0)

! Kidney compartment

RK = QK*(CPlasmaFree-CVK)
AK = Integ(RK,0.0)
CK = AK/VK
CVK = AK/(VK*PK)

!Rapidly perfused tissue

RR = QR*(CPlasmaFree-CVR)
AR = Integ(RR,0)
CR = AR/VR
CVR = AR/(VR*PR)

!Slowly perfused tissue
RS = QS*(CPlasmaFree-CVS)
AS = Integ(RS,0)
```

```
CS = AS/VS
CVS = AS/(VS*PS)

QbalATR = QC-QL-QR-QK-QBR-QS


!Mass balance
!TMASS = MASS balance (umol)
TMASS = Ablood+AL+AK+ABR+AS+AR+AATR_DEmet+AATR_DIPmet
BALATR= AAO-TMASS

!**********Submodel for DE**************************************
! DE in blood
CV1 = ((CVL1*QL+CVBR1*QBR+CVR1*QR1+CVS1*QS)/QC)
Rblood1 = QC*(CV1-CA1)
Ablood1 = Integ(Rblood1,0)
CA1 = Ablood1/Vblood

! DE in the liver
! AL1 = Amount of DE in the liver (umol)
RAL1 = QL*(CA1-CVL1)+RATR_DEmet-RDE_DACTmet
AL1 = Integ(RAL1,0) !amount of DE in the liver
CL1 = AL1/VL ! concentration of DE in the liver, uM
CVL1 = AL1/(VL*PL1)!concentration of DE in venous liver blood, uM

! metabolism of DE in the liver
RDE_DACTmet = VmaxDEDACT*CVL1/(Km1+CVL1) !rate of metabolism of DE to DACT in the liver
ADE_DACTmet = Integ(RDE_DACTmet,0)

!DE in the brain
RABR1 = QBR*(CA1-CVBR1)
ABR1 = Integ(RABR1,0)
```

```
CBR1 = ABR1/VBR
CVBR1 = ABR1/(VBR*PBR1)

!DE in the richly perfused tissue
!AR1 = Amount of DE in richly perfused tissue
RAR1 = QR1*(CA1-CVR1)-Rurine1
AR1 = Integ(RAR1,0)
CR1 = AR1/VR1
CVR1 = AR1/(VR1*PR1)

! urinary excretion of DE
Rurine1 = Kurine1*CVR1*VR1
Aurine1 = Integ(Rurine1,0)

! DE in the slowly perfused tissue
!AS1 = Amount of DE in slowly perfused tissue
RAS1 = QS*(CA1-CVS1)
AS1 = Integ(RAS1,0)
CS1 = AS1/VS
CVS1 = AS1/(VS*PS1)

QbalDE = QC-QL-QR1-QBR-QS

! Mass balance of DE
! TMASS1 = mass balance of DE (umol)
TMASS1 = Ablood1 + AL1 + ABR1 + AR1 + AS1 + ADE_DACTmet+Aurine1
BALDE = AATR_DEmet- TMASS1

!********************Submodel for DIP*****************************
! DIP in the blood
CV2 = ((CVL2*QL+CVBR2*QBR+CVS2*QS+CVR2*QR1)/QC)
Rblood2 = QC*(CV2-CA2)
```

```
Ablood2 = Integ(Rblood2,0)
CA2 = Ablood2/Vblood


! DIP in the liver
!AL2 =  Amount of DIP in the liver tissue (umol)
RAL2 = QL*(CA2-CVL2)+RATR_DIPmet-RDIP_DACTmet
AL2 = Integ(RAL2,0)
CL2 = AL2/VL
CVL2 = AL2/(VL*PL2)

! metabolism of DIP
RDIP_DACTmet = VmaxDIPDACT*CVL2/(Km2+CVL2)
ADIP_DACTmet = Integ(RDIP_DACTmet,0)

! DIP in the brain tissue
! ABR2 = Amount of DIP in the brain tissue
RABR2 = QBR*(CA2-CVBR2)
ABR2 = Integ(RABR2,0)
CBR2 = ABR2/VBR
CVBR2 = ABR2/(VBR*PBR2)

! DIP in the richly perfused tissue
!AR2 = Amount of DIP in the richly perfused tissue
RAR2 = QR1*(CA2-CVR2)-Rurine2
AR2 = Integ(RAR2,0)
CR2 = AR2/VR1
CVR2 = AR2/(VR1*PR2)

! urinary excretion of DIP
Rurine2 = Kurine2*CVR2*VR1
Aurine2 = Integ(Rurine2,0)
```

```
! DIP in the slowly perfused tissue
! AS2 = Amount of DIP in the slowly perfused tissue
RAS2 = QS*(CA2-CVS2)
AS2 = Integ(RAS2,0)
CS2 = AS2/VS
CVS2 = AS2/(VS*PS2)

QbalDIP= QC-QL-QR1-QBR-QS

! Mass balance
! TMASS2 = MASS balance of DIP (umol)
TMASS2 = Ablood2+AL2+ABR2+AS2+AR2+ADIP_DACTmet+Aurine2
BALDIP = AATR_DIPmet - TMASS2

!**********submodel for DACT**********

! DACT in the blood
RAPlasmaFree3 = QC*(CV3 - CPlasmaFree3) +RARBCunbind3-RARBCbind3+ RAplasmaunbind3-RAplasmabind3
APlasmaFree3 = Integ(RAPlasmaFree3,0.0)
CPlasmaFree3 = APlasmaFree3/VPlasma

RAPlasmabound3= RAPlasmabind3-RAPlasmaunbind3
APlasmabound3 = Integ(RAPlasmabound3,0)
CPlasmabound3 = APlasmabound3/VPlasma

RARBCbound3 = RARBCbind3-RARBCunbind3
ARBCbound3 = Integ(RARBCbound3,0)
CRBCbound3 = ARBCbound3/VRBC

Ablood3 = APlasmaFree3 + APlasmabound3+ ARBCbound3
Cblood3 = Ablood3/Vblood
```

```
Aplasma3 = APlasmaFree3 + APlasmabound3
Cplasma3 = Aplasma3/Vplasma
AUCCplasma3 = Integ(Cplasma3,0)

RAplasmabind3 = KaDACTplasma*BMaxPlasmaRemain3*APlasmaFree3
RAplasmaunbind3 = KdDACTplasma*Aplasmabound3
RARBCbind3 = KaDACTrbc*BMaxRBCRemain3*APlasmaFree3
RARBCunbind3 = KdDACTrbc*ARBCbound3


BMaxPlasmaRemain3 = BMaxPlasma3 - APlasmabound3
BMaxRBCRemain3 = BMaxRBC3 - ARBCbound3

CV3 = ((CVL3*QL+CVBR3*QBR+CVK3*QK+CVS3*QS+CVR3*QR)/QC)

! DACT in the liver

RL3 = QL*(CPlasmaFree3-CVL3)+RDE_DACTmet+RDIP_DACTmet!
AL3 = Integ(RL3,0)
CL3 = AL3/VL
CVL3 = AL3/(VL*PL3)

! Brain compartment

RBR3 = QBR*(CPlasmaFree3-CVBR3)
ABR3 = Integ(RBR3,0)
CBR3 = ABR3/VBR
CVBR3 = ABR3/(VBR*PBR3)
AUCCBR3 = Integ(CBR3,0)
```

```
! DACT in the richly perfused tissue
RR3 = QR*(CPlasmaFree3-CVR3)
AR3 = Integ(RR3,0)
CR3 = AR3/VR
CVR3 = AR3/(VR*PR3)

! DACT in the slowly perfused tissue

RS3 = QS*(CPlasmaFree3-CVS3)
AS3 = Integ(RS3,0)
CS3 = AS3/VS
CVS3 = AS3/(VS*PS3)

! Kidney compartment

RK3 = QK*(CPlasmaFree3-CVK3)-Rurine3
AK3 = Integ(RK3,0.0)
CK3 = AK3/VK
CVK3 = AK3/(VK*PK3)
! urinary excretion of DACT
Rurine3 = Kurine3*CVK3*VK
Aurine3 = Integ(Rurine3,0)

QbalDACT = QC-QL-QR-QK-QBR-QS

! Mass balance of DACT
! TMASS3 = mass balance of DACT (umol)
TMASS3 = Ablood3+AL3+ABR3+AR3+AS3+AK3+Aurine3
BALDACT = ADE_DACTmet+ADIP_DACTmet-TMASS3

                END ! DERIVATIVE
```

```
            ! Add discrete events here as needed
            !  DISCRETE
            !  END
            ! code that is executed once at each communication interval goes here

            CONSTANT TSTOP = 24.0
            TERMT (T .GE. TSTOP, 'checked on communication interval: REACHED TSTOP')

        END ! DYNAMIC
        TERMINAL
            ! code that is executed once at the end of a simulation run goes here
        END ! TERMINAL
END ! PROGRAM
```

APPENDIX C

SUPPLEMENTARY MATERIALS FOR CHAPTER 5

Supplementary data

Sensitivity analysis

Sensitivity analysis-methods

A normalized sensitivity analysis was performed (based on a 5 mg/kg exposure dose) to identify critical model parameters by examining the influences of each model parameter on key dose metrics of interest: maternal plasma/maternal brain/placental/fetal ATR and DACT concentration AUCs from GD14–20 (gestational model) or milk ATR/DACT and neonatal plasma/brain DACT concentration AUCs from PND0-10 (lactational model). Each parameter was examined separately. The normalized sensitivity coefficient (NSC) was calculated using the following equation (Yoon et al., 2009a; Loccisano et al., 2012):

$$NSC = \Delta r/r * p/\Delta p \quad \text{(C1)}$$

where p is the original parameter value, Δp is 1% percent of the original parameter value, r is the dose metric derived from the original parameter value, and Δr is the change of the dose metric value resulting from 1% increase in the parameter value. For parameters describing the growth or changes during gestation/lactation, a 1% increase in the parameter was calculated using the following equation:

$$\Delta p = 0.01 * \text{original growth equation} \quad \text{(C2)}$$

where original growth equation is the equation used to describe the growth or changes during the simulation time. The relative impact of each model parameter on the dose metrics of interest was

classified as: low: |NSC|<0.2; medium: 0.2≤|NSC|<0.5; high: 0.5≤|NSC| (Yoon et al., 2009a; Lin et al., 2011).

Sensitivity analysis-results

The results for NSCs of model parameters are presented in Tables C15 (gestational model) and C16 (lactational model). Only moderately and highly sensitive parameters were reported (|NSC|≥ 0.2). In the gestational model, bidirectional placental transfer and fetus PC parameters of ATR and DACT had high impacts on their respective fetal dose metrics. All ATR related dose metrics were highly sensitive to the metabolic rate parameters from ATR to DIP, while all DACT associated dose metrics were highly sensitive to maternal plasma volume and urine elimination rate constant of DACT. The maternal brain or placenta PC parameters of ATR and DACT had high influences on their respective dose metrics in the maternal brain or placenta. The intestinal absorption rate constant had moderate influence on all selected dose metrics. The maternal plasma ATR, maternal brain ATR and maternal plasma DACT AUCs were all moderately sensitive to their respective protein binding parameters.

In the lactational model, neonatal BW had high impact on all selected dose metrics, and milk clearance rate parameters of ATR and DACT had high influences on their respective dose metrics. In addition, neonatal plasma and brain DACT AUCs were both highly sensitive to fractional absorption, plasma volumes and DACT's urine elimination rates of the dam and the neonate. Milk ATR AUC was highly sensitive to maternal BW and metabolic rate parameters from ATR to DIP, whereas milk DACT AUC was highly sensitive to maternal plasma volume and urine elimination rate of DACT.

Sensitivity analysis-discussion

The majority of parameters had |NSC|≤1, indicating a less than or equal to one-to-one relationship between changes in parameter value and resulting changes in model output. The only exception was the neonatal BW on neonatal plasma/brain DACT dosimetry, with |NSC| around 1.5. This is not unexpected because it has been observed in an earlier lactational PBPK model, which we used in constructing the present one (Yoon et al., 2009b). The facts that (1) the PC, placental transfer rate and milk clearance rate parameters of ATR and DACT have high impacts on selected dose metrics associated with ATR and DACT, respectively and (2) most of these parameters were estimated based on relatively limited data sets (Fraites et al., 2011) underscore the importance of these parameters on the model outputs and the importance of continued experimental work in this area.

Supplementary tables

Table C1. Urineflowfactor changes during pregnancy compared to nonpregnant rats[a].

Physiological stages	Urine flow (ml/day)	Urineflowfactor (unitless)
Nonpregnant (on average)	16.35	1.000
Pregnant (gestational day)		
2	18.05	1.104
3	19.37	1.185
4	20.04	1.225
5	19.10	1.168
6	18.48	1.130
7	17.97	1.099
8	16.18	0.990
9	19.53	1.194
10	18.59	1.137
11	16.58	1.014
12	19.29	1.180
13	25.10	1.535
14	23.41	1.432
15	22.37	1.368
16	22.18	1.357
17	22.42	1.371
18	21.91	1.340
19	21.08	1.290
20	21.86	1.337
21	16.85	1.031

[a] Sprague Dawley rats (Atherton et al., 1982).

Table C2. Age-dependent differences in rat hepatic P450 content[a].

PND	P450 content[b]	Proportion relative to the adult[c]
0	13.1	0.34
5	25.2	0.65
6	25.8	0.67
7	25.7	0.67
10	25.3	0.66
20	30.3	0.79
30	33.9	0.88
45	45.6	1.18
60	38.5	1.00
90	38.1	0.99

[a] Watanabe et al. (1993).
[b] Unit: nmol/g liver.
[c] Values of the parameter Kneomet, set the level on PND60 as the adult level.

Table C3. Age-dependent differences in rat hepatic P450 activity[a].

PND	P450 activity[b]	Proportion relative to the adult female[c]
0	6.32	0.24
2.5	6.06	0.23
5	6.07	0.23
7	6.08	0.23
10.5	6.36	0.24
13	6.10	0.23
17	7.43	0.28
21	9.82	0.37
24	14.04	0.53
25	20.10	0.76
26	23.52	0.90
35	26.71	1.02
50	26.24	1.00
60	26.28	1.00
90	25.87	0.99
124	26.00	0.99

[a] Henderson (1971).
[b] Unit: μmoles formaldehyde/(g dry weight*h).
[c] Values of the parameter Kneomet2, set the level on PND60 as the adult level.

Table C4. Liver weight changes with age in the rat.

PND	Liver weight[a] (kg)	Proportion relative to the adult female[b]
0	0.00033933	0.0386
1	0.00033966	0.0387
2	0.00034163	0.0389
3	0.00034654	0.0395
4	0.00035555	0.0405
5	0.00036973	0.0421
6	0.00039011	0.0444
7	0.00041761	0.0475
8	0.00045315	0.0516
9	0.00049754	0.0566
10	0.00055153	0.0628
11	0.00061580	0.0701
12	0.00069096	0.0787
13	0.00077750	0.0885
14	0.00087585	0.0997
15	0.00098630	0.1123
16	0.00110908	0.1263
17	0.00124428	0.1417
18	0.00139190	0.1585
19	0.00155180	0.1767
20	0.00172378	0.1962
21	0.00190748	0.2172
Adult female	0.00878400	1.0000

[a] Neonatal liver weights from PND0 to PND21 were calculated using the equation reported in Mirfazaelian and Fisher (2007). Adult female liver weight was calculated by multiplying the adult female body weight (0.24 kg; Yoon et al., 2009a) by the fractional liver weight (0.0366) for the rat (Brown et al., 1997). Unit: kg.

[b] Values of the parameter KliverR.

Table C5. Equations for describing growth and changing parameters during pregnancy in the gestational model.

Parameters	Equations	References
Pregnant dam		
Body weight (BW, kg)	BW0[a] + Increased tissue volumes during gestation[b]	Clewell et al. (2003); Yoon et al. (2009a)
Cardiac output index (QCC, L/h/kg)[c]	QCC=24.56-0.1323*GD[d]; QC0=QCC*BW0; QC=QCC*BW	Dowell and Kauer (1997); Yoon et al. (2009a)
Tissue volume (L, actual volume, changing during pregnancy)		
Mammary gland (VM)	VM0=0.01*BW0; VM=VM0*(1+0.2*GD)	Hanwell and Linzell (1973); Rosso et al. (1981); Yoon et al. (2009a)
Fat (VF)[e]	VF0=0.07*BW0; VF=VF0*(1+0.0182*GD)	Naismith et al. (1982); Brown et al. (1997); Yoon et al. (2009a)
Placenta (Vpla, for a whole litter)[f]	GD0-6: Vpla=0; GD6-10: Vpla=N*8*(GD-6)/10^6; GD10-22: Vpla=N*32*$e^{(-0.23*(GD-10))}$+40*$e^{(0.28(GD-10)-1)}$	O'Flaherty et al. (1992); Clewell et al. (2003); Yoon et al. (2009a)
Rest of body (Voth)	Voth=BW-VBR-VL-VK-VM-Vpla-Vfetus	
Tissue blood flow (L/h, actual flow changing during pregnancy)		
Mammary gland (QM)	QM0=0.002*QC0; QM=QM0*(VM/VM0)	Hanwell and Linzell (1973); Clewell et al. (2003); Yoon et al. (2009a)
Placenta (Qpla, for a whole litter)	Qpla=N*(0.02*QDEC+QCAP)/24, where QDEC and QCAP as follows: GD0-6: QDEC=0, QCAP=0; GD6-10: QDEC=0.55*(GD-6), QCAP=0; GD10-12: QDEC=2.2*$e^{(-0.23*(GD-10))}$, QCAP=0; GD12-22: QDEC=2.2*$e^{(-0.23*(GD-10))}$, QCAP=$(0.1207*(GD-12))^{4.36}$	O'Flaherty et al. (1992); Clewell et al. (2003); Yoon et al. (2009a)
Rest of body (Qoth)	Qoth=QC-QBR-QL-QK-QM-Qpla	
Body weight for individual fetus (V1fetus, kg)	V1fetus=(0.1089+(16.0*$e^{(-X)}$))/1000, where X=$e^{(5.515-0.2565*GD)}$	Sikov and Thomas (1970); Yoon et al. (2009a)

[a] "0" indicates parameter values on GD0 or for nonpregnant female rats.

[b] These tissues include mammary gland, fat, placenta and fetuses.

[c] Scaled to the actual changing body weight during pregnancy, not the BW0.

[d] GD represents gestational day.

[e] The fat was not described as a separate compartment. Fat volume was included for the purpose of calculating maternal body weight only.

[f] N=12, litter size.

Table C6. Equations for describing pup-specific growth-related changing parameters in the lactational model.

Parameters	Equations	References
Body weight (BWpup, kg)	$(0.0067X71.47^{2.02}+0.604XPND^{2.02})/(71.47^{2.02}+PND^{2.02})$	Mirfazaelian and Fisher (2007)
Cardiac output (Qcpup, L/h)	8.72XBWpup/(0.189+BWpup)	Rodriguez et al. (2007a)
Tissue volume (L, actual volume, changing during lactation)		
Liver (VLpup, L)	$(0.0003X45.7^{2.82}+0.016XPND^{2.82})/(45.7^{2.82}+PND^{2.82})$	Mirfazaelian and Fisher (2007)
Brain (VBRpup, L)	$(0.00021X12.26^{1.55}+0.0021XPND^{1.55})/(12.26^{1.55}+PND^{1.55})$	Mirfazaelian and Fisher (2007)
Kidney (VKpup, L)	$(0.000075X70.07^{2.36}+0.0039XPND^{2.36})/(70.07^{2.36}+PND^{2.36})$	Mirfazaelian and Fisher (2007)
Rest of body (Vothpup, L)	Vothpup=BWpup-VBRpup-VLpup-VKpup	

Values used for simulating physiological parameters in the dam and pups using TABLE function in the lactational model are shown in Table C7-C12.

Table C7. Body weight of the lactating dam (kg)[a].

Postnatal day (PND)	Body weight (BW, kg)
0	0.257
2	0.262
3	0.258
5	0.274
6	0.274
8	0.276
9	0.280
11	0.284
12	0.282
14	0.295
15	0.292
17	0.292
18	0.290
20	0.294
21	0.292

[a] Shirley (1984); Yoon et al. (2009b).

Table C8. Cardiac output index of the dam during lactation[a].

Postnatal day (PND)	Cardiac output index (QCC, L/h/kg)
0	29.5
0.5	29.5
2.5	35.8
4.5	40.4
9.5	39.6
14.5	38.7
21.5	48.8

[a] Hanwell and Linzell (1973); Dowell and Kauer (1997); Yoon et al. (2009b).

Table C9. Volume of mammary gland, liver and kidney in the lactating dam (fraction of BW)[a].

Postnatal day (PND)	Mammary gland (VMC)	Liver (VLC)	Kidney (VKC)
0	0.049	0.0376	0.0073
0.5	0.049	0.0376	0.0073
2.5	0.042	0.0396	0.0077
4.5	0.044	0.0425	0.0084
9.5	0.049	0.0475	0.0080
14.5	0.054	0.0515	0.0086
21.5	0.054	0.0524	0.0080

[a] Hanwell and Linzell (1973); Rosso et al. (1981); Yoon et al. (2009b).

Table C10. Blood flow to mammary gland, liver and kidney in the lactating dam (fraction of QC)[a].

Postnatal day (PND)	Mammary gland (QMC)	Liver (QLC)	Kidney (QKC)
0	-	0.2408	0.1410
0.5	0.09	0.2408	0.1410
2.5	0.11	0.2328	0.1646
4.5	0.10	0.2408	0.1483
9.5	0.12	0.2930	0.1424
14.5	0.14	0.3492	0.1297
21.5	0.13	0.3853	0.1008

[a] Hanwell and Linzell (1973); Yoon et al. (2009b).
- indicates data not available.

Table C11. Milk suckling rate per kg body weight of the pup[a].

Postnatal day (PND)	Milk suckling rate (KlacC, L/h/kg BWpup)
2	0.0216
6	0.0155
7	0.0144
8	0.0144
9	0.0144
10	0.0144
11	0.0144
12	0.0134
13	0.0134
14	0.0134
15	0.0134
16	0.0134
17	0.0119
18	0.0111
19	0.0107
20	0.0096
21	0.0073

[a] Mirfazaelian et al. (2007); Yoon and Barton (2008); Yoon et al. (2009b).

Table C12. Blood flow to brain, liver and kidney in the pup (fraction of QCpup)[a].

Postnatal day (PND)	Brain (QBRCpup)	Liver (QLCpup)	Kidney (QKCpup)
0	-	0.045	0.0150
9	0.093	0.199	0.0364
18	0.085	0.235	0.0571
25	0.049	0.188	0.0769
42	0.034	0.186	0.0880
64	0.046	0.128	0.0764
80	0.020	0.183	0.1410
200	0.020	0.183	0.1410

[a] Stulcová (1977); Yoon et al. (2009b); Loccisano et al. (2012).
- indicates data not available.

Table C13. Comparison of partition coefficients (PC) for ATR and its metabolites derived from different studies and/or methods.

Chemical	Compartment	Current models	Tremblay et al. (2012)[a]	McMullin et al. (2007b)	Time-point tissue/plasma concentration ratio[b]	Algorithm-calculated[e]
ATR	Liver	0.69	0.69	2.36	-	9.45
	Brain	0.73	0.73	-	1.19 ± 0.27	12.21
	Kidney	1	-	-	-	-
	Mammary	5	-	-	6.08 ± 3.58	-
	Placenta	1	-	-	-	-
	Other tissues	1	-	-	-	-
	Fetus	1	-	-	2.09 ± 0.43	-
	Milk[c]	6.1[d]	-	-	0.86 ± 0.36	-
	Milk:mammary[c]	0.35	-	-	0.35 ± 0.04	-
	Muscle	-	-	-	-	2.96
	Body	-	-	1	-	-
DE	Liver	1	-	0.92	-	2.09
	Brain	0.5	-	-	0.45 ± 0.04	2.58
	Kidney	1	-	-	-	-
	Mammary	1	-	-	1.08 ± 0.17	-
	Placenta	1	-	-	-	-
	Other tissues	1	-	-	-	-
	Fetus	1	-	-	1.07 ± 0.16	-
	Milk[c]	0.47	-	-	0.47 ± 0.01	-
	Milk:mammary[c]	0.51	-	-	0.51 ± 0.08	-
	Muscle	-	-	-	-	1.14
	Body	-	-	1	-	-

Table C13 (continued). Comparison of partition coefficients (PC) for ATR and its metabolites derived from different studies and/or methods.

Chemical	Compartment	Current models	Tremblay et al. (2012)[a]	McMullin et al. (2007b)	Time-point tissue/plasma concentration ratio[b]	Algorithm-calculated[e]
DIP	Liver	1	-	0.86	-	1.28
	Brain	0.5	-	-	0.33 ± 0.04	1.52
	Kidney	1	-	-	-	-
	Mammary	1	-	-	0.71 ± 0.07	-
	Placenta	1	-	-	-	-
	Other tissues	1	-	-	-	-
	Fetus	1	-	-	1.03 ± 0.10	-
	Milk[c]	0.51	-	-	0.51 ± 0.03	-
	Milk:mammary[c]	0.67	-	-	0.67 ± 0.03	-
	Muscle	-	-	-	-	0.91
	Body	-	-	1	-	-
DACT	Liver	1	-	0.82	-	0.70
	Brain	0.9	-	-	0.77 ± 0.04	0.78
	Kidney	1	-	-	-	-
	Mammary	0.8	-	-	0.61 ± 0.17	-
	Placenta	1	-	-	-	-
	Other tissues	1	-	-	-	-
	Fetus	1	-	-	1.11 ± 0.09	-
	Milk[c]	0.48	-	-	0.48 ± 0.11	-
	Milk:mammary[c]	0.58	-	-	0.58 ± 0.08	-
	Muscle	-	-	-	-	0.69
	Body	-	-	1	-	-

[a] These parameters were experimentally-determined using a negligible depletion solid phase microextration method (Tremblay et al., 2012).

[b] These parameters were calculated using the single time-point tissue/plasma concentration ratio method reported by Lin et al. (2011) and Fisher et al. (2011) based on data from Fraites et al. (2011). Data represent means ± SD.

[c] These parameters were used in the process of optimizing the description of lactational transfer of ATR and its metabolites based on the methods reported by Fisher et al. (1990), but were not included in the final lactational model.

[d] This parameter was calculated by dividing the human milk:water partition coefficient (29.26; Geisler et al., 2011) by the rat blood:saline partition coefficient (4.8; Tremblay et al., 2012).

[e] These parameter values were calculated using the algorithm reported in Poulin and Krishnan (1995) or Poulin and Theil (2000).

Table C14. Comparison of estimated placental transfer rates and organ blood flow rates.

	Placental transfer rate[a]		Placental transfer rate[b]		Organ blood flow rate[b]		
	KtransinC[c]	KtransoutC[d]	Ktransin[c]	Ktransout[d]	Liver[e]	Brain[e]	Kidney[e]
ATR	1.1	1.0	0.31073	0.28248	1.41937	0.11788	0.83111
DE	1.1	1.0	0.31073	0.28248			
DIP	1.2	1.0	0.33897	0.28248			
DACT	1.4	1.0	0.39547	0.28248			

[a] $L/h/kg^{0.75}$.

[b] L/h.

[c] Diffusion rate constant from maternal placenta to fetal venous blood.

[d] Diffusion rate constant from fetal arterial blood to maternal placenta.

[e] Organ blood flow rates are organ-specific and chemical-independent (Brown et al., 1997).

Table C15. Gestational model normalized sensitivity coefficients (NSCs)[a].

Parameter[b]	Description	Response variable (AUC from GD14 to GD20)							
		ATR				DACT			
		Maternal plasma	Maternal brain	Placenta	Fetus	Maternal plasma	Maternal brain	Placenta	Fetus
Maternal physiological parameters									
BW	Body weight	0.47	-	-	-	- 0.49	- 0.77	- 0.78	- 0.78
VplasmaC	fractional volume of plasma	0.28	-	-	-	- 0.69	- 0.97	- 0.98	- 0.98
VBRC	fractional volume of brain	-	0.24	-	-	-	-	-	-
Maternal tissue partition coefficients									
PBR	Brain:blood PC* for ATR	-	0.76	-	-	-	-	-	-
PP	Placenta:blood PC* for ATR	-	-	1.00	-	-	-	-	-
PBR3	Brain:blood PC* for DACT	-	-	-	-	-	0.82	-	-
PP3	Placenta:blood PC* for DACT	-	-	-	-	-	-	1.00	-
Plasma/tissue binding parameters									
Kaatrplasma	Ka* of ATR with plasma proteins	0.28	-	-	-	-	-	-	-
Kdatrplasma	Kd* of ATR-plasma protein adduct	0.28	-	-	-	-	-	-	-
Bmaxplasmac	BmaxC* of ATR in plasma	0.28	-	-	-	-	-	-	-
Kaatrbrain	Ka* of ATR with brain proteins	-	0.24	-	-	-	-	-	-
Kdatrbrain	Kd* of ATR-brain protein adduct	-	0.24	-	-	-	-	-	-
Bmaxbrainc	BmaxC* of ATR in brain	-	0.24	-	-	-	-	-	-
Kadactplasma	Ka* of DACT with plasma proteins	-	-	-	-	0.29	-	-	-
Kddactplasma	Kd* of DACT-plasma protein adduct	-	-	-	-	0.28	-	-	-
Bmaxplasmac3	BmaxC* of DACT in plasma	-	-	-	-	0.29	-	-	-

Table C15 (continued). Gestational model normalized sensitivity coefficients (NSCs)[a].

Parameter[b]	Description	Response variable (AUC from GD14 to GD20)							
		ATR				DACT			
		Maternal plasma	Maternal brain	Placenta	Fetus	Maternal plasma	Maternal brain	Placenta	Fetus
Absorption, metabolism and elimination parameters									
Vmaxcatr_dip	Maximal metabolic rate from ATR to DIP	- 0.90	- 0.90	- 0.90	- 0.90	-	-	-	-
Kmatr_dip	Michaelis-Menten constant	0.90	0.90	0.90	0.90	-	-	-	-
Kurine3c	KurineC* of DACT	-	-	-	-	- 0.97	- 0.97	- 0.97	- 0.97
K3c	Intestinal absorption rate constant	0.31	0.31	0.31	0.31	0.28	0.29	0.29	0.28
Placental transfer parameters									
Katrtransinc	KtransinC* of ATR	-	-	-	1.00	-	-	-	-
Katrtransoutc	KtransoutC* of ATR	-	-	-	- 0.98	-	-	-	-
Kdacttransinc	KtransinC* of DACT	-	-	-	-	-	-	-	0.99
Kdacttransoutc	KtransoutC* of DACT	-	-	-	-	-	-	-	- 0.98
Fetal parameter									
Pfetus	Fetus:blood PC* of ATR	-	-	-	0.95	-	-	-	-
Pfetus3	Fetus:blood PC* of DACT	-	-	-	-	-	-	-	0.93

- indicates a |NSC| smaller than 0.2.

[a] NSCs were calculated based on Yoon et al. (2009a) and Loccisano et al. (2012).

[b] Only parameters with at least one absolute value of NSC greater than 0.2 are presented.

* Detailed description of these parameters refers to Table 5.2.

Table C16. Lactational model normalized sensitivity coefficients (NSCs)[a].

		Response variable (AUC from PND0 to PND10)			
Parameter[b]	Description	Neonatal plasma DACT	Neonatal brain DACT	Milk ATR	Milk DACT
Maternal parameter					
BW	Body weight	-	-	0.96	-
VplasmaC	fractional volume of plasma	- 0.88	- 0.88	-	- 0.96
K3c	Intestinal absorption rate constant	0.28	0.28	0.29	0.25
Vmaxcatr_dip	Maximal metabolic rate from ATR to DIP	-	-	- 0.90	-
Kmatr_dip	Michaelis-Menten constant	-	-	0.90	-
Kurine3c	KurineC* of DACT	- 0.87	- 0.87	-	- 0.95
Milk clearance					
Kmilkc	Kmilkc* of ATR	-	-	1.00	-
Kmilk3c	Kmilkc* of DACT	0.92	0.92	-	0.98
Neonatal parameter					
Bwpup	Body weight of the pup	- 1.48	- 1.50	- 0.99	- 0.99
Vplasmacpup	Fractional volume of plasma for the pup	- 0.68	- 0.70	-	-
Frac	Fractional absorption of the pup	1.00	1.00	-	-
Pbr3pup	Brain:blood PC* of DACT in the pup	-	0.89	-	-
Poth3pup	Rest of body:blood PC* of DACT in the pup	- 0.27	- 0.27	-	-
Kurine3cpup	KurineC* of DACT in the pup	- 0.68	- 0.68	-	-

[a] NSCs were calculated based on Yoon et al. (2009a) and Loccisano et al. (2012).

[b] Only parameters with at least one absolute value of NSC greater than 0.2 are presented.

- indicates a |NSC| smaller than 0.2.

* Detailed description of these parameters refers to Table 5.2.

Supplementary figures

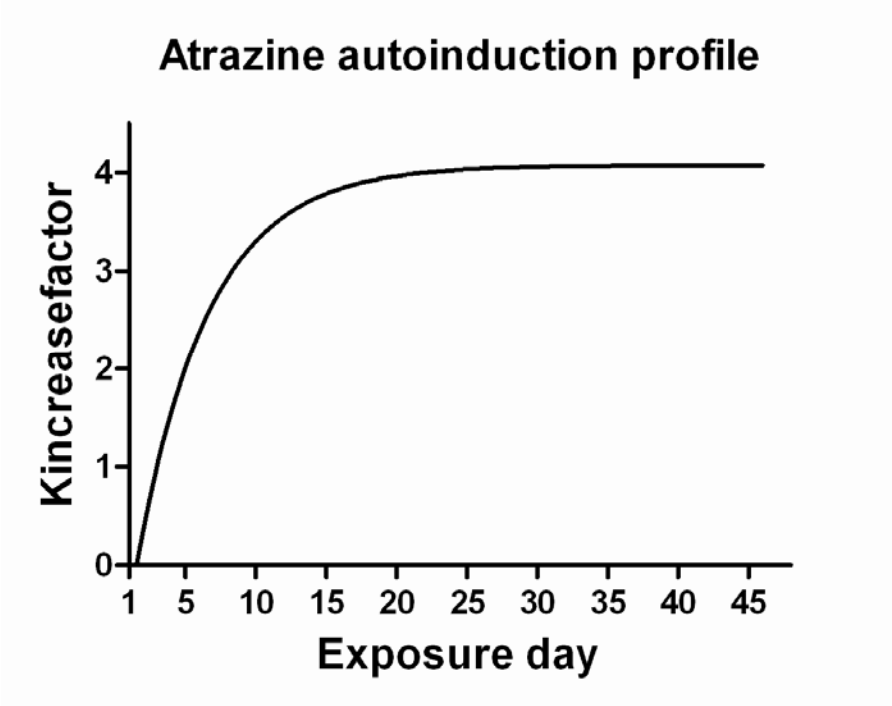

Figure C1. A time-course of autoinduction metabolism of ATR. Kincreasefactor (y axis) represents the extent of net increase of the metabolic rate, which is exposure-dependent, irrespective of physiological stages during which exposure takes place.

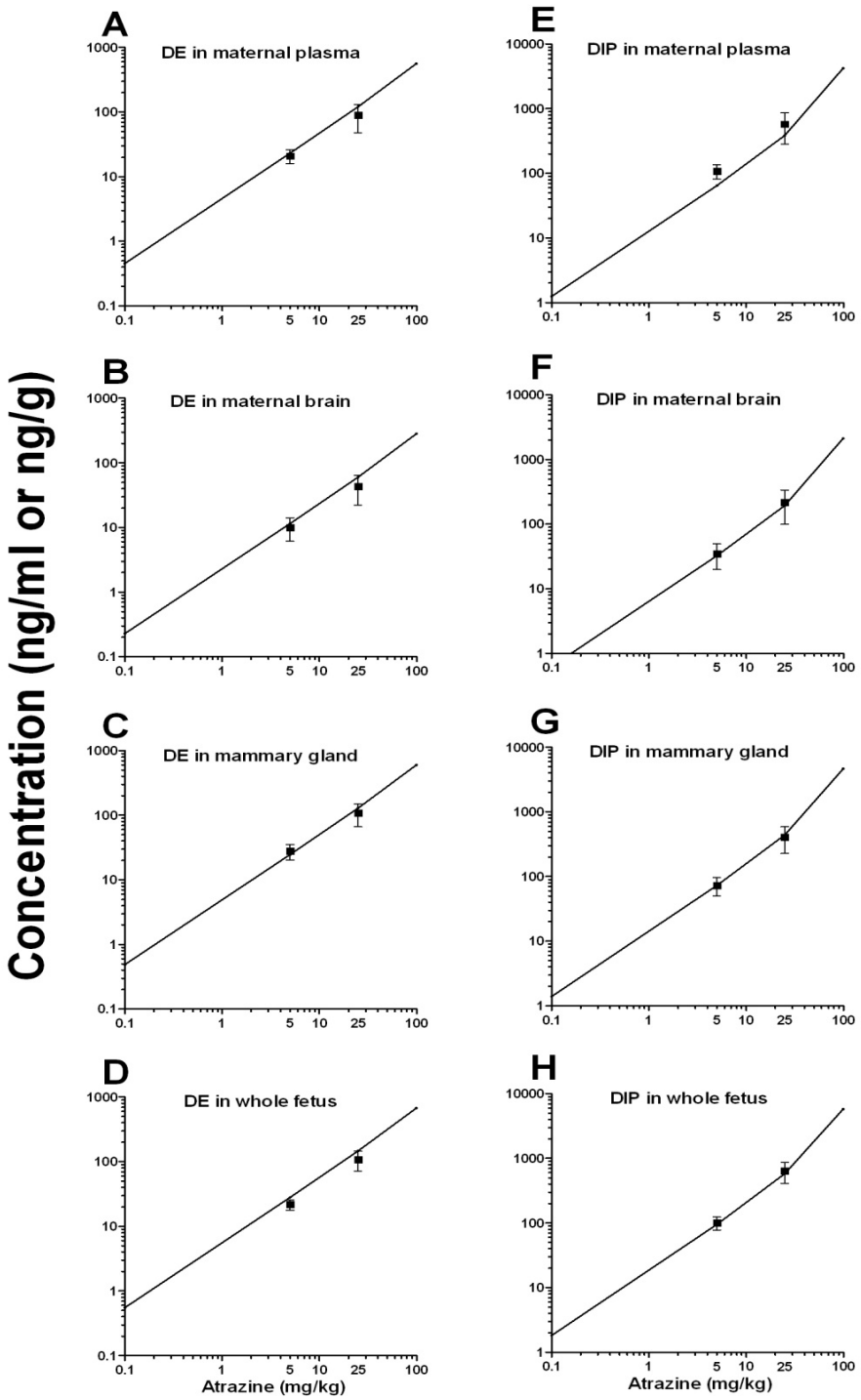

Figure C2. Comparison of gestational model predictions (solid lines) and measured concentrations (Fraites et al., 2011) of DE (A-D) and DIP (E-H) at 2 h after the last dosing on GD20 in maternal plasma, maternal brain, mammary gland and whole fetus of pregnant rats exposed to ATR (5 or 25 mg/kg) by daily oral gavage from GD14 to GD20.

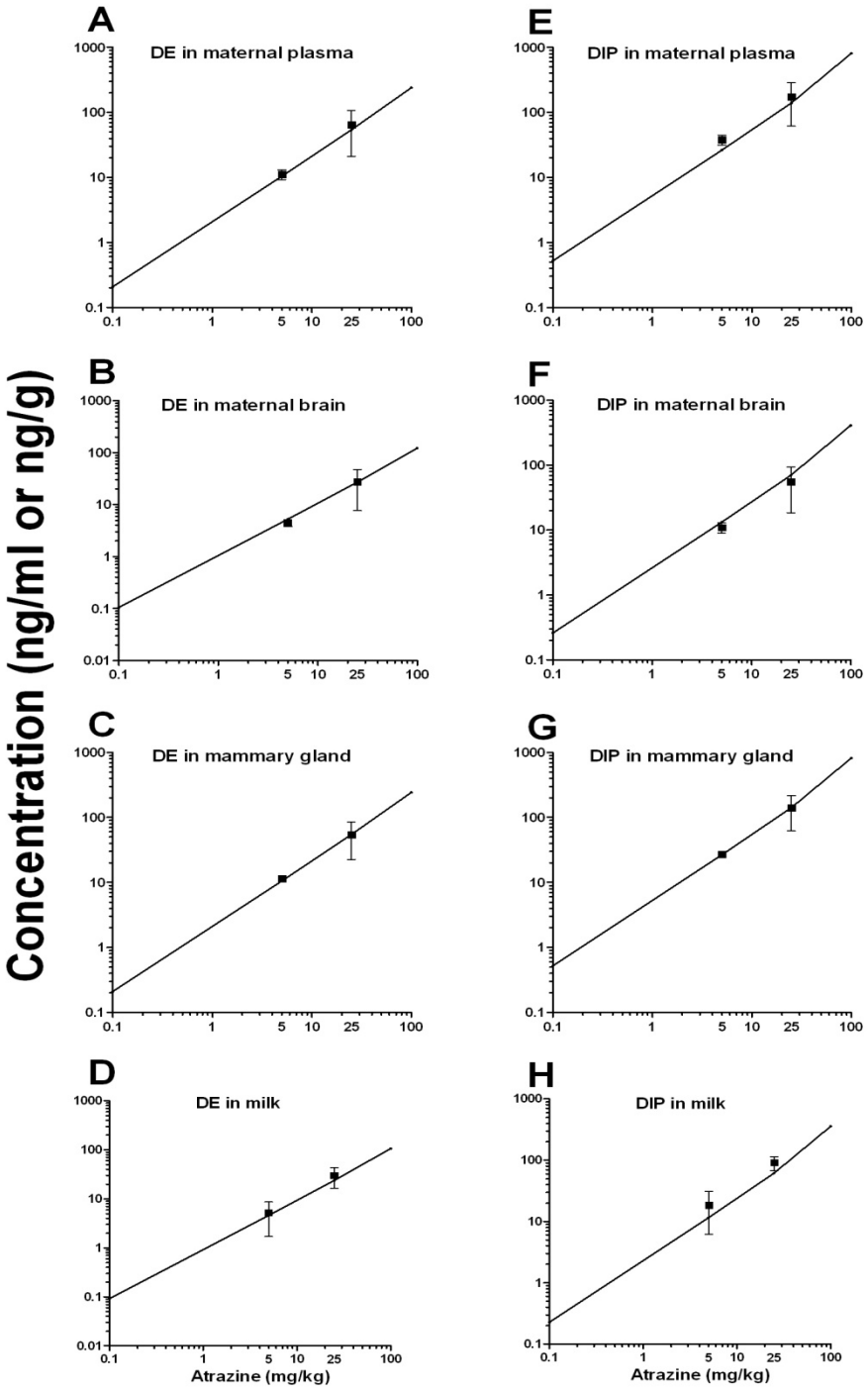

Figure C3. Comparison of lactational model predictions (solid lines) and measured concentrations (Fraites et al., 2011) of DE (A-D) and DIP (E-H) at 2 h after the last dosing on PND10 in maternal plasma, maternal brain, mammary gland and milk following maternal exposure to ATR (5 or 25 mg/kg) by daily oral gavage from GD14 to PND10.

The PBPK model code (csl. file) for atrazine in pregnant rats and fetuses

```
PROGRAM

INITIAL
  ! Code that is executed once at the beginning of a simulation run goes here
  ! Original version initiated by Zhoumeng Lin in July, 2011, based on the code by Yoon et al., 2009, done by the end of 2011
  ! Revised by Zhoumeng Lin in March, 2012
  ! Double-checked and finalized by Zhoumeng Lin in August, 2013

  !!!...Dam: Physiological parameters
  !...Tissue Volumes, Dam (Fraction of true body weight, not including fetus)
  CONSTANT BW0 = 0.240        ! Body weight at the beginning of gestation (kg), assume same as Yoon et al., 2009.
  ! In the distribution study, dams arrived on GD6. There is not initial body weight (Fraites et al., 2011).
  CONSTANT VbloodC = 0.074    ! Brown et al., 1997, Table 21. (0.0676, Yoon 2009 cited from Brown 1997)
  CONSTANT VplasmaC = 0.047   ! Clewell et al., 2003, Brown et al., 1997, Altman and Dittmer, 1971
  CONSTANT VrbcC = 0.027      ! 0.0274 Clewell et al., 2003, Brown et al., 1997, Altman and Dittmer, 1971
  CONSTANT VBRC = 0.0057      ! Brown et al., 1997, Table 5 (0.006, Brown et al., 1997, Table 21. Yoon et al., 2009.)
  CONSTANT VLC = 0.0366       ! Brown et al., 1997, Table 5 (0.0402, Buelke-Sam, et al, 1982, SD rat)
  CONSTANT VKC = 0.0073       ! Brown et al., 1997, Table 5
  CONSTANT VMC = 0.01         ! Mammary gland (non-pregnant), Hanwell & Linzell, 1973
  CONSTANT VFC = 0.07  ! Fat (non-pregnant) for BW changing calculation, Brown et al., 1997, P417, Table 12 (Yoon et al., 2009)

  !...Blood flows (fraction of cardiac output)
  CONSTANT QBRC = 0.02  !fraction of blood flow to brain (Brown et al., 1997, Table 23) same as Yoon et al., 2009
  CONSTANT QLC = 0.2408!fraction of blood flow to liver (Brown et al., 1997, Table 23) (0.2408, Ahokas, 1984, Yoon et al., 2009)
  CONSTANT QKC = 0.141        ! fraction of blood flow to kidney (Brown et al., 1997, Table 23)
  CONSTANT QMC = 0.002        ! fraction of blood flow to mammary gland (Yoon et al., 2009 cited from Hanwell and Linzell 1983)

  !!!...Fetal physiological parameters
  CONSTANT N = 12             ! N = 13 in Yoon et al., 2009; In Fraites et al., 2011, N = 13 for implantation sites, N = 12 for live pups
  CONSTANT mgkg = 1.0e6  ! Unit coversion factor
```

```
  CONSTANT QCCfetus = 22.8     ! Cardiac output index in individual fetus, (L/h/kg) Yoon et al., 2009 cited from Girard, 1983 for guinea pig.
  CONSTANT VbloodCfetus = 0.074  ! Brown et al., 1997, Table 21. (0.0676, Yoon 2009 cited from Brown 1997)

  !!!...Dam: Chemical specific parameters

  !!...Partition coefficients/Distribution coefficients (Set all PCs to be 1 initially, then do minor adjustment to fit the data.)

  !...PCs for ATR, unitless
  CONSTANT PL = 0.69       ! Liver: blood PC,
  CONSTANT PBR = 0.73    ! Brain: blood PC,
  CONSTANT PK = 1          ! Kidney: blood PC,
  CONSTANT PM = 5          ! mammry gland: blood PC,
  CONSTANT PP = 1          ! placenta: blood PC,
  CONSTANT Poth = 1        ! other tissues: blood PC

  !...PCs for DE, unitless
  CONSTANT PL1 = 1         ! Liver: blood PC,
  CONSTANT PBR1 = 0.5    ! Brain: blood PC,
  CONSTANT PK1 = 1         ! Kidney: blood PC,
  CONSTANT PM1 = 1         ! mammry gland: blood PC,
  CONSTANT PP1 = 1         ! placenta: blood PC,
  CONSTANT Poth1 = 1       ! other tissues: blood PC

  !...PCs for DIP, unitless
  CONSTANT PL2 = 1         ! Liver: blood PC,
  CONSTANT PBR2 = 0.5    ! Brain: blood PC,
  CONSTANT PK2 = 1         ! Kidney: blood PC,
  CONSTANT PM2 = 1         ! mammry gland: blood PC,
  CONSTANT PP2 = 1         ! placenta: blood PC,
  CONSTANT Poth2 = 1       ! other tissues: blood PC
```

```
!...PCs for DACT, unitless
CONSTANT PL3 = 1        ! Liver: blood PC,
CONSTANT PBR3 = 0.9   ! Brain: blood PC,
CONSTANT PK3 = 1        ! Kidney: blood PC,
CONSTANT PM3 = 0.8    ! mammry gland: blood PC,
CONSTANT PP3 = 1        ! placenta: blood PC,
CONSTANT Poth3 = 1      ! other tissues: blood PC

!!...Metabolic constants
!...Metabolic constants for ATR, (ATR to DE)
CONSTANT VmaxcATR_DE = 35925.3264              !in vivo = 3 fold in vitro, 11975.1088 ug/h/kg^0.75, Maximum velocity of metabolism of ATR to DE, scalable by (BW)^0.75, original in vitro data see Hanioka et al., 1999.
CONSTANT KmATR_DE = 9598.205                   !ug/l, 44.5 umol/l, Michaelis-Menten constant, Hanioka et al., 1999

!...Metabolic constants for ATR, (ATR to DIP)
CONSTANT VmaxcATR_DIP = 388265.6181            !in vivo = 3 fold in vitro, 129421.8727 ug/h/kg^0.75, Maximum velocity of metabolism of ATR to DIP, scalable by (BW)^0.75, original in vitro data see Hanioka et al., 1999.
CONSTANT KmATR_DIP = 10870.776                 !ug/l, 50.4 umol/l, Michaelis-Menten constant, Hanioka et al., 1999

!...Metabolic constants for DE to DACT
CONSTANT Vmaxc1 = 2626.820             !ug/h/kg^0.75 !14 umol/h/kg^0.75, Maximum velocity of metabolism of DE to DACT, scalable by (BW)^0.75, estimated, data from mouse in Lin et al., 2011
CONSTANT Km1 = 2439.190                !ug/l !13 umol/l, Michaelis-Menten constant, rat in vitro value, in McMullin et al., 2007

!...Metabolic constants for DIP to DACT
CONSTANT Vmaxc2 = 7291.200             !ug/h/kg^0.75 !42 umol/h/kg^0.75, Maximum velocity of metabolism of DIP to DACT, scalable by (BW)^0.75, estimated, data from mouse in Lin et al., 2011
CONSTANT Km2 = 2256.800                !ug/l !13 umol/l, Michaelis-Menten constant, rat in vitro value, in McMullin et al., 2007

!!...Parameters for plasma, red blood cells, tissue (brain) binding, association/disociation rate constants and maximal binding capacities
!...Dam, ATR and plasma, bound ATR account for 26% (18% - 37%) of the total plasma ATR, Lu et al., 1998
```

CONSTANT KaATRplasma = 0.05 !/(ug*h), fitting to meet the 26% criteria, ATR and plasma (albumin) second order association rate constant,
CONSTANT KdATRplasma = 1 !h-1, set to be 1, ATR-plasma protein complex first order dissociation rate constant, same as Lin et al., 2011
CONSTANT BMaxplasmac = 601.7751 !ug/l or ug/kg !2.79 umol/l (or umol/kg), maximal binding capacity of ATR with plasma protein, estimated, highest concentration of plasma ATR at the highest dose group, 250 mg/kg, Lin et al., 2011

!...Dam, ATR and red blood cells,
CONSTANT KaATRrbc = 0.01 !/(ug*h), fitting to meet the 26% criteria, ATR and red blood cells (hemoglobin) second order association rate constant,
CONSTANT KdATRrbc = 1 !h-1, set to be 1, ATR-RBC complex first order dissociation rate constant, same as Lin et al., 2011
CONSTANT BMaxrbcc = 12725.710 !ug/l or ug/kg !59 umol/l (or umol/kg), maximal binding capacity of ATR with red blood cells, estimated, Lin et al., 2011

!...Dam, ATR and brain
CONSTANT KaATRbrain = 0.6 !/(ug*h), fitting to meet the 26% criteria, ATR and brain tissue second order association rate constant,
CONSTANT KdATRbrain = 1 !h-1, set to be 1, ATR-brain tissue protein complex first order dissociation rate constant,
CONSTANT BMaxbrainc = 284.7108 !ug/l or ug/kg !1.32 umol/l (or umol/kg), maximal binding capacity of ATR with brain tissue protein,

!...Whole litter/fetus, ATR
CONSTANT KaATRfetus = 0.15 !/(ug*h), fitting to meet the 26% criteria, ATR and whole fetus tissue second order association rate constant,
CONSTANT KdATRfetus = 1 !h-1, set to be 1, ATR-whole fetus tissue protein complex first order dissociation rate constant,
CONSTANT BMaxfetusc = 284.7108 !ug/l or ug/kg !set equal to dam brain value, maximal binding capacity of ATR with whole fetus tissue protein,

!...Dam, DACT and plasma, set DACT similar binding property as ATR, bound ATR account for 26% (18% - 37%) of the total plasma ATR, Lu et al., 1998

```
  CONSTANT KaDACTplasma = 0.002              !/(ug*h), fitting to meet the 26% criteria, DACT and plasma protein (Albumin) second order association rate constant, estimated, mouse data in Lin et al., 2011
  CONSTANT KdDACTplasma = 1                  !h-1, set to be 1, DACT-plasma protein complex first order dissociation rate constant
  CONSTANT BMaxplasmac3 = 15974.84025        !ug/l or ug/kg !109.755 umol/l (or umol/kg), maximal binding capacity of DACT with plasma protein, estimated, highest concentration of plasma DACT at the highest dose group (250 mg/kg), Lin et al., 2011

  !...Dam, DACT and red blood cells, based on McMullin et al., 2003, 1.5% of total chlorotriazine was bound to red blood cells.
  CONSTANT KaDACTrbc = 0.0002                !/(ug*h), fitting to meet the 26% criteria, DACT and red blood cell (hemoglobin) second order association rate constant,
  CONSTANT KdDACTrbc = 1                     !h-1,set to be 1, DACT-RBC complex first order dissociation rate constant
  CONSTANT BMaxrbcc3 = 1228296.450           !ug/l or ug/kg !8439, umol/l (or umol/kg), maximal binding capacity of DACT with red blood cells, estimated, Lin et al., 2011

  !...Dam, DACT and brain
  CONSTANT KaDACTbrain = 0.02                !/(ug*h), fitting to meet the 26% criteria, DACT and brain tissue second order association rate constant,
  CONSTANT KdDACTbrain = 1                   !h-1, set to be 1, DACT-brain tissue protein complex first order dissociation rate constant,
  CONSTANT BMaxbrainc3 = 7503.1025           !ug/l or ug/kg !51.55 umol/l (or umol/kg), maximal binding capacity of DACT with brain tissue protein,

  !...Whole litter/fetus, DACT
  CONSTANT KaDACTfetus = 0.006               !/(ug*h), fitting to meet the 26% criteria, DACT and whole fetus tissue second order association rate constant,
  CONSTANT KdDACTfetus = 1                   !h-1, set to be 1, DACT-whole fetus tissue protein complex first order dissociation rate constant,
  CONSTANT BMaxfetusc3 = 7503.1025           !ug/l or ug/kg !51.55 umol/l (or umol/kg), maximal binding capacity of DACT with whole fetus tissue protein, set equal to dam brain value

  !!...Elimination constants
  CONSTANT Kurine1C = 1                      ! /(h*kg^(+0.75)), First order urinary elimination rate constant for DE,
  CONSTANT Kurine2C = 0.5                    ! /(h*kg^(+0.75)), First order urinary elimination rate constant for DIP,
  CONSTANT Kurine3C = 14                     ! /(h*kg^(+0.75)), First order urinary elimination rate constant for DACT,
```

```
!!... Urine flow/output change of pregnant rats relative to non-pregnant rats (Atherton et al., 1982)
!...Urine flow for nonpregnant SD rats, unit, ml per day (Get average)
! TABLE DURINEFLOWNON, 1,20/2,3,4,5,6,7,8,9,10,11,12,13,14,15,16,17,18,19,20,21,&
! 13.77,14.87,16.50,15.78,14.84,17.76,16.50,15.14,16.45,17.12,16.72,15.24,16.77,14.98,16.83,17.28,16.13,17.87,18.54,17.93/

!...Urine flow/output for pregnant SD rats, unit, ml per day
! TABLE DURINEFLOWPREG, 1,20/2,3,4,5,6,7,8,9,10,11,12,13,14,15,16,17,18,19,20,21,&
! 18.05,19.37,20.04,19.10,18.48,17.97,16.18,19.53,18.59,16.58,19.29,25.10,23.41,22.37,22.18,22.42,21.91,21.08,21.86,16.85/

!...Urine flow/output change factor, unitless
TABLE DURINEFLOWFACTOR,1,20/2,3,4,5,6,7,8,9,10,11,12,13,14,15,16,17,18,19,20,21,&
1.104,1.185,1.225,1.168,1.130,1.099,0.990,1.194,1.137,1.014,1.180,1.535,1.432,1.368,1.357,1.371,1.340,1.290,1.337,1.031/

!!...Oral absorption rate constant
CONSTANT K1C = 0.2          ! (kg^0.25)/h, gastric absorption rate constant
CONSTANT K2C = 0.7          ! (kg^0.25)/h, gastric intestinal transfer rate constant
CONSTANT K3C = 0.018        ! (kg^0.25)/h, intestinal absorption rate constant
CONSTANT K4C = 0.006        ! (kg^0.25)/h, fecal elimination rate constant (fit data in Bakke et al., 1972)

!!... Molecular weight
CONSTANT MWATR = 215.69      ! Molecular weight of ATR, g/mol
CONSTANT MWDE = 187.63       ! Molecular weight of DE, g/mol
CONSTANT MWDIP = 173.6       ! Molecular weight of DIP, g/mol
CONSTANT MWDACT = 145.55     ! Molecular weight of DACT, g/mol

!!...Conversion ratios for metabolites
ATR_DE = MWDE/MWATR
ATR_DIP = MWDIP/MWATR
DE_DACT = MWDACT/MWDE
DIP_DACT = MWDACT/MWDIP
```

```
!!!...Fetus: Chemical specific parameters
!!...Partition coefficients/distribution coefficients (Set all PCs to be 1 initially, then do minor adjustment to fit the data. )
!...PC for ATR
CONSTANT Pfetus = 1.0     ! Fetus PC for ATR,
!...PC for DE
CONSTANT Pfetus1 = 1.0      ! Fetus PC for DE,
!...PC for DIP
CONSTANT Pfetus2 = 1.0    ! Fetus PC for DIP,
!...PC for DACT
CONSTANT Pfetus3 = 1.0    ! Fetus PC for DACT,

!!...Fetal-Placental transfer parameters
CONSTANT KATRtransinC = 1.1  ! Placenta to fetal vein blood diffusion rate constant (L/h/kg^0.75)
CONSTANT KATRtransoutC = 1.  ! Fetal art blood to placenta diffusion rate constant (L/h/kg^0.75)
CONSTANT KDEtransinC = 1.1   ! Placenta to fetal vein blood diffusion rate constant (L/h/kg^0.75)
CONSTANT KDEtransoutC = 1.   ! Fetal art blood to placenta diffusion rate constant (L/h/kg^0.75)
CONSTANT KDIPtransinC = 1.2  ! Placenta to fetal vein blood diffusion rate constant (L/h/kg^0.75)
CONSTANT KDIPtransoutC = 1.  ! Fetal art blood to placenta diffusion rate constant (L/h/kg^0.75)
CONSTANT KDACTtransinC = 1.4 ! Placenta to fetal vein blood diffusion rate constant (L/h/kg^0.75)
CONSTANT KDACTtransoutC = 1. ! Fetal art blood to placenta diffusion rate constant (L/h/kg^0.75)

!!!...Dosing, multiple oral gavage
CONSTANT TSTOP = 22.         ! End simulation (days)
CONSTANT tlen = 0.001        ! Length of oral gavage exposure (h/day)
CONSTANT DGAV = 5000       ! Oral gavage dose (ug/kg)
CONSTANT Dstart = 14.        ! Initiation day of oral gavage (day)
CONSTANT Dstop = 21.         ! Termination day of oral gavage (day)

CONSTANT MAXT = 1.           ! maximum comm. interval
CONSTANT CINTC = 0.1         ! Communication interval
CINT = CINTC                 ! Communication interval
```

```
Tsim = TSTOP*24              ! Tstop in hours
DS = Dstart*24               ! Initiation time point of oral gavage (h)
Doff = (Dstop - Dstart)*24   ! Oral gavage duration (h)

TimeOn = Dstart*24           ! Initiation time point of oral gavage (h)
TimeOff = Dstop*24+tlen      ! Termination time point of oral gavage (h)

!...Initials
Exposure = 0.

QCAP = 0.
QDEC = 0.

      END ! INITIAL
      DYNAMIC

            ALGORITHM IALG = 2
            NSTEPS    NSTP = 10
            MAXTERVAL MAXT = 1.0e9
            MINTERVAL MINT = 1.0e-9
            CINTERVAL CINT = 0.1

            DERIVATIVE
            ! code for calulating the derivative goes here

Dose = DGAV*BW
Exposure = PULSE(0, 24, tlen)*PULSE(DS, Tsim, Doff)
RDose = (Dose/tlen)*Exposure          ! Rate of oral dosing (ug/h)
RAST = RDose-K2*AST-K1*AST
AST = INTEG(RAST,0)
RAI = K2*AST-K3*AI-K4*AI
AI = INTEG(RAI,0.)
```

```
RAO = K1*AST+K3*AI
AAO = INTEG(RAO,0.)
RAfecal = K4*AI
Afecal  = INTEG(RAfecal,0)

GD = T/24.                    ! Simulation in days, Gestational day (GD)

!!!...Equations for changing values in dams
!...Volume of rat placenta (L) from O'Flaherty based on Buelke-Sam (1982) data, (Yoon et al., 2009)

IF (GD.LE.6) THEN
VPLA = 1.0e-10
ELSE IF (GD.LT.10) THEN
VPLA = (N*(8*(GD-6)))/mgkg
ELSE
VPLA = (N*((32*exp(-0.23*(GD-10)))+(40*(exp(0.28*(GD-10))-1))))/mgkg
END IF

!...Blood flow to placenta (L/h), (Yoon et al., 2009)

IF (GD.LE.6.0) THEN
QDEC = 0.0
ELSE IF (GD.LE.10.0) THEN
QDEC = ((0.55*(GD-6)))
ELSE IF (GD.LE.12) THEN
QDEC = (((2.2*(exp(-0.23*(GD-10))))))
ELSE IF (GD.GT.12) THEN
QDEC = (((2.2 * (exp(-0.23 * (GD - 10))))))
QCAP = (0.1207*(GD-12))**4.36
END IF
QPLA = N*(0.02*QDEC+QCAP)/24
```

```
!!!...Changing parameters, Dam
!!...Physiological parameters
!...Tissue volumes
! For constant tissue volumes during gestation, scaled to initial Body weight (BW0)
! For changing tissue volume during gestation, scaled to body weight (BW)

PNBW = BW-VPLA-Vfetus            ! Dam BW just after birth

Vblood = Vbloodc*BW              ! Blood volume (L)
Vplasma = VplasmaC*BW            ! Plasma volume (L)
Vrbc = VrbcC*BW                  ! Red blood cell volume (L)
VBR = VBRC*BW0                   ! Brain volume (L)
VL = VLC*BW0                     ! Liver volume(L)
VK = VKC*BW0                     ! Kidney volume(L)
VM0 = VMC*BW0                    ! non-pregnant mammary volume (L)
VM = VM0*(1.0+0.201*GD)          ! Mammary volume increase (L), Yoon et al., 2009. (Rosso, 1981 on GD21, SD rat)
VF0 = VFC*BW0                    ! non-pregnant fat volume (L)
VF = VF0*(1.0+0.01818*GD)        ! Assuming 40% fat increase (L), Yoon et al., 2009; Clewell 2003, Naismith, 1982

BW = BW0+Vpla+Vfetus+(VM-VM0)+(VF-VF0) ! Initial BW + Increased volume (kg)
BWINC = Vpla+Vfetus+(VM-VM0)+(VF-VF0)  ! BW increment (kg)

VOth = BW-VBR-VL-VK-VM-Vpla-Vfetus
Vbal = BW-VBR-VL-VK-VM-Vpla-Voth-Vfetus !For tissue volume balance checking in dam

!...Blood flows in Dam
QCC = 24.56-0.1323*GD            ! Cardiac Index (L/h/kg), Dowell, 1997, for total BW
QC = QCC*BW                      ! Cardiac output (L/h), for total BW

QCC0 = 24.56-0.1323*0            ! QCC on GD0, non-pregnant, Dowell, 1997
QC0 = QCC0*BW0                   ! Initial QC, non-pregnant, for non-changing tissue flows
QL = QLC*QC0                     ! Liver blood flow, (L/h)
```

```
QBR = QBRC*QC0                  ! Brain blood flow, (L/h)
QK = QKC*QC0                   ! Kidney blood flow, (L/h)
QM0 = QMC*QC0                   ! Mammary blood flow, (L/h), non-pregnant (Hanwell and Linzell, 1983)
QM = QM0*(VM/VM0) ! Mammary blood flow, (L/h), proportional to mammary volume increase (O'Flaherty, Clewell et al., 2003)

Qoth = QC-QBR-QL-QK-QM-Qpla       ! Other tissue blood flow, (L/h)
Qbal = QC-QBR-QL-QK-QM-Qpla-Qoth  ! Dam blood flow balance checking

!...Scaled parameters
! First order absorption or fecal elimination rate constant
K1 = K1C/BW^0.25
K2 = K2C/BW^0.25
K3 = K3C/BW^0.25
K4 = K4C/BW^0.25

!...Metabolic parameters
! Increasing evidence suggests that ATR exposure induces total P450 content and P450 enzyme activity. Increased expression of specific enzyme has been shown to increase metabolism of ATR.

Dexp = GD+1-Dstart ! The number of days exposed to ATR
Kincreasefactor1 = 0
Kincreasefactor2 = 0
IF (Dexp.LT.2) THEN
Kincreasefactor = 0.0
ELSE IF ((Dexp.GE.2).AND.(Dexp.LE.11)) THEN
Kincreasefactor = 0.4*(Dexp-1)
ELSE IF (Dexp.GT.11) THEN
Kincreasefactor = 4.0
END IF

VmaxcATR_DE_current = VmaxcATR_DE+VmaxcATR_DE*Kincreasefactor
VmaxcATR_DIP_current = VmaxcATR_DIP+VmaxcATR_DIP*Kincreasefactor
```

```
Vmaxc1_current = Vmaxc1*(1+Kincreasefactor1)
Vmaxc2_current = Vmaxc2*(1+Kincreasefactor2)

VmaxATR_DE = VmaxcATR_DE_current*BW**0.75    ! ug/h, maximum velocity of metabolism of ATR to DE,
VmaxATR_DIP = VmaxcATR_DIP_current*BW**0.75  ! ug/h, maximum velocity of metabolism of ATR to DIP,

VmaxDEDACT = Vmaxc1_current*BW**0.75             ! ug/h, maximum velocity of metabolism of DE to DACT,
VmaxDIPDACT = Vmaxc2_current*BW**0.75            ! ug/h, maximum velocity of metabolism of DIP to DACT,

!....increased urinary elimination because of:
!Increased urine output, increased kidney blood flow rate, increased grumerular filtration rate during pregnancy,
Urineflowfactor = DURINEFLOWFACTOR(GD)

Kurine1C_current = Kurine1C*Urineflowfactor
Kurine2C_current = Kurine2C*Urineflowfactor
Kurine3C_current = Kurine3C*Urineflowfactor

Kurine1 = Kurine1C_current*(BW**(+0.75))
Kurine2 = Kurine2C_current*(BW**(+0.75))
Kurine3 = Kurine3C_current*(BW**(+0.75))

!...(Plasma, red blood cell, tissue) protein binding parameter
BMaxplasma = BMaxplasmac*Vplasma         ! ug, maximal binding capacity of ATR with plasma protein
BMaxrbc = BMaxrbcc*Vrbc                  ! ug, maximal binding capacity of ATR with red blood cells
BMaxbrain = BMaxbrainc*VBR               ! ug, maximal binding capacity of ATR with brain
BMaxfetus = BMaxfetusc*Vfetus            ! ug, maximal binding capacity of ATR with whole fetus
BMaxplasma3 = BMaxplasmac3*Vplasma       ! ug, maximal binding capacity of DACT with plasma protein
BMaxrbc3 = BMaxrbcc3*Vrbc                ! ug, maximal binding capacity of DACT with red blood cells
BMaxbrain3 = BMaxbrainc3*VBR             ! ug, maximal binding capacity of DACT with brain
BMaxfetus3 = BMaxfetusc3*Vfetus          ! ug, maximal binding capacity of DACT with whole fetus
```

```
KATRtransin = KATRtransinC*((V1fetus**0.75)*N)     ! Placental diffusion rate constant (Maternal to Fetal) (L/h)
KATRtransout = KATRtransoutc*((V1fetus**0.75)*N)   ! Placental diffusion rate constant (Fetal to Maternal) (L/h)
KDEtransin = KDEtransinC*((V1fetus**0.75)*N)       ! Placental diffusion rate constant (Maternal to Fetal) (L/h)
KDEtransout = KDEtransoutC*((V1fetus**0.75)*N)     ! Placental diffusion rate constant (Fetal to Maternal) (L/h)
KDIPtransin = KDIPtransinC*((V1fetus**0.75)*N)     ! Placental diffusion rate constant (Maternal to Fetal) (L/h)
KDIPtransout = KDIPtransoutC*((V1fetus**0.75)*N)   ! Placental diffusion rate constant (Fetal to Maternal) (L/h)
KDACTtransin = KDACTtransinC*((V1fetus**0.75)*N)   ! Placental diffusion rate constant (Maternal to Fetal) (L/h)
KDACTtransout = KDACTtransoutC*((V1fetus**0.75)*N) ! Placental diffusion rate constant (Fetal to Maternal) (L/h)

!!!...Changing parameters in Fetus
!...Physiological parameters as a whole litter (=sum of N fetuses)

V1fetus = (0.1089+(16.0*exp(-exp(5.515-0.2565*gd))))/1000 ! Individual fetus BW (kg), Sikov & Thomas, 1970. (Yoon et al., 2009)
Vfetus = V1fetus*N                                ! Whole litter weight (kg)

Vbloodfetus = VbloodCfetus*Vfetus
QCfetus = QCCfetus*Vfetus

!!!...Model equations
!!...ATR sub-model
!...ATR in blood compartment
!...APlasmaFree = Amount of free ATR in plasma (ug)
RAPlasmaFree = QC*(CV-CPlasmaFree)+RARBCunbind-RARBCbind+RAplasmaunbind-RAplasmabind
APlasmaFree = Integ(RAPlasmaFree,0.0)
CPlasmaFree = APlasmaFree/Vplasma

!...APlasmabound = Amount of ATR bound plasma protein (ug)
RAPlasmabound = RAPlasmabind-RAPlasmaunbind
APlasmabound = Integ(RAPlasmabound,0.0)
CPlasmabound = APlasmabound/Vplasma
```

```
!...ARBCbound = Amount of ATR bound to red blood cells (ug)
RARBCbound = RARBCbind-RARBCunbind
ARBCbound = Integ(RARBCbound,0.0)
CRBCbound = ARBCbound/VRBC

!...Ablood = Total amount of ATR in the blood compartment (ug)
!...Aplasma = Total amount of ATR in the plasma compartment (ug)
Ablood = APlasmaFree+APlasmabound+ARBCbound
Cblood = Ablood/Vblood
Aplasma = APlasmaFree+Aplasmabound
Cplasma = Aplasma/Vplasma
AUCCplasma = Integ(Cplasma,0.0)

RAplasmabind = KaATRplasma*BMaxPlasmaRemain*AplasmaFree
RAplasmaunbind = KdATRplasma*Aplasmabound
RARBCbind = KaATRrbc*BMaxRBCRemain*AplasmaFree
RARBCunbind = KdATRrbc*ARBCbound

BMaxPlasmaRemain = BMaxPlasma-APlasmabound
BMaxRBCRemain = BMaxRBC-ARBCbound

CV= (CVL*QL+CVBR*QBR+CVK*QK+CVoth*Qoth+CVM*QM+CVPla*QPla)/QC

!...ATR in liver compartment
!...Total amount of ATR in liver
RL = QL*(CPlasmaFree-CVL)+RAO-RATR_DEmet-RATR_DIPmet
AL = Integ(RL,0.0)
CL = AL/VL
CVL = AL/(VL*PL)

! Metabolism of ATR in liver
RATR_DEmet = VmaxATR_DE*CVL/(KmATR_DE+CVL)          ! Metabolic rate of ATR to DE, ug/h,
```

```
AATR_DEmet = Integ(RATR_DEmet,0.0)

RformDE = RATR_DEmet*ATR_DE                    ! Rate of formation of DE from ATR, ug/h
AformDE = Integ(RformDE,0.0)

RATR_DIPmet = VmaxATR_DIP*CVL/(KmATR_DIP+CVL)      ! Metabolic rate of ATR to DIP, ug/h,
AATR_DIPmet = Integ(RATR_DIPmet,0.0)

RformDIP = RATR_DIPmet*ATR_DIP                 ! Rate of formation of DIP from ATR, ug/h
AformDIP = Integ(RformDIP,0.0)
AATRmet = AATR_DEmet+AATR_DIPmet               ! Amount of ATR metabolized, ug

!...ATR in brain compartment
!...ABRfree = Amount of ATR  free in brain (ug)
RBRfree = QBR*(CPlasmaFree-CVBR)+KdATRBrain*ABrainbound-KaATRBrain*BMaxBrainRemain*AVBR
ABRfree = Integ(RBRfree,0.0)
CBRfree = ABRfree/VBR
CVBR = ABRfree/(VBR*PBR)
AVBR = ABRfree/PBR

!...ABrainbound = Amount of ATR bound in brain (ug)
RABrainbound = KaATRBrain*BMaxBrainRemain*AVBR-KdATRBrain*ABrainbound
ABrainbound = Integ(RABrainbound,0.0)
CBrainbound = ABrainbound/VBR

!...BMaxBrainRemain = Remaining binding capacity of brain for ATR (ug)
BMaxBrainRemain = BMaxBrain-ABrainbound

!...ABR = Total amount of ATR in the brain (ug)
ABR = ABRfree+ABrainbound
CBR = ABR/VBR
AUCCBR = Integ(CBR,0.0)
```

```
!...ATR in kidney compartment
!...AK = Total amount of ATR in kidney (ug)
RK = QK*(CPlasmaFree-CVK)
AK = Integ(RK,0.0)
CK = AK/VK
CVK = AK/(VK*PK)

!...ATR in other tissue compartment
!...Aoth = Total amount of ATR in other tissues (ug)
Roth = Qoth*(CPlasmaFree-CVoth)
Aoth = Integ(Roth,0.0)
Coth = Aoth/Voth
CVoth = Coth/Poth

!...ATR in mammary gland compartment
!...AM = Total amount of ATR in mammary gland (ug)
RM = QM*(CPlasmaFree-CVM)
AM = Integ(RM,0.0)
CM = AM/VM
CVM = CM/PM

!...ATR in placenta compartment
!...APla = Total amount of ATR in placenta (ug)
RPla = QPla*(CPlasmaFree-CVpla)+RATRtransout-RATRtransin
APla = Integ(RPla,0.0)
CPla = APla/VPla
CVPla = CPla/PP

!...AATRtransin = Amount of ATR transferred to fetus from dam, ug
RATRtransin = KATRtransin*CVPla
AATRtransin = Integ(RATRtransin,0.0)
```

```
!...AATRtransout = Amount of ATR transferred to dam from fetus, ug
 RATRtransout = KATRtransout*Cbloodfetus
 AATRtransout = Integ(RATRtransout,0.0)

 !!...Fetal compartment, as a whole litter, single compartment model

 !...Afetusfree = Amount of ATR free in the whole fetuses, ug
Rfetusfree = RATRtransin-RATRtransout+KdATRfetus*Afetusbound-KaATRfetus*BMaxFetusRemain*Abloodfetus
Afetusfree = Integ(Rfetusfree,0.0)
Cfetusfree = Afetusfree/Vfetus
Cbloodfetus = Cfetusfree/Pfetus
Abloodfetus = Cbloodfetus*Vbloodfetus

!...Afetusbound = Amount of ATR bound in the whole fetuses, ug
RAfetusbound = KaATRfetus*BMaxFetusRemain*Abloodfetus-KdATRfetus*Afetusbound
Afetusbound = Integ(RAfetusbound,0.0)
Cfetusbound = Afetusbound/Vfetus

!...BMaxFetusRemain = Remaining binding capacity of whole fetuses for ATR (ug)
BMaxFetusRemain = BMaxFetus-AFetusbound

!...Afetus = Total amount of ATR in the fetus (ug)
Afetus = Afetusfree+Afetusbound
Cfetus = Afetus/Vfetus
AUCCfetus = Integ(Cfetus,0.0)
!...Mass balance for ATR
!...Tmass = Mass balance for ATR (total amount of ATR absorpted or in the body), ug
Tmass = Ablood+AL+ABR+AK+Aoth+AM+AATR_DEmet+AATR_DIPmet+Apla+Afetus
BalATR = AAO-Tmass   ! Checking mass balance of ATR sub-model, Absorption = remaining in the tissues + metabolized

!!...DE sub-model
!...DE in blood compartment, We consider binding kinetics of DE in blood and tissues are negligible.
```

```
!...Ablood1 = Amount of DE in the blood compartment, ug
Rblood1 = QC*(CV1-CA1)
Ablood1 = Integ(Rblood1,0.0)
CA1 = Ablood1/Vblood  ! DE concentration in artery, ug/l

CV1 = (CVL1*QL+CVBR1*QBR+CVK1*QK+CVoth1*Qoth+CVM1*QM+CVpla1*Qpla)/QC ! DE concentration in venous blood, ug/l

!...DE in liver compartment
!...AL1 = Amount of DE in the liver compartment, ug
RL1 = QL*(CA1-CVL1)+RformDE-RDE_DACTmet
AL1 = Integ(RL1,0.0)
CL1 = AL1/VL          ! DE concentration in liver tissue, ug/l
CVL1 = AL1/(VL*PL1)   ! DE concentration in liver venous blood, ug/l

!...Metabolism of DE in the liver
!...ADE_DACTmet = Amount of DE metabolized to DACT in the liver, ug
RDE_DACTmet = VmaxDEDACT*CVL1/(Km1+CVL1)    ! Rate of metabolism of DE to DACT in the liver, ug/h
ADE_DACTmet = Integ(RDE_DACTmet,0.0)

RformDACTDE = RDE_DACTmet*DE_DACT          ! Rate of formation of DACT from DE in the liver, ug/h
AformDACTDE = Integ(RformDACTDE,0.0)

!...DE in the brain compartment
!...ABR1 = Amount of DE in the brain compartment, ug
RBR1 = QBR*(CA1-CVBR1)
ABR1 = Integ(RBR1,0.0)
CBR1 = ABR1/VBR                    ! DE concentration in brain tissue, ug/l
CVBR1 = CBR1/PBR1                   ! DE concentration in brain venous blood, ug/l

!...DE in the kidney compartment
!...AK1 = Amount of DE in the kidney compartment, ug
```

```
RK1 = QK*(CA1-CVK1)-Rurine1
AK1 = Integ(RK1,0.0)
CK1 = AK1/VK                          ! DE concentration in kidney tissue, ug/l
CVK1 = CK1/PK1                        ! DE concentration in kidney venous blood, ug/l

!...DE in the other tissue compartment
!...Aoth1 = Amount of DE in the other tissue compartment, ug
Roth1 = Qoth*(CA1-CVoth1)
Aoth1 = Integ(Roth1,0.0)
Coth1 = Aoth1/Voth                    ! DE concentration in other tissue, ug/l
CVoth1 = Coth1/Poth1                  ! DE concentration in other tissue venous blood, ug/l

!...DE in the mammary gland compartment
!...AM1 = Amount of DE in the mammary gland compartment, ug
RM1 = QM*(CA1-CVM1)
AM1 = Integ(RM1,0.0)
CM1 = AM1/VM                          ! DE concentration in mammary gland, ug/l
CVM1 = CM1/PM1                        ! DE concentration in mammary gland venous blood, ug/l
!...DE in the placenta compartment
!...Apla1 = Amount of DE in the placenta compartment, ug
Rpla1 = Qpla*(CA1-CVpla1)+RDEtransout-RDEtransin
Apla1 = Integ(Rpla1,0.0)
Cpla1 = Apla1/Vpla                    ! DE concentration in placenta, ug/l
CVpla1 = Cpla1/PP1                    ! DE concentration in placenta venous blood, ug/l

!...ADEtransin = Amount of DE transferred to fetus from dam, ug
RDEtransin = KDEtransin*CVpla1
ADEtransin = Integ(RDEtransin,0.0)

!...ADEtransout = Amount of DE transferred to dam from fetus, ug
RDEtransout = KDEtransout*Cbloodfetus1
ADEtransout = Integ(RDEtransout,0.0)
```

```
!!...fetal compartment, as a whole litter, single compartment
!... Afetus1 = Amount of DE transferred to fetus from dam, ug
Rfetus1 = RDEtransin-RDEtransout
Afetus1 = Integ(Rfetus1,0.0)
Cfetus1 = Afetus1/Vfetus
Cbloodfetus1 = Cfetus1/Pfetus1

!...Urinary excretion of DE
Rurine1 = Kurine1*CV1*Vplasma
Aurine1 = Integ(Rurine1,0.0)

!...Mass balance for DE
!TMASS1 = Mass balance of DE, ug (total amount of DE produced)
Tmass1 = Ablood1+AL1+ABR1+AK1+Aoth1+AM1+Apla1+Afetus1+ADE_DACTmet+Aurine1
BalDE = AformDE-Tmass1

!!...DIP sub-model
   !...DIP in blood compartment, we consider binding kinetics of DIP in blood and tissues are negligible.
!...Ablood2 = Amount of DIP in the blood compartment, ug
Rblood2 = QC*(CV2-CA2)
Ablood2 = Integ(Rblood2,0.0)
CA2 = Ablood2/Vblood                    ! DIP concentration in artery blood, ug/l
CV2 = (CVL2*QL+CVBR2*QBR+CVK2*QK+CVoth2*Qoth+CVM2*QM+CVpla2*Qpla)/QC       ! DIP concentration in venous
blood, ug/l
!...DIP in liver compartment
!...AL2 = Amount of DIP in the liver compartment, ug
RL2 = QL*(CA2-CVL2)+RformDIP-RDIP_DACTmet
AL2 = Integ(RL2,0.0)
CL2 = AL2/VL                        ! DIP concentration in liver tissue, ug/l
CVL2 = AL2/(VL*PL2)                     ! DIP concentration in liver venous blood, ug/l
```

```
!...Metabolism of DIP in the liver
!...ADIP_DACTmet = Amount of DIP metabolized to DACT in the liver, ug
RDIP_DACTmet = VmaxDIPDACT*CVL2/(Km2+CVL2)    ! Rate of metabolism of DIP to DACT in the liver, ug/h
ADIP_DACTmet = Integ(RDIP_DACTmet,0.0)
RformDACTDIP = RDIP_DACTmet*DIP_DACT          ! Rate of formation of DACT from DIP in the liver, ug/h
AformDACTDIP = Integ(RformDACTDIP,0.0)

!...DIP in the brain compartment
!...ABR2 = Amount of DIP in the brain compartment, ug
RBR2 = QBR*(CA2-CVBR2)
ABR2 = Integ(RBR2,0.0)
CBR2 = ABR2/VBR                    ! DIP concentration in brain tissue, ug/l
CVBR2 = CBR2/PBR2                   ! DIP concentration in brain venous blood, ug/l

!...DIP in the kidney compartment
!...AK2 = Amount of DIP in the kidney compartment, ug
RK2 = QK*(CA2-CVK2)-Rurine2
AK2 = Integ(RK2,0.0)
CK2 = AK2/VK                       ! DIP concentration in kidney tissue, ug/l
CVK2 = CK2/PK2                      ! DIP concentration in kidney venous blood, ug/l

!...DIP in the other tissue compartment
!...Aoth2 = Amount of DIP in the other tissue compartment, ug
Roth2 = Qoth*(CA2-CVoth2)
Aoth2 = Integ(Roth2,0.0)
Coth2 = Aoth2/Voth                 ! DIP concentration in other tissues, ug/l
CVoth2 = Coth2/Poth2                ! DIP concentration in other tissue venous blood, ug/l

!...DIP in the mammary gland compartment
!...AM2 = Amount of DIP in the mammary gland compartment, ug
RM2 = QM*(CA2-CVM2)
AM2 = Integ(RM2,0.0)
```

```
CM2 = AM2/VM                    ! DIP concentration in mammary gland tissue, ug/l
CVM2 = CM2/PM2                  ! DIP concentration in mammary gland venous blood, ug/l

!...DIP in the placenta compartment
!...Apla2 = Amount of DIP in the placenta compartment, ug
Rpla2 = Qpla*(CA2-CVpla2)+RDIPtransout-RDIPtransin
Apla2 = Integ(Rpla2,0.0)
Cpla2 = Apla2/Vpla              ! DIP concentration in placenta tissue, ug/l
CVpla2 = Cpla2/PP2              ! DIP concentration in placenta venous blood, ug/l

!...ADIPtransin = Amount of DIP transferred to fetus from dam, ug
RDIPtransin = KDIPtransin*CVpla2
ADIPtransin = Integ(RDIPtransin,0.0)
!...ADIPtransout = Amount of DIP transferred to dam from fetus, ug
RDIPtransout = KDIPtransout*Cbloodfetus2
ADIPtransout = Integ(RDIPtransout,0.0)

!...fetal compartment, as a whole litter, single compartment
!...Afetus2 = Amount of DIP transferred to fetus from dam, ug
Rfetus2 = RDIPtransin-RDIPtransout
Afetus2 = Integ(Rfetus2,0.0)
Cfetus2 = Afetus2/Vfetus
Cbloodfetus2 = Cfetus2/Pfetus2

!...Urinary excretion of DIP
Rurine2 = Kurine2*CV2*Vplasma
Aurine2 = Integ(Rurine2,0.0)

!...Mass balance for DIP
!...Tmass2 = Mass balance of DIP, ug (total amount of DIP produced)
Tmass2 = Ablood2+AL2+ABR2+AK2+Aoth2+AM2+Apla2+Afetus2+ADIP_DACTmet+Aurine2
BalDIP = AformDIP-Tmass2
```

!!!...DACT sub-model
!...DACT in blood compartment, we consider ATR and DACT, but not DE and DIP, bind to maternal plasma, red blood cell, brain tissue, and whole fetus.

!...APlasmaFree3 = Amount of free DACT in plasma (ug)
RAPlasmaFree3 = QC*(CV3-CPlasmaFree3)+RARBCunbind3-RARBCbind3+RAplasmaunbind3-RAplasmabind3
APlasmaFree3 = Integ(RAPlasmaFree3,0.0)
CPlasmaFree3 = APlasmaFree3/VPlasma

!...APlasmabound3 = Amount of DACT bound to plasma protein (ug)
RAPlasmabound3 = RAPlasmabind3-RAPlasmaunbind3
APlasmabound3 = Integ(RAPlasmabound3,0.0)
CPlasmabound3 = APlasmabound3/VPlasma

!...ARBCbound3 = Amount of DACT bound to red blood cells (ug)
RARBCbound3 = RARBCbind3-RARBCunbind3
ARBCbound3 = Integ(RARBCbound3,0.0)
CRBCbound3 = ARBCbound3/VRBC

!...Ablood3 = Total amount of DACT in the blood compartment (ug)
!...Aplasma3 = Total amount of DACT in the plasma compartment (ug)
Ablood3 = APlasmaFree3+APlasmabound3+ARBCbound3
Cblood3 = Ablood3/Vblood
Aplasma3 = APlasmaFree3+APlasmabound3
Cplasma3 = Aplasma3/Vplasma
AUCCplasma3 = Integ(Cplasma3,0.0)
RAplasmabind3 = KaDACTplasma*BMaxPlasmaRemain3*APlasmaFree3
RAplasmaunbind3 = KdDACTplasma*Aplasmabound3
RARBCbind3 = KaDACTrbc*BMaxRBCRemain3*APlasmaFree3
RARBCunbind3 = KdDACTrbc*ARBCbound3
BMaxPlasmaRemain3 = BMaxPlasma3-APlasmabound3
BMaxRBCRemain3 = BMaxRBC3-ARBCbound3

```
CV3 = (CVL3*QL+CVBR3*QBR+CVK3*QK+CVoth3*Qoth+CVM3*QM+CVpla3*Qpla)/QC    ! DACT concentration in venous
blood, ug/l

!...DACT in liver compartment
!...AL3 = Amount of DACT in the liver compartment, ug
RL3 = QL*(CPlasmaFree3-CVL3)+RformDACTDE+RformDACTDIP
AL3 = Integ(RL3,0.0)
CL3 = AL3/VL                        ! DACT concentration in liver tissue, ug/l
CVL3 = CL3/PL3                      ! DACT concentration in liver venous blood, ug/l

!...DACT in brain compartment
!...ABRfree3 = Amount of DACT free in brain, ug
RBRfree3 = QBR*(CPlasmaFree3-CVBR3)+KdDACTBrain*ABrainbound3-KaDACTBrain*BMaxBrainRemain3*AVBR3
ABRfree3 = Integ(RBRfree3,0.0)
CBRfree3 = ABRfree3/VBR
CVBR3 = CBRfree3/PBR3                   ! DACT concentration in brain venous blood, ug/l
AVBR3 = ABRfree3/PBR3
!...ABrainbound3 = Amount of DACT bound to brain tissue, ug
RABrainbound3 = KaDACTBrain*BMaxBrainRemain3*AVBR3-KdDACTBrain*ABrainbound3
ABrainbound3 = Integ(RABrainbound3,0.0)
CBrainbound3 = ABrainbound3/VBR

!...BMaxBrainRemain3 = Remaining binding capacity of brain for DACT, ug
BMaxBrainRemain3 = BMaxBrain3-ABrainbound3

!...ABR3 = Total amount of DACT in the brain, ug
ABR3 = ABRfree3+ABrainbound3
CBR3 = ABR3/VBR                     ! DACT concentration in brain tissue, ug/l

!...DACT in kidney compartment
!...AK3 = Amount of DACT in the kidney compartment, ug
RK3 = QK*(CPlasmaFree3-CVK3)-Rurine3
```

```
AK3 = Integ(RK3,0.0)
CK3 = AK3/VK                    ! DACT concentration in kidney tissue, ug/l
CVK3 = CK3/PK3                  ! DACT concentration in kidney venous blood, ug/l

!...DACT in the other tissue compartment
!...Aoth3 = Amount of DACT in the other tissue compartment, ug
Roth3 = Qoth*(CPlasmaFree3-CVoth3)
Aoth3 = Integ(Roth3,0.0)
Coth3 = Aoth3/Voth              ! DACT concentration in other tissue, ug/l
CVoth3 = Coth3/Poth3            ! DACT concentration in other tissue venous blood, ug/l

!...DACT in the mammary gland compartment
!...AM3 = Amount of DACT in the mammary gland compartment, ug
RM3 = QM*(CPlasmaFree3-CVM3)
AM3 = Integ(RM3,0.0)
CM3 = AM3/VM                    ! DACT concentration in mammary gland tissue, ug/l
CVM3 = CM3/PM3                  ! DACT concentration in mammary gland venous blood, ug/l

!...DACT in the placenta compartment
!...Apla3 = Amount of DACT in the placenta compartment, ug
Rpla3 = Qpla*(CPlasmaFree3-CVpla3)+RDACTtransout-RDACTtransin
Apla3 = Integ(Rpla3,0.0)
Cpla3 = Apla3/Vpla              ! DACT concentration in placenta tissue, ug/l
CVpla3 = Cpla3/PP3              ! DACT concentration in placenta venous blood, ug/l

!...ADACTtransin = Amount of DACT transferred to fetus from dam, ug
RDACTtransin = KDACTtransin*CVpla3
ADACTtransin = Integ(RDACTtransin,0.0)

!...ADACTtransout = Amount of DACT transferred to dam from fetus, ug
RDACTtransout = KDACTtransout*Cbloodfetus3
ADACTtransout = Integ(RDACTtransout,0.0)
```

```
!!...fetal compartment, as a whole litter, single compartment
!...Afetusfree3 = Amount of DACT free in the whole fetuses, ug
Rfetusfree3 = RDACTtransin-RDACTtransout+KdDACTfetus*Afetusbound3-KaDACTfetus*BMaxFetusRemain3*Abloodfetus3
Afetusfree3 = Integ(Rfetusfree3,0.0)
Cfetusfree3 = Afetusfree3/Vfetus
Cbloodfetus3 = Cfetusfree3/Pfetus3
Abloodfetus3 = Cbloodfetus3*Vbloodfetus

!...Afetusbound3 = Amount of DACT bound to the whole fetus tissue, ug
RAfetusbound3 = KaDACTfetus*BMaxFetusRemain3*Abloodfetus3-KdDACTfetus*Afetusbound3
Afetusbound3 = Integ(RAfetusbound3,0.0)
Cfetusbound3 = Afetusbound3/Vfetus

!...BMaxFetusRemain3 = Remaining binding capacity of whole fetus for DACT, ug
BMaxFetusRemain3 = BMaxFetus3-Afetusbound3

!...Afetus3 = Total amount of DACT in the fetus, ug
Afetus3 = Afetusfree3+Afetusbound3
Cfetus3 = Afetus3/Vfetus
AUCCfetus3 = Integ(Cfetus3,0.0)

!...Urinary excretion of DACT
Rurine3 = Kurine3*CV3*Vplasma
Aurine3 = Integ(Rurine3,0.0)

!...Mass balance for DACT
!...Tmass3 = Mass balance of DACT, ug (total amount of DACT produced)
TMass3 = Ablood3+AL3+ABR3+AK3+Aoth3+AM3+Apla3+Afetus3+Aurine3
BalDACT = AformDACTDE+AformDACTDIP-Tmass3

 END ! DERIVATIVE
```

```
            ! Add discrete events here as needed
            !  DISCRETE
            !  END
            ! code that is executed once at each communication interval goes here

            !CONSTANT TSTOP = 10.0
            TERMT (T .GE. (TSTOP*24), 'checked on communication interval: REACHED TSTOP')

        END ! DYNAMIC

        TERMINAL
            ! code that is executed once at the end of a simulation run goes here
        END ! TERMINAL

END ! PROGRAM
```

The PBPK model code (csl. file) for atrazine in lactating rats and neonates

```
PROGRAM: LactationATR.csl

! ATR lactation model by Zhoumeng Lin, July 21, 2011
! Modified by Zhoumeng Lin, March 22, 2012
! Based on adult mouse model (Lin et al., 2011) and Mnlactation model (Yoon et al., 2009) and PFOSlactation model (Loccisano et al., 2011)
! Cl(clearance) used instead of Vmax & Km for milk ATR and metabolites excretion
! No residual vol of milk assumed, production = suckled assumed
! PND0 physiology matched with GD22 values except BW
! & Total BW-(fetuses+placenta) used as BWdam for PND0,
! Initial tissue conc from GestationATR model (GD22).
! Double-checked and finalized in August, 2013

      INITIAL
      ! code that is executed once at the beginning of a simulation run goes here
      !...Parameters changing with time

 !...Body weight of the dam (kg, shirley 1984), GD22 BW-Vpla-Vfet=PND0 BW
 TABLE DBW,1,15/0.,2.,3.,5.,6.,8.,9.,11.,12.,14.,15.,17.,18.,20.,21.,&
 0.257,0.262,0.258,0.274,0.274,0.276,0.280,0.284,0.282,0.295,0.292,0.292,0.29,0.294,0.292/

 !...Cardiac output during lactation (QCC, L/h/kg) (Hanwell & Linzell, 1973, changing pattern; and Dowell, 1997 GD0=adult)
 TABLE DQCC,1,7/0.,0.5,2.5,4.5,9.5,14.5,21.5,29.5,29.5,35.8,40.4,39.6,38.7,48.8/

 !...Volume of Mammary gland (Fraction of BW) (Knight et al., 1984)
 ! GD22 = PND0 from gestation model, 4.9% of true BW (without fetus & placenta)
 ! Changing pattern deduced by using Wistar data in Hanwell & Linzell based on GD22 = PND0 VMC
 TABLE DVMC,1,7/0.,0.5,2.5,4.5,9.5,14.5,21.5,0.049,0.049,0.042,0.044,0.049,0.054,0.054/
```

```
!...Volume of liver (fraction of BW) (Hanwell & Linzell, 1973)
!...GD21=PND0 from gestation model, 3.7% of true BW (without fetus & placenta)
!changing pattern deduced by using Wistar data in Hanwell & Linzell based on GD21=PND0 VLC
TABLE DVLC,1,7/0.,0.5,2.5,4.5,9.5,14.5,21.5,0.0376,0.0376,0.0396,0.0425,0.0475,0.0515,0.0524/

!...Volume of kidney (fraction of BW) (Hanwell & Linzell, 1973)
!...GD22=PND0 from gestation model, 0.73% of true BW (without fetus & placenta)
!..changing pattern deduced by using Wistar data in Hanwell & Linzell based on GD22=PND0 VKC
TABLE DVKC,1,7/0.,0.5,2.5,4.5,9.5,14.5,21.5,0.0073,0.0073,0.0077,0.0084,0.008,0.0086,0.008/

! ...Volume of fat (fraction of BW) from Naismith, et al., 1982.
TABLE DVFatC,1,3/0.,2.,16.,0.1245,0.152,0.07/

!...Blood flow to mammary gland (Fraction of QC) (Hanwell & Linzell, 1973)
!...GD22=PND0 from gestation model--~1% of QC
TABLE DQMC,1,6/0.5,2.5,4.5,9.5,14.5,21.5,0.09,0.11,0.10,0.12,0.14,0.13/

!...Blood flow to liver (fraction of QC) (Hanwell & Linzell, 1973)
! GD21=PND0 value, Wistar pattern adopted
TABLE DQLC,1,7/0.,0.5,2.5,4.5,9.5,14.5,21.5,0.2408,0.2408,0.2328,0.2408,0.293,0.3492,0.3853/

!...Blood flow to kidney (fraction of QC) (Hanwell & Linzell, 1973)
!Initial QKC = 0.141 based on adult SD rat, changing pattern during lactation follows Wistar rat
TABLE DQKC,1,7/0.,0.5,2.5,4.5,9.5,14.5,21.5,0.141,0.141,0.1646,0.1483,0.1424,0.1297,0.1008/

  !...Milk suckling rate (L/h/kg BWpup) (Yoon et al., 2007 + Mirfazelian 2007)
 TABLE
DKLacC,1,17/2.,6.,7.,8.,9.,10.,11.,12.,13.,14.,15.,16.,17.,18.,19.,20.,21.,0.0216,0.0155,0.0144,0.0144,0.0144,0.0144,0.0144,0.0134,0.
0134,0.0134,0.0134,0.0134,0.0119,0.0111,0.0107,0.0096,0.0073/

!...Constants for BW curve for SD rat pup (Mirfazaelian et al., 2007)
CONSTANT Wt0bw = 0.00674640!0.0067526 (Yoon 2009)  ! GD22 BW = BW at birth
```

```
CONSTANT Kbw = 71.47
CONSTANT rbw = 2.02
CONSTANT Wtmaxbw = 0.60411950

!...Constants for Brain growth (Mirfazaelian et al., 2007)
CONSTANT Wt0brain = 0.00020901      ! GD22 = 0.00022445 = Brain weight at birth (kg), Yoon et al., 2009
CONSTANT Kbrain = 12.26             ! PND at half maximal growth (days)
CONSTANT rbrain = 1.55              ! Hill coefficient
CONSTANT Wtmaxbrain = 0.00205933    ! Maximal brain weight (kg)

!...Constants for liver growth (Mirfazaelian et al., 2007)
CONSTANT Wt0liver = 0.00033933      ! GD22 = 0.00029644 = liver weight at birth (kg), Yoon et al., 2009
CONSTANT Kliver = 45.70             ! PND at half maximal growth (days)
CONSTANT rliver = 2.82              ! Hill coefficient
CONSTANT Wtmaxliver = 0.01595805    ! Maximal liver weight (kg)

!...Constants for kidney growth (Mirfazaelian et al., 2007)
CONSTANT Wt0kidney = 0.00007503     ! kidney weight at birth (kg)
CONSTANT Kkidney = 70.07            ! PND at half maximal growth (days)
CONSTANT rkidney = 2.36             ! Hill coefficient
CONSTANT Wtmaxkidney = 0.00388297   ! Maximal kidney weight (kg)
!...Constants for QC for SD rat pups (Rodriguez et al., 2007)
CONSTANT QCmax = 8.72               ! L/h
CONSTANT BW50 = 0.189               ! kg BWpup

!...Blood flow to pup brain (fraction of QCpup) (Stulcova 1977)
! Adult QBRNC=0.02 was put as PND80 to prevent continuous increase in Table function
TABLE DQBRCpup,1,7/9.,18.,25.,42.,64.,80.,200.,0.093,0.085,0.049,0.034,0.046,0.02,0.02/

!...Blood flow to pup liver (fraction of QCpup) (Stulcova 1977)
! Adult QLC=0.2408 was put as PND80 to prevent negative slope in Table function
TABLE DQLCpup,1,8/0.,9.,18.,25.,42.,64.,80.,200.,0.045,0.199,0.235,0.188,0.186,0.128,0.2408,0.2408/
```

```
!...Blood flow to pup kidney (fraction of QCpup) (Stulcova 1977)
! Adult QKC=0.141 was put as PND80 to prevent negative slope in Table function
TABLE DQKCpup,1,8/0.,9.,18.,25.,42.,64.,80.,200.,0.015,0.0364,0.0571,0.0769,0.088,0.0764,0.141,0.141/

!...Neonatal metabolism rate factor (neonatal liver P450 content compared to adult level)
TABLE DKneomet, 1,10/0.,5.,6.,7.,10.,20.,30.,45.,60.,90.,&
0.34,0.65,0.67,0.67,0.66,0.79,0.88,1.18,1,0.99/

!...Neonatal metabolism rate factor (neonatal liver P450 activity compared to female adult level)
TABLE DKneomet2, 1,16/0.,2.5,5.,7.,10.5,13.,17.,21.,24.,25.,26.,35.,50.,60.,90.,124.,&
0.24,0.23,0.23,0.23,0.24,0.23,0.28,0.37,0.53,0.76,0.9,1.02,1.,1.,0.99,0.99/

!!...Physiological parameters for dam
!...Factional blood flows (Fraction of QC of dam, Brown et al., 1997)
CONSTANT PNBW = 0.257       ! from gestation model, GD21 BW-placenta-fetuses
CONSTANT QBRC = 0.02        ! Fraction of blood flow to brain (Brown et al., 1997, Table 23)

!...Fractional tissue volumes (Fraction of BW, Brown et al., 1997)
CONSTANT VbloodC = 0.074    ! Blood from GD21 value for PNBW, Yoon et al., 2009 (0.074, Brown et al., 1997, Table 21)
CONSTANT VplasmaC = 0.047   ! Clewell et al., 2003, Brown et al., 1997, Altman and Dittmer, 1971
CONSTANT VrbcC = 0.027      ! 0.0274, Clewell et al., 2003, Brown et al., 1997, Altman and Dittmer, 1971
CONSTANT VBRC = 0.0057      ! Brain GD21 fraction of PNBW, Yoon et al., 2009 (0.0057, Brown et al., 1997, Table 4)
CONSTANT Vmilk = 0.002      ! volume of milk compartment (L); Fisher 1990
CONSTANT QFatC = 0.07       ! fractional blood flow to fat

!!...Physiological parameters for pups
CONSTANT N = 12
!...Fractional tissue volume (fraction of BWpup)
CONSTANT Vbloodcpup = 0.074    ! Brown et al., 1997, Table 21 (0.0676 Yoon et al., 2009)
CONSTANT VplasmaCpup = 0.047   ! Clewell et al., 2003, Brown et al., 1997, Altman and Dittmer, 1971
CONSTANT VrbcCpup = 0.027      ! 0.0274, Clewell et al., 2003, Brown et al., 1997, Altman and Dittmer, 1971
```

```
!!!...Chemical specific parameters
!!...Dam chemical specific parameters
!!...Partition coefficients for Dam
!...PCs for ATR, unitless (All these PC values are the same as those in gestation model.)
CONSTANT PL = 0.69   ! Liver: blood PC, Tremblay et al., 2012
CONSTANT PBR = 0.73  ! Brain: blood PC, Tremblay et al., 2012
CONSTANT PK = 1      ! Kidney: blood PC, McMullin et al., 2007
CONSTANT PM = 5      ! Mammry gland: blood PC, McMullin et al., 2007
CONSTANT Poth = 1    ! Remaining tissues: blood PC, McMullin et al., 2007

!...PCs for DE, unitless (All these PC values are the same as those in gestation model.)
CONSTANT PL1 = 1       ! Liver: blood PC, McMullin et al., 2007
CONSTANT PBR1 = 0.5    ! Brain: blood PC, estimated by fitting to Fraites et al., 2011
CONSTANT PK1 = 1       ! Kidney: blood PC, McMullin et al., 2007
CONSTANT PM1 = 1       ! Mammry gland: blood PC, McMullin et al., 2007
CONSTANT Poth1 = 1     ! Remaining tissues: blood PC, McMullin et al., 2007

!...PCs for DIP, unitless (All these PC values are the same as those in gestation model.)
CONSTANT PL2 = 1       ! Liver: blood PC, McMullin et al., 2007
CONSTANT PBR2 = 0.5    ! Brain: blood PC, estimated by fitting to Fraites et al., 2011
CONSTANT PK2 = 1       ! Kidney: blood PC, McMullin et al., 2007
CONSTANT PM2 = 1       ! Mammry gland: blood PC, McMullin et al., 2007
CONSTANT Poth2 = 1     ! Remaining tissues: blood PC, McMullin et al., 2007

!...PCs for DACT, unitless (All these PC values are the same as those in gestation model.)
CONSTANT PL3 = 1       ! Liver: blood PC, McMullin et al., 2007
CONSTANT PBR3 = 0.9    ! Brain: blood PC, estimated by fitting to Fraites et al., 2011
CONSTANT PK3 = 1       ! Kidney: blood PC, McMullin et al., 2007
CONSTANT PM3 = 0.8     ! Mammry gland: blood PC, estimated by fitting to Fraites et al., 2011
CONSTANT Poth3 = 1     ! Remaining tissues: blood PC, McMullin et al., 2007
```

```
!...Metabolic constants for ATR for dam, ATR to DE
CONSTANT VmaxcATR_DE = 35925.3264 !ug/h/kg^0.75, Maximum velocity of metabolism of ATR to DE, scalable by (BW)^0.75, in vivo = 3-fold in vitro, original in vitro data see Hanioka et al., 1999.
CONSTANT KmATR_DE = 9598.205      !ug/l, 44.5 umol/l, Michaelis-Menten constant, Hanioka et al., 1999

!...Metabolic constants for ATR for dam, ATR to DIP
CONSTANT VmaxcATR_DIP = 388265.6181!ug/h/kg^0.75, Maximum velocity of metabolism of ATR to DIP, scalable by (BW)^0.75, in vivo = 3-fold in vitro, original in vitro data see Hanioka et al., 1999.
CONSTANT KmATR_DIP = 10870.776     !ug/l, 50.4 umol/l, Michaelis-Menten constant, Hanioka et al., 1999

!...Metabolic constants for DE to DACT
CONSTANT Vmaxc1 = 2626.820     !ug/h/kg^0.75, Maximum velocity of metabolism of DE to DACT, scalable by (BW)^0.75, in Lin et al., 2011
CONSTANT Km1 = 2439.190       !ug/l, 13 umol/l, Michaelis-Menten constant, rat in vitro value, in McMullin et al., 2007

!...Metabolic constants for DIP to DACT
CONSTANT Vmaxc2 = 7291.200     !ug/h/kg^0.75, Maximum velocity of metabolism of DIP to DACT, scalable by (BW)^0.75, in Lin et al., 2011
CONSTANT Km2 = 2256.800       !ug/l, 13, umol/l, Michaelis-Menten constant, rat in vitro value, in McMullin et al., 2007

!!...Parameters for plasma, red blood cells, brain tissue binding, association/disociation rate constant and maximal binding capacity
!...Dam, ATR and plasma, bound ATR account for 26% (18% - 37%) of the total plasma ATR, Lu et al., 1998
CONSTANT KaATRplasma = 0.05       !/(ug*h), ATR and plasma protein (Albumin) second order association rate constant, in Lin et al., 2011
CONSTANT KdATRplasma = 1          !h-1, ATR-plasma protein complex first order dissociation rate constant, in Lin et al., 2011
CONSTANT BMaxplasmac = 601.7751   !ug/l or ug/kg, maximal binding capacity of ATR with plasma protein, Lin et al., 2011

!...Dam, ATR and red blood cells, based on McMullin et al., 2003, 1.5% of total chlorotriazine was bound to red blood cells.
CONSTANT KaATRrbc = 0.01          !/(ug*h), ATR and red blood cell (hemoglobin) second order association rate constant, in Lin et al., 2011
CONSTANT KdATRrbc = 1             !h-1, ATR-RBC complex first order dissociation rate constant, Lin et al., 2011
CONSTANT BMaxrbcc = 12725.710     !ug/l or ug/kg, maximal binding capacity of ATR with red blood cells, Lin et al., 2011
```

```
 !...Dam, ATR and brain
 CONSTANT KaATRbrain = 0.6        !/(ug*h), ATR and brain tissue second order association rate constant.
 CONSTANT KdATRbrain = 1          !h-1, ATR-brain tissue protein complex first order dissociation rate constant.
 CONSTANT BMaxbrainc = 284.7108   !ug/l or ug/kg, maximal binding capacity of ATR with brain tissue protein.

 !...Dam, DACT and plasma, set DACT similar binding property as ATR, bound ATR account for 26% (18% - 37%) of the total plasma ATR, Lu et al., 1998
 CONSTANT KaDACTplasma = 0.002       !/(ug*h), DACT and plasma protein (Albumin) second order association rate constant, Lin et al., 2011
 CONSTANT KdDACTplasma = 1           !h-1, DACT-plasma protein complex first order dissociation rate constant
 CONSTANT BMaxplasmac3 = 15974.84025 !ug/l or ug/kg, maximal binding capacity of DACT with plasma protein, Lin et al., 2011

 !...Dam, DACT and red blood cells, based on McMullin et al., 2003, 1.5% of total chlorotriazine was bound to red blood cells.
 CONSTANT KaDACTrbc = 0.0002         !/(ug*h), DACT and red blood cell (hemoglobin) second order association rate constant, in Lin et al., 2011
 CONSTANT KdDACTrbc = 1              !h-1, DACT-RBC complex first order dissociation rate constant
 CONSTANT BMaxrbcc3 = 1228296.450    !ug/l or ug/kg, maximal binding capacity of DACT with red blood cells, Lin et al., 2011

 !...Dam, DACT and brain
 CONSTANT KaDACTbrain = 0.02         !/(ug*h), DACT and brain tissue second order association rate constant.
 CONSTANT KdDACTbrain = 1            !h-1, DACT-brain tissue protein complex first order dissociation rate constant.
 CONSTANT BMaxbrainc3 = 7503.1025    !ug/l or ug/kg, maximal binding capacity of DACT with brain tissue protein.

 !...Urine elimination rate constants of metabolites in the dam
 CONSTANT Kurine1C = 1         !/(h*kg^(+0.75)), First order urinary elimination rate constant for DE,
 CONSTANT Kurine2C = 0.5       !/(h*kg^(+0.75)), First order urinary elimination rate constant for DIP,
 CONSTANT Kurine3C = 14        !/(h*kg^(+0.75)), First order urinary elimination rate constant for DACT,

 !...Oral absorption rate constants of ATR in the dam
 CONSTANT K1C = 0.2          !kg^0.25/h, gastric absorption rate constant
 CONSTANT K2C = 0.7          !kg^0.25/h, gastric intestinal transfer rate constant
```

```
CONSTANT K3C = 0.018        !kg^0.25/h, intestinal absorption rate constant
CONSTANT K4C = 0.006        !kg^0.25/h, fecal elimination rate constant

!!...Molecular weight
CONSTANT MWATR = 215.69       ! Molecular weight of ATR, g/mol
CONSTANT MWDE = 187.63        ! Molecular weight of DE, g/mol
CONSTANT MWDIP = 173.6        ! Molecular weight of DIP, g/mol
CONSTANT MWDACT = 145.55      ! Molecular weight of DACT, g/mol

!!..Conversion ratios for metabolites
ATR_DE = MWDE/MWATR
ATR_DIP = MWDIP/MWATR
DE_DACT = MWDACT/MWDE
DIP_DACT = MWDACT/MWDIP

!...Initial tissue and blood amounts of ATR and its metabolites in dam, ug, will be from gestation model
CONSTANT APlasmaFree0 = 0
CONSTANT APlasmabound0 = 0
CONSTANT ARBCbound0 = 0
CONSTANT Cplasma0 = 0
CONSTANT AL0 = 0
CONSTANT ABRfree0 = 0
CONSTANT ABrainbound0 = 0
CONSTANT AK0 = 0
CONSTANT Aoth0 = 0
CONSTANT AM0 = 0
CONSTANT Ablood10 = 0
CONSTANT AL10 =0
CONSTANT ABR10 = 0
CONSTANT AK10 = 0
CONSTANT Aoth10 = 0
CONSTANT AM10 = 0
```

```
CONSTANT Ablood20 = 0
CONSTANT AL20 = 0
CONSTANT ABR20 = 0
CONSTANT AK20 = 0
CONSTANT Aoth20 = 0
CONSTANT AM20 = 0
CONSTANT APlasmaFree30 = 0
CONSTANT APlasmabound30 = 0
CONSTANT ARBCbound30 = 0
CONSTANT Cplasma30 = 0
CONSTANT AL30 = 0
CONSTANT ABRfree30 = 0
CONSTANT Abrainbound30 = 0
CONSTANT AK30 = 0
CONSTANT Aoth30 = 0
CONSTANT AM30 = 0

!...Calculation of initial tissue and blood amounts
Ablood0 = APlasmaFree0+APlasmabound0+ARBCbound0
ABR0 = ABRfree0+ABrainbound0
Ablood30 = APlasmaFree30+APlasmabound30+ARBCbound30
ABR30 = ABRfree30+Abrainbound30

!...Lactational transfer constant
CONSTANT KmilkC = 0.0035      ! Milk clearance for ATR (L/h/kg^0.75)
CONSTANT Kmilk1C = 0.0035     ! Milk clearance for DE (L/h/kg^0.75)
CONSTANT Kmilk2C = 0.0035     ! Milk clearance for DIP (L/h/kg^0.75)
CONSTANT Kmilk3C = 0.0035     ! Milk clearance for DACT (L/h/kg^0.75)

!...Chemical specific parameters for pups
!...fractional absorption via milk, 82% of oral dose was absorbed in adults. (Bakke et al., 1972; Timchalk et al., 1990)
CONSTANT Frac = 1    ! (Xu, 1996)
```

```
  !...Partition coefficients for pups
  !...PCs for ATR in the pups, unitless (All these PC values for the pups are same as those for the dams.)
  CONSTANT PLpup = 0.69  ! Liver: blood PC, same as that in the dams
  CONSTANT PBRpup = 0.73 ! Brain: blood PC, same as that in the dams
  CONSTANT PKpup = 1     ! Kidney: blood PC, same as that in the dams
  CONSTANT PMpup =  5    ! Mammry gland: blood PC, same as that in the dams
  CONSTANT Pothpup = 1   ! Remaining tissues: blood PC, same as that in the dams

  !...PCs for DE in the pups, unitless (All those PC values for the pups are same as those for the dams.)
  CONSTANT PL1pup = 1      ! Liver: blood PC, same as that in the dams
  CONSTANT PBR1pup = 0.5   ! Brain: blood PC, same as that in the dams
  CONSTANT PK1pup = 1      ! Kidney: blood PC, same as that in the dams
  CONSTANT PM1pup = 1      ! Mammry gland: blood PC, same as that in the dams
  CONSTANT Poth1pup = 1    ! Remaining tissues: blood PC, same as that in the dams

  !...PCs for DIP in the pups, unitless (All those PC values for the pups are same as those for the dams, which are from AUC method
based on the lowest dose dataset - 5 mg/kg.)
  CONSTANT PL2pup = 1       ! Liver: blood PC, same as that in the dams
  CONSTANT PBR2pup = 0.5    ! Brain: blood PC, same as that in the dams
  CONSTANT PK2pup = 1       ! Kidney: blood PC, same as that in the dams
  CONSTANT PM2pup = 1       ! Mammry gland: blood PC, same as that in the dams
  CONSTANT Poth2pup = 1     ! Remaining tissues: blood PC, same as that in the dams

  !...PCs for DACT in the pups, unitless (All those PC values for the pups are same as those for the dams, which are from AUC method
based on the lowest dose dataset - 5 mg/kg.)
  CONSTANT PL3pup = 1       ! Liver: blood PC, same as that in the dams
  CONSTANT PBR3pup = 0.9    ! Brain: blood PC, same as that in the dams
  CONSTANT PK3pup = 1       ! Kidney: blood PC, same as that in the dams
  CONSTANT PM3pup = 0.8     ! Mammry gland: blood PC, same as that in the dams
  CONSTANT Poth3pup = 1     ! Remaining tissues: blood PC, same as that in the dams
```

!...Metabolic constants for ATR for pups, ATR to DE
CONSTANT KmATR_DEpup = 9598.205 !ug/l, 44.5 umol/l, Michaelis-Menten constant, Hanioka et al., 1999, set same as dam's

!...Metabolic constants for ATR for pups, ATR to DIP
CONSTANT KmATR_DIPpup = 10870.776 !ug/l, 50.4 umol/l, Michaelis-Menten constant, Hanioka et al., 1999, set same as dam's

!...Metabolic constants for pups, DE to DACT
CONSTANT Km1pup = 2439.190 !ug/l, 13 umol/l, Michaelis-Menten constant, rat in vitro value, in McMullin et al., 2007, set same as dam's

!...Metabolic constants for pups, DIP to DACT
CONSTANT Km2pup = 2256.800 !ug/l, 13 umol/l, Michaelis-Menten constant, rat in vitro value, in McMullin et al., 2007, set same as dam's

!!...(Pup), Parameters for plasma, red blood cells, brain tissue binding, association/disociation rate constant and maximal binding capacity
!...Pup, ATR and plasma, bound ATR account for 26% (18% - 37%) of the total plasma ATR in adult, Lu et al., 1998, set same as that in adult
CONSTANT KaATRplasmaPup = 0.05 !/(ug*h), ATR and plasma protein (Albumin) second order association rate constant, set same as that in adult
CONSTANT KdATRplasmaPup = 1 !h-1, ATR-plasma protein complex first order dissociation rate constant, set same as that in adult
CONSTANT BMaxplasmacPup = 601.7751!ug/l or ug/kg, maximal binding capacity of ATR with plasma protein, set same as that in adult

!...(Pup), ATR and red blood cells, based on McMullin et al., 2003, 1.5% of total chlorotriazine was bound to red blood cells.
CONSTANT KaATRrbcPup = 0.01 !/(ug*h), ATR and red blood cell (hemoglobin) second order association rate constant, set same as that in adult
CONSTANT KdATRrbcPup = 1 !h-1, ATR-RBC complex first order dissociation rate constant, set same as that in adult
CONSTANT BMaxrbccPup = 12725.710 !ug/l or ug/kg, maximal binding capacity of ATR with red blood cells, set same as that in adult

!...(Pup), ATR and brain
CONSTANT KaATRbrainPup = 0.6 !/(ug*h), ATR and brain tissue second order association rate constant, set same as that in adult.
CONSTANT KdATRbrainPup = 1 !h-1, ATR-brain tissue protein complex first order dissociation rate constant, set same as that in adult
CONSTANT BMaxbraincPup = 284.7108 !ug/l or ug/kg, maximal binding capacity of ATR with brain tissue protein, set same as that in adult.

!...(Pup), DACT and plasma, set DACT similar binding property as ATR, bound ATR account for 26% (18% - 37%) of the total plasma ATR in the adult, Lu et al., 1998, set same as that in adult
CONSTANT KaDACTplasmaPup = 0.002 !/(ug*h), DACT and plasma protein (Albumin) second order association rate constant, set same as that in adult
CONSTANT KdDACTplasmaPup = 1 !h-1, DACT-plasma protein complex first order dissociation rate constant, set same as that in adult
CONSTANT BMaxplasmac3Pup = 15974.84025 !ug/l or ug/kg, maximal binding capacity of DACT with plasma protein, set same as that in adult

!...(Pup), DACT and red blood cells, based on McMullin et al., 2003, 1.5% of total chlorotriazine was bound to red blood cells.
CONSTANT KaDACTrbcPup = 0.0002 !/(ug*h), DACT and red blood cell (hemoglobin) second order association rate constant, set same as that in adult
CONSTANT KdDACTrbcPup = 1 !h-1, DACT-RBC complex first order dissociation rate constant, set same as that in adult
CONSTANT BMaxrbcc3Pup = 1228296.450 !ug/l or ug/kg, maximal binding capacity of DACT with red blood cells, set same as that in adult

!...(Pup), DACT and brain
CONSTANT KaDACTbrainPup = 0.02 !/(ug*h), DACT and brain tissue second order association rate constant, set same as that in adult.
CONSTANT KdDACTbrainPup = 1 !h-1, DACT-brain tissue protein complex first order dissociation rate constant,set same as that in adult
CONSTANT BMaxbrainc3Pup = 7503.1025 !ug/l or ug/kg, maximal binding capacity of DACT with brain tissue protein, set same as that in adult.

```
!...Elimination constants of metabolites in the pup
CONSTANT Kurine1CPup = 1      !/(h*kg^(+0.75)),First order urinary elimination rate constant for DE,
CONSTANT Kurine2CPup = 0.5    !/(h*kg^(+0.75)),First order urinary elimination rate constant for DIP,
CONSTANT Kurine3CPup = 14     !/(h*kg^(+0.75)),First order urinary elimination rate constant for DACT,

!...Calculation for pup initial condition
!...Initial tissue concentrations of ATR and its metabolites in pup (ug/kg or ug/l) on GD22 = PND0 from gestation model
CONSTANT Cfetus0 = 0
CONSTANT Cfetusfree0 = 0
CONSTANT Cfetusbound0 = 0
CONSTANT Cfetus10 = 0
CONSTANT Cfetus20 = 0
CONSTANT Cfetus30 = 0
CONSTANT Cfetusfree30 = 0
CONSTANT Cfetusbound30 = 0
CONSTANT Cbloodfetus0 = 0
CONSTANT Cbloodfetus10 = 0
CONSTANT Cbloodfetus20 = 0
CONSTANT Cbloodfetus30 = 0

!...Initial tissue amount of ATR and its metabolites in pup (ug/kg or ug/l) on GD22 = PND0 from gestation model
APlasmaFreepup0 = Cbloodfetus0*Vplasmapup*0.74
APlasmaboundpup0 = Cbloodfetus0*Vplasmapup*0.26
ARBCboundpup0 = Cbloodfetus0*Vrbcpup
Cplasmapup0 = Cbloodfetus0

ALpup0 = Cfetus0*Wt0liver
ABRpup0 = Cfetus0*Wt0brain
ABRfreepup0 = Cfetusfree0*Wt0brain
Abrainboundpup0 = Cfetusbound0*Wt0brain
AKpup0 = Cfetus0*Wt0kidney
Aothpup0 = Cfetus0*(Wt0BW-Wt0liver-Wt0brain-Wt0kidney)
```

```
Ablood1pup0 = Cbloodfetus10*Vbloodcpup*Wt0BW
AL1pup0 = Cfetus10*Wt0liver
ABR1pup0 = Cfetus10*Wt0brain
AK1pup0 = Cfetus10*Wt0kidney
Aoth1pup0 = Cfetus10*(Wt0BW-Wt0liver-Wt0brain-Wt0kidney)

Ablood2pup0 = Cbloodfetus20*Vbloodcpup*Wt0BW
AL2pup0 = Cfetus20*Wt0liver
ABR2pup0 = Cfetus20*Wt0brain
AK2pup0 = Cfetus20*Wt0kidney
Aoth2pup0 = Cfetus20*(Wt0BW-Wt0liver-Wt0brain-Wt0kidney)

APlasmaFree3pup0 = Cbloodfetus30*Vplasmapup*0.74
APlasmabound3pup0 = Cbloodfetus30*Vplasmapup*0.26
ARBCbound3pup0 = Cbloodfetus30*Vrbcpup
Cplasma3pup0 = Cbloodfetus30

AL3pup0 = Cfetus30*Wt0liver
ABR3pup0 = Cfetus30*Wt0brain
ABRfree3pup0 = Cfetusfree30*Wt0brain
ABrainbound3pup0 = Cfetusbound30*Wt0brain
AK3pup0 = Cfetus30*Wt0kidney
Aoth3pup0 = Cfetus30*(Wt0BW-Wt0liver-Wt0brain-Wt0kidney)

 !!!...Dosing, multiple oral gavage
  CONSTANT TSTOP = 22.         ! End simulation (hs)
  CONSTANT tlen = 0.001        ! Length of oral gavage exposure (h/day)
  CONSTANT DGAV = 5000           ! Oral gavage dose (mg/kg)

  CONSTANT Dstart = 0.         ! Initiation day of oral gavage (day)
  CONSTANT Dstop = 11.         ! Termination day of oral gavage (day)
```

```
  CONSTANT MAXT = 1.          ! maximum comm. interval
  CONSTANT CINTC = 0.1        ! Communication interval
  CINT = CINTC                ! Communication interval
  CONSTANT GDexpday = 8       ! the number of days exposed to ATR during gestation
  Tsim = TSTOP*24             ! Tstop in (hours)
  DS = Dstart*24              ! Initiation time point of oral gavage (h)
  Doff = (Dstop - Dstart)*24  ! Oral gavage duration (h)

  !...Initials
  Daily = 0.0
  Exposure = 0.0

  WEAN = 0.0         ! Weaning

  QCAP = 0.
  QDEC = 0.
END ! INITIAL


      DYNAMIC

            ALGORITHM IALG = 2
            NSTEPS    NSTP = 10
            MAXTERVAL MAXT = 1.0e9
            MINTERVAL MINT = 1.0e-9
            CINTERVAL CINT = 0.1

            DERIVATIVE
                  ! code for calulating the derivative goes here
  !...ATR oral gavage to dam
  DOSE = DGAV*BW
  Exposure = PULSE(0,24,tlen)*PULSE(DS,Tsim,Doff)
```

```
RDOSE = (Dose/tlen)*Exposure            ! Rate of oral dosing (ug/h)
RAST = RDOSE-K2*AST-K1*AST
AST = Integ(RAST,0.0)
RAI = K2*AST-K3*AI-K4*AI
AI = Integ(RAI,0.0)
RAO = K1*AST+K3*AI
AAO = Integ(RAO,0.0)
RAfecal = K4*AI
Afecal  = INTEG(RAfecal,0)

PND = T/24
!...ATR and its metabolite uptake to the individual pup
Rmilkpup = Frac*Rmilk/N          ! ATR Milk dose (ug/h, individual pup)
Rmilk1pup = Frac*Rmilk1/N        ! DE Milk dose (ug/h, individual pup)
Rmilk2pup = Frac*Rmilk2/N        ! DIP Milk dose (ug/h, individual pup)
Rmilk3pup = Frac*Rmilk3/N        ! DACT Milk dose (ug/h, individual pup)

D = T/24

PROCEDURAL

!...Dam

BW = DBW(D)       ! Dam BW (kg), Shirley
BW0 = DBW(0.0)    ! Dam BW on PND0

QCC = DQCC(D)     ! Dam QCC (L/h/kg)
QCC0 = DQCC(0.0)

QMC = DQMC(D)     ! fractional blood flow to mammary gland
VMC = DVMC(D)     ! Mammary gland volume scalar
```

```
QLC = DQLC(D)     ! Fractional blood flow to liver
VLC = DVLC(D)     ! Liver volume

QKC = DQKC(D)     ! Fractional blood flow to kidney
VKC = DVKC(D)     ! Kidney volume (L)

KLacC = DKLacC(D) ! milk production/suckling rate (L/h/kg BWpup)

Kneomet = DKneomet(D)   ! fractional neonatal metabolism rate to adult level, enzyme expression
Kneomet2 = DKneomet2(D) ! fractional neonatal metabolism rate to adult level, enzyme activity

!...Pup
QBRCpup = DQBRCpup(D)  ! Fractional blood flow to pup brain
QLCpup = DQLCpup(D)    ! Fractional blood flow to pup liver
QKCpup = DQKCpup(D)    ! Fractional blood flow to pup kidney

END  ! of Procedural

!...Changing values, pup
BWpup = (Wt0bw*Kbw**rbw+Wtmaxbw*((D)**rbw))/(Kbw**rbw+((D)**rbw))       ! Individual Pup BW (kg)
BWpup0 = (Wt0bw*Kbw**rbw+Wtmaxbw*((0.)**rbw))/(Kbw**rbw+((0.)**rbw))    ! Individual Pup BW (kg)
KLac = KLacC*BWpup*N    ! Daily milk production rate for a litter (L/h)

QCpup = (QCmax*BWpup/(BW50+BWpup))    ! Rodriguez et al., 2007

VLpup = (Wt0liver*Kliver**rliver+Wtmaxliver*((D)**rliver))/(Kliver**rliver+((D)**rliver)) !Individual pup liver (kg)
VBRpup = (Wt0brain*Kbrain**rbrain+Wtmaxbrain*((D)**rbrain))/(Kbrain**rbrain+((D)**rbrain))!Individual pup brain (Kg)
VKpup  =  (Wt0kidney*Kkidney**rkidney+Wtmaxkidney*((D)**rkidney))/(Kkidney**rkidney+((D)**rkidney))  !Individual  pup
kidney (Kg)

!...Scaled parameters for Dam
QC = QCC*BW                 ! Cardiac output (L/h)
```

```
QC0 = QCC0*PNBW
QL = QLC*QC                  ! Liver blood flow (L/h)
QM = QMC*QC                   ! Mammary blood flow (L/h)
QBR = QBRC*QC                  ! Brain blood flow (L/h)
QK = QKC*QC                  ! Kidney blood flow (L/h)
Qoth = QC-QL-QM-QBR-QK        ! Other tissue blood flow (L/h)
PAmilk = PAmilkC*(BWpup**0.75)*N
PAmilk1 = PAmilk1C*(BWpup**0.75)*N
PAmilk2 = PAmilk2C*(BWpup**0.75)*N
PAmilk3 = PAmilk3C*(BWpup**0.75)*N

Vblood = Vbloodc*BW
Vplasma = Vplasmac*BW
Vrbc = VrbcC*BW
VM = VMC*BW
VL = VLC*BW
VK = VKC*BW
VBR = VBRC*PNBW        ! Keep constant brain volume
Voth = BW-VM-VBR-VL-VK  ! Other tissue volume (L)

!...Blood flow and volume balance for dam
Qbal = QC-QL-QBR-QK-QM-Qoth ! Mass balance for blood flow (should be 0)
Vbal = BW-VBR-VL-VK-VM-Voth ! Mass balance for tissue (should be 0)

!...Scaled parameters
!...First order absorption and fecal elimination rate constants
K1 = K1C/BW^0.25
K2 = K2C/BW^0.25
K3 = K3C/BW^0.25
K4 = K4C/BW^0.25
K1pup = K1C/BWpup^0.25
K2pup = K2C/BWpup^0.25
```

```
K3pup = K3C/BWpup^0.25
K4pup = K4C/BWpup^0.25

!...metabolic parameters in the dam
! Lots of evidence show ATR exposure induces total P450 content and P450 enzyme activity. Increased expression of specific enzyme has been shown to increase metabolism of ATR.
Dexp = GDexpday+PND+1-Dstart ! The number of days exposed to ATR
Kincreasefactor1 = 1
Kincreasefactor2 = 1
IF (Dexp.LT.2) THEN
Kincreasefactor = 0.0
ELSE IF ((Dexp.GE.2).AND.(Dexp.LE.11)) THEN
Kincreasefactor = 0.4*(Dexp-1)
ELSE IF (Dexp.GT.11) THEN
Kincreasefactor = 4.0
END IF

VmaxcATR_DE_current = VmaxcATR_DE+VmaxcATR_DE*Kincreasefactor
VmaxcATR_DIP_current = VmaxcATR_DIP+VmaxcATR_DIP*Kincreasefactor
Vmaxc1_current = Vmaxc1*(1+Kincreasefactor1)
Vmaxc2_current = Vmaxc2*(1+Kincreasefactor2)

VmaxATR_DE = VmaxcATR_DE_current*BW**0.75
VmaxATR_DIP = VmaxcATR_DIP_current*BW**0.75
VmaxDEDACT = Vmaxc1_current*BW**0.75          ! ug/h,(umol/h), maximum velocity of metabolism of DE to DACT,
VmaxDIPDACT = Vmaxc2_current*BW**0.75         ! ug/h,(umol/h), maximum velocity of metabolism of DIP to DACT,

!...urine elimination parameters in the dam
Kurine1 = Kurine1C*(BW**(+0.75))
Kurine2 = Kurine2C*(BW**(+0.75))
Kurine3 = Kurine3C*(BW**(+0.75))
```

```
!...plasma, red blood cell, brain protein binding parameters for the dam
BMaxplasma = BMaxplasmac*Vplasma         ! ug, (umol), maximal binding capacity of ATR with plasma protein
BMaxrbc = BMaxrbcc*Vrbc                  ! ug, (umol), maximal binding capacity of ATR with red blood cells
BMaxbrain = BMaxbrainc*VBR               ! ug, (umol), maximal binding capacity of ATR with brain
BMaxplasma3 = BMaxplasmac3*Vplasma       ! ug, (umol), maximal binding capacity of DACT with plasma protein
BMaxrbc3 = BMaxrbcc3*Vrbc                ! ug, (umol), maximal binding capacity of DACT with red blood cells
BMaxbrain3 = BMaxbrainc3*VBR             ! ug, (umol), maximal binding capacity of DACT with brain

Kmilk = KmilkC*(BW**(0.75))              ! ATR Clearance through milk, (L/h)
Kmilk1 = Kmilk1C*(BW**(0.75))            ! DE Clearance through milk, (L/h)
Kmilk2 = Kmilk2C*(BW**(0.75))            ! DIP Clearance through milk, (L/h)
Kmilk3 = Kmilk3C*(BW**(0.75))            ! DACT Clearance through milk, (L/h)

!...Scaled parameters for the pup
QLpup = QLCpup*QCpup                     ! Liver blood flow (L/h)
QBRpup = QBRCpup*QCpup                   ! Brain blood flow (L/h)
QKpup = QKCpup*QCpup                     ! Kidney blood flow (L/h)
Qothpup = QCpup-QLpup-QBRpup-QKpup       ! Other tissue blood flow (L/h)

Vbloodpup = Vbloodcpup*BWpup             ! blood volume (L)
Vplasmapup = Vplasmacpup*BWpup           ! Plasma volume (L)
Vrbcpup = Vrbccpup*BWpup                 ! Red blood cell volume (L)
Vothpup = BWpup-VLpup-VBRpup-VKpup       ! Other tissue volume (L)

!...Blood flow and volume balance for the pup
Qbalpup = QCpup-QLpup-QBRpup-QKpup-Qothpup   ! Mass balance for blood flow for the pup, should be 0
Vbalpup = BWpup-VLpup-VBRpup-VKpup-Vothpup   ! Mass balance for volume for the pup, should be 0

!...metabolic parameters in the pup
KliverR = VLpup/(0.24*0.0366) ! dam liver weight: pup liver weight ratio
VmaxATR_DEpup = VmaxATR_DE*Kneomet*KliverR*Kneomet2   ! ug/h, Maximum velocity of metabolism of ATR to DE,
VmaxATR_DIPpup = VmaxATR_DIP*Kneomet*KliverR*Kneomet2 ! ug/h, Maximum velocity of metabolism of ATR to DIP,
```

```
VmaxDEDACTpup = VmaxDEDACT*Kneomet*KliverR*Kneomet2   ! ug/h, maximum velocity of metabolism of DE to DACT,
VmaxDIPDACTpup = VmaxDIPDACT*Kneomet*KliverR*Kneomet2 ! ug/h, maximum velocity of metabolism of DIP to DACT,

!...plasma, red blood cell, brain protein binding parameters for the pup
BMaxplasmapup = BMaxplasmacpup*Vplasmapup     ! ug, maximal binding capacity of ATR with plasma protein
BMaxrbcpup = BMaxrbccpup*Vrbcpup              ! ug, maximal binding capacity of ATR with red blood cells
BMaxbrainpup = BMaxbraincpup*VBRpup           ! ug, maximal binding capacity of ATR with brain
BMaxplasma3pup = BMaxplasmac3pup*Vplasmapup   ! ug, maximal binding capacity of DACT with plasma protein
BMaxrbc3pup = BMaxrbcc3pup*Vrbcpup            ! ug, maximal binding capacity of DACT with red blood cells
BMaxbrain3pup = BMaxbrainc3pup*VBRpup         ! ug, maximal binding capacity of DACT with brain

!...urine elimination for the pup
Kurine1pup = Kurine1Cpup*(BWpup**(+0.75))
Kurine2pup = Kurine2Cpup*(BWpup**(+0.75))
Kurine3pup = Kurine3Cpup*(BWpup**(+0.75))

!!!...ATR sub model
!!...model equations for dam
!...ATR in the blood compartment
!...APlasmaFree = Amount of free ATR in plasma (ug)
RAPlasmaFree = QC*(CV-CPlasmaFree)+RARBCunbind-RARBCbind+RAplasmaunbind-RAplasmabind
APlasmaFree = Integ(RAPlasmaFree,APlasmaFree0)
CPlasmaFree = APlasmaFree/Vplasma

!...APlasmabound = Amount of ATR bound to plasma protein (ug)
RAPlasmabound = RAPlasmabind-RAPlasmaunbind
APlasmabound = Integ(RAPlasmabound,APlasmabound0)
CPlasmabound = APlasmabound/Vplasma

!...ARBCbound = Amount of ATR bound to red blood cells (ug)
RARBCbound = RARBCbind-RARBCunbind
ARBCbound = Integ(RARBCbound,ARBCbound0)
```

```
CRBCbound = ARBCbound/VRBC
!...Ablood = Total amount of ATR in the blood compartment (ug)
!...Aplasma = Total amount of ATR in the plasma compartment (ug)
Ablood = APlasmaFree+APlasmabound+ARBCbound
Cblood = Ablood/Vblood
Aplasma = APlasmaFree+Aplasmabound
Cplasma = Aplasma/Vplasma
AUCCplasma = Integ(Cplasma,Cplasma0)

RAplasmabind = KaATRplasma*BMaxPlasmaRemain*AplasmaFree
RAplasmaunbind = KdATRplasma*Aplasmabound
RARBCbind = KaATRrbc*BMaxRBCRemain*AplasmaFree
RARBCunbind = KdATRrbc*ARBCbound

BMaxPlasmaRemain = BMaxPlasma-APlasmabound
BMaxRBCRemain = BMaxRBC-ARBCbound

CV= (CVL*QL+CVBR*QBR+CVK*QK+CVoth*Qoth+CVM*QM)/QC

!...ATR in the liver compartment
!...Total amount of ATR in liver
RL = QL*(CPlasmaFree-CVL)+RAO-RATR_DEmet-RATR_DIPmet
AL = Integ(RL,AL0)
CL = AL/VL
CVL = AL/(VL*PL)

! Metabolism of ATR in liver
RATR_DEmet = VmaxATR_DE*CVL/(KmATR_DE+CVL)          ! Metabolic rate of ATR to DE, ug/h,
AATR_DEmet = Integ(RATR_DEmet,0.0)

RformDE = RATR_DEmet*ATR_DE                         ! Rate of formation of DE from ATR, ug/h
AformDE = Integ(RformDE,0.0)
```

```
RATR_DIPmet = VmaxATR_DIP*CVL/(KmATR_DIP+CVL)       ! Metabolic rate of ATR to DIP, ug/h,
AATR_DIPmet = Integ(RATR_DIPmet,0.0)

RformDIP = RATR_DIPmet*ATR_DIP                    ! Rate of formation of DIP from ATR, ug/h
AformDIP = Integ(RformDIP,0.0)

AATRmet = AATR_DEmet+AATR_DIPmet                  ! Amount of ATR metabolized, ug/h,

!...ATR in brain compartment
!...ABRfree = Amount of ATR  free in brain (ug)
RBRfree = QBR*(CPlasmaFree-CVBR)+KdATRBrain*ABrainbound-KaATRBrain*BMaxBrainRemain*AVBR
ABRfree = Integ(RBRfree,ABRfree0)
CBRfree = ABRfree/VBR
CVBR = ABRfree/(VBR*PBR)
AVBR = ABRfree/PBR

!...ABrainbound = Amount of ATR bound in brain (ug)
RABrainbound = KaATRBrain*BMaxBrainRemain*AVBR-KdATRBrain*ABrainbound
ABrainbound = Integ(RABrainbound,ABrainbound0)
CBrainbound = ABrainbound/VBR

!...BMaxBrainRemain = Remaining binding capacity of brain for ATR (ug)
BMaxBrainRemain = BMaxBrain-ABrainbound

!...ABR = Total amount of ATR in the brain (ug)
ABR = ABRfree+ABrainbound
CBR = ABR/VBR

!...ATR in kidney compartment
!...AK = Total amount of ATR in kidney (ug)
RK = QK*(CPlasmaFree-CVK)
```

```
AK = Integ(RK,AK0)
CK = AK/VK
CVK = AK/(VK*PK)

!...ATR in other tissue compartment
!...Aoth = Total amount of ATR in other tissues (ug)
Roth = Qoth*(CPlasmaFree-CVoth)
Aoth = Integ(Roth,Aoth0)
Coth = Aoth/Voth
CVoth = Coth/Poth

!...ATR in mammary gland compartment
!...AM = Total amount of ATR in mammary gland (ug)
RM = QM*(CPlasmaFree-CVM)-RMilk
AM = Integ(RM,AM0)
CM = AM/VM
CVM = CM/PM

RMilk = Kmilk*CVM
AMilk = Integ(RMilk,0.0)
CMilk = RMilk/Klac          ! Milk concentration of ATR, ug/l
AUCcmilk = integ(cmilk,0)

!...Mass balance for ATR in the dam
!...Tmassdam = mass balance for ATR (total amount of ATR absorbed), ug
Tmassdam = Ablood+AL+ABR+AK+Aoth+AM+AATR_DEmet+AATR_DIPmet+Amilk
BalATRdam = AAO-Tmassdam     ! Checking mass balance of ATR sub-model, Absorption = remaining in the tissues + metabolized

!!...model equations for pup
!...ATR in the blood compartment
!...APlasmaFreepup = Amount of free ATR in plasma (ug)
```

RAPlasmaFreepup = QCpup*(CVpup-CPlasmaFreepup)+RARBCunbindpup-RARBCbindpup+RAplasmaunbindpup-RAplasmabindpup
APlasmaFreepup = Integ(RAPlasmaFreepup,APlasmaFreepup0)
CPlasmaFreepup = APlasmaFreepup/Vplasmapup

!...APlasmaboundpup = Amount of ATR bound to plasma protein (ug)
RAPlasmaboundpup = RAPlasmabindpup-RAPlasmaunbindpup
APlasmaboundpup = Integ(RAPlasmaboundpup,APlasmaboundpup0)
CPlasmaboundpup = APlasmaboundpup/Vplasmapup

!...ARBCboundpup = Amount of ATR bound to red blood cells (ug)
RARBCboundpup = RARBCbindpup-RARBCunbindpup
ARBCboundpup = Integ(RARBCboundpup,ARBCboundpup0)
CRBCboundpup = ARBCboundpup/VRBCpup

!...Abloodpup = Total amount of ATR in the blood compartment (ug)
!...Aplasmapup = Total amount of ATR in the plasma compartment (ug)
Abloodpup = APlasmaFreepup+APlasmaboundpup+ARBCboundpup
Cbloodpup = Abloodpup/Vbloodpup
Aplasmapup = APlasmaFreepup+Aplasmaboundpup
Cplasmapup = Aplasmapup/Vplasmapup
AUCCplasmapup = Integ(Cplasmapup,Cplasmapup0)

RAplasmabindpup = KaATRplasmapup*BMaxPlasmaRemainpup*AplasmaFreepup
RAplasmaunbindpup = KdATRplasmapup*Aplasmaboundpup
RARBCbindpup = KaATRrbcpup*BMaxRBCRemainpup*AplasmaFreepup
RARBCunbindpup = KdATRrbcpup*ARBCboundpup

BMaxPlasmaRemainpup = BMaxPlasmapup-APlasmaboundpup
BMaxRBCRemainpup = BMaxRBCpup-ARBCboundpup

CVpup= (CVLpup*QLpup+CVBRpup*QBRpup+CVKpup*QKpup+CVothpup*Qothpup)/QCpup

```
!...ATR in the liver compartment
!...Total amount of ATR in liver
RLpup = QLpup*(CPlasmaFreepup-CVLpup)+Rmilkpup-RATR_DEmetpup-RATR_DIPmetpup
ALpup = Integ(RLpup,ALpup0)
CLpup = ALpup/VLpup
CVLpup = ALpup/(VLpup*PLpup)

Amilkpup = Integ(Rmilkpup,0.0)

! Metabolism of ATR in liver
RATR_DEmetpup = VmaxATR_DEpup*CVLpup/(KmATR_DEpup+CVLpup)      ! Metabolic rate of ATR to DE, ug/h, (umol/h)
AATR_DEmetpup = Integ(RATR_DEmetpup,0.0)

RformDEpup = RATR_DEmetpup*ATR_DE                              ! Rate of formation of DE from ATR, ug/h
AformDEpup = Integ(RformDEpup,0.0)

RATR_DIPmetpup = VmaxATR_DIPpup*CVLpup/(KmATR_DIPpup+CVLpup)    ! Metabolic rate of ATR to DIP, ug/h, (umol/h)
AATR_DIPmetpup = Integ(RATR_DIPmetpup,0.0)

RformDIPpup = RATR_DIPmetpup*ATR_DIP                           ! Rate of formation of DIP from ATR, ug/h
AformDIPpup = Integ(RformDIPpup,0.0)

AATRmetpup = AATR_DEmetpup+AATR_DIPmetpup                      ! Amount of ATR metabolized, ug/h, (umol/h)

!...ATR in brain compartment
!...ABRfreepup = Amount of ATR  free in brain (ug)
RBRfreepup                    =                    QBRpup*(CPlasmaFreepup-CVBRpup)+KdATRBrainpup*ABrainboundpup-
KaATRBrainpup*BMaxBrainRemainpup*AVBRpup
ABRfreepup = Integ(RBRfreepup,ABRfreepup0)
CBRfreepup = ABRfreepup/VBRpup
CVBRpup = ABRfreepup/(VBRpup*PBRpup)
AVBRpup = ABRfreepup/PBRpup
```

```
!...ABrainboundpup = Amount of ATR bound in brain (ug)
RABrainboundpup = KaATRBrainpup*BMaxBrainRemainpup*AVBRpup-KdATRBrainpup*ABrainboundpup
ABrainboundpup = Integ(RABrainboundpup,Abrainboundpup0)
CBrainboundpup = ABrainboundpup/VBRpup

!...BMaxBrainRemainpup = Remaining binding capacity of brain for ATR (ug)
BMaxBrainRemainpup = BMaxBrainpup-ABrainboundpup

!...ABR = Total amount of ATR in the brain (ug)
ABRpup = ABRfreepup+ABrainboundpup
CBRpup = ABRpup/VBRpup

!...ATR in kidney compartment
!...AKpup = Total amount of ATR in kidney (ug)
RKpup = QKpup*(CPlasmaFreepup-CVKpup)
AKpup = Integ(RKpup,AKpup0)
CKpup = AKpup/VKpup
CVKpup = AKpup/(VKpup*PKpup)

!...ATR in other tissue compartment
!...Aothpup = Total amount of ATR in other tissues (ug)
Rothpup = Qothpup*(CPlasmaFreepup-CVothpup)
Aothpup = Integ(Rothpup,Aothpup0)
Cothpup = Aothpup/Vothpup
CVothpup = Cothpup/Pothpup

!...Mass balance for ATR in the pup
!...Tmasspup = mass balance for ATR (total amount of ATR absorbed), ug
Tmasspup = Abloodpup+ALpup+ABRpup+AKpup+Aothpup+AATR_DEmetpup+AATR_DIPmetpup
BalATRpup = Amilkpup-Tmasspup    ! Checking mass balance of ATR sub-model, Absorption = remaining in the tissues + metabolized
```

```
!!...DE sub-model
!...DE in the dam
!...DE in blood compartment, We consider binding kinetics of DE in blood and tissues are negligible.
!...Ablood1 = Amount of DE in the blood compartment, ug
Rblood1 = QC*(CV1-CA1)
Ablood1 = Integ(Rblood1,Ablood10)
CA1 = Ablood1/Vblood  ! DE concentration in artery, ug/l
CV1 = (CVL1*QL+CVBR1*QBR+CVK1*QK+CVoth1*Qoth+CVM1*QM)/QC ! DE concentration in venous blood, ug/l

!...DE in liver compartment
!...AL1 = Amount of DE in the liver compartment, ug
RL1 = QL*(CA1-CVL1)+RformDE-RDE_DACTmet
AL1 = Integ(RL1,AL10)
CL1 = AL1/VL          ! DE concentration in liver tissue, ug/l
CVL1 = AL1/(VL*PL1)   ! DE concentration in liver venous blood, ug/l

!...Metabolism of DE in the liver
!...ADE_DACTmet = Amount of DE metabolized to DACT in the liver, ug
RDE_DACTmet = VmaxDEDACT*CVL1/(Km1+CVL1)    ! Rate of metabolism of DE to DACT in the liver, ug/h
ADE_DACTmet = Integ(RDE_DACTmet,0.0)

RformDACTDE = RDE_DACTmet*DE_DACT          ! Rate of formation of DACT from DE in the liver, ug/h
AformDACTDE = Integ(RformDACTDE,0.0)

!...DE in the brain compartment
!...ABR1 = Amount of DE in the brain compartment, ug
RBR1 = QBR*(CA1-CVBR1)
ABR1 = Integ(RBR1,ABR10)
CBR1 = ABR1/VBR                    ! DE concentration in brain tissue, ug/l
CVBR1 = CBR1/PBR1                   ! DE concentration in brain venous blood, ug/l
```

```
!...DE in the kidney compartment
!...AK1 = Amount of DE in the kidney compartment, ug
RK1 = QK*(CA1-CVK1)-Rurine1
AK1 = Integ(RK1,AK10)
CK1 = AK1/VK                        ! DE concentration in kidney tissue, ug/l
CVK1 = CK1/PK1                      ! DE concentration in kidney venous blood, ug/l

!...DE in the other tissue compartment
!...Aoth1 = Amount of DE in the other tissue compartment, ug
Roth1 = Qoth*(CA1-CVoth1)
Aoth1 = Integ(Roth1,Aoth10)
Coth1 = Aoth1/Voth                  ! DE concentration in other tissue, ug/l
CVoth1 = Coth1/Poth1                ! DE concentration in other tissue venous blood, ug/l

!...DE in the mammary gland compartment
!...AM1 = Amount of DE in the mammary gland compartment, ug
RM1 = QM*(CA1-CVM1)-RMilk1
AM1 = Integ(RM1,AM10)
CM1 = AM1/VM                        ! DE concentration in mammary gland, ug/l
CVM1 = CM1/PM1                      ! DE concentration in mammary gland venous blood, ug/l
RMilk1 = Kmilk1*CVM1
AMilk1 = Integ(RMilk1,0.0)
CMilk1 = RMilk1/Klac        ! Milk concentration of ATR, ug/l

!...Urinary excretion of DE
Rurine1 = Kurine1*CV1*Vplasma
Aurine1 = Integ(Rurine1,0.0)

!...Mass balance for DE
!TMASS1dam = Mass balance of DE, ug (total amount of DE produced)
Tmass1dam = Ablood1+AL1+ABR1+AK1+Aoth1+AM1+ADE_DACTmet+Aurine1+AMilk1
BalDEdam = AformDE-Tmass1dam
```

```
!...DE in the pup
!...DE in blood compartment, We consider binding kinetics of DE in blood and tissues are negligible.
!...Ablood1pup = Amount of DE in the blood compartment, ug
Rblood1pup = QCpup*(CV1pup-CA1pup)
Ablood1pup = Integ(Rblood1pup,Ablood1pup0)
CA1pup = Ablood1pup/Vbloodpup  ! DE concentration in artery, ug/l

CV1pup = (CVL1pup*QLpup+CVBR1pup*QBRpup+CVK1pup*QKpup+CVoth1pup*Qothpup)/QCpup ! DE concentration in venous blood, ug/l

!...DE in liver compartment
!...AL1pup = Amount of DE in the liver compartment, ug
RL1pup = QLpup*(CA1pup-CVL1pup)+Rmilk1pup+RformDEpup-RDE_DACTmetpup
AL1pup = Integ(RL1pup,AL1pup0)
CL1pup = AL1pup/VLpup          ! DE concentration in liver tissue, ug/l
CVL1pup = AL1pup/(VLpup*PL1pup)   ! DE concentration in liver venous blood, ug/l

Amilk1pup = Integ(Rmilk1pup,0.0)

!...Metabolism of DE in the liver
!...ADE_DACTmetpup = Amount of DE metabolized to DACT in the liver, ug
RDE_DACTmetpup = VmaxDEDACTpup*CVL1pup/(Km1pup+CVL1pup) ! Rate of metabolism of DE to DACT in the liver, ug/h
ADE_DACTmetpup = Integ(RDE_DACTmetpup,0.0)
RformDACTDEpup = RDE_DACTmetpup*DE_DACT                ! Rate of formation of DACT from DE in the liver, ug/h
AformDACTDEpup = Integ(RformDACTDEpup,0.0)

!...DE in the brain compartment
!...ABR1pup = Amount of DE in the brain compartment, ug
RBR1pup = QBRpup*(CA1pup-CVBR1pup)
ABR1pup = Integ(RBR1pup,ABR1pup0)
CBR1pup = ABR1pup/VBRpup                    ! DE concentration in brain tissue, ug/l
CVBR1pup = CBR1pup/PBR1pup                   ! DE concentration in brain venous blood, ug/l
```

```
!...DE in the kidney compartment
!...AK1pup = Amount of DE in the kidney compartment, ug
RK1pup = QKpup*(CA1pup-CVK1pup)-Rurine1pup
AK1pup = Integ(RK1pup,AK1pup0)
CK1pup = AK1pup/VKpup                    ! DE concentration in kidney tissue, ug/l
CVK1pup = CK1pup/PK1pup                  ! DE concentration in kidney venous blood, ug/l

!...DE in the other tissue compartment
!...Aoth1 = Amount of DE in the other tissue compartment, ug
Roth1pup = Qothpup*(CA1pup-CVoth1pup)
Aoth1pup = Integ(Roth1pup,Aoth1pup0)
Coth1pup = Aoth1pup/Vothpup              ! DE concentration in other tissue, ug/l
CVoth1pup = Coth1pup/Poth1pup            ! DE concentration in other tissue venous blood, ug/l

!...Urinary excretion of DE
!Rurine1pup = Kurine1pup*CVK1pup*VKpup
Rurine1pup = Kurine1pup*CV1pup*Vplasmapup
Aurine1pup = Integ(Rurine1pup,0.0)

!...Mass balance for DE
!TMASS1pup = Mass balance of DE, ug (total amount of DE produced)
Tmass1pup = Ablood1pup+AL1pup+ABR1pup+AK1pup+Aoth1pup+ADE_DACTmetpup+Aurine1pup
BalDEpup = Amilk1pup+AformDEpup-Tmass1pup

!!...DIP sub-model
!...DIP in the dam
!...DIP in blood compartment, We consider binding kinetics of DIP in blood and tissues are negligible.
!...Ablood2 = Amount of DIP in the blood compartment, ug
Rblood2 = QC*(CV2-CA2)
Ablood2 = Integ(Rblood2,Ablood20)
CA2 = Ablood2/Vblood  ! DIP concentration in artery, ug/l
CV2 = (CVL2*QL+CVBR2*QBR+CVK2*QK+CVoth2*Qoth+CVM2*QM)/QC ! DIP concentration in venous blood, ug/l
```

```
!...DIP in liver compartment
!...AL1 = Amount of DIP in the liver compartment, ug
RL2 = QL*(CA2-CVL2)+RformDIP-RDIP_DACTmet
AL2 = Integ(RL2,AL20)
CL2 = AL2/VL          ! DIP concentration in liver tissue, ug/l
CVL2 = AL2/(VL*PL2)   ! DIP concentration in liver venous blood, ug/l

!...Metabolism of DIP in the liver
!...ADIP_DACTmet = Amount of DIP metabolized to DACT in the liver, ug
RDIP_DACTmet = VmaxDIPDACT*CVL2/(Km2+CVL2)    ! Rate of metabolism of DIP to DACT in the liver, ug/h
ADIP_DACTmet = Integ(RDIP_DACTmet,0.0)

RformDACTDIP = RDIP_DACTmet*DIP_DACT          ! Rate of formation of DACT from DIP in the liver, ug/h
AformDACTDIP = Integ(RformDACTDIP,0.0)

!...DIP in the brain compartment
!...ABR2 = Amount of DIP in the brain compartment, ug
RBR2 = QBR*(CA2-CVBR2)
ABR2 = Integ(RBR2,ABR20)
CBR2 = ABR2/VBR                    ! DIP concentration in brain tissue, ug/l
CVBR2 = CBR2/PBR2                  ! DIP concentration in brain venous blood, ug/l

!...DIP in the kidney compartment
!...AK2 = Amount of DIP in the kidney compartment, ug
RK2 = QK*(CA2-CVK2)-Rurine2
AK2 = Integ(RK2,AK20)
CK2 = AK2/VK                       ! DIP concentration in kidney tissue, ug/l
CVK2 = CK2/PK2                     ! DIP concentration in kidney venous blood, ug/l

!...DIP in the other tissue compartment
!...Aoth1 = Amount of DIP in the other tissue compartment, ug
Roth2 = Qoth*(CA2-CVoth2)
```

```
Aoth2 = Integ(Roth2,Aoth20)
Coth2 = Aoth2/Voth                    ! DIP concentration in other tissue, ug/l
CVoth2 = Coth2/Poth2                  ! DIP concentration in other tissue venous blood, ug/l

!...DIP in the mammary gland compartment
!...AM2 = Amount of DIP in the mammary gland compartment, ug
RM2 = QM*(CA2-CVM2)-RMilk2
AM2 = Integ(RM2,AM20)
CM2 = AM2/VM                          ! DIP concentration in mammary gland, ug/l
CVM2 = CM2/PM2                        ! DIP concentration in mammary gland venous blood, ug/l

RMilk2 = Kmilk2*CVM2
AMilk2 = Integ(RMilk2,0.0)
CMilk2 = RMilk2/Klac        ! Milk concentration of DIP, ug/l

!...Urinary excretion of DIP
!Rurine2 = Kurine2*CVK2*VK
Rurine2 = Kurine2*CV2*Vplasma
Aurine2 = Integ(Rurine2,0.0)

!...Mass balance for DIP
!TMASS2dam = Mass balance of DIP, ug (total amount of DIP produced)
Tmass2dam = Ablood2+AL2+ABR2+AK2+Aoth2+AM2+ADIP_DACTmet+Aurine2+AMilk2
BalDIPdam = AformDIP-Tmass2dam

!...DIP in the pup
!...DIP in blood compartment, We consider binding kinetics of DIP in blood and tissues are negligible.
!...Ablood2pup = Amount of DIP in the blood compartment, ug
Rblood2pup = QCpup*(CV2pup-CA2pup)
Ablood2pup = Integ(Rblood2pup,Ablood2pup0)
CA2pup = Ablood2pup/Vbloodpup  ! DIP concentration in artery, ug/l
```

```
  CV2pup = (CVL2pup*QLpup+CVBR2pup*QBRpup+CVK2pup*QKpup+CVoth2pup*Qothpup)/QCpup ! DIP concentration in
venous blood, ug/l

  !...DIP in liver compartment
  !...AL2pup = Amount of DIP in the liver compartment, ug
  RL2pup = QLpup*(CA2pup-CVL2pup)+Rmilk2pup+RformDIPpup-RDIP_DACTmetpup
  AL2pup = Integ(RL2pup,AL2pup0)
  CL2pup = AL2pup/VLpup          ! DIP concentration in liver tissue, ug/l
  CVL2pup = AL2pup/(VLpup*PL2pup)   ! DIP concentration in liver venous blood, ug/l

  Amilk2pup = Integ(Rmilk2pup,0.0)

  !...Metabolism of DIP in the liver
  !...ADIP_DACTmetpup = Amount of DIP metabolized to DACT in the liver, ug
  RDIP_DACTmetpup = VmaxDIPDACTpup*CVL2pup/(Km2pup+CVL2pup)  ! Rate of metabolism of DIP to DACT in the liver,
ug/h
  ADIP_DACTmetpup = Integ(RDIP_DACTmetpup,0.0)

  RformDACTDIPpup = RDIP_DACTmetpup*DIP_DACT                ! Rate of formation of DACT from DIP in the liver, ug/h
  AformDACTDIPpup = Integ(RformDACTDIPpup,0.0)

  !...DIP in the brain compartment
  !...ABR2pup = Amount of DIP in the brain compartment, ug
  RBR2pup = QBRpup*(CA2pup-CVBR2pup)
  ABR2pup = Integ(RBR2pup,ABR2pup0)
  CBR2pup = ABR2pup/VBRpup                          ! DIP concentration in brain tissue, ug/l
  CVBR2pup = CBR2pup/PBR2pup                         ! DIP concentration in brain venous blood, ug/l

  !...DIP in the kidney compartment
  !...AK2pup = Amount of DIP in the kidney compartment, ug
  RK2pup = QKpup*(CA2pup-CVK2pup)-Rurine2pup
  AK2pup = Integ(RK2pup,AK2pup0)
```

```
CK2pup = AK2pup/VKpup                    ! DIP concentration in kidney tissue, ug/l
CVK2pup = CK2pup/PK2pup                  ! DIP concentration in kidney venous blood, ug/l

!...DIP in the other tissue compartment
!...Aoth1 = Amount of DIP in the other tissue compartment, ug
Roth2pup = Qothpup*(CA2pup-CVoth2pup)
Aoth2pup = Integ(Roth2pup,Aoth2pup0)
Coth2pup = Aoth2pup/Vothpup              ! DIP concentration in other tissue, ug/l
CVoth2pup = Coth2pup/Poth2pup            ! DIP concentration in other tissue venous blood, ug/l

!...Urinary excretion of DIP
!Rurine2pup = Kurine2pup*CVK2pup*VKpup
Rurine2pup = Kurine2pup*CV2pup*Vplasmapup
Aurine2pup = Integ(Rurine2pup,0.0)

!...Mass balance for DIP
!TMASS2pup = Mass balance of DIP, ug (total amount of DIP produced)
Tmass2pup = Ablood2pup+AL2pup+ABR2pup+AK2pup+Aoth2pup+ADIP_DACTmetpup+Aurine2pup
BalDIPpup = Amilk2pup+AformDIPpup-Tmass2pup

!!!...DACT sub-model
!...DACT in the dam
!...DACT in blood compartment, we consider ATR and DACT, but not DE and DIP, bind to maternal plasma, red blood cells, brain
tissue.
!...APlasmaFree3 = Amount of free DACT in plasma (ug)
RAPlasmaFree3 = QC*(CV3-CPlasmaFree3)+RARBCunbind3-RARBCbind3+RAplasmaunbind3-RAplasmabind3
APlasmaFree3 = Integ(RAPlasmaFree3,APlasmaFree30)
CPlasmaFree3 = APlasmaFree3/VPlasma
!...APlasmabound3 = Amount of DACT bound to plasma protein (ug)
RAPlasmabound3 = RAPlasmabind3-RAPlasmaunbind3
APlasmabound3 = Integ(RAPlasmabound3,APlasmabound30)
CPlasmabound3 = APlasmabound3/VPlasma
```

```
!...ARBCbound3 = Amount of DACT bound to red blood cells (ug)
RARBCbound3 = RARBCbind3-RARBCunbind3
ARBCbound3 = Integ(RARBCbound3,ARBCbound30)
CRBCbound3 = ARBCbound3/VRBC

!...Ablood3 = Total amount of DACT in the blood compartment (ug)
!...Aplasma3 = Total amount of DACT in the plasma compartment (ug)
Ablood3 = APlasmaFree3+APlasmabound3+ARBCbound3
Cblood3 = Ablood3/Vblood
Aplasma3 = APlasmaFree3+APlasmabound3
Cplasma3 = Aplasma3/Vplasma
AUCCplasma3 = Integ(Cplasma3,Cplasma30)

RAplasmabind3 = KaDACTplasma*BMaxPlasmaRemain3*APlasmaFree3
RAplasmaunbind3 = KdDACTplasma*Aplasmabound3
RARBCbind3 = KaDACTrbc*BMaxRBCRemain3*APlasmaFree3
RARBCunbind3 = KdDACTrbc*ARBCbound3

BMaxPlasmaRemain3 = BMaxPlasma3-APlasmabound3
BMaxRBCRemain3 = BMaxRBC3-ARBCbound3

CV3 = (CVL3*QL+CVBR3*QBR+CVK3*QK+CVoth3*Qoth+CVM3*QM)/QC    ! DACT concentration in venous blood, ug/l

!...DACT in liver compartment
!...AL3 = Amount of DACT in the liver compartment, ug
RL3 = QL*(CPlasmaFree3-CVL3)+RformDACTDE+RformDACTDIP
AL3 = Integ(RL3,AL30)
CL3 = AL3/VL                    ! DACT concentration in liver tissue, ug/l
CVL3 = CL3/PL3                  ! DACT concentration in liver venous blood, ug/l

!...DACT in brain compartment
!...ABRfree3 = Amount of DACT free in brain, ug
```

```
RBRfree3 = QBR*(CPlasmaFree3-CVBR3)+KdDACTBrain*ABrainbound3-KaDACTBrain*BMaxBrainRemain3*AVBR3
ABRfree3 = Integ(RBRfree3,ABRfree30)
CBRfree3 = ABRfree3/VBR
CVBR3 = CBRfree3/PBR3                    ! DACT concentration in brain venous blood, ug/l
AVBR3 = ABRfree3/PBR3
!...ABrainbound3 = Amount of DACT bound to brain tissue, ug
RABrainbound3 = KaDACTBrain*BMaxBrainRemain3*AVBR3-KdDACTBrain*ABrainbound3
ABrainbound3 = Integ(RABrainbound3,ABrainbound30)
CBrainbound3 = ABrainbound3/VBR

!...BMaxBrainRemain3 = Remaining binding capacity of brain for DACT, ug
BMaxBrainRemain3 = BMaxBrain3-ABrainbound3

!...ABR3 = Total amount of DACT in the brain, ug
ABR3 = ABRfree3+ABrainbound3
CBR3 = ABR3/VBR                          ! DACT concentration in brain tissue, ug/l

!...DACT in kidney compartment
!...AK3 = Amount of DACT in the kidney compartment, ug
RK3 = QK*(CPlasmaFree3-CVK3)-Rurine3
AK3 = Integ(RK3,AK30)
CK3 = AK3/VK                             ! DACT concentration in kidney tissue, ug/l
CVK3 = CK3/PK3                           ! DACT concentration in kidney venous blood, ug/l

!...DACT in the other tissue compartment
!...Aoth3 = Amount of DACT in the other tissue compartment, ug
Roth3 = Qoth*(CPlasmaFree3-CVoth3)
Aoth3 = Integ(Roth3,Aoth30)
Coth3 = Aoth3/Voth                       ! DACT concentration in other tissue, ug/l
CVoth3 = Coth3/Poth3                     ! DACT concentration in other tissue venous blood, ug/l
```

```
!...DACT in the mammary gland compartment
!...AM3 = Amount of DACT in the mammary gland compartment, ug
RM3 = QM*(CPlasmaFree3-CVM3)-RMilk3
AM3 = Integ(RM3,AM30)
CM3 = AM3/VM                    ! DACT concentration in mammary gland tissue, ug/l
CVM3 = CM3/PM3                  ! DACT concentration in mammary gland venous blood, ug/l

RMilk3 = Kmilk3*CVM3
AMilk3 = Integ(RMilk3,0.0)
CMilk3 = RMilk3/Klac        ! Milk concentration of DIP, ug/l
AUCcmilk3 = integ(cmilk3,0)

!...Urinary excretion of DACT
!Rurine3 = Kurine3*CVK3*VK
Rurine3 = Kurine3*CV3*Vplasma
Aurine3 = Integ(Rurine3,0.0)

!...Mass balance for DACT
!...Tmass3dam = Mass balance of DACT, ug (total amount of DACT produced)
TMass3dam = Ablood3+AL3+ABR3+AK3+Aoth3+AM3+Aurine3+AMilk3
BalDACTdam = AformDACTDE+AformDACTDIP-Tmass3dam

!!...DACT in the pup
!...DACT in the blood compartment
!...APlasmaFree3pup = Amount of free DACT in plasma (ug)
RAPlasmaFree3pup    =    QCpup*(CV3pup-CPlasmaFree3pup)+RARBCunbind3pup-RARBCbind3pup+RAplasmaunbind3pup-
RAplasmabind3pup
APlasmaFree3pup = Integ(RAPlasmaFree3pup,APlasmaFree3pup0)
CPlasmaFree3pup = APlasmaFree3pup/VPlasmapup

!...APlasmabound3pup = Amount of DACT bound to plasma protein (ug)
RAPlasmabound3pup = RAPlasmabind3pup-RAPlasmaunbind3pup
```

```
   APlasmabound3pup = Integ(RAPlasmabound3pup,APlasmabound3pup0)
   CPlasmabound3pup = APlasmabound3pup/VPlasmapup

   !...ARBCbound3pup = Amount of DACT bound to red blood cells (ug)
   RARBCbound3pup = RARBCbind3pup-RARBCunbind3pup
   ARBCbound3pup = Integ(RARBCbound3pup,ARBCbound3pup0)
   CRBCbound3pup = ARBCbound3pup/VRBCpup

   !...Ablood3pup = Total amount of DACT in the blood compartment (ug)
   !...Aplasma3pup = Total amount of DACT in the plasma compartment (ug)
   Ablood3pup = APlasmaFree3pup+APlasmabound3pup+ARBCbound3pup
   Cblood3pup = Ablood3pup/Vbloodpup
   Aplasma3pup = APlasmaFree3pup+APlasmabound3pup
   Cplasma3pup = Aplasma3pup/Vplasmapup
   AUCCplasma3pup = Integ(Cplasma3pup,Cplasma3pup0)

   RAplasmabind3pup = KaDACTplasmapup*BMaxPlasmaRemain3pup*APlasmaFree3pup
   RAplasmaunbind3pup = KdDACTplasmapup*Aplasmabound3pup
   RARBCbind3pup = KaDACTrbcpup*BMaxRBCRemain3pup*APlasmaFree3pup
   RARBCunbind3pup = KdDACTrbcpup*ARBCbound3pup

   BMaxPlasmaRemain3pup =  BMaxPlasma3pup-APlasmabound3pup
   BMaxRBCRemain3pup = BMaxRBC3pup-ARBCbound3pup

   CV3pup = (CVL3pup*QLpup+CVBR3pup*QBRpup+CVK3pup*QKpup+CVoth3pup*Qothpup)/QCpup     ! DACT concentration
in venous blood, ug/l

   !...DACT in liver compartment
   !...AL3pup = Amount of DACT in the liver compartment, ug
   RL3pup = QLpup*(CPlasmaFree3pup-CVL3pup)+Rmilk3pup+RformDACTDEpup+RformDACTDIPpup
   AL3pup = Integ(RL3pup,AL3pup0)
   CL3pup = AL3pup/VLpup                        ! DACT concentration in liver tissue, ug/l
```

```
  CVL3pup = CL3pup/PL3pup                    ! DACT concentration in liver venous blood, ug/l

  AMilk3pup = Integ(Rmilk3pup,0.0)

  !...DACT in brain compartment
  !...ABRfree3pup = Amount of DACT free in brain, ug
  RBRfree3pup = QBRpup*(CPlasmaFree3pup-CVBR3pup)+KdDACTBrainpup*ABrainbound3pup-
KaDACTBrainpup*BMaxBrainRemain3pup*AVBR3pup
  ABRfree3pup = Integ(RBRfree3pup,ABRfree3pup0)
  CBRfree3pup = ABRfree3pup/VBRpup
  CVBR3pup = CBRfree3pup/PBR3pup             ! DACT concentration in brain venous blood, ug/l
  AVBR3pup = ABRfree3pup/PBR3pup
  !...ABrainbound3pup = Amount of DACT bound to brain tissue, ug
  RABrainbound3pup = KaDACTBrainpup*BMaxBrainRemain3pup*AVBR3pup-KdDACTBrainpup*ABrainbound3pup
  ABrainbound3pup = Integ(RABrainbound3pup,ABrainbound3pup0)
  CBrainbound3pup = ABrainbound3pup/VBRpup

  !...BMaxBrainRemain3pup = Remaining binding capacity of brain for DACT, ug
  BMaxBrainRemain3pup = BMaxBrain3pup-ABrainbound3pup

  !...ABR3pup = Total amount of DACT in the brain, ug
  ABR3pup = ABRfree3pup+ABrainbound3pup
  CBR3pup = ABR3pup/VBRpup                   ! DACT concentration in brain tissue, ug/l
  AUCCBR3pup = Integ(CBR3pup,cfetus30)
  !...DACT in kidney compartment
  !...AK3pup = Amount of DACT in the kidney compartment, ug
  RK3pup = QKpup*(CPlasmaFree3pup-CVK3pup)-Rurine3pup
  AK3pup = Integ(RK3pup,AK3pup0)
  CK3pup = AK3pup/VKpup                      ! DACT concentration in kidney tissue, ug/l
  CVK3pup = CK3pup/PK3pup                    ! DACT concentration in kidney venous blood, ug/l
```

```
  !...DACT in the other tissue compartment
  !...Aoth3 = Amount of DACT in the other tissue compartment, ug
  Roth3pup = Qothpup*(CPlasmaFree3pup-CVoth3pup)
  Aoth3pup = Integ(Roth3pup,Aoth3pup0)
  Coth3pup = Aoth3pup/Vothpup                    ! DACT concentration in other tissue, ug/l
  CVoth3pup = Coth3pup/Poth3pup                  ! DACT concentration in other tissue venous blood, ug/l

  !...Urinary excretion of DACT
  Rurine3pup = Kurine3pup*CV3pup*Vplasmapup
  Aurine3pup = Integ(Rurine3pup,0.0)

  !...Mass balance for DACT
  !...Tmass3dam = Mass balance of DACT, ug (total amount of DACT produced)
  TMass3pup = Ablood3pup+AL3pup+ABR3pup+AK3pup+Aoth3pup+Aurine3pup
  BalDACTpup = AMilk3pup+AformDACTDEpup+AformDACTDIPpup-Tmass3pup

            END ! DERIVATIVE

            ! Add discrete events here as needed
            !  DISCRETE
            !  END
            ! code that is executed once at each communication interval goes here

            !CONSTANT TSTOP = 10.0
            TERMT (T .GE. (TSTOP*24), 'checked on communication interval: REACHED TSTOP')

      END ! DYNAMIC

      TERMINAL
            ! code that is executed once at the end of a simulation run goes here
      END ! TERMINAL
END ! PROGRAM
```

APPENDIX D

SUPPLEMENTARY DATA FOR CHAPTER 7

Table D1. Body weights and selected organ weights: dams.

	Vehicle	3 mg/L ATR	p value
Body weight (g)			
Initial (GD1)	21.64 ± 0.638	21.79 ± 0.372	0.841
GD5	22.57 ± 0.602	22.79 ± 0.414	0.767
GD12	26.72 ± 0.586	26.32 ± 0.466	0.600
GD17	33.69 ± 0.957	33.09 ± 0.664	0.613
PND6	28.49 ± 0.707	29.08 ± 0.611	0.536
PND13	30.61 ± 0.830	30.84 ± 0.840	0.848
PND20	30.00 ± 1.062	29.73 ± 0.634	0.832
Sacrifice day (PND23-24)	26.84 ± 0.742	27.17 ± 0.737	0.756
Organ weight (g/kg BW)			
Brain	17.756 ± 0.493	16.943 ± 0.400	0.216
Liver	60.334 ± 2.333	65.112 ± 2.568	0.185
Spleen	2.546 ± 0.145	2.603 ± 0.151	0.789
Thymus	1.585 ± 0.117	1.356 ± 0.135	0.216
Uterus	3.001 ± 0.252	2.939 ± 0.176	0.843
Ovary	0.358 ± 0.0226	0.362 ± 0.0239	0.902

Table D2. Body weights and selected organ weights: offspring.

	Male		Female		p value		
	Vehicle	3 mg/L ATR	Vehicle	3 mg/L ATR	ATR	Sex	ATR X Sex
PND21-22							
Body weight (g)	7.975 ± 0.335	7.878 ± 0.315	7.312 ± 0.335	7.578 ± 0.315	0.798	0.149	0.581
Organ weight (g/kg BW)							
Brain	51.314 ± 2.258	51.663 ± 2.129	55.005 ± 2.258	52.396 ± 2.219	0.610	0.322	0.506
Liver	38.797 ± 2.094	40.999 ± 1.975	37.760 ± 2.094	40.127 ± 1.975	0.271	0.642	0.968
Spleen	4.468 ± 0.454	4.794 ± 0.428	4.680 ± 0.454	4.813 ± 0.428	0.606	0.795	0.828
Thymus	6.219 ± 0.524	6.360 ± 0.494	6.625 ± 0.524	5.911 ± 0.494	0.579	0.966	0.408
Testis	4.588 ± 0.177	4.681 ± 0.171	-	-	0.712	-	-
Uterus	-	-	0.993 ± 0.0492	1.008 ± 0.0656	0.857	-	-
Ovary	-	-	0.741 ± 0.0451	0.723 ± 0.0795	0.842	-	-
Weaning day (PND23-24)							
Body weight (g)	8.685 ± 0.302	8.926 ± 0.323	8.601 ± 0.285	8.472 ± 0.285	0.852	0.376	0.541
PND38-39							
Body weight (g)	18.40 ± 0.306	17.781 ± 0.306	15.30 ± 0.306	15.305 ± 0.274	0.312	<0.001	0.305
Organ weight (g/kg BW)							
Brain	23.978 ± 0.523	24.250 ± 0.523	27.565 ± 0.523	27.543 ± 0.468	0.807	<0.001	0.775
Liver	57.255 ± 1.620	55.646 ± 1.620	54.040 ± 1.620	53.373 ± 1.449	0.477	0.092	0.768
Spleen	2.960 ± 0.162	2.873 ± 0.162	2.824 ± 0.162	2.806 ± 0.145	0.739	0.524	0.828
Thymus	2.960 ± 0.321	2.807 ± 0.321	3.521 ± 0.321	3.019 ± 0.287	0.303	0.226	0.581
Testis	6.570 ± 0.240	6.917 ± 0.288	-	-	0.371	-	-
Uterus	-	-	0.900 ± 0.134	0.804 ± 0.0920	0.548	-	-
Ovary	-	-	0.627 ± 0.0510	0.577 ± 0.0312	0.389	-	-

Table D2 (continued). Body weights and selected organ weights: offspring.

	Male		Female		p value		
	Vehicle	3 mg/L ATR	Vehicle	3 mg/L ATR	ATR	Sex	ATR X Sex
PND73-74							
Body weight (g)	23.438 ± 0.653	23.163 ± 0.653	18.550 ± 0.698	19.350 ± 0.653	0.696	<0.001	0.425
Organ weight (g/kg BW)							
Brain	19.257 ± 0.902	19.267 ± 0.902	24.200 ± 0.964	23.361 ± 0.902	0.655	<0.001	0.647
Liver	50.708 ± 1.249	49.972 ± 1.249	47.756 ± 1.335	47.874 ± 1.249	0.810	0.057	0.739
Spleen	2.134 ± 0.154	2.211 ± 0.154	2.458 ± 0.165	2.914 ± 0.154	0.101	0.003	0.238
Thymus	1.450 ± 0.193	1.407 ± 0.193	2.354 ± 0.206	2.442 ± 0.193	0.910	<0.001	0.741
Testis	7.947 ± 0.361	7.909 ± 0.387	-	-	0.944	-	-
Uterus	-	-	2.983 ± 0.504	2.309 ± 0.321	0.267	-	-
Ovary	-	-	0.832 ± 0.0842	0.719 ± 0.0423	0.236	-	-

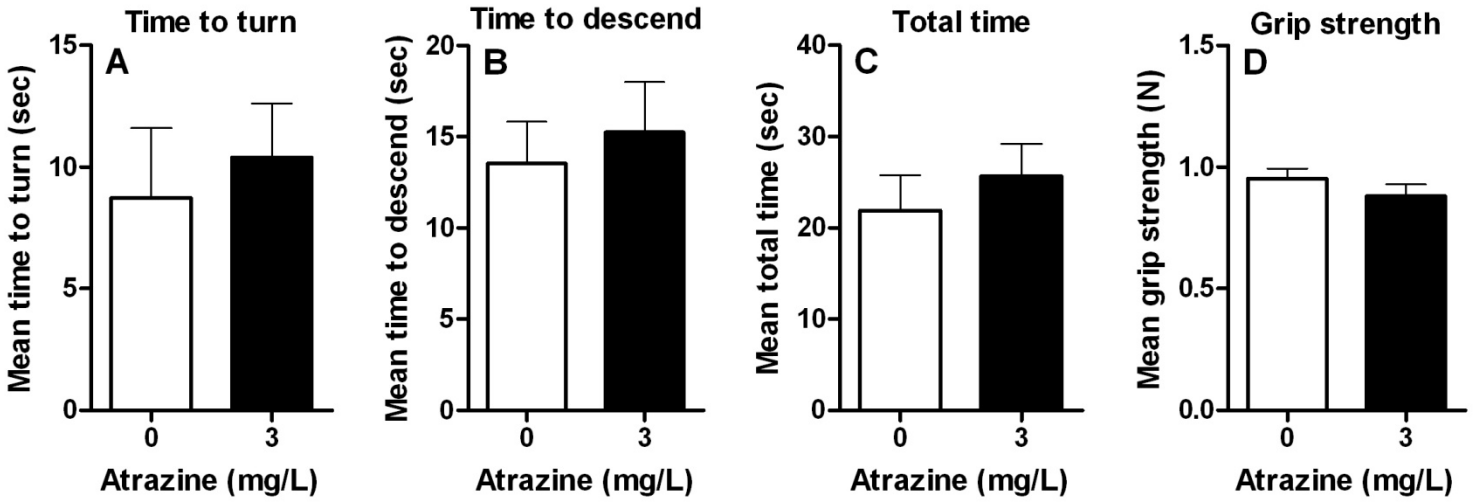

Figure D1. Effects of drinking water atrazine (3 mg/L) exposure from gestational day 6 to postnatal day 21-22 on the time to turn (A), time to descend (B), and total time (C) spent in a pole test and on the forelimb grip strength (D) in mouse dams. There were no significant differences ($p \geq 0.28$) between control and ATR-treated groups among these endpoints. Data are expressed as means ± SEM.

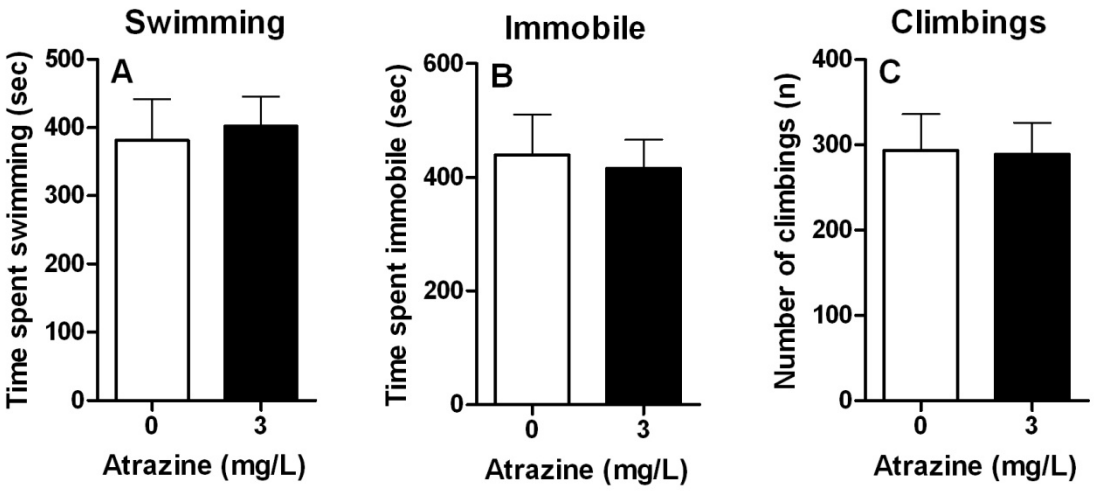

Figure D2. Effects of drinking water atrazine (3 mg/L) exposure from gestational day 6 to postnatal day 22-23 on the time spent swimming (A), time spent immobile (B), and the number of climbings (B) in a forced swim test in mouse dams. There were no significant differences ($p \geq 0.79$) between control and ATR-treated groups among these endpoints. Data are expressed as means ± SEM.

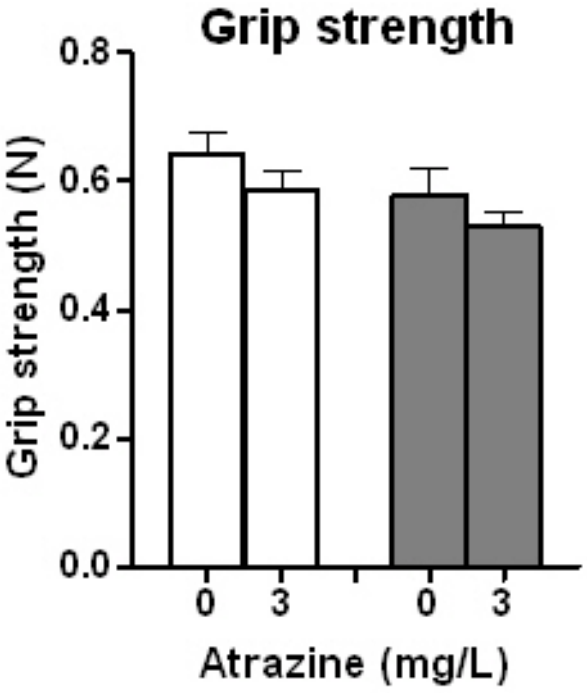

Figure D3. Effects of drinking water atrazine (3 mg/L) exposure from gestational day 6 to postnatal day 23-24 on the forelimb grip strength in juvenile mouse offspring. There were no significant differences ($p \geq 0.23$) between control and ATR-treated groups in both males and females. Data are expressed as means ± SEM.

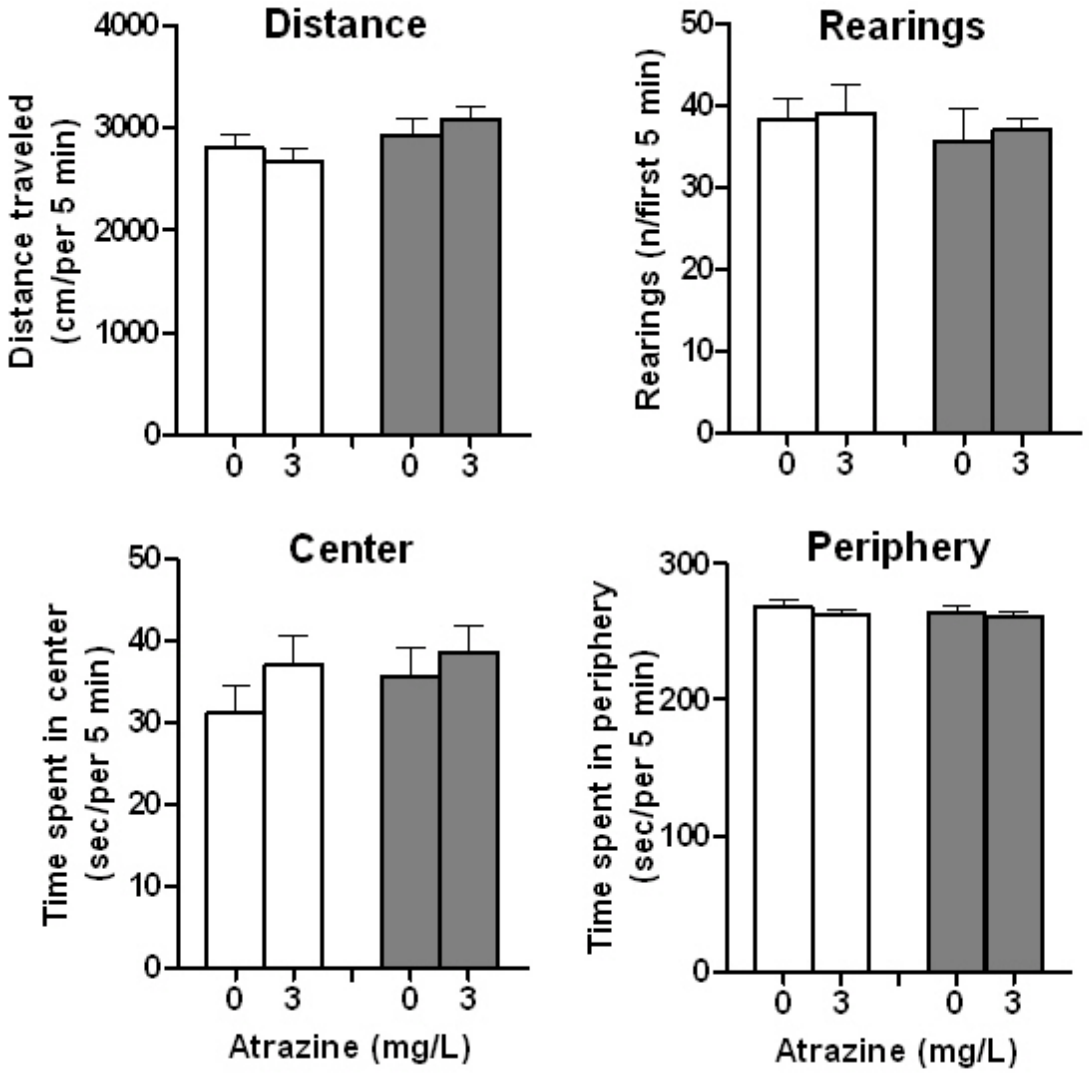

Figure D4. Effects of drinking water atrazine (3 mg/L) exposure from gestational day 6 to postnatal day 23-24 on the locomotor activity in an open field test in adult mouse offspring. There were no significant differences ($p \geq 0.23$) between control and ATR-treated groups in both males and females. Data are expressed as means ± SEM.

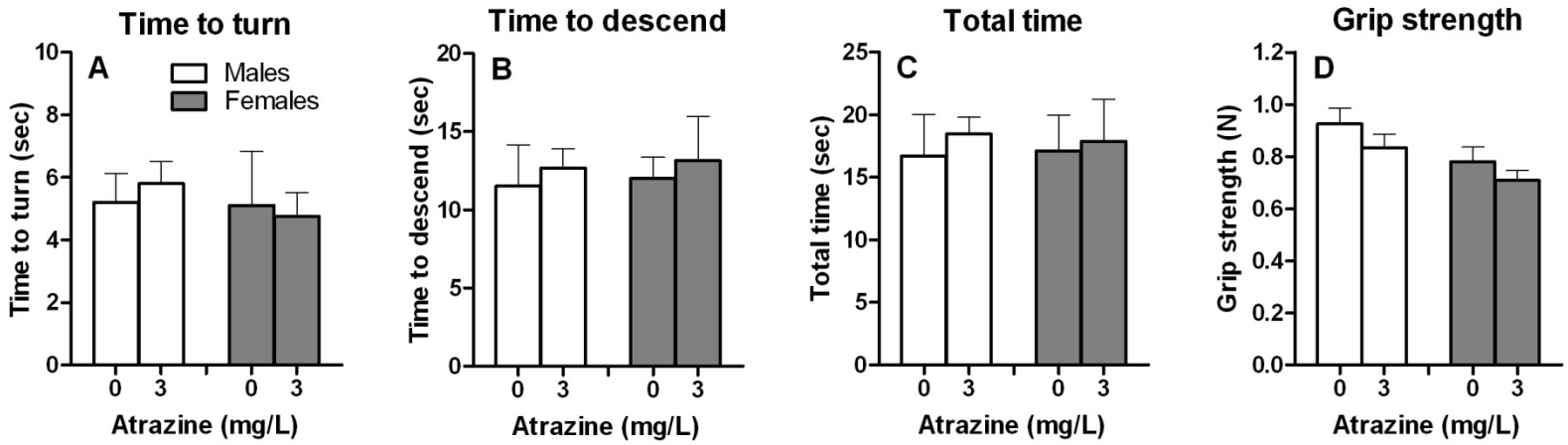

Figure D5. Effects of drinking water atrazine (3 mg/L) exposure from gestational day 6 to postnatal day 23-24 on the time to turn (A), time to descend (B), and total time (C) spent in a pole test and on the forelimb grip strength (D) in adult mouse offspring. There were no significant differences ($p \geq 0.27$) between control and ATR-treated groups in both males and females in these endpoints. Data are expressed as means ± SEM.

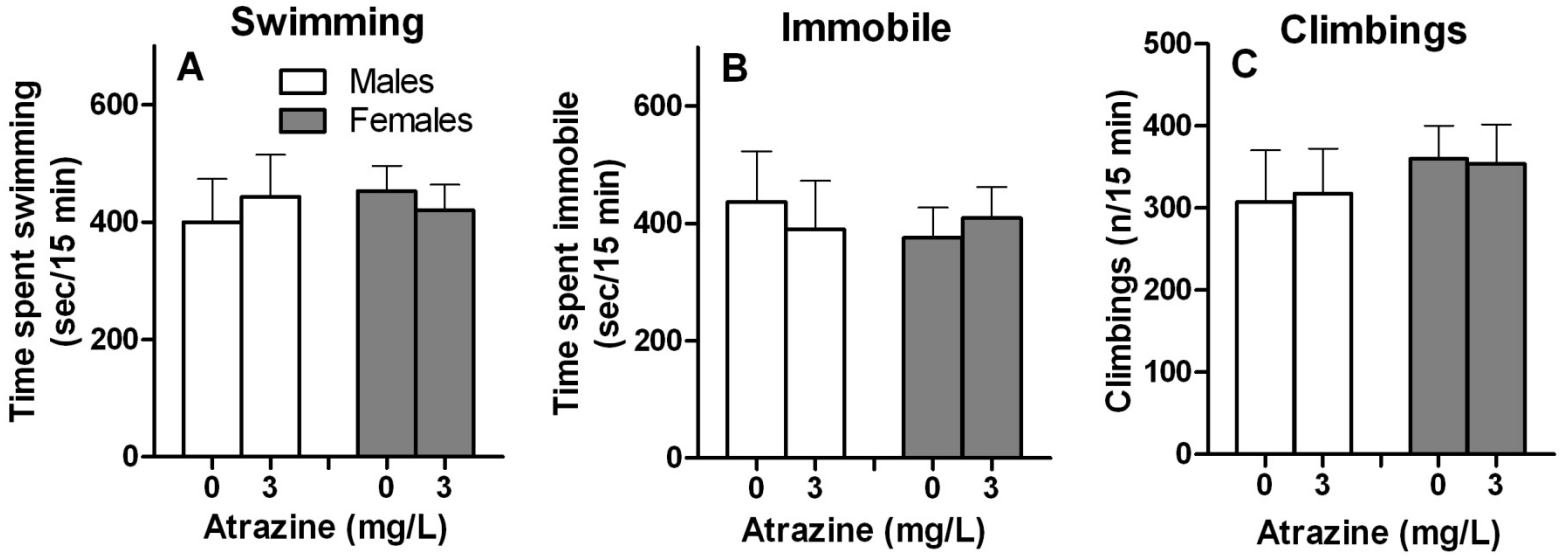

Figure D6. Effects of drinking water atrazine (3 mg/L) exposure from gestational day 6 to postnatal day 23-24 on the time spent swimming (A), time spent immobile (B), and the number of climbings (C) in a forced swim test in adult mouse offspring. There were no significant differences ($p \geq 0.60$) between control and ATR-treated groups in both males and females in these endpoints. Data are expressed as means ± SEM.

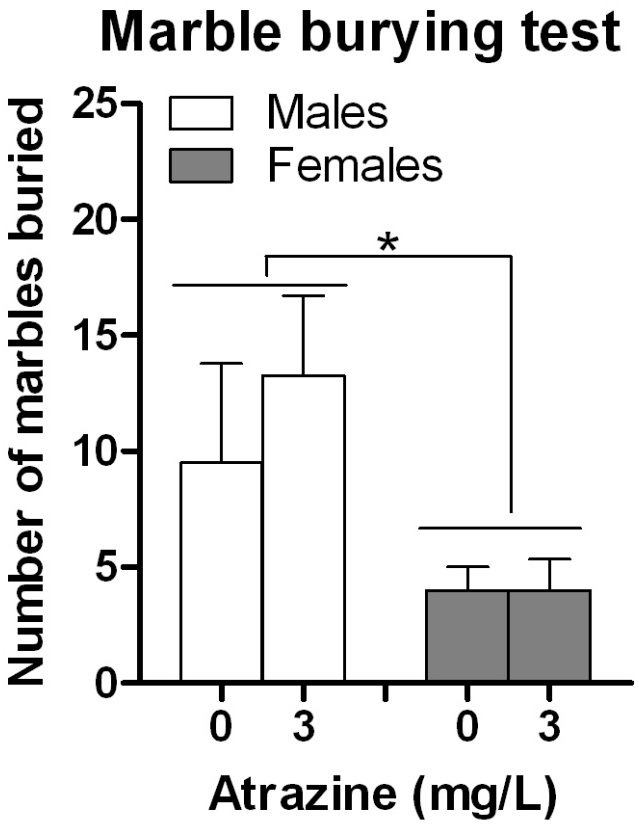

Figure D7. Effects of drinking water atrazine (3 mg/L) exposure from gestational day 6 to postnatal day 23-24 on the number of marbles buried in a marble burying test in adult mouse offspring. There were no significant differences ($p \geq 0.60$) between control and ATR-treated groups in both males and females. * Indicates significant difference between males and females ($p \leq 0.05$). Data are expressed as means ± SEM.

Table D3. Concentrations of monoamines and their metabolites in selected brain regions of mouse dams exposed to ATR from GD6 to PND23-24[a].

	DA	DOPAC	HVA	3-MT	5-HT	5-HIAA	NE	MHPG
Nucleus accumbens								
Vehicle	169.54 ± 8.22	19.41 ± 0.53	11.43 ± 0.96	14.36 ± 1.71	0.66 ± 0.15	0.81 ± 0.11	0.98 ± 0.13	17.19 ± 1.31
3 mg/L ATR	**128.56 ± 12.66^**	18.42 ± 1.27	**8.56 ± 0.66***	**9.12 ± 0.34***	0.77 ± 0.13	1.13 ± 0.14	1.31 ± 0.14	17.68 ± 1.25
Prefrontal cortex								
Vehicle	0.51 ± 0.17	-	1.15 ± 0.25	-	1.90 ± 0.18	1.08 ± 0.10	7.89 ± 0.38	-
3 mg/L ATR	0.78 ± 0.17	-	0.91 ± 0.25	-	**1.45 ± 0.09***	1.17 ± 0.10	7.85 ± 0.38	-
Perirhinal cortex								
Vehicle	1.68 ± 0.78	-	1.15 ± 0.41	-	1.27 ± 0.20	0.84 ± 0.16	7.69 ± 0.36	5.76 ± 1.91
3 mg/L ATR	1.89 ± 1.16	-	1.16 ± 0.35	-	1.48 ± 0.51	1.01 ± 0.29	**6.67 ± 0.12***	6.41 ± 2.48
Hippocampus								
Vehicle	0.60 ± 0.08	-	0.29 ± 0.08	-	1.40 ± 0.12	2.23 ± 0.18	10.54 ± 0.36	4.81 ± 0.26
3 mg/L ATR	0.56 ± 0.08	-	**0.58 ± 0.08***	-	1.46 ± 0.12	2.20 ± 0.18	10.52 ± 0.37	4.60 ± 0.26

[a] Data represent means ± SEM; unit: ng/mg protein. DA: dopamine; DOPAC: dihydroxyphenylacetic acid; HVA: homovanillic acid; 3-MT: 3-methoxytyramine; 5-HT: serotonin; 5-HIAA: 5-hydroxyindoleacetic acid; NE: norepinephrine; MHPG: 3-methoxy-4-hydroxyphenylglycol.

* Different from control group ($p \leq 0.05$). ^ $p = 0.06$. - indicates not detectable.

Table D4. Concentrations of monoamines and their metabolites in selected brain regions of juvenile mouse offspring exposed to ATR from GD6 to PND23-24[a].

	DA	HVA	5-HT	5-HIAA	NE	MHPG
Males						
Prefrontal cortex						
Vehicle	0.47 ± 0.10	0.62 ± 0.35	1.10 ± 0.16	0.87 ± 0.07	6.05 ± 0.28	-
3 mg/L ATR	0.40 ± 0.12	0.67 ± 0.41	1.25 ± 0.19	1.02 ± 0.09	6.08 ± 0.32	-
Hippocampus						
Vehicle	0.70 ± 0.06	0.33 ± 0.06	1.07 ± 0.25	1.51 ± 0.28	9.28 ± 0.43	4.17 ± 0.31
3 mg/L ATR	0.83 ± 0.07	0.48 ± 0.07	1.11 ± 0.51	1.62 ± 0.48	9.29 ± 0.50	4.16 ± 0.36
Females						
Prefrontal cortex						
Vehicle	0.50 ± 0.16	0.37 ± 0.09	1.17 ± 0.20	0.89 ± 0.10	6.61 ± 0.40	-
3 mg/L ATR	0.78 ± 0.14	0.45 ± 0.08	1.45 ± 0.18	0.98 ± 0.09	5.97 ± 0.35	-
Hippocampus						
Vehicle	0.64 ± 0.10	0.41 ± 0.05	1.13 ± 0.41	1.64 ± 0.37	8.49 ± 0.52	4.53 ± 0.19
3 mg/L ATR	0.80 ± 0.09	0.31 ± 0.04	1.61 ± 0.39	1.92 ± 0.35	8.38 ± 0.49	4.09 ± 0.18

[a] Data represent means ± SEM; unit: ng/mg protein. DA: dopamine; HVA: homovanillic acid; 5-HT: serotonin; 5-HIAA: 5-hydroxyindoleacetic acid; NE: norepinephrine; MHPG: 3-methoxy-4-hydroxyphenylglycol.
* Different from control group ($p \leq 0.05$). - indicates not detectable.

Table D5. Concentrations of monoamines and their metabolites in selected brain regions of the adult mouse offspring exposed to ATR from GD6 to PND23-24[a].

	DA	DOPAC	HVA	3-MT	5-HT	5-HIAA	NE	MHPG
Males								
Nucleus accumbens								
Vehicle	102.434 ± 16.18	10.65 ± 1.23	8.03 ± 1.45	14.32 ± 1.80	3.31 ± 1.24	0.79 ± 0.10	2.89 ± 0.77	4.67 ± 0.40
3 mg/L ATR	83.597 ± 24.42	10.91 ± 2.82	9.29 ± 1.81	**7.12 ± 2.08***	1.81 ± 0.24	0.98 ± 0.13	4.35 ± 1.70	4.92 ± 0.81
Prefrontal cortex								
Vehicle	1.74 ± 0.13	-	0.48 ± 0.13	-	1.87 ± 0.27	2.01 ± 0.31	8.32 ± 0.33	-
3 mg/L ATR	**0.85 ± 0.13***	-	0.71 ± 0.13	-	2.49 ± 0.27	1.72 ± 0.31	8.32 ± 0.33	-
Perirhinal cortex								
Vehicle	3.67 ± 0.89	0.98 ± 0.12	1.54 ± 0.27	-	0.65 ± 0.16	1.53 ± 0.41	8.93 ± 0.54	-
3 mg/L ATR	5.11 ± 1.01	0.76 ± 0.06	1.58 ± 0.64	-	0.82 ± 0.27	1.02 ± 0.27	9.26 ± 0.98	-
Hippocampus								
Vehicle	0.53 ± 0.08	-	0.44 ± 0.15	-	2.95 ± 0.52	2.96 ± 0.44	10.76 ± 0.78	-
3 mg/L ATR	0.58 ± 0.08	-	0.53 ± 0.15	-	2.77 ± 0.52	3.02 ± 0.44	10.12 ± 0.78	-

Table D5 (continued). Concentrations of monoamines and their metabolites in selected brain regions of the adult mouse offspring exposed to ATR from GD6 to PND23-24[a].

	DA	DOPAC	HVA	3-MT	5-HT	5-HIAA	NE	MHPG
Females								
Nucleus accumbens								
Vehicle	115.29 ± 4.32	13.52 ± 0.97	9.73 ± 0.99	12.42 ± 2.50	1.95 ± 0.79	0.80 ± 0.04	2.02 ± 0.53	4.30 ± 0.31
3 mg/L ATR	105.20 ± 11.48	15.75 ± 0.86	11.65 ± 1.14	15.33 ± 2.85	2.23 ± 0.40	**1.01 ± 0.03***	1.85 ± 0.27	**8.34 ± 1.48^**
Prefrontal cortex								
Vehicle	0.82 ± 0.47	-	0.67 ± 0.23	-	2.19 ± 0.19	1.59 ± 0.24	6.90 ± 0.35	-
3 mg/L ATR	1.10 ± 0.38	-	0.62 ± 0.19	-	1.97 ± 0.14	1.67 ± 0.20	7.33 ± 0.28	-
Perirhinal cortex								
Vehicle	3.69 ± 1.65	1.24 ± 0.28	1.76 ± 0.22	-	1.38 ± 0.41	0.72 ± 0.34	6.81 ± 0.88	-
3 mg/L ATR	2.69 ± 0.98	**0.50 ± 0.03***	0.83 ± 0.57	-	**0.36 ± 0.16***	0.61 ± 0.20	6.95 ± 0.67	-
Hippocampus								
Vehicle	0.67 ± 0.07	-	0.45 ± 0.09	-	3.75 ± 0.75	3.91 ± 0.40	9.71 ± 0.45	-
3 mg/L ATR	0.70 ± 0.06	-	0.64 ± 0.07	-	3.53 ± 0.60	3.57 ± 0.32	9.04 ± 0.37	-

[a] Data represent means ± SEM; unit: ng/mg protein. DA: dopamine; DOPAC: dihydroxyphenylacetic acid; HVA: homovanillic acid; 3-MT: 3-methoxytyramine; 5-HT: serotonin; 5-HIAA: 5-hydroxyindoleacetic acid; NE: norepinephrine; MHPG: 3-methoxy-4-hydroxyphenylglycol.
* Different from control group ($p \leq 0.05$). ^ $p = 0.06$. - indicates not detectable.